The Roles of HIFα Transcription Factors in Kidney Tumour Initiation and Kidney Function

Dissertation
zur
Erlangung der naturwissenschaftlichen Doktorwürde
(Dr. sc. nat.)

vorgelegt der
Mathematisch-naturwissenschaftlichen Fakultät
der
Universität Zürich
von

Désirée Schönenberger
von
Arbon TG

Promotionskomitee

Prof. Dr. Carsten A. Wagner
Prof. Dr. Michael Detmar
Dr. Jaya Krishnan
Prof. Dr. Ian J. Frew
(Vorsitz und Leitung der Dissertation)

Zürich, 2014

Table of Contents

1 Summary

The von Hippel-Lindau (VHL) tumour suppressor gene is biallelically inactivated in 70 - 90% of sporadic clear cell renal carcinomas (ccRCC). However, loss of pVHL function alone is not sufficient to cause tumour formation in human or mouse kidneys, indicating that additional cooperating mutations are likely to be involved in tumour initiation. The protein product of the VHL locus, pVHL, possesses numerous potential tumour suppressor functions, including regulation of the HIFα transcription factors. Numerous recent studies have suggested that HIF1α inhibits and HIF2α promotes the proliferation of established ccRCCs, however the roles of these proteins in the initiation of ccRCC remain unclear. We show that simultaneous deletion of *Vhl* and *Hif1a* or *Vhl* and *Hif2a* in mouse kidneys does not induce cyst or tumour formation, indicating that either Hif1α or Hif2α stabilization alone does not represent an oncogenic event, even when combined with loss of the multiple tumour suppressor activities of pVHL. Cell culture studies, however, support the notion that Hif1α activation inhibits cellular proliferation. Ablation of *Vhl* in primary mouse embryonic fibroblasts (pMEFs) causes *Trp53*-dependent senescence and is accompanied by changes in cellular metabolism that decrease O_2 consumption and impair ATP production. These effects are rescued by the additional deletion of *Hif1a*, but not of *Hif2a*, implying that Hif1α stabilization induces metabolic stress that inhibits cellular proliferation. Consistently, downregulation of *Hif1a* in *Vhl/p53*-deficient pMEFs accelerates proliferation of pMEFs and enhances the transformation capacity of primary kidney cells (PKCs), supporting the hypothesis that loss of Hif1α activity is beneficial for renal tumour evolution. In contrast, loss of *Hif1a* prevents the formation of cysts and neoplasms in *Vhl/Trp53* double mutant kidneys, demonstrating that *Hif1a* is necessary for the first stages of tumour formation *in vivo*. These findings suggest that HIF1α is necessary for tumour initiation but later acts as a tumour suppressor and inhibits the proliferation of established ccRCCs.

Maintenance of the correct activity of the HIFα transcription factors is also important for the physiological function of various organs. In the second part of this thesis we aimed to understand the underlying mechanisms of a previously published hydronephrosis phenotype, which is induced by the deletion of *Vhl* in the renal epithelium. Hydronephrosis is characterized by the expansion of the renal pelvis and the collecting system and is the most frequently diagnosed prenatal abnormality, occurring in approximately 1% of all pregnancies. Untreated hydronephrosis causes chronic kidney insufficiency and end stage renal disease, however, the precise mechanism is not yet fully understood. Histological analysis of *Vhl*-deficient mouse kidneys at different time points revealed the formation of a bilateral non-obstructive hydronephrosis between postnatal days 10 and 14. Furthermore, adult *Vhl*-deficient mice display

severe polydipsia and polyuria, which is accompanied by decreased urine osmolality and reduced hematocrit and hemoglobin levels. Detailed analyses of kidney morphogenesis by RT-qPCR and immunohistochemistry revealed a decreased abundance of specific renal markers in the medulla and papilla, suggesting a shortening of the respective parts of the nephron, presumably as a secondary effect of polyuria and subsequent development of hydronephrosis. Intriguingly, *Vhl*-deficient mice do not show any signs of renal failure and blood creatinine and electrolyte levels remain unchanged. Co-deletion of *Hif1a*, but not of *Hif2a*, fully restored kidney morphology and function, indicating that the activation of specific Hif1α-target genes in the renal epithelium causes polyuria and the subsequent formation of hydronephrosis. Gene expression analysis of kidney lysates demonstrated a *Hif1a*-dependent increase in *Vegf-a* expression, the major molecular mediator of angiogenesis. Consistently, *Vhl*-deficient and *Vhl/Hif2a*-deficient, but not *Vhl/Hif1a* deficient kidneys exhibit an increased medullary vascularization. We hypothesize that changes in medullary blood flow disrupts the osmotic gradient, washing out salt from the renal interstitium and thereby preventing urinary concentration and urine reabsorption. The excess production of urine causes a back pressure on the kidney, leading to the expansion of the renal pelvis. Taken together, our study characterizes a new mouse model for non-obstructive hydronephrosis and gives new insights in the physiological and pathophysiological effects of *Hif1a* stabilization in the kidney.

2 Zusammenfassung

Der Tumorsuppressor von Hippel Lindau ist in 70-90% der nicht erblich bedingten klarzelligen Nierenzellkarzinome (kNK) inaktiviert. Der Verlust von pVHL, dem Proteinprodukt von *VHL*, ist allerdings alleine nicht ausreichend um das Wachstum von Tumoren auszulösen, was darauf hindeutet, dass dafür zusätzliche Mutationen notwendig sind. pVHL erfüllt zahlreiche potenzielle Tumorsuppressorfunktionen, wie zum Beispiel die Regulation der Transkriptionsfaktoren HIFα. Obwohl unzählige Studien darauf hinweisen, dass HIF1α das Wachstum von kNK vermindert wohingegen es von HIF2α gefördert wird, bleibt die Rolle dieser Proteine in der Tumorentstehung unklar. Unsere Studie zeigt, dass die gleichzeitige Inaktivierung von *Vhl* und *Hif1a* oder *Vhl* und *Hif2a* in der Mauseniere nicht zur Entstehung von Tumoren oder Zysten führt. Dies beweist, dass weder die Stabilisierung von Hif1α noch von Hif2α alleine oder kombiniert mit dem Verlust der mannigfaltigen tumorverhindernden Aktivitäten von pVhl ein onkogenes Ereignis darstellt. Das Ausschalten von *Vhl* in primären embryonischen Fibroblasten von Mäusen (pMEFs) führt zur Seneszenz dieser Zellen, welche durch die Inaktivierung von *Trp53* verhindert werden kann. Gleichzeitig verändert sich der Metabolismus dieser Zellen, was einen verminderten Sauerstoffverbrauch und eine tiefere ATP Produktion zur Folge hat. Diese Prozesse werden durch die zusätzliche Inaktivierung von *Hif1a,* jedoch nicht durch die Inaktivierung von *Hif2a* verhindert, was darauf hindeutet, dass die Stabilisierung von Hif1α einen metabolischen Stress verursacht, der die Zellvermehrung hemmt. Die Herabregulierung von *Hif1a* beschleunigt das Zellwachstum auch in pMEFs ohne funktionellem *Vhl* und *Trp53* und fördert die maligne Transformation von primären Nierenzellen. Diese Resultate unterstützen die Hypothese, dass die Inaktivierung von *Hif1a* die Tumorentstehung begünstigt. Allerdings scheint *Hif1a* im frühen Stadium der Krebsentstehung notwendig zu sein, da die Inaktivierung von *Hif1a* in Mausnieren die Entstehung von Zysten und Neoplasmen, die durch Mutationen in *Vhl* und *Trp53* ausgelösten wurden, verhindert. Diese Resultate legen ein neues Model für die Entstehung von kNK nahe, in dem HIF1α für die Initiation der Tumore notwendig ist, im weiteren Verlauf jedoch als Tumorsuppressor agiert und das Wachstum von etablierten kNK vermindert.

Die korrekte Regulierung der HIFα Transkriptionsfaktoren ist auch für die Funktion unterschiedlicher Organe notwendig. Im zweiten Teil dieser Doktorarbeit wurde untersucht, wie die Inaktivierung von *Vhl* im Nierenepithel zur Expansion des Nierenbeckens und der Sammelrohre führt. Die sogenannte Hydronephrose ist mit rund einem Prozent aller Schwangerschaften die am häufigsten diagnostizierte pränatale Fehlentwicklung. Unbehandelt führt sie zu einer chronischen Niereninsuffizienz und zu Nierenversagen, allerdings ist der dafür verantwortliche Mechanismus noch nicht vollständig geklärt. Die histologische Analyse von

Maus-Nieren an unterschiedlichen Entwicklungs-Zeitpunkten zeigt, dass der Verlust von *Vhl* die Entstehung einer bilateralen, nicht-obstruktiven Hydronephrose zwischen dem zehnten und 14 Tag nach der Geburt auslöst. Ausserdem weisen adulte Mäuse mit einer Mutation in *Vhl* eine starke Polydipsie und Polyurie auf, welche von niedrigen Hämatokrit- und Hämoglobinwerten und reduzierter Urinosmolalität begleitet werden. Die detaillierte Untersuchung der Nierenmorphogenese mit Hilfe von RT-qPCR und Immunohistochemie zeigt eine reduzierte Menge mehrerer Proteinen, die nur in bestimmten Nephronabschnitten im Nierenmark und Nierenbecken exprimiert werden. Dies deutet auf eine Verkürzung der Nephrone hin, möglicherweise infolge der übermässigen Urinentwicklung und der dadurch entstehenden Hydronephrose. Bemerkenswert ist, dass diese Mäuse keine Anzeichen von Nierenversagen aufweisen und auch die Blutwerte für Kreatinin und verschiedene Elektrolyte unverändert sind. Die zusätzliche Inaktivierung von *Hif1α* aber nicht von *Hif2α* führt zu einer vollständigen Wiederherstellung der Nierenfunktion und Nierenmorphologie. Dies beweist, dass die Aktivität eines oder mehrerer von Hif1α regulierten Gene im Nierenepithel für den oben beschriebenen Phenotype verantwortlich ist. Die Analyse der Genexpression zeigt, dass die Stabilisierung von Hif1α zu einem Anstieg der Vegf-a Synthese in der Niere führt, einem zentralen Regulator der Angiogenese. Damit übereinstimmend weisen Nieren ohne *Vhl* oder *Vhl* und *Hif2α* im Gegensatz zu Nieren mit Mutationen in *Vhl* und *Hif1α* eine erhöhte Gefässbildung im Nierenmark auf. Wir vermuten, dass der veränderte Blutfluss im Nierenmark die Aufrechterhaltung des osmotischen Gradienten stört, was zu einer tieferen Osmolalität im Niereninterstitium führt und dadurch die Wasserabsorption im Nephron beeinträchtigt. Die erhöhte Urinproduktion übt einen ständigen Druck auf die Nieren aus, wodurch sich das Nierenbecken erweitert. Zusammengefasst charakterisiert unsere Studie ein neues Mausmodel für die nicht-obstruktive Hydronephrose und gibt neue Einblicke in physiologische und pathophysiologische Funktionen von HIFα in der Niere.

3 Acknowledgment

First of all I want to thank Ian Frew for giving me the possibility to work on this exciting project, for his great supervision and for always having time for any kind of questions. He not only created a stimulating scientific environment but also supported a social and cheerful atmosphere in the lab. It was great to be part of a new lab and to contribute to its development.

I am also thankful to Carsten Wagner, Jaya Krishnan and Michael Detmar for supporting me as members of my PhD committee with valuable feedback and ideas. Furthermore, I appreciate the courses that where organized by the Cancer Biology PhD program Zürich, which further strengthened my education in Cancer Biology.

Special thanks go to the people that started more or less simultaneously with me in the lab, especially to the other PhD students Holger Lehmann, Sabine Harlander and Tomas Hejhal, and later also Tamara Hüsser and Laura Brandt that brought fresh wind to our group. I am happy that I could share all the ups and downs of my PhD with these people and I will always remember the BBQs, Fondues, zvieri breaks and lab beers we had together. I enjoyed the great atmosphere in the lab that motivated me every day to come to work, even in moments of frustrating experiments and results. I especially want to thank Daniele Vicari for a lot of help when everything was still new to me, Joachim Albers for many very valuable advices and Michal Rajski for working together on the same project. I am also thankful to Holger Lehmann for always bringing selfbaked cookies and other sweets to the lab (except of the Thyme chocolate!) and to Tomas Hejhal for discussions about science and the world, for always giving a helping hand and for constant computer support, especially for being my last hope when my computer once again refused to convert a pdf out of my posters. Special thanks go to Sabine Harlander. Always being a little bit ahead of me, she supported me whenever help was needed, starting with the first western blot until to the printing of my thesis. I was lucky to get such a great person sitting next to me. I am also grateful for all the food I borrowed from her desk during the last years, without that I probably would have starved to death several times.

Special thanks also go to Claudia Danzer-Baltzer and Mojca Adlesic. They have been supporting my scientific career from the very beginning, sharing all their wisdom with me during these years and investing a lot of time in proofreading my thesis. I am very happy that they have become good friends during this time and appreciate all the great moments we had together.

I am thankful that I had the chance to meet so many interesting and fun people during my studies at ETH, at the Institute of Physiology (especially people from the Wenger group), in the cancer biology PhD program and in the kidney.ch NCCR program. I enjoyed the scientific and non-scientific discussions and I appreciate the social moments that made my PhD to a great experience.

I also want to thank my family, especially my mother, for support and care during my whole life. It is good to know that there are always people that are there for you if it is needed. Finally, I am grateful to Andreas for being a part of my life and for opening a door to a different world.

4 Preface

A number of people have directly contributed to the work described in this thesis. I am grateful that these people enabled the investigation of this project in a bigger context and enjoyed their collaboration.

Ian Frew wrote the manuscript in chapter 8.2.1. Sabine Harlander, Tatjana Simka and Ian Frew performed the metabolic analysis of *Vhl* and *Vhl/Trp53*-deficient pMEFs. Michal Rajski, Robert A. Jacobs and Anne-Kristine Lundby analysed the renal oxygen consumption rate and Tomas Hejhal provided RNA for the gene expression analysis of *Vhl/Hif1α*-deficient pMEFs.

Furthermore, Claudia Danzer-Baltzer established the deep-sequencing protocol for the screen in 8.2.2 and Michal Rajski performed all the experiments with $Hif2a^{fl/fl}$ and $Vhl^{fl/fl}$ $Hif2a^{fl/fl}$ mice in chapter 8.3. Holger Lehmann, Sabine Harlander and Tomas Hejal contributed to chapter 7.

5 Abbreviations

ANH	antenatally diagnosed hydronephrosis
Aqp	Aquaporin
ATP	Adenosine triphosphate
AVP	Arginine vasopressin, also known as antidiuretic hormone (ADH)
BUN	Blood urea nitrogen
ccRCC	clear cell renal cell carcinoma
Epo	erythropoietin
Hct	hematocrit
Hifα	Hypocia inducible transcription factor alpha
NaPi-IIa	Na/phosphate cotransporter
NCC	Na/Cl co-transporter
NDI	nephrogenic diabetes insipidus
NKCC2	sodium-potassium chloride co-transporter
P53	transformation related protein 53 (mouse homologue)
PKCs	primary kidney cells
pMEFs	primary mouse embryo fibroblasts
pVhl	von Hippel Lindau protein
TAL	thick ascending limb of Henle
TP53	tumour protein 53 gene (human homologue)
Trp53	transformation related protein 53 gene (mouse homologue)
Vhl	von Hippel Lindau gene
ROS	reactive oxygen species
MBL	medullary blood flow

6 Introduction

6.1 Kidney anatomy and function

A broad range of genetic or acquired diseases including polycystic kidney disease, virus infections, exogenous stress (toxins, drugs, obesity) or kidney cancer are affecting kidney function, finally causing kidney insufficiency. The kidney is the main excretory organ in mammals and is responsible for various physiological processes such as osmoregulation, urine excretion, blood cell production and the regulation of the blood pressure and acid/base homeostasis. The precise regulation of these processes is very complex and many questions are still not fully answered. In this thesis, we focused on clear cell renal cell carcinoma (ccRCC) and hydronephrosis, on two common disorders of the kidney. We aimed to understand the underlying mechanisms that are involved in the formation of these diseases and how specific genetic deletions influence the function and structural integrity of the organ. The following paragraphs focus on the processes and mechanisms of kidney structure and function that are important for the understanding of the experimental goals of the work described in this thesis.

The functional unit of the kidney is the nephron, a tubular epithelial structure composed of the glomerulus, proximal tubule (PT), descending and ascending loop of Henle, macula densa, distal tubule (DCT) and the connecting tubule (CT) (Fig. 6.1A) (Treuting and Kowalewska 2012). The connecting tubule leads into the collecting ducts, which converge into the renal papilla and finally extend in the pelvis, the funnel-like dilated part of ureter. The human kidney consists of around 1 Mio nephrons, whereas there are approximately 14 000 nephrons in mice. Importantly, the nephron number does not change with age. Macroscopically, the kidney consists of two major regions, the cortex (outer region) and the medulla (inner region), the latter being further divided in an outer and inner part (Fig. 6.1B). In contrast to the mouse kidney, which is a unilobular organ, the human kidney consists of 7-9 papillae which form the renal calyxes and then open into the renal pelvis (Fig. 6.1C) (Treuting and Kowalewska 2012). The glomeruli, the proximal and the distal tubules are located in the cortex, whereas the loop of Henle and the collecting ducts reach into the medulla. Peritubular capillaries surround the tubules in the medulla, taking up the reabsorbed solutes from interstitial space (Fig. 6.2). Therefore, the capillaries are essential for the maintenance of the osmotic gradient, the driving force for renal reabsorption (see below) (W F Boron 2009).

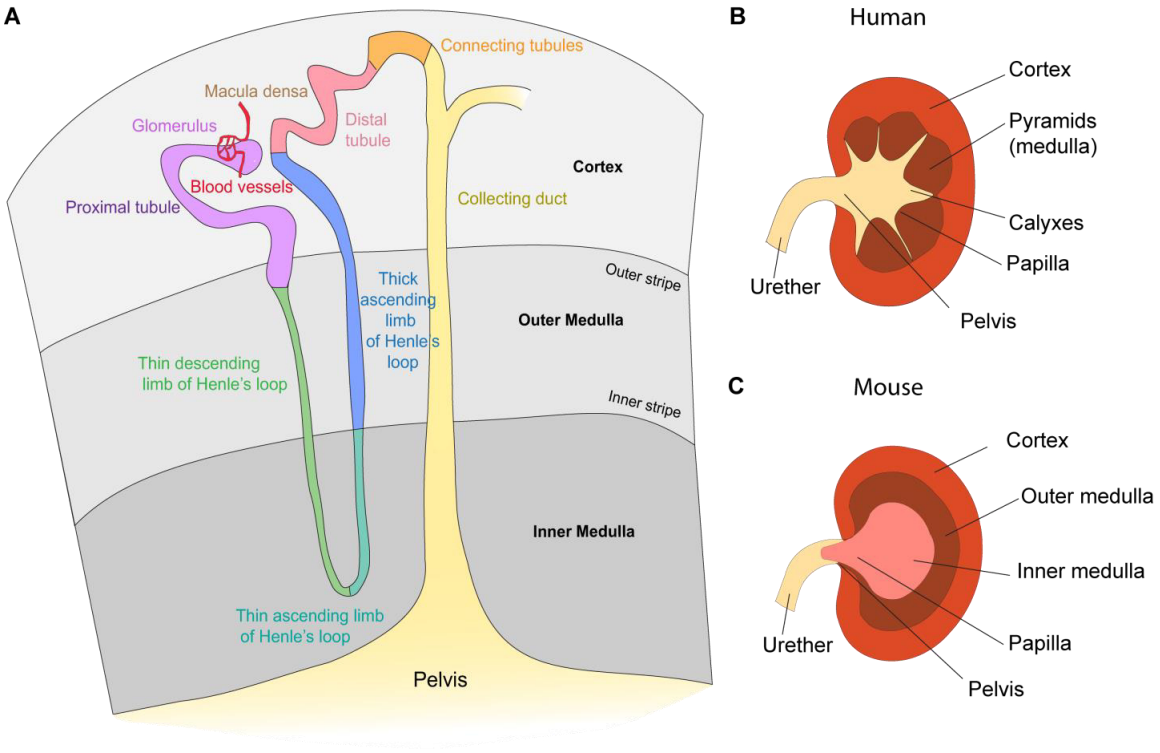

Fig. 6.1: Schematic view of kidney anatomy. (A) The renal glomerulus is located in the renal cortex and gives rise to the tubular system that is reaching into the inner medulla of the kidney. Several connecting tubules fuse into a collecting duct which finally ends in the renal pelvis. Different tubular segments are depicted in corresponding colors. (B) The human kidney consists of several pyramids that fuse via the renal calyxes into the pelvis, whereas (C) the mouse kidney is a unilobar organ.

The glomerulus consists of a network of capillaries and is surrounded by podocytes, modified epithelial tubular cells. Together, they create the Bowman's space, which is the proximal end of the tubular lumen of the nephron. This unit is called the Bowman's capsule. The basement membrane is located between endothelial cells and podocytes and in cooperation they represent the actual filter unit. Together, they prevent large solutes (molecular weight < 1 kDa) and large negatively charged solutes in the blood from entering the Bowman's space (W F Boron 2009). After filtration, the primary urine is transported along the nephron and specific molecules (ions, water) are reabsorbed by specialized nephron segments (S Silbernagl 2003). The proximal tubule reabsorbs NaCl, $NaHCO_3$, nutrients (glucose, amino acids etc.), water and divalent ions (Ca^{2+}, HPO_4^{2-}, SO_4^{2-}) and secretes NH_4^+ and other endogenous and exogenous solutes into the lumen. The loop of Henle is mainly responsible for water reabsorption and maintenance of the osmotic gradient. In the descending limb of Henle water crosses the membrane along the osmotic gradient, which is recreated by the thick ascending limb, where specialized ion transporters (NKCC2) actively pump NaCl in the medullary interstitial space to make it hypertonic. The distal tubules and the collecting duct are responsible for the fine tuning of NaCl uptake and water

absorption by hormone-dependent regulation of ion transporters and water channels (see below) (W F Boron 2009).

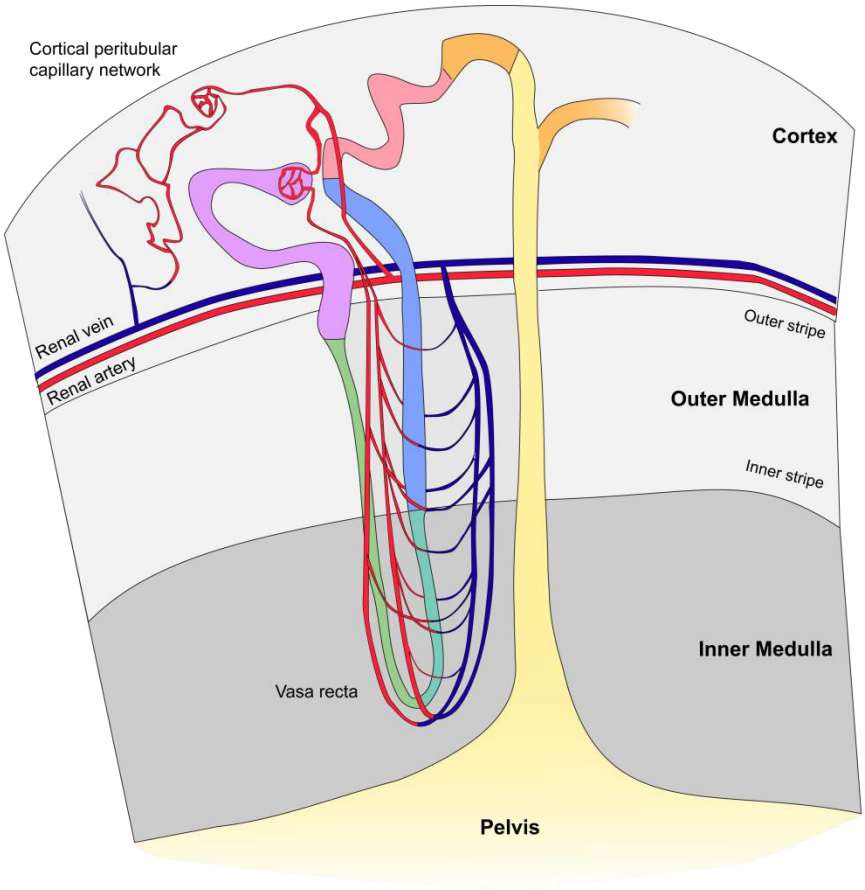

Fig, 6.2: Simplified view on renal capillary system. The renal arteries give rise to numerous afferent arterioles which subsequently form the glomerular capillaries. The efferent arterioles of the juxtamedullary glomeruli descend into the renal papillae and form hairpin-shaped vessels called the vasa recta, providing the capillary network for the medulla. However, the majority of the efferent arterioles give rise to the peritubular capillary network that supplies the cortex with nutrients and oxygen (superficial glomeruli).

A broad range of distinct transporters is expressed in the apical and basolateral side of the renal tubular cells to enable water reabsorption and to prevent loss of important molecules or ions in the urine. Solutes can be transported through epithelial cells either passively along their electro-chemical gradient or actively by different types of transporter (transcellular pathway). Finally, they are reabsorbed from the interstitial space by the capillaries. The sodium-potassium-chloride co-transporter (NKCC2) is an example of an apically coupled co-transporter expressed in the thick ascending limp of Henle (TAL), where the uptake of the ions by the cell is driven by downhill concentration gradients of Na^+ and Cl^-. On the basolateral side of the cell, the ATP-dependent Na-K-pump, an antiporter, actively transports Na^+ into the interstitial space, through which the Na^+ gradient is maintained. On the other hand, sodium and chloride are transported by NCC, a Na/Cl co-transporter, into the distal convoluted tubule. In addition to the transcellular pathway, small solutes can also travel from the primary urine to the blood via a fully extracellular pathway through the tight junctions of cells (paracellular pathway). Water flows passively through different renal aquaporins due to the difference in the osmotic gradient in the medulla. Since Na^+ is the most important contributor to the osmolality of the extracellular fluid, a common rule is:

where Na^+ goes, water follows. Importantly, there are no aquaporins expressed in the TAL (Verkman 2008), which therefore enables the reconstitution of the osmotic gradient by NKCC2. Increased plasma osmolality causes the secretion of arginine vasopressin (AVP, also called antidiuretic hormone (ADH)) from the posterior pituitary that in turn binds to their receptors at the basolateral side of target cells, leading to increased absorption of water by several mechanisms. In the collecting duct, AVP stimulation causes the translocation of AQP2 (Aquaporin 2) to the apical membrane and NKCC2 and K^+ channels are stimulated in the TAL (W F Boron 2009). Furthermore, the kidney is crucial for the control of plasma levels of solutes like phosphate, calcium, magnesium and amino acids that are only present at low concentrations. Interestingly, some molecules including urea or HCO_3^- are not only reabsorbed but can also be secreted by the kidney (W F Boron 2009).

Some renal transporters are often used as markers for specific tubular segments, due to their very distinct expression patter. In this thesis, we used NCC as a marker for distal tubules, NKCC2 for the TAL (Kaplan et al. 1996) and AQP2 for collecting ducts. Additionally, NaPi-IIa (Na/phosphate cotransporter), SGLT1, Cubulin, Pendrin, Tamm-Horsfall and ATP V1B1 were used. NaPI-IIa, SGLT1 and Cubulin are all markers for proximal tubules. NaPi-IIa is the most abundant phosphate transporter in humans and specifically expressed in proximal tubules, where 80% of the filtered phosphate is reabsorbed (Berndt and Knox 1992). SGLT1 is expressed in the later part of the proximal tubule and is responsible for the apical glucose uptake, whereas Cubulin binds albumin in the urine and hence mediates its endocytosis (Sahali et al. 1988; Birn et al. 2000; Wright et al. 2007). ATPV1B is the B1 subunit of the vacuolar proton-pumping ATPase (V-ATPase) and used as a marker for distal tubules and collecting ducts (Paunescu et al. 2007). Pendrin is a chloride iodide transporter that is expressed in the proximal tubules and the cortical collecting duct (Scott et al. 1999; Soleimani et al. 2001). Mutations in these genes cause the Pendred syndrome, a recessively inherited disorder characterized by congenital deafness (Everett et al. 1997). Similarly, mutations in ATPV1B1 can also lead to loss of hearing (Yashima et al. 2010). (Paunescu et al. 2007). Tamm-Horsfall protein (also called uromodulin) is a glycoprotein expressed in the thick ascending limb and presumably in a part of the distal tubules. Although it has been shown to be involved in several pathways and human disorders, its precise function is still not fully understood (Hoyer et al. 1979; Sikri et al. 1981; Mao et al. 2014)

Finally, the kidney also functions as an endocrine organ. At the macula densa the kidney senses the amount of fluid and NaCl passing through the nephron and regulates the glomerular filtration rate accordingly. Furthermore, the macula densa also controls the pressure of afferent arterioles by induction of renin excretion into the circulation by granular cells of the juxtaglomerular

apparatus (JGA) (W F Boron 2009). Another endocrine function of the kidney is the regulation of erythrocyte production in adults. When renal oxygen content drops, erythropoietin (EPO)-producing, fibroblast-like cells are recruited to the border of the subcapsular tissue, elevating EPO secretion in the blood (Koury et al. 1989; Eckardt et al. 1993). In the bone marrow, Epo stimulates erythropoiesis and therefore enables increased oxygen transport in the body (Wenger and Hoogewijs 2010).

6.2 Kidney development

In amniotes nephrogenesis consists of 3 phases, each of them marked by the formation of a more advanced kidney (Gilbert 2003). In the first phase, the pronephros is formed from the intermediate mesoderm in the neck region of the embryo, forming the pronephric ducts and pronephric tubules which open into the cloacae. In mammals, the pronephros does not fulfil any excretory function and regresses again. The most caudal part, however, persists as the nephric duct (also known as Wolffian duct) and participates in the formation of the male reproduction organs (Gilbert 2003; Joseph et al. 2009). Subsequently, the formation of the mesonepheros is induced from the adjacent mesenchyme. The mesonephros is a large, tubular structure that consists of primitive glomeruli and functions as an interim kidney in some mammalian species until the metanephros has developed (Saxén L 1987; Gilbert 2003). Whereas the mesonephros does not function as a kidney in rodents, its contribution to fetal blood filtration remains unknown (Gilbert 2003). Next, the nephric duct starts to evaginate at day E10.5 in mice (fifth week of gestation in humans) and forms an uretic bud at its caudal end that invades the metanephric mesenchyme (Costantini and Kopan 2010; Song and Yosypiv 2012). After invading the metanephric mesenchyme the uretic bud starts extending and branching repeatedly (Fig. 6.3A-G) (Srinivas et al. 1999). The metanephric mesenchyme condenses around the ureteric bud tips, undergoes mesenchymal-epithelial transition and forms the renal vesicles. Subsequently, the vesicles fuse with the ureteric stalk, creating the so-called S-shaped bodies. The most proximal part of the S-shaped body will give rise to the future glomerulus and most of the renal tubules, whereas the very distal end of the S-shaped body and the ureteric bud will form the collecting ducts (Dressler 2009). At this stage, the different parts of the S-shaped body show a distinct gene expression pattern presumably reflecting the regionalization into the different segments (Georgas et al. 2009). However, the detailed mechanism of subdivision of the nephron is not fully understood yet. Eventually, renal medulla becomes identifiable at E15.5 and expands longitudinally to increase in size. Importantly, nephrogenesis is not completed at birth in rodents. For instance, the medulla of newborn rats is not separated into an outer and inner zone yet. In the first 2 weeks after birth, the immature thick limbs of Henle are transformed by a series of

apoptotic deletions and growth of the segment (Song and Yosypiv 2012). Very recent data shows that tubulogenesis continuous in the adult mouse kidney. Linage-tracing experiments indicate that a subset of adult epithelial cells keep dividing, thus leading to a complete renewal of the renal epithelium approximately every 6 weeks (Rinkevich et al. 2014).

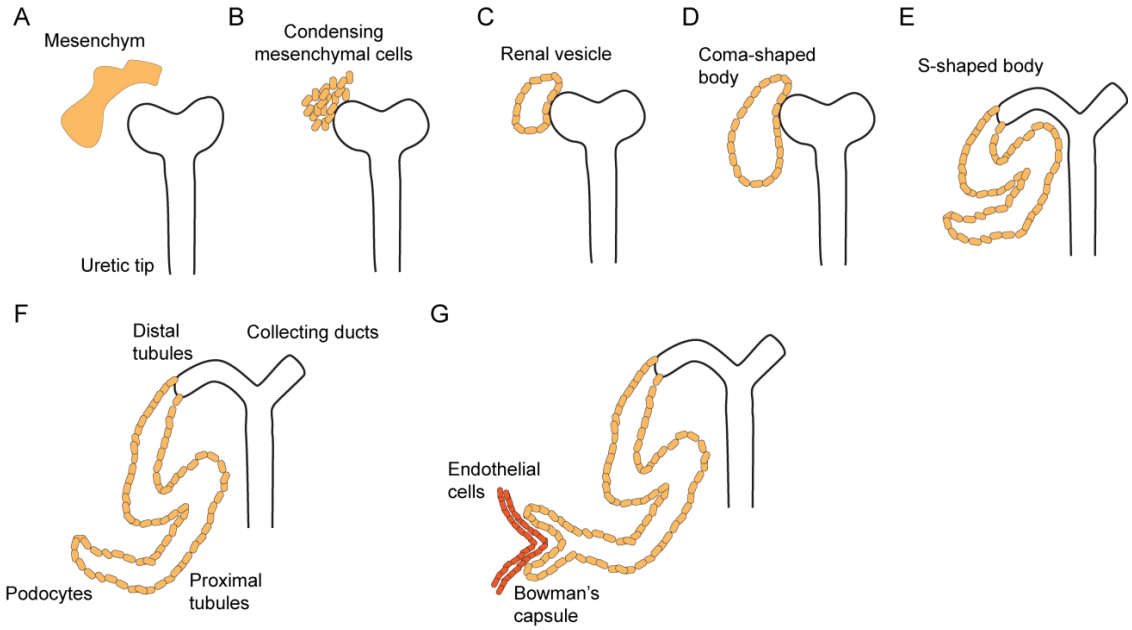

Fig. 6.3: Development of the adult kidney (Pronephros): (A-B) Mesenchymal cells condense at the uretic bud, (C) subsequently forming the renal vessels, (D-E) comma-and S-shaped body, (F) finally giving rise to the tubular system. (G) The most proximal cells associate with endothelial cells to build up the Bowman's capsule.

Nephrogenesis is synchronized with kidney vascularization. Although it is believed that kidney vascularization is mainly achieved by angiogenesis (sprouting from existing vessels), vasculogenesis (de novo synthesis from endothelial progenitor cells) has also been postulated (Saxén L 1987). Hence, endothelial cells may sprout from pre-existing vessels in the surrounding tissue of the mesenchyme or could alternatively differentiate *in situ* from mesenchymal or epithelial cells within the S-shaped body (Gomez et al. 1997). During kidney organogenesis a broad spectrum of growth factors such as VEGF, TGFα, PDGF, IGF etc. are secreted, presumably also supporting development of the vascular system (Gomez et al. 1997). For instance, Kitamoto et al. show that correct VEGF signalling is important for the correct formation of vascular morphology and glomeruli (Kitamoto et al. 1997). Additionally, VEGF is crucial for the maintenance of glomeruli in adults indicating a crosstalk between epithelial and endothelial cells (Kitamoto et al. 1997).

Finally, the renal interstitium and the renal nerves have to develop. The adult cortical and medullary interstitium arises from two distinct populations of metanephric stroma cells. The knowledge of the role of renal neuronal cells in metanephric development is still very limited,

although it has been shown that sympathetic nerves follow the track of blood vessels while growing into the embryonic kidney (Song and Yosypiv 2012). These two processes are not further discussed in the context of this thesis.

Various signalling pathways are involved in renal organogenesis, including integrins or Wnt, Notch and Pi3K signalling pathways (Costantini and Kopan 2010). Mutations of these pathways can lead to severe malformations (see 6.4) (Schedl 2007; Wu et al. 2009). Furthermore, the hypoxia-inducible factors α, transcription factors induced upon low oxygen tension are essential for intact kidney development (see below for a detailed discussion of Hifα signalling). In new born mice *Hif1α* and *Hif2α* mRNA is highly expressed in the renal medulla, especially in the medullary collecting ducts (Freeburg and Abrahamson 2003). Moreover VEGF mRNA, a Hifα target gene, was found in the medulla from rat kidneys at day 14 and inhibition of VEGF activity in developing mouse kidneys cause renal malformations (Kitamoto et al. 1997; Madsen et al. 2010) .

In this thesis we examined the effects of HIFα dysregulation in the renal epithelium on renal function and on the formation of clear cell renal carcinoma (ccRCC). We used the Cre/LoxP system to induce tissue-specific gene deletions in transgenic mice. The Ksp1.3-Cre transgene induces the expression of a Cre-recombinase in the ureteric bud, the Wolffian and Müllerian ducts, the developing ureter and in the developing tubules in the mesonephros and the metanephros and thereby causes gene deletions by homologous recombination in the epithelium of the uterus, epididymis, vesicular glands and in the renal nephron. Furthermore, the use of a tamoxifen-inducible variation of the Cre-recombinase (Ksp1.3-Cre-ER^{T2}) enabled us to cause gene deletion only in adult mice, circumventing any effects caused by changes in early development. Since the Ksp.1.3 promoter is only transiently active in the Wolffian and Müllerian ducts, this transgene causes gene recombination only in the renal epithelium (Shao et al., 2002a; Shao et al., 2002b; Patel et al., 2008).

6.3 Renal cell carcinoma (RCC)

6.3.1 Inherited and sporadic forms of RCC

Renal cell carcinoma (RCC) is the general term for a group of cancers arising from the renal tubular epithelium. Currently these diseases represent the eighth leading cause of cancer-related death in the United States of America (Hakimi et al. 2013). Clear cell RCC (ccRCC) is the most common subtype with approximately 65% of all reported cases, followed by papillary RCC (pRCC, type 1 and 2) accounting for 15-20% and chromophobe RCC with 5% of all RCC patients. Moreover, a few very rare carcinomas including MiTF-TFE translocations and spindle cell carcinomas are also

accounted to RCC (Jonasch et al. 2012). The different types of RCC are distinguished by morphology, prognosis and their underlying genetics. Similar to other types of cancer, RCCs occur in sporadic and hereditary forms, the latter accounting for 4% of all cases. Several familiar cancer syndromes predispose to different types of hereditary RCC. For instance, ccRCC often occurs in patients suffering from the von Hippel-Lindau (VHL) syndrome, which is characterized by germline mutations of *VHL*, a gene coding for pVHL, the recognition component of a ubiquitin ligase (Latif et al. 1993). Additionally, ccRCC is sometimes found in patients with the Tuberous Sclerosis syndrome, caused by germline mutations in the tuberous sclerosis complex (TSC) 1 and 2 genes. Mutations in the *MET* genes cause hereditary papillary renal carcinoma and increase the risk for type 1 pRCC (Zbar et al. 1994; Schmidt et al. 1997). In contrast, fumarate hydratase (FH) mutations occur in hereditary leiomyomatosis and renal cell carcinoma syndrome (HLRCC) and predispose for pRCC type 2 (Tomlinson et al. 2002). The Birt-Hogg-Dubé syndrome is associated with mutations in the folliculin (FLCN) gene which predisposes to the development of chromophobe RCC (Nickerson et al. 2002). Finally, mutations in the succinate dehydrogenase subunit B (SDHB) give rise to the paraganglioma syndrome and these patients display an increased risk of developing multiple types of RCC. The genetic events that cause tumourigenesis in sporadic cases of RCC are less well understood. VHL is somatically mutated or silenced in up to 92% of patients with ccRCC, indicating that loss of VHL function is a crucial step in the development of the cancer (Sato et al. 2013). In contrast, MET or FLCN mutations only occur in a small fraction of patients with sporadic pRCC or chromophobe RCC, respectively (Schmidt et al. 1997; Kiuru et al. 2002). Similarly, to date no mutations in SDHB or TSC1/2 have been found in sporadic RCC (Parry et al. 2001).

The goal of this thesis was to better understand the initial events in kidney cancer formation, focusing on ccRCC. To address this question, we developed different mouse models harbouring epithelium-specific deletions of the most common genetic alterations occurring in ccRCC. This system allowed us to investigate the cooperative effects of gene deletion directly in the murine kidney as well as in different cell culture models.

6.3.2 Treatment of RCC

The 5-year survival for patients with RCC largely depends on the stage of the disease. Whereas stage I RCC (tumour ≤ 7 cm, limited to the kidney) has an overall survival rate of 88%, stage II (tumour ≥ 7 cm, limited to the kidney) and stage III disease (expansion into major veins, adrenal glands or perinephric fat) display a reduced survival rate of 63% and 65%, respectively. Only 15% of patients suffering from stage IV disease (invasion beyond Gerota's fascia, >1 lymph node metastasis or distant metastasis) are still alive 5 years after diagnosis (data from patients

diagnosed between 1964 and 1997) (Greene 2002; Sunela et al. 2009). In general, overall prognosis is rather poor since 30% of RCCs have already metastasized at the time of the first diagnosis and another 30% develop metastasis after initial resection of the primary tumour (Sandock et al. 1995; Mekhail et al. 2005).

Currently, the most efficient treatment for ccRCC is surgery combined with targeted therapy using multiple anti-angiogenic agents, such as sorafenib (Raf kinase inhibitor (Bukowski et al. 2007)), sunitinib (small-molecule tyrosine kinase inhibitor targeting VEGFR-2, PDGFR-B, FLT3 and KIT), bevacizumab (recombinant humanized monoclonal antibody against VEGF (Presta et al. 1997)) and pazopanib (tyrosine-kinase inhibitor (Hutson et al. 2010)). Treatment of patients with metastatic ccRCC with the kinase inhibitors sorafenib and sunitinib have been shown to extend the overall survival to 28.8 months compared to only 10 months in patients treated with conventional chemotherapy (Motzer et al. 1999; Herrmann et al. 2011; Qian 2013). Unfortunately, patients undergoing anti-angiogenic therapy inevitably develop a resistance or already present primary resistance at the time of the treatment. Therefore, several novel agents are currently being tested as adjuvants in clinical trials. For instance, a phase II study of sunitinib plus trebananib, an angiopoietin peptibody disrupting the Ang/Tie-2 axis, has shown encouraging results with a progression-free survival of 16 months and a high overall response rate of 59% (Atkins 2012). Other promising newly developed agents are currently undergoing clinical trials such as cabozantinib (a small-molecule kinase inhibitor targeting MET receptor and VEGFR-2) and dalantercept (a soluble fusion protein of the extracellular domain of ALK-1 and human IgF1-Fc that binds BMP9 and BMP10, functioning as a ligand trap), both inhibiting angiogenesis by different mechanisms. Additionally, several other targets that have been associated with angiogenic resistance are currently being investigated in animal models, such as IL-8 neutralizing antibodies, HDM2/HDMX antagonists, improved mTOR inhibitors or the inhibition of the Hippo pathway. Direct inhibition of HIF2α, a transcription factor regulating VEGF expression, has also been proposed as potential potent therapeutic, however clinically applicable inhibitors have not yet been developed (Philips and Atkins 2014). Finally, recent studies have identified immunoregulatory pathways that protect tumour cells from the destruction by the immune system. Newly developed antibodies such as nivolumab blocking these immune checkpoints have been shown to exhibit anti-tumour activity in several cancers, including RCC and may be promising agents for new combination therapies. However, very recent clinical trials indicate an inacceptable dose-limiting toxicity for some patients and demonstrate the need of a suitable ccRCC mouse model that enables the development of new therapeutic agents that not only prolong a patient's life but eventually cure the disease (Asim Amin 2014).

6.3.3 Von Hippel-Lindau (VHL) Disease

Von Hippel-Lindau disease is an autosomal dominant disorder that is characterized by a germline mutation of the *VHL* gene, coded on chromosome 3p25 (see below) (Latif et al. 1993). VHL patients are at high risk of developing ccRCC and various other benign and malignant tumours including pancreatic cysts and neuroendocrine tumours, pheochromocytoma (tumour of the adrenal gland (Santos et al. 2014)), retinal haemangioblastomas, central nervous system hemangioblastoma and endolymphatic sac tumours (tumour of the inner ear) (Linehan et al. 2009). Tumours are initiated by the inactivation of the second allele of the *VHL* gene. VHL disease is divided into different subtypes, depending on the kind of inherited mutations in the *VHL* gene (missense, nonsense, deletions). Importantly, this genetic variability is also reflected by the clinical manifestation of the disorder. For instance, phaeochromocytoma is only a feature of type 2 VHL diseases but not of type 1. Type 2 is further divided into 3 subtypes that differ in the risk of developing renal cancers. Type 2C is associated with a high risk of phaeochromocytoma, but a low risk of renal cell carcinoma and hemangioblastoma (Barontini and Dahia 2010). Genetic analyses of these patients reveal a specific missense mutation in the *VHL* gene that causes no or only very weak activation of the hypoxia-inducible transcription factor alpha (HIFα), a protein targeted for proteolytic degradation by VHL. This is in contrast to the mutations in other subtypes of the VHL disease that cause high HIFα levels, correlating with a high risk for renal cancer and therefore indicating that HIF stabilization is an important step in the formation of ccRCC (Raval et al. 2005)

VHL disease occurs with an incidence of 1 in 39 000 live births in England (Maher et al. 1991). Retinal haemangiomas or phaeochromocytomas are often the first manifestations of the syndrome in childhood or adolescence, presented by loss of visual acuity and visual field or severe hypertension and headaches, respectively. Central nervous system (CNS) haemangioblastomas are the most common lesion, occurring in 60-80% of all cases (Maher et al. 2011). These are highly vascularized benign tumours that cause important neurological deficits and are associated with a significant mortality rate. Furthermore, ccRCC or multiple renal cysts occur in 60-70% of patients depending on the subtype of VHL disease and are commonly diagnosed when patients reach the age of 40 years. ccRCC can arise from frequently observed multiple renal cysts or from non-cystic renal parenchyma and is a common cause of death in VHL patients (Maher et al. 2011). Additionally, 35-77% of patients develop pancreatic tumours or cysts. Whereas cysts are normally benign, tumours metastasize in 8-50% of the cases, commonly to the liver. Endolymphatic sac tumours can cause tinnitus, vertigo or irreversible loss of hearing in early adults (Barontini and

Dahia 2010). Finally, up to 60% of males with VHL disease develop epididymal cystadenomas, which are usually asymptomatic and do not require further treatment (Choyke et al. 1997).

Treatment of patients depends on the manifestation of the disease. Children with a familiar history of VHL disease should be genetically screened for germline mutations in the *VHL* gene and clinical screening is recommended when mutations are identified (Johnston et al. 2001). However, 20% of VHL disease patients result from *de novo* mutations and are first identified by the manifestation of typical tumours found in VHL disease (Richards et al. 1995). Pancreatic and renal tumours are resected when larger than 3 cm in diameter. Also, early removal of endolymphatic sac tumours is recommended, possibly preventing or alleviating the neurological symptoms. Importantly, patients require life-long follow-ups due to the risk of recurrence (Barontini and Dahia 2010). Moreover, retinal angiomas mostly respond well to laser photocoagulation or cryotherapy. Several anti-angiogenic agents including small-molecule VEGF receptor inhibitors or anti-VEGF antibodies are currently used for the treatment of advanced tumours in clinics or in clinical trials, partially with good responses in some tumours (Barontini and Dahia 2010).

Inherited *VHL* mutations can also cause Cuvash polycythaemia, an autosomal recessive disorder characterized by increased HIFα and EPO levels (Ang et al. 2002). These patients suffer from erythrocytosis but lack the typical tumoural phenotype of VHL disease, therefore Cuvash polycythaemia is categorized as a separate disorder.

6.3.4 Clear cell renal cell Carcinoma (ccRCC)

6.3.4.1 Origin of ccRCC

Only 1% of ccRCC are caused by inherited VHL mutations (see 6.3.3) and the majority occur as sporadic cases (Neumann et al. 1998). The clear cell form of renal carcinoma is characterized by a high lipid and glycogen content and represents the most common and aggressive subtype (Linehan et al. 2009). ccRCC originates from the renal epithelium, however the type of tubular segment or segments that serves as the cell of origin of this tumour is still under debate. Examinations of pre-cancerous kidneys of VHL patients reveal that the majority of *VHL*-deficient proximal cells remain as single cells, whereas multicellular *VHL* null lesions almost exclusively arise from the distal tubules, possibly reflecting intrinsic differences in the response of the different segments to the loss of *VHL* function (Mandriota et al. 2002). Several studies with human ccRCC biopsies indicate that most tumours stain positively for proteins that are specifically expressed by the proximal tubules, while other studies suggest the distal tubules and collecting duct cells as the origin for ccRCC (Droz et al. 1990; Motzer et al. 1996; Paraf et al. 2000;

Mandriota et al. 2002; Straube et al. 2011). However, tubular cells may change their gene expression pattern during transformation possibly leading to up or down regulation of specific markers and therefore limiting the significance of these studies. Consistently, examination of kidneys from VHL patients show that clusters of *VHL* null cells lose the expression of epithelial markers such as E-cadherin and Tamm-Horsfall protein, yet they are positive for Vimentin, a mesenchymal marker for de-differentiation (Mandriota et al. 2002; Esteban et al. 2006). In summary, it appears that ccRCC most often arises from proximal tubular cells, but can also arise from epithelial cells of other nephron segments.

For the generation of a ccRCC mouse model, we used the Ksp1.3 promoter, which specifically induces gene deletions in epithelial cells throughout the whole nephron, therefore targeting all segments that have been postulated as the origin of ccRCC. While the Cre-recombinase is only weakly expressed in the proximal tubules in comparison to expression levels in other nephron segments, our unpublished reporter studies, together with published data, show that approximately 5-10% of proximal tubular epithelial cells undergo Cre-mediated recombination (Shao et al. 2002a; Shao et al. 2002b; Frew et al. 2008b, Goncalves unpublished data). This observation suggests that the Ksp1.3-Cre mouse line is a good choice for the generation of ccRCC mouse models but also has implications for the physiological analyses that were carried out in this thesis.

6.3.4.2 Common genetic alterations in ccRCC

The most prominent mutation in ccRCC is the loss of function of pVHL, encoded by the *VHL* gene. Detailed molecular analysis has recently revealed that *VHL* is biallelically inactivated, either by loss of function mutations, DNA hypermethylation or loss of one copy of chromosome 3p in up to 92% of sporadic cases of ccRCC (Sato et al. 2013). This extremely high prevalence of genetic alterations in a specific gene indicates an important role of pVHL in tumourigenesis. This notion is further supported by the observation that 42% of the remaining cases of ccRCC that are wild type for pVHL harbour a biallelic inactivation of *TCEB1* (encoding Elongin C) another member of the pVHL ubiquitin ligase complex (Kamura et al. 2000; Sato et al. 2013). However, examination of kidneys of VHL patients demonstrates that loss of pVHL function alone is not sufficient to induce tumour formation since kidneys exhibit a large number of *VHL* null cells but only a few finally develop into cysts or tumours. This notion indicates that additional oncogenic events have to occur to drive tumour formation (Mandriota et al. 2002; Montani et al. 2010)

During the last years, whole-genome, whole-exome and transcriptome analyses have been performed using large collections of ccRCC samples, providing a deeper understanding of the underlying genetic alteration in ccRCC formation (Hakimi et al. 2013). These studies demonstrate

that loss of heterogocity (LOH) of chromosome 3p is a fundamental event in ccRCC pathogenesis, occurring in over 90% of the cases (The Cancer Genome Atlas Research 2013). On this chromosome segment the *VHL*, *PBRM1*, *BAP1* and *SETD2* genes are closely located. Further, these genes also belong to the top four mutated genes in ccRCC, hence leading to a lack of functional protein expression in a very high number of ccRCC cases. Together, these findings support the importance of pVHL inactivation in tumour formation and also indicate a fundamental role of epigenetic alteration in the formation of kidney cancer, as PBRM1, BAP1, and SETD2 are involved in chromatin remodelling (Sato et al. 2013). This goes in line with the findings in several other cancer types, where epigenetic changes are important drivers for tumour formation (Wilting and Dannenberg 2012).

Genetic alteration in the tumour suppressor *TP53* occurs in approximately 50% of all human cancers (Hollstein et al. 1994). In ccRCC, mutations in *TP53* have been reported in 2.3-9% of the cases, representing only a minor fraction of tumours. However, when other members of the p53 pathway such as ATM, MDM2 and CDKN2A and MYC are considered as well, 40% of the ccRCC tumours show disturbed p53 signalling, indicating an important function also in the formation of kidney cancers (Albers et al. 2013; Sato et al. 2013).

Another frequent event in ccRCC is the deletion of chromosome 14q, which locates *HIF1a* (Hypoxia inducible transcription factor 1a*)* as well as S*AV1 (Salvador 1)* and *FRMD6 (*FERM domain-containing protein 6), two members of the Hippo pathway. This indicates a putative tumour suppressor activity for these genes (Shen et al. 2011). Moreover, investigations of phosphoinositide 3-kinase (PI3K)-Akt-mTOR signalling pathway show that approximately 27% of ccRCCs exhibit mutations in various members including PTEN, PI3K, Akt, TSC1, TSC2 and mTOR, leading to a constitutive activation of the pathway (Sato et al. 2013; The Cancer Genome Atlas Research 2013). The mTOR (mammalian target of rapamycin) signalling network serves as a global regulator of cell growth and cell proliferation. It senses the cellular energy and nutrient status and subsequently regulates several pro-proliferative processes such as transcription, translation, ribosome biogenesis, autophagy and cellular metabolism (Wullschleger et al. 2006). Constitutively active mTOR signalling is a common feature in various cancers, further supporting the relevance of these mutations in tumourigenesis.

Despite these extensive studies, the interplay of the different genetic alterations and their contribution to tumour initiation and progression are poorly understood. Therefore, another goal of this thesis was to investigate the cooperative effects of the inactivation of *Vhl, Hif1a* and *Trp53,* representing some of the most common mutagenic alterations in ccRCC.

6.3.5 The Von Hippel Lindau protein (pVHL)

As mentioned above, over 90% of ccRCC tumours exhibit loss of function of pVHL, demonstrating an essential role of this protein in tumourigenesis. The VHL locus is encoded on chromosome 3p and gives rise to a long and a short isoform (referred to as $pVHL_{30}$ and $pVHL_{19}$ in humans and $pVHL_{25}$ and $pVHL_{20}$ in mice) that are derived from alternate translational initiation sites (Iliopoulos et al. 1998; Blankenship et al. 1999). Studies in human cell lines show that the long form co-localises predominantly with cytoplasmic microtubules, whereas in mice the short form localises mainly in the nucleus (Hergovich et al. 2003). Nevertheless, both isoforms can function separately as tumour suppressors, since reintroduction of $pVHL_{30}$ as well as of $pVHL_{19}$ in renal cancer cells inhibits tumour development in mouse xenografts (Blankenship et al. 1999). pVHL is a multipurpose adaptor protein involved in various cancer related processes. For instance, pVHL promotes the activity of the tumour suppressor p53 by suppressing the Mdm2-mediated ubiquitination and subsequent degradation of p53. pVHL is also associated with microtubules, inhibits their depolymerisation and regulates the orientation of the mitotic spindle and cellular division planes (Hergovich et al. 2003; Thoma et al. 2009; Hell et al. 2014). Consistently, pVHL is important for the maintenance of the primary cilium, a microtubule-based sensory organelle which is important for renal tubular integrity and suppression of renal epithelial cysts (Thoma et al. 2007). Furthermore, pVHL has been shown to bind to collagen and fibronectin and is therefore associated with the regulation of the extracellular matrix (ECM) (Ohh et al. 1998; Grosfeld et al. 2007). pVHL also inhibits the NF-kB transcription factors, which are involved in the regulation of the immune system and promote cell survival and proliferation (Yang et al. 2007; Hayden and Ghosh 2008). pVHL supresses several cellular processes such as canonical Wnt signalling and cellular senescence (Chitalia et al. 2008; Young et al. 2008; Welford et al. 2010). Senescence is defined as irreversible growth arrest that occurs when cells encounter oncogenic stress and therefore is an important mechanism for preventing the proliferation of potential cancer cells (Rodier and Campisi 2011). Finally, pVHL serves as a recognition subunit of an E3 ubiquitin ligase complex consisting of Elongin B, Elongin C, Cullin 2 and Rbx-1 (VCB complex) (Pause et al. 1997; Lonergan et al. 1998; Lisztwan et al. 1999; Stebbins et al. 1999; Kamura et al. 2000). Under normoxic conditions this complex targets the HIFα transcription factors for oxygen-dependent proteolytic degradation (Maxwell et al. 1999). Under hypoxia, or in ccRCC cells where functional pVHL or Elongin B are missing, the HIFα transcription factors are stabilized and induce the expression of target genes involved in glycolysis, proliferation, angiogenesis and other cellular processes, which have been shown to be important in tumourigenesis (see 6.3.6). The investigation of the role of dysregulation of Hif1α and Hif2α in *Vhl* null cells in the initiation of tumour formation was one of the major goals of this thesis. The pVHL ubiquitin ligase complex

also facilitates the proteosomal degradation of other proteins including certain isoforms of protein kinase C (PCK) and the large subunit of the RNA polymerase II complex (Rbp1) (Okuda et al. 2001; Kuznetsova et al. 2003).

Although loss of pVHL is associated with several potential tumour-promoting pathways it remains unclear which of the distinct functions of pVHL contribute to its tumour suppressor activity. To address this question a broad range of different *Vhl*-deficient mouse models have been developed during the past years. In 1997, Gnarra *et al.* reported that the homozygous germ-line mutation of *Vhl* causes embryonic lethality due to a failure of the vascularization of the placenta (Gnarra et al. 1997). To circumvent this problem, several conditional mouse models have been developed using different segment specific promoters to induce gene deletions in the proximal tubule (Rankin et al. 2006), all nephron segments (Frew et al. 2008a; Schley et al. 2011; Mathia et al. 2013), the thick ascending loop of Henle or in the distal tubules and collecting ducts (Pritchett et al. 2014). Although some models led to fibrosis or mild cyst formation, *Vhl*-deletion in renal epithelium did not cause tumour growth in any of the mouse models.

Together with the notion that only a few *VHL* null cells in VHL patients develop into tumours, these findings clearly show that the loss of pVHL alone is insufficient for the initiation of ccRCC and that additional alterations are necessary for the further transformation of *VHL*-deficient cells into tumour forming cells. Given that animal models for human cancers are an important tool for the development of efficient anti-cancer treatments, the main aim of this thesis was the generation of an autochthonous mouse model for ccRCC focusing on the specific role of *Vhl*, *Hifα* and *Trp53*.

6.3.6 The hypoxia inducible factor α (HIFα) transcription factor family

The hypoxia inducible transcription factor (HIF) family consists of three members: HIF1α, HIF2α and HIF3α. HIF1α and HIF2α (also known as EPAS1) harbour a transcription activating domain, whereas the function of HIF3α is still unclear (Gu et al. 1998; Hara et al. 2001). HIF1α is ubiquitously expressed, while HIF2α is restricted to endothelial cells, lung, kidney, liver and tumours of various tissues (Semenza 2003; Wiesener et al. 2003). Under hypoxic conditions, HIF1α and HIF2α (collectively HIFα) translocate into the nucleus where they dimerize with the stable β subunit HIF1β (also known as ARNT) and interact with the transcriptional co-activator p300/CBP and bind to a consensus hypoxia-responsive element (HRE) to induce the expression of a broad range of target genes (Fig. 6.4) (Banumathy and Cairns 2010). Under normoxic conditions a family of prolyl hydroxylases (PHD1-3) catalyses the hydroxylation of HIFα using molecular oxygen and 2-oxoglutarate as substrates (Schofield and Ratcliffe 2004; Lofstedt et al.

2007). These modifications allow the binding of the VCB complex mediated by direct interaction between the pVHL protein and prolyl hydroxylated residues in HIFα, resulting in the targeting of HIFα for proteasomal degradation (Maxwell et al. 1999; Ohh et al. 2000). Additionally, the factor inhibiting HIF (FIH) hydroxylates HIFα on a specific asparaginyl residue, blocking the interaction of the transcription factor with the p300 co-activator and therefore preventing the induction of gene expression (Mahon et al. 2001). In a variety of tumours the E3 ubiquitin ligase hypoxia associated factor (HAF) mediates the degradation of HIF1α, but not of HIF2α, in an oxygen-dependent but pVHL-independent mechanism. HAF also directly binds to HIF2α, thereby promoting its transactivation activity without causing its degradation (Koh et al. 2008; Koh et al. 2011).

In addition to the regulation of HIFα activity by the availability of oxygen, HIFα expression is influenced by growth factors and diverse pathways that are commonly hyperactivated in human tumours (Bardos and Ashcroft 2004). For instance, activation of PI3K/Akt signalling under normoxia results in increased HIFα levels through upregulation of mTOR-dependent HIFα translation (Zundel et al. 2000). Interestingly, mTOR signalling also regulates the expression of HIFα. Expression of HIF1α depends on the activity of mTORC1 and mTORC2, whereas HIF2α expression is only induced by mTORC2 (Toschi et al. 2008). HIFα phosphorylation by the Ras/Raf/MAPK pathway increases the stability of HIFα, though the molecular mechanism is not yet clear (Bardos and Ashcroft 2004). Furthermore, PHDs can be inhibited by the Krebs cycle intermediates oxaloacetate, succinate and fumarate, connecting HIFα regulation to intracellular metabolism (Sudarshan et al. 2007; Lisy and Peet 2008).

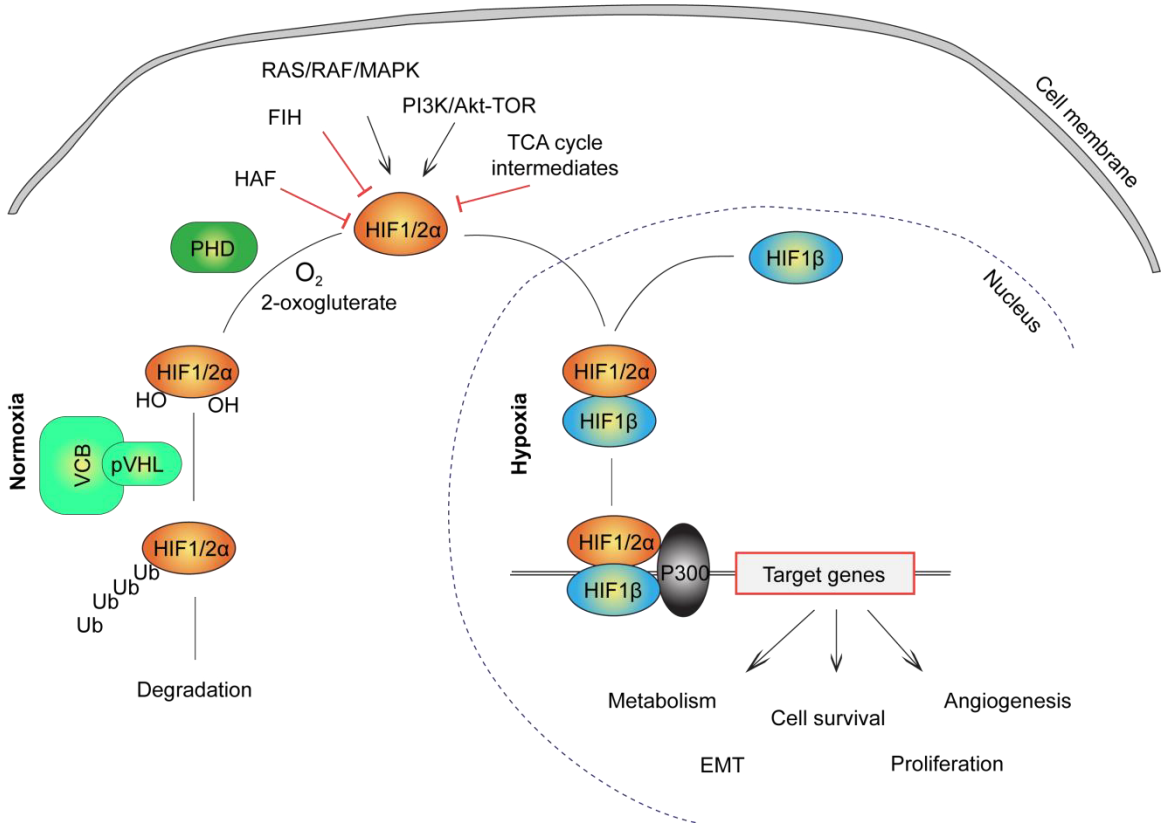

Fig. 6.4: Regulation of HIFα activity. Under normoxic conditions, PHD1-3 hydroxylate HIFα, which is recognized by pVHL, a member of a E3 ubiquitin ligase complex (VCB), and targeted for proteosomal degradation. In hypoxia, PHDs do not hydroxylate HIFα escapes the hydroxylation and shuttles into the nucleus, where it dimerizes with HIFβ and the transcriptional cofactor p300. Subsequently, this complex binds to the hypoxia-responsive element (HRE), leading to the expression of various target genes. Further, HIFα activity is regulated on transcriptional or translational level by several additional pathways

Physiological HIFα stabilization results in the cellular adaption to changed environmental condition by the regulation of the expression of target genes involved in numerous pathways. However, most these processes are also associated with tumour formation, including changes in energy metabolism (e.g. glucose transporter 1 (GLUT1), phosphoglycerate kinase (PKG) and lactose dehydrogenase A (LDHA)), angiogenesis (e.g. vascular endothelial growth factor (VEGF), erythropoiesis (erythropoietin (EPO)), epithelial-to-mesenchymal transition (EMT, cell survival (e.g. transforming growth factor-α (TGF α)) and invasion (eg. MMP) (Gunaratnam et al. 2003; Higgins et al. 2007; Koh et al. 2011). In 2005, over 70 direct HIF target genes had been validated and numerous additional targets have been published since (Wenger et al. 2005). Importantly, cell culture experiments have shown that HIF1α and HIF2α respond differently to environmental cues. Experiments using different cell lines demonstrate that HIF2α accumulates at moderate O_2 concentration (2-5%), whereas Hif1α stabilizes only at lower concentration (0-2% O_2) (Holmquist-Mengelbier et al. 2006). Additionally, the HIF1α response is associated with acute hypoxia, on the other hand HIF2α mediates the cellular adaption to chronic hypoxia (Uchida et al. 2004). These functional differences are reflected by distinct expression profiles of the two isoforms.

Although they share a consensus sequence, HIF1α preferably induces the expression of genes regulating cell metabolism, while HIF2α is associated with the expression of OCT4 and pro-proliferative genes (Gordan et al. 2008; Keith et al. 2012). Furthermore, HIF1α and HIF2α reciprocally regulate each other's protein levels at least in renal cancer cell lines, since suppression of HIF1α enhances the expression of HIF2α and vice versa (Raval et al. 2005). In the following sections, the role of HIFα in the regulation of cellular metabolism and proliferation are discussed in more detail.

6.3.6.1 HIFα in the Warburg effect

Several studies characterize ccRCC as a metabolic disease (Linehan et al. 2010; Hakimi et al. 2013). For instance, mRNA expression and proteomic profiling by the TCGA study demonstrate a global metabolic shift in ccRCC, characterized by the decreased activity of AMPK and the TCA cycle, increased cellular glutamine transport and higher fatty acid production, as well as an increased dependence on the pentose phosphate shunt (The Cancer Genome Atlas Research 2013). HIF1α controls the expression of a large panel of genes involved in cellular metabolism and is associated with the metabolic reprogramming of cancer cells. One important function of HIF1α is the adaptation of cellular metabolism under hypoxic conditions. In the presence of oxygen, quiescent cells mostly metabolize glucose to pyruvate, which then enters the tricarboxylic acid (TCA) cycle and is subsequently oxidized to CO_2 by oxidative phosphorylation in the mitochondria, leading to the production of ATP, NADH (nicotinamide adenine dinucleotide) and NADPH (Fig. 6.5) (Vander Heiden et al. 2009). In this process oxygen is required as final electron acceptor, therefore the cells have to reprogram their metabolism under hypoxia to avoid the production of reactive oxygen species (ROS) (Hamanaka and Chandel 2009). When oxygen is limited, HIF1α induces the transcription of a set of genes that cooperatively mediate the so-called "metabolic switch". Elevated gene expression of the cellular glucose transporter 1 (Glut1) and several glycolytic genes (including hexokinases 1 and 2 (HK1/2), phosphofructokinases L (PFKL), aldolase A (ALDA), phosphoglycerate kinase (PGK) and enolase 1 (ENO1) and Pyruvate kinase M2 (PKM2)) accelerates glycolytic flux and enables the increased production of ATP (Semenza et al. 1994; Luo et al. 2011). Furthermore, the HIF1α target PDK1 (pyruvate dehydrogenase) inhibits the enzyme PDH (pyruvate dehydrogenase), which converts pyruvate to acetyl-CoA (Kim et al. 2006). In concert with LDHA (lactate dehydrogenase) PDK1 causes the preferential conversion of pyruvate to lactate, thereby diminishing energy production by oxidative phosphorylation and favouring aerobic glycolysis (Kim et al. 2006). Since these changes result in elevated lactate levels and lactate secretion, the cell increases HIF1α dependent expression of NHE 1 (sodium-hydrogen exchanger 1), MCT-4 (monocarboxylate transporter 4) and CA9 (carbonic anhydrase 9) to maintain the alkaline intracellular pH and the acidic extracellular pH (Fang et al. 2008; Kroemer

and Pouyssegur 2008). Additionally, HIF1α modifies the abundance of mitochondrial proteins, resulting in impaired mitochondrial activity and decreased ROS production. On one hand, HIF1α regulates the composition of the cytochrome c oxidase (COX, electron transport complex IV) by the induction of COX4-2 and LON synthesis. COX4-2 replaces COX4-1 at complex IV, facilitating a more efficient mitochondrial respiration without ROS production. LON functions as a mitochondrial protease and is required for the degradation of COX4-1 (Fukuda et al. 2007). Moreover, the expression of the Complex 1 inhibitor NDUFA4L2 (NADH dehydrogenase [ubiquinone] 1 alpha subcomplex, 4-like 2) is also regulated by HIF1α, thereby attenuating mitochondrial activity (Tello et al. 2011). On the other hand, *Hif1α*-dependent BNIP3 expression selectively triggers the autophagy of mitochondria (Zhang et al. 2008). Finally, HIF1α further reduces mitochondrial abundance by blocking the activity of the transcriptional coactivator PGC-1β by the repression of MYC activity via MXI-1 (see 6.3.6.2) (Liang and Ward 2006; Zhang et al. 2007b)

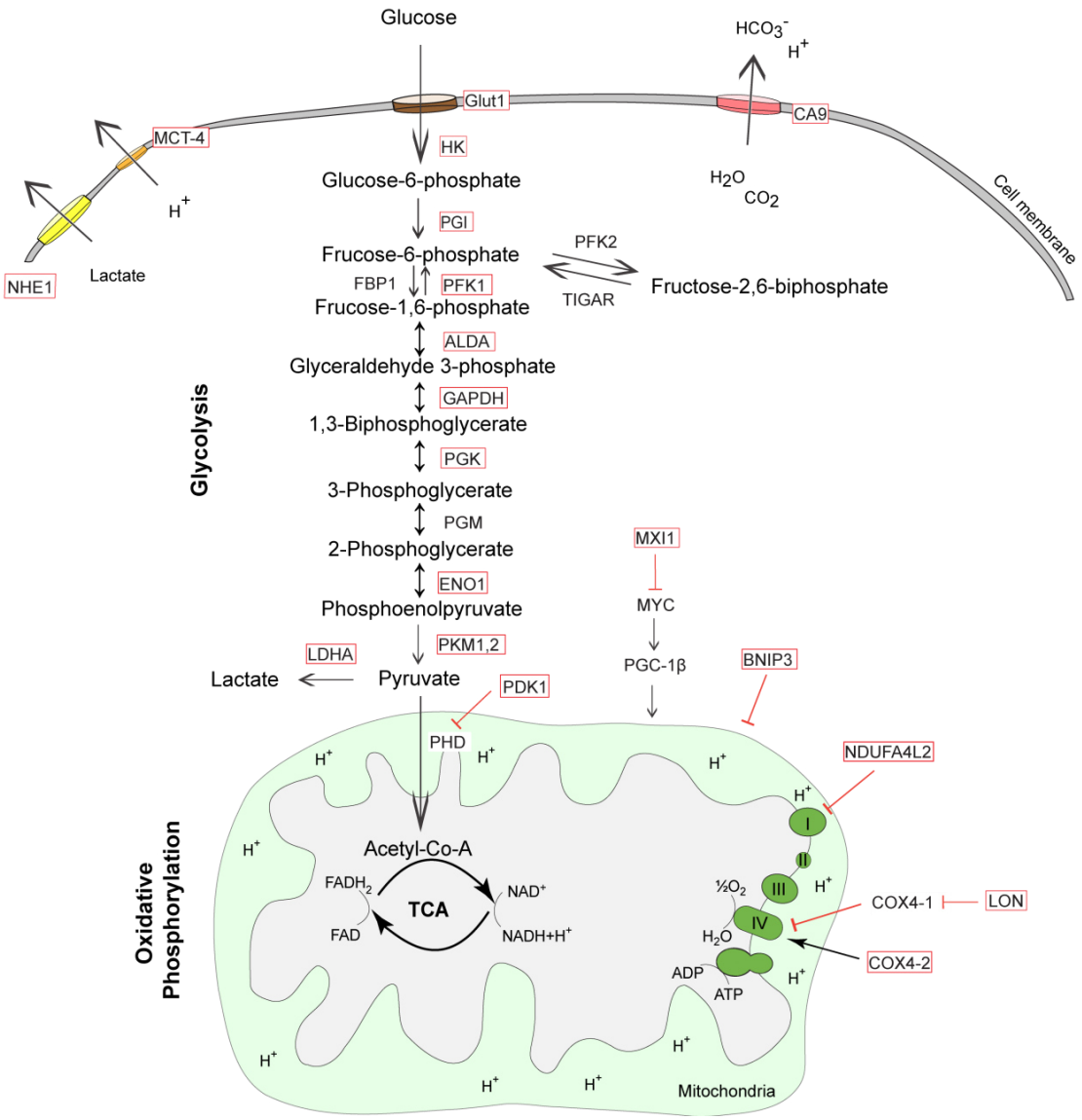

Fig. 6.5: Induction of the metabolic switch by HIFα. Activation of HIFα leads to an increased glycolytic flux by the elevated expression of glycolytic enzymes. Furthermore, mitochondrial activity is decreased by preventing the entry of pyruvate in the TCA cycle and simultaneous inhibition of specific complexes of the respiratory chain. The increased expression of acid and lactate transporters ensures the maintenance of cellular pH levels. HIF1α target genes are highlighted in red.

Anaerobic glycolysis does not only serve as a protective mechanism for differentiated cells under hypoxic condition. Also proliferating cells metabolize 85% of their pyruvate to lactate under normoxia. Although aerobic glycolysis is less efficient than oxidative phosphorylation in terms of ATP production per glucose-derived carbon, proliferating cells benefit from the increased availability of intermediates for the production of nucleotides, amino acids and lipids that are required for further proliferation (Lehninger et al. 1993; Vander Heiden et al. 2009). Consistently, the metabolic reprogramming from oxidative phosphorylation to glycolysis is a common feature of cancer cells even in the presence of sufficient oxygen. This phenomenon is widely known as anaerobic glycolysis or Warburg effect and represents one of the hallmarks of cancer (Hanahan

and Weinberg 2000). Already in 1942 Otto Warburg observed a fundamental difference in the metabolism of cancer cells compared to normal tissues. He found that unlike most normal tissues cancer cells tend to metabolize glucose into lactate even in the presence of sufficient oxygen, indicating a shift from oxidative phosphorylation to glycolysis (Warburg, 1956). Since the function of mitochondria is not impaired in most cancer cells, these changes in cell metabolism enable the cell to employ aerobic glycolysis and oxidative phosphorylation to maximize the availability of energy (ATP), reducing equivalents (NADH, NADPH) and macromolecules for biogenesis (Vander Heiden et al. 2009).

A big body of data based on tumour biopsies and cancer cells lines document a HIFα-dependent metabolic reprogramming in ccRCC (Papandreou et al. 2006; Zhang et al. 2007a; Langbein et al. 2008; Luo et al. 2011; The Cancer Genome Atlas Research 2013; Li et al. 2014). Consistently, a very recent study of 200 ccRCCs revealed the depletion of the fructose-1,6bisphosphatase 1 (FBP1) in almost 100% of ccRCC tumours examined, leading to increased glycolytic flux and promotion of HIFα activity (Li et al. 2014), further arguing that there is a selection for enhanced glycolysis during the formation of ccRCC. However, the importance of these metabolic changes in tumour initiation remains unclear, since they could be a requirement for or a consequence of disease progression. Using the genetically engineered mouse models escribed above, we aimed to understand the impact of *Hif1α*-dependent metabolic alterations in regulating cellular behaviour and proliferation *in culture* and their consequences *in vivo*.

6.3.6.2 HIFα in cell proliferation

Although HIF1α and HIF2α bind to the same consensus sequence on common target genes, an increasing amount of data indicates that they have opposing effects on cell proliferation: Hif2α promotes while Hif1α rather restrains proliferation. Tissue microarrays show that ccRCC expressing only HIF2α, but not HIF1α, are significantly larger in volume and display a stronger staining for the proliferation marker Ki67 when compared to tumours expressing both HIFα isoforms. Furthermore, HIF2α stabilization is associated with more advanced disease as HIF1α expression gradually decreases whereas HIF2α protein becomes more abundant during ccRCC progression (Mandriota et al. 2002). Consistently, loss of chromosome 14q which harbours the *HIF1α* allele is a frequent event ccRCC associated with poor disease outcome (Shen et al. 2011). Xenograft studies showed that silencing of HIF2α in RCC increases growth rates compared to control tumours, whereas HIF1α decelerates cell growth (Biswas et al. 2010). Moreover, silencing of HIF2α in pVHL-deficient RCC cells is sufficient to suppress tumour formation (Kondo et al. 2002; Kondo et al. 2003). Intriguingly, most ccRCC cell lines exhibit a biallelic inactivation of *HIF1α* and reintroduction of Hif1α impairs proliferation *in vitro*. Consistently, downregulation of HIF1α in

RCC4 cells, a ccRCC cell line expression both HIFα isoforms, promotes cell proliferation *in vitro* and *in vivo,* as shown by the implantation of cells in the kidney of nude mice (Shen et al. 2011).

The different effects of HIF1α and HIF2α on proliferation may at least partly be explained by the opposing effects of HIFα isoforms on the activity of the transcription factor MYC. Several studies have shown that HIF1α antagonizes MYC-dependent gene expression, while HIF2α promotes MYC activity by several mechanisms. HIF2α enhances MYC activity by the stabilisation of the binding between MYC and its cofactor MAX, thereby augmenting the expression of genes involved in cell cycle progression such as cyclin D1 and D2 and inhibiting the synthesis of the cell cycle inhibitors p21 and p27 (Mack et al. 2005; Gordan et al. 2007). In contrast, HIF1α antagonizes MYC activity either by the direct binding to MYC itself or by the competitive binding to MAX and SP1, which is another MYC cofactor (Koshiji and Huang 2004; Koshiji et al. 2004). Moreover, HIF1α stabilization promotes the proteasomal degradation of MYC and elevates the transcription of MX1-1, a MYC inhibitor (Zhang et al. 2007a). Concordantly, amplification of MYC on chromosome 5c is another frequent event in ccRCC (Shen et al. 2011). While tumours expressing only HIF2α tend to display high levels of MYC expression and activation of MYC target genes, VHL wild type and HIF1α/HIF2α expressing ccRCC show increased activity of MAP kinases and TOR signalling pathways (Gordan et al. 2008).

Taken together, these data suggest that a shift in the balance between HIF1α and HIF2α is a critical step in ccRCC formation and raise the hypothesis that the loss of HIF1α activity in *VHL*-deficient cells represents an oncogenic event (Gordan et al. 2008). However, most of these studies were performed in transformed cancer cell lines and it remains unclear whether the opposing effects of HIF1α and HIF2α also play a role in the initial steps of ccRCC formation. Therefore, we aimed to dissect the different roles of HIFα isoforms on proliferation and transformation capacity *in vivo.*

6.3.7 The tumour suppressor gene *Trp53*

The transcription factor p53, encoded by the *TP53* gene (*Trp53* in mice), is mutated in 50% of all human cancers and controls various cancer-related processes as a tumour suppressor (Hollstein et al. 1994). The main regulator of p53 activity is the proto-oncogene Mdm2 (murine double minute 2), which acts as an E3 ubiquitin ligase, targeting p53 for degradation (Freedman and Levine 1999). Additionally, Mdm2 binds to p53 and prevents its transcriptional activity by interfering with the transcriptional machinery (Kubbutat et al. 1997; Thut et al. 1997). Intriguingly, Mdm2 itself is a transcriptional target of p53, enabling a fine-tuned balance between both proteins (Wu et al. 1993). Stress stimuli such as DNA damage, hypoxia, oncogene activation

or nutrient deprivation disturb the balance between Mdm2 and p53 and therefore activate a broad range of downstream processes including cell cycle arrest, apoptosis and genome stability. All these pathways are major mechanisms for tumour suppression, explaining the importance of p53 in tissue integrity. pVHL and hypoxia activate p53 signalling on several levels. For example, pVHL associates with p53 and thereby prevents the Mdm2-mediated ubiquitination and nuclear export of p53 (Roe et al. 2006). Further, studies in RCC cell lines demonstrated that inhibition of HIF2α promotes p53-dependent cell death and, in contrast to HIF1α, enhances the response to radiotherapy, again underlying the pro-tumourigenic activity of HIF2α (Bertout et al. 2009) (Roberts et al. 2009). One example for p53 downstream signalling is the regulation of cell cycle progression: DNA damage causes the p53-dependent expression of the cell cycle inhibitor p21 (coded by *Cdkn1a*), which facilitates the accumulation of pRb and induces cell cycle arrest. If DNA repair is successful, p53 levels drop, allowing the entry into S-Phase. If not, p53 triggers apoptosis to prevent the establishment of oncogenic mutations (Sebastian et al. 2010). Similarly, the activation of oncogenes including RAS and MYC cause p53-dependent senescence or apoptosis (Sebastian et al. 2010). Recent findings also suggest a role of p53 in the regulation of cellular metabolism. Depending on oxygen and nutrient availability p53 modulates the expression of numerous of genes involved in glycolysis, oxidative phosphorylation, mitochondrial integrity, autophagy, mTOR signalling and other metabolic pathways (Jiang et al. 2011; Maddocks and Vousden 2011). Together, these changes promote the use of catabolic pathways to maintain energy production in periods of limited nutrients to ensure cell survival.

Loss of p53 signalling activity or other cell cycle regulators disables the most important cellular self-protection mechanisms and facilitates the formation of cancers. To identify whether mutations in cell cycle regulators might represent another oncogenic event in the formation of ccRCC, we screened for pro-proliferative combinations in *Vhl* and *Vhl/Hif1α* negative primary kidney cells using a lentiviral based shRNA library targeting cell cycle regulators.

6.3.8 Aim

The goal of this thesis was to gain a better understanding of the initial events in the formation of ccRCC. ccRCC accounts for approximately 2.5 % of all adult malignancies and cannot be cured once it spreads beyond the kidney (Jonasch et al. 2012). Despite extensive research, the generation of suitable animal models has failed so far, indicating an insufficient knowledge about the molecular mechanism of the disease. Nevertheless, it has become clear over the last years that loss of function of the tumour suppressor pVHL is necessary but not sufficient to drive tumourigenesis in the renal epithelium. Furthermore, genetic profiling of human biopsies show that a high number of ccRCC tumours harbour a deletion of *HIF1A*, presumably promoting the

transformation of cancer cells (Monzon et al. 2011). We developed several mouse models harbouring specific deletions of *Vhl*, *Hif1α* or *Hif2α* and *Trp53* either together or alone to investigate their cooperative effect in tumour initiation and progression *in vivo.* One of my main goals was to analyse the effects of the specific gene deletions in *Vhl/Hif1α* and *Vhl/Hif1α/Trp53* deficient mice. Primary cells from these mice also allowed us to further dissect the roles of Hif1α and Hif2α in the early stages of tumour formation, focusing on their effect on cell metabolism and cell transformation capacity. Moreover, we investigated whether the inactivation of specific cell cycle regulatory proteins, especially the deletion of the tumour suppressor *Trp53* further transforms *Vhl* and *Vhl/Hif1α* negative cells, potentially representing another oncogenic event during cancer evolution.

6.4 Hydronephrosis

6.4.1 Prevalence and management of hydronephrosis

Hydronephrosis is defined as an increase in the diameter of one or more components of the renal collecting duct (Thom and Rosenblum 2013). Antenatal ultrasound screening at 18-20 weeks gestation revealed congenital abnormalities in 1-2% of all pregnancies, whereas congenital hydronephrosis is with an overall prevalence of approximately 0.6% the most frequently detected abnormality (Livera et al. 1989; Dudley et al. 1997). In fifty percent of the patients both kidneys were affected (Dudley et al. 1997). Most cases of prenatally diagnosed hydronephrosis stabilize or even resolve spontaneously after birth or within the first two years of life (Woodward and Frank 2002). However, 10 – 25% of the cases show persistent severe dilatation and require medical or surgical intervention to prevent kidney insufficiency. Therefore, the decision for therapy is critical and the need for better treatment guidelines has been recently reported (Braga et al. 2014). In general, the likelihood of a patient for having significant postnatal abnormalities is proportional to the severity of the antenatally detected hydronephrosis (ANH) (Grignon et al. 1986). In very rare cases hydronephrosis progresses significantly during pregnancy, requiring prenatal intervention to prevent further renal dysplasia (Yamacake and Nguyen 2013). In most cases conservative management of hydronephrosis is conducted, including antibiotic therapy to prevent urinary tract infections and regular ultrasound scans. However, progressive hydronephrosis, decreasing renal function and recurrent infection are clear indications for surgical intervention. Untreated hydronephrosis – or more precisely lack of treatment of the underlying etiology – leads to proteinuria, degeneration of nephrons, glomerulosclerosis and tubular atrophy, which eventually leads to chronic kidney insufficiency and end stage renal disease (Bailey et al. 1994; Rasouly and Lu 2013). Nevertheless, surgery for hydronephrosis

especially in neonates is technically challenging, leading to a high risk of complications and should therefore be considered carefully (Peters et al. 1989). Thanks to improved conservative management of urological conditions over the years only about 5% of patients with ANH will ultimately require surgery (Woodward and Frank 2002).

In the literature, hydronephrosis is divided in an obstructive or a non-obstructive form. The most commonly used diagnostic tool to asses for obstruction is the diuretic renography using Mercaptoacetyltriglycine (Tc99m-MAG3) as radiolabelled agent (Hashim and Woodhouse 2012), where delayed MAG3 clearance is used as an indicator for obstruction (Kathel 1971). Although several disorders have been associated with the formation of congenital or acquired hydronephrosis, the underlying etiologies are often not fully understood and further research is required. We recently reported that specific deletion of the tumour suppressor *Vhl* in renal epithelial cells causes hydronephrosis in mice, however, the underlying mechanism remained unclear (Frew et al. 2008b). In the second part of this thesis, we aimed to identify these mechanisms by the investigation of possible molecular or obstructive causes. In the following sections, we present a review of the current literature on obstructive and non-obstructive hydronephrosis.

6.4.2 Obstructive hydronephrosis

6.4.2.1 Description

Congenital anormalities of the ureter often cause impaired urine transport from the kidney to the bladder, causing urinary obstruction (blockage of urine transport by functional or physical obstruction) or vesicoureteral reflux (VUR) – the abnormal, retrograde flow of urine from bladder to the upper urinary tract (Gargollo and Diamond 2007). Both events increase the pressure in the ureter and renal pelvis eventually causing hydronephrosis and hydroureter, the dilation of the ureter (Rasouly and Lu 2013). Ureteropelvic junction obstruction (UJP) is the most common cause for marked hydronephrosis (renal pelvic diameter (RPD) > 10 mm), diagnosed in 10-30% of the cases (Podevin et al. 1996; Yamacake and Nguyen 2013). UJP is generally thought to be due to an abnormal development of the ureter just at the ureterojunction or proximal ureter (Peters 1995). In contrast, VUR is the most likely diagnosis in mild hydronephrosis (RPD = 5-9 mm) with a prevalence of 10-40% (Podevin et al. 1996; Yamacake and Nguyen 2013). Other causes of congenital hydronephrosis such as the obstruction of urterovesical junction (UVJ) (5-15%), multicystic dysplastic kidney (2-5%), posterior urethral valves (1-5%) and ureterocele (1-3%) are much less common (Yamacake and Nguyen 2013).

Mechanical obstructions caused by kidney stones, pregnancy or by tumours such as pelvic neuroblastoma can lead to hydronephrosis (Au et al. 1985; Woo et al. 2013). Interestingly, hydronephrosis can be observed in around 80% of all pregnancies, mostly caused by the mechanical compression of the ureter (Cheung and Lafayette 2013) (Au et al. 1985). Furthermore, hydronephrosis caused by obstructions due to impaired neuronal control of the upper urinary tract are a well-known complication of patients with spinal cord injury (Tsai et al. 2001; Vaidyanathan et al. 2009; Lai et al. 2014).

The generation of non-genetic mouse models have enabled to study the effect of fetal obstructions of the urinary system, such as surgical induction of obstructions in guinea pigs (Chevalier and Kaiser 1984) or in fetal sheep. The latter is the most widely used model as the sheep kidney resembles the human kidney in terms of gestation time and pattern of renal development. These studies have shown that the surgical induction of partial or complete ureteral obstruction at different time points of gestation have profound effects on kidney function, such as decreased creatinine clearance and glomerular filtration rate, increased fractional excretion of sodium, and formation of hydronephrosis (Glick et al. 1983). Additionally, increased blastemal apoptosis leading to the formation of hydronephrosis was observed in a model of urinary bladder outflow obstruction. (Samnakay et al. 2006).

6.4.2.2 Molecular mechanisms

The genetic mechanisms causing obstructive uropathy are largely undefined. The generation of different mouse models and the investigation of human disorders have associated various pathways with urinary tract development including Wnt signalling (Yu et al. 2002; Trowe et al. 2012), TGF-β signalling (Miyazaki et al. 2000; Tripathi et al. 2012), Receptor tyrosine kinases (RTK) and the Hedgehog signalling pathway (Caubit et al. 2008). Mutations in genes involved in these pathways potentially lead to malformations of the kidney, ureter or bladder (Rasouly and Lu 2013), possibly resulting in obstructive or non-obstructive hydronephrosis. One example of a human disorder characterized by developmental abnormalities such as urethral obstruction and mesodermal developmental defects is the Prune-Belly Syndrome (PBS) (Manivel et al. 1989). Antenatal sonography of children with this syndrome revealed bilateral hydroureter and hydronephrosis, thin-walled bladder and a deficiency in amniotic fluid due to impaired kidney function (Woods and Brandon 2007; Chen et al. 2010). Although mutations in *HNF1B* (hepatocyte nuclear factor 1B) and *CHRM3* (muscarinic cholineric receptor 3) have recently been associated with cases of familial PBS, the molecular mechanisms of the syndrome are widely unknown (Haeri et al. 2010; Hassett et al. 2012) (Weber et al. 2011). Moreover, defects in the ureteric budding, ureter differentiation and elongation, peristalsis, UVJ formation and bladder development have

been associated with vesicoureteral reflux (VUR), all being possible causes for obstructive hydronephrosis. Recently, mutations in several genes such as *PAX2*, *Sox17* and *Ret* have been connected to the development of VUR (Rasouly and Lu 2013).

6.4.3 Non-obstructive hydronephrosis

6.4.3.1 Description

Hydronephrosis can also occur without clinically significant obstruction and some studies report that the majority of cases are non-obstructive in nature (Woodward and Frank 2002; Thom and Rosenblum 2013). Excess urine production due to diverse underlying disorders can cause a back pressure on the kidney, leading to expansion of the renal pelvis and the collecting system. For instance, prolonged polyuria has been described as cause of bilateral non-obstructive hydronephrosis in cases of nephropathic diabetes insipidus (NDI), neurogenic diabetes insipidus, psychogenic polydipsia and the Batter's syndrome (see below) (Wheeler and Hanchey 1971; Harrison et al. 1979; Uribarri and Kaskas 1993). Furthermore, renal urine overload might also be the cause of some cases of antenatally diagnosed hydronephrosis. Fetal urine production is four to six times higher than after birth, possibly causing transient or persistent dilation of the renal pelvis (Walsh PC 2002; Thom and Rosenblum 2013). Finally, studies on rare human disorders such as the Pallistor-Hall Syndrome (PHS) revealed that congenital malformation of structures supporting the urinary tract can lead to non-obstructive hydronephrosis (Chang et al., 2004).

6.4.3.2 Molecular mechanisms

NDI is characterized by an impaired renal response to arginine vasopressin (AVP) stimulation and subsequent failure to regulate renal water reabsorption (Fujiwara, Morgan et al. 1995). In contrast, neurogenic diabetes insipidus is caused by an impaired production of vasopressin (AVP) in the brain (Di Iorgi et al. 2012). Genetic studies demonstrated that NDI is caused by mutations in the V2 type vasopressin receptor or in Aquaporin 2 (AQP2), an AVP-sensitive water channel (Pan et al. 1992; Moon et al. 2009). This notion is also supported by the generation of several mouse models with mutations in AQP2 or the Vasopressin receptor. Interestingly, hydronephrosis occurs only in a small subset of patients , whereas it is a common feature in mouse models for NDI (van Lieburg et al. 1999; Yun et al. 2000; McDill et al. 2006; Jin et al. 2009).

Furthermore, decreased expression of AQP1, 2, 3 and 4 were observed in children with congenital hydronephrosis as well as in a spontaneous mutation model for hydronephrosis in mice (Ampawong et al. 2012). Although the degree of hydronephrosis correlates with the grade of AQP downregulation in humans, in both studies it remains unclear whether altered AQP expression is the cause for or a consequence of hydronephrosis. This question becomes relevant in the light of

a study of Li et al. in rats, where the authors surgically induced a bilateral ureteral obstruction (BUO) for 24h. Subsequent analysis of animals revealed the down regulation of AQP1, 2 and 3, which persisted up to 30 days after release of BUO. Moreover, these features correlated with polyuria and impaired urine concentration (Li et al. 2001).

The Bartter syndrome is a group of rare autosomal-recessive disorders that are characterized by the severe reduction or lack of salt absorption by the thick ascending limb of Henle (TAL). Patients suffer from polyuria, renal salt wasting, hypokalemic metabolic alkalosis and elevated renin and aldosterone levels (Hebert 2003). So far, mutations in five genes have been identified in patients that lead to the classification of type I-IV Bartter syndrome. Three genes encode ion transporters (Type I-III): *SLC12A* (sodium-potassium chloride co-transporter NKCC2), *KCNJ1* (renal outer medulla potassium channel, ROMK) and *Clcnk* (Cloride channel-K b, ClC-Kb). The other two genes identified are responsible for the regulation of TAL ion transporters (*BSND* and *CaSR,* type IV and V*)*. Interestingly, patients with Type IV disease also suffer from sensorineuronal deafness since Barttin, the gene product of *BSND,* is required for the function of ClC-K channels in the inner ear (Jeck et al. 2001). Inactivation of NKCC2 and ROMK in the TAL enabled the generation of mouse models of Bartter's syndrome (Takahashi et al. 2000; Wagner et al. 2008; Yan et al. 2008). Whereas hydronephrosis is only occasionally observed in Batter's patients, these mouse models exhibit a severe phenotype. Since the grade of polyuria correlates with the grade of hydronephrosis, the authors speculated that the back pressure produced by excess urine volume causes the hydronephrosis (Takahashi et al. 2000). Interspecies differences might be explained by differences in kidney structure or maturity after birth.

As mentioned above, developmental malformation can also cause non-obstructive hydronephrosis. For example, Cain et al discovered a critical role of the Hedgehog signalling pathway in urogenital tract morphogenesis and function in a mouse model for the Pallister-Hall syndrome (PHS) (Cain et al. 2011). PHS, a rare disorder characterized by abnormalities of the kidney and other organs, is caused by mutations in the transcriptional repressor GLI3, a member of the Hedgehog pathway (Narumi et al. 2010). In mice, pathway inactivation by the deletion of Smoothened (Smo) in the renal pelvic and the upper ureteric mesenchyme resulted in non-obstructive hydronephrosis and hydroureter, probably due to impaired unidirectional ureter peristalsis (Cain et al. 2011).

6.4.4 Aim

We recently reported that specific deletion of the tumour suppressor *Vhl* in renal epithelial cells causes hydronephrosis in mice, however, the underlying mechanism remained unclear (Frew et

al. 2008b). *Vhl* is a multipurpose protein involved in several pathways that are associated with the formation of hydronephrosis (see 6.3.5 for detailed discussion of pVhl function). For instance, numerous studies report interactions between *Vhl* activity and Wnt-β-catenin signalling presumably in a cell-specific manner, although the precise mechanism remains unclear (Berndt et al. 2009). For instance, *Vhl* decreases Wnt signalling by promoting the stabilization of Jade-1, an ubiquitinase responsible for the degradation of β-catenin (Zhou et al. 2004; Chitalia et al. 2008). In contrast, Hif1α hampers the activation of β-catenin whereas Hif2a stimulates Wnt signalling (Lim et al. 2008; Choi et al. 2010). Furthermore, a recent study has shown that *Vhl* inhibits Hedgehog signalling by the direct interaction with Gli 1 (Cho et al. 2013). Finally, Abreu-Rodriguez at al. showed that hypoxic stabilization of Hif1α increased Aqp1 expression in mouse hemangioendothelioma endothelial (EOMA) cells. This finding is supported by elevated Aqp1 levels in brain and lung of mice exposed to hypoxia (Abreu-Rodriguez et al. 2011). Interestingly, decreased AQP1 abundance has also been described as a positive prognostic marker in ccRCC (Huang et al. 2009). A recent study directly links *Hif1a* with bladder outlet obstruction in rats. Six weeks after surgical creation of obstruction, increased Hifα abundance and expression of glycolytic enzymes were measured in the bladder. However no hydronephrosis was reported. The authors hypothesize that a switch to anaerobic glycolysis ensures maintained contractility and thereby upholds a normal micturition cycle (Ekman et al. 2014).

In the second part of this thesis, we aim to understand the underlying mechanism of hydronephrosis in *Vhl* deficient mice. Hydronephrosis is a common complication in several human diseases and causes chronic kidney insufficiency and end stage renal disease when not or only insufficiently treated (Bailey et al. 1994; Rasouly and Lu 2013). Although several urinary tract malformations or genetic mutations have been associated with the formation of hydronephrosis, many questions remain unclear. For instance, little is known about the contribution of these malformations to chronic kidney disease and renal failure (Rasouly and Lu 2013). In this context, our mouse model is of special interest, since the mice display a normal life span and even aged kidneys show an intact morphology – except of the expanded renal pelvis. We therefore investigated possible molecular and obstructive causes potentially leading to hydronephrosis and its effect on kidney function.

7 Materials and Methods

7.1 Materials

7.1.1 General Chemicals

Reagent	Supplier
30% Acrylamide/Bisacrylamide Solution	Bio-Rad
4',6-Diamidino-2-phenylindole dihydrochloride (DAPI)	Sigma-Aldrich
Acetic acid (glacial)	Merck
Acetone	Sigma-Aldrich
Agar	Sigma-Aldrich
Agarose, D1 low EEO	Conda
Agarose, low melting point	Sigma-Aldrich
Albumin from bovine serum	Sigma-Aldrich
Ammonium carbonate	Sigma-Aldrich
Ammonium chloride	Fluka
Boric acid	Sigma-Aldrich
Bovine serum albumin (BSA)	Invitrogen
Bromophenol blue	Sigma-Aldrich
Citric acid monohydrate	Sigma-Aldrich
Crystal violet	Sigma-Aldrich
CSA detection kit	Dako
Dimethylsulfoxide (DMSO)	Sigma-Aldrich
di-sodium hydrogen orthophosphate (Na_2HPO_4)	Sigma-Aldrich
Dithiothreitol (DTT)	Sigma-Aldrich
Entellan	Merck
Eosin 1% (aqueous)	BioSystems
Ethanol	AUL
Ethidium bromide	Sigma-Aldrich
Ethylenediamine tetra-acetic acid (EDTA) disodium salt dihydrate	Sigma-Aldrich
Formalin 10%, neutral buffered	Sigma-Aldrich
Glycerol	Sigma-Aldrich
Haematoxylin (Mayer's)	J.T.Baker
Hydrochloric acid, 32%	Sigma-Aldrich
Hydrogen peroxide	Sigma-Aldrich
Isopropanol	AUL
Lactate assay Kit II	Biovision
Magnesium chloride	Sigma-Aldrich
Magnesium sulfate	Sigma-Aldrich
Methanol	AUL
Mineral oil	Sigma-Aldrich
Mowiol	Sigma-Aldrich
N,N,N',N'-Tetramethylethylenediamine (TEMED)	Bio-Rad
N-2-Hydroxyethylpiperazine-N'-2-ethanesulfonic acid (HEPES)	Sigma-Aldrich
NP-40	Sigma-Aldrich
NucleoBond Xtra Midi	Macherey-Nagel
NucleoSpin RNA kit	Macherey-Nagel
Paraformaldehyde	Sigma-Aldrich

Reagent	Supplier
p-coumaric acid	Sigma-Aldrich
Phenyl-methyl-sulphonyl-fluoride (PMSF)	Sigma-Aldrich
Potassium acetate	
Potassium chloride	Sigma-Aldrich
Propidium iodide (PI)	Sigma-Aldrich
Protease inhibitor cocktail	Sigma-Aldrich
Protein assay Dye Reagent	Bio-Rad
Safflower oil	Migros
Sodium acetate	Sigma-Aldrich
Sodium azide	Sigma-Aldrich
Sodium chloride	Sigma-Aldrich
Sodium deoxycholate	Sigma-Aldrich
Sodium dihydrogen orthophosphate (NaH_2PO_4)	Sigma-Aldrich
Sodium Dodecyl Sulfate (SDS)	Sigma-Aldrich
Sodium hydroxide	Sigma-Aldrich
Sulforhodamine B sodium salt (SRB)	Sigma-Aldrich
SYBR FAST Universal 2X qPCR Master Mix	KapaBiosystems
SYBR Green JumpStart Taq ReadyMix	Sigma-Aldrich
Trichloroacetic acid	Sigma-Aldrich
Tris(hydroxymethyl)aminomethane (Tris base)	Sigma-Aldrich
Tris(hydroxymethyl)aminomethane hydrochloride (Tris HCl)	Sigma-Aldrich
Tri-Sodium citrate	Sigma-Aldrich
Triton X-100	Sigma-Aldrich
Tween-20	Sigma-Aldrich
Visipaque 270	GE Healthcare
Xylene	Thommen-Furler AG

7.1.2 Drugs & tissue culture reagents

Reagent	Supplier
2–Mercaptoethanol	Bio-Rad
2´,7´-dichlorodihydrofluorescein diacetate	Invitrogen
3,3,5 Triiodothyronine (T3)	Sigma-Aldrich
5-Bromo-2'-deoxyuridine (BrdU)	Sigma-Aldrich
Acridine Orange 10-nonyl bromide	Sigma-Aldrich
Ampicillin	Sigma-Aldrich
Apo-Transferrin (TF), human	Sigma-Aldrich
Calcium chloride	Sigma-Aldrich
Collagenase Type II	Gibco
Cycloheximid	Sigma-Aldrich
D-glucose	Sigma-Aldrich
DMEM without L-methionine, L-cystine	Sigma-Aldrich
DMEM/F12	Sigma-Aldrich
Dulbecco’s Modified Eagle Medium (DMEM)	Sigma-Aldrich

Reagent	Supplier
Epidermal Growth factor (EGF), murine	PeproTech
Fetal Calf Serum (FCS)	Biochrome AG
G418 (geneticin)	Sigma-Aldrich
HBSS	Gibco
Hepatocyte Growth factor (HGF)	PeproTech
HEPES 1M	Sigma-Aldrich
Hydrocortisone (HC)	Sigma-Aldrich
Insulin, human	Sigma-Aldrich
Kanamycin	Sigma-Aldrich
L-Glutamine	Sigma-Aldrich
Matrigel (growth factor reduced)	Corning
Met-[S35]-label (SCIS-103)	Hartmann Analytics
Penicillin/Streptomycin	PAA
Phosphate Buffered Saline (PBS)	Biochrome Ag
Polybrene (Hexadimethrine Bromide)	Sigma-Aldrich
Prostagladin E1 (PGE1)	Sigma-Aldrich
Puromycin	InvivoGen
Sodium bicarbonate	Sigma-Aldrich
Sodium Selenite (SS)	Sigma-Aldrich
Tamoxifen	Sigma-Aldrich
Trypsin EDTA	Gibco
Trypsin inhibitor, soybean	Gibco

7.1.3 Kits

Name	$upplier
ABC Kit (PK6100)	Vectorstain
Avidin/Biotin Blocking Kit (SP 2001)	VectorLaboratories
CellTiter-Glo Luminescent Cell Viability Assay	Promega
DAB Substrate Kit (SK-4100)	VectorLaboratories
GenElute Mammalian Genomic DNA Miniprep Kit	Sigma-Aldrich
Glucose assay Kit II	Biovision
Lactate assay Kit II	Biovision
NucleoBond Xtra Midi	Macherey-Nagel
NucleoSpin RNA kit	Macherey-Nagel
Ready-To-Go You-Prime First-Strand Beads	GE Healthcare

7.1.4 Antibodies

Name	Vendor	Order number	Source	Dilution	Application
AE1	Gift from Wagner Lab	-	Rabbit	1:250	IF
Alexa-488 Anti-mouse	Life technologies	A11029	Goat	1:1000	IF
Alexa-488 Anti-rabbit	Life technologies	A11008	Goat	1:1000	IF
Alexa-488 Anti-rat	Life technologies	A11006	Goat	1:1000	IF
Alexa-568 Anti-mouse	Life technologies	A11031	Goat	1:1000	IF
Alexa-568 Anti-rabbit	Life technologies	A11036	Goat	1:1000	IF
Alexa-568 Anti-rat	Life technologies	A11077	Goat	1:1000	IF
AMPKα (F6)	Cell Signaling Technologies	2793	mouse	1:1000	WB
Aquaporin 2	Gift from Loffing Lab	-	Rabbit	1:3500	IF
ATP V1B1	Gift from Wagner Lab	-	Rabbit	1:250	IF
BrdU	Milipore	MAP3510	Mouse		IF
Glut1	Abcam	Ab14683	Rabbit	1:500	WB/IF
Hif1α	Novus Biotechnologies	NB-100-479	Mouse	1:500	Wb
Hif1α (H1α67)	Novus Biotechnologies	NB-100-105	Mouse	1:20000	IHC
Hif2α	Pollard et al. 2007	PM8	rabbit	1:2500	IHC
HRP anti-mouse	ThermoScientific	31430	Goat	1:1000	IHC
HRP anti-rabbit	ThermoScientific	31460	Goat	1:1000	IHC
LDH-A (N-14)	Santa Cruz Biotechnology	Sc-27230	Goat	1:1000	WB
NaPi2	Gift from Biber Lab	-	Rabbit	1:500	IF
NCC	Millipore	AB3553	Rabbit	1:500	IF

NKCC2	Gift from Loffing Lab	-	Rabbit	1:250	IF
p53	Leica Microsystems	NCL-p53-CM5p	Rabbit	1:1000	WB
PDK-1	Enzo Life Sciences	ADI-KAP-PK112-D	Rabbit	1:1000	WB
Pendrin	Gift from Wagner Lab	-	Rabbit	1:250	IF
Tamm Horsfall Protein (H-135)	Santa Cruz Biotechnologies	Sc-20631	Rabbit	1:250	IF
Tubulin, acetylated	Sigma-Aldrich	T6793	Mouse	1:1000	IF
Vhl (FL-181)	Santa Cruz Biotechnologies	Sc-5575	Rabbit	1:100	WB
β-Actin (AC-74)	Sigma-Aldrich	A2228	Mouse	1:1000	WB

7.1.5 Oligonucleotide sequences

Name	Sequence	Application
Control band cre fwd	ATA ATG CCT TTC CTC AGT AAA CCA G	Genotyping
Control band cre rev	GGA TCC CAT TAC AGA TGG TTG TG	Genotyping
Cre fwd	AGG TTC GTG CAC TCA TGG A	Genotyping
Cre rev	TCG ACC AGT TTA GTT ACC C	Genotyping
Hif1a fwd	GGA GCT ATC TCT CTA GAC C	Genotyping
Hif1a rev	GCA GTT AAG AGC ACT AGT TG	Genotyping
Hif2a fwd	GAG AGC AGC TTC TCC TGG AA	Genotyping
Hif2a rev	TGT AGG CAA GGA AAC CAA GG	Genotyping
p53 fwd	GCC CTC TCT TAT CGC CAG AT	Genotyping
p53 rev	GCT TAT GGG CTT CTC CAA ACT	Genotyping
Vhl fwd	GGA GTA GGA TAA GTC AGC TG	Genotyping
Vhl rev	GTA CAC CTG AGA GCG GCT TC	Genotyping
Aqp1 fwd	AGG CTT CAA TTA CCC ACT GGA	RT-qPCR
Aqp1 rev	GTG AGC ACC GCT GAT GTGA	RT-qPCR
Aqp11 fwd	TGG GGC TAA TGC TGC TGT TC	RT-qPCR
Aqp11 rev	CAC CCA TTT CGG GG GAC ATA	RT-qPCR
Aqp2 fwd	ATG TGG GAA CTC CGG TCC ATA	RT-qPCR
Aqp2 rev	ACG GCA ATC TGG AGC ACAG	RT-qPCR
Aqp3 fwd	GCT TTT GGC TTC GCT GTCAC	RT-qPCR
Aqp3 rev	TAG ATG GGC AGC TTG ATC CAG	RT-qPCR
Aqp4 fwd	CTTT CTG GAA GGC AGT CTC AG	RT-qPCR
Aqp4 rev	CCA CAC CGA GCA AAA CAAA GAT	RT-qPCR

Aqp6 fwd	GTG TAG CAG GGC TTA CCT TCT	RT-qPCR
Aqp6 rev	GAT GGC GAT CTG GAG CAC A	RT-qPCR
Aqp7 fwd	AAT ATG GTG CGA GAG TTT CTG G	RT-qPCR
Aqp7 rev	ACC CAA GTT GAC ACC GAG ATA	RT-qPCR
Atp6v1b1 fwd	AAG TTT GCC CAG TAT GCT GAG	RT-qPCR
Atp6v1b1r rec	GCA GGA TGT CCC CTG TGA A	RT-qPCR
Chd1 fwd	CAG CCT TCT TTT CGG AAG ACT	RT-qPCR
Chd1 rev	TTA CAG CTA CCT GCC ACT TTT C	RT-qPCR
Cubulin fwd	CAC TTT AGG TTG TGG TGG AAC A	RT-qPCR
Cubulin rev	TTG CTG TCA AAG CTA ATC TCC C	RT-qPCR
Epo fwd	ACT CTC CTT GCT ACT GAT TCC T	RT-qPCR
Epo rev	ATC GTG ACA TTT TCT GCC TCC	RT-qPCR
Hif1a fwd	TGC TCAT CAG TTG CCA CTT C	RT-qPCR
Hif1a rev	CCT CAT GGT CAC ATG GAT GA	RT-qPCR
Hif2a fwd	CTG ATG GCC AGG CGC ATG ATG	RT-qPCR
Hif2a rev	CTG ATG GCC AGG CGC ATG ATG	RT-qPCR
Ldh-a fwd	TGG CTT TCC CAA AAA CCG AGT	RT-qPCR
Ldh-a rev	CCA TCA GGT AAC GGA ACC GC	RT-qPCR
Lkb1 fwd	TTG GGC CTT TTC TCC GAG G	RT-qPCR
Lkb1 rev	CAG GTC CCC CAT CAG GTA CT	RT-qPCR
p53 fwd	GCG TAA ACG CTT CGA GAT GTT	RT-qPCR
p53 rev	TTT TTA TGG CGG GAA GTA GAC TG	RT-qPCR
Pdk1 fwd	AGG ATC AGA AAC CGG CAC AAT	RT-qPCR
Pdk1 rev	GTG CTG GTT GAG TAG CAT TCT A	RT-qPCR
Pfkfb3 fwd	CAA CTC CCC AAC CGT GAT TGT	RT-qPCR
Pfkfb3 rev	TGA GGT AGC GAG TCA GCT TCT	RT-qPCR
Pgk1 fwd	TGG AGC CAA CTC CGT TGT C	RT-qPCR
Pgk1 rev	CAG GCA TTC TCG ACT TCT GGG	RT-qPCR
Pk-m1 fwd	TTG TGC GAG CCT CCA GTC	RT-qPCR
Pk-m1 rev	ACT CCG TGA GAA CTA TCA AAG C	RT-qPCR
Pk-m2 fwd	TCG AGG AAC TCC GCC GCC TG	RT-qPCR
Pk-m2 rev	CCA CGG CAC CCA CGG CGG CA	RT-qPCR
S12 fwd	GAA GCT GCC AAA GCC TTA GA	RT-qPCR
S12 rev	AAC TGC AAC CAA CCA CCT TC	RT-qPCR

Slc12a1 (NKCC2) fwd	TGG GTT GTC AAC TTC TGC AAT	RT-qPCR
Slc12a1 (NKCC2) rev	CCG GGA AAT CAG GTA GTA GGC	RT-qPCR
Slc12a3 (NCC) fwd	ACA CGG CAG CAC CTT ATA CAT	RT-qPCR
Slc12a3 (NCC) rev	GAG GAA TGA ATG CAG GTCA GC	RT-qPCR
Slc26a4 (Pendrin) fwd	AAG AGA GCC TTT GGT GTG GTA	RT-qPCR
Slc26a4 (Pendrin) rev	CAG GGC ATA AGC CAT CCC TTG	RT-qPCR
Slc34a1 (NaPi-IIa) fwd	TGC CTC TGA TGC TGG CTTT C	RT-qPCR
Slc34a1 (NaPi-IIa) fwd	TTG TGG GTT GCC AAC ATG ATG	RT-qPCR
Slc34a1 (NaPi-IIa) rev	GATA GGA TGG CAT TGT CCTT GAA	RT-qPCR
Slc34a1 (NaPi-IIa) rev	CCA GCT TGG TAG GTA GTG GGT	RT-qPCR
Slc4a1 (AE1) fwd	AGA TCC CAG ATC GAG ACA GC	RT-qPCR
Slc4a1 (AE1) rev	GCT CCA CAT AGA CCT GAC CG	RT-qPCR
SLC5A1 (SGLT1) fwd	ATG CGG CTG ACA TCT CAG TC	RT-qPCR
SLC5A1 (SGLT1) rev	ACC AAG GCG TTC CAT TCA AAG	RT-qPCR
Umod (THP) fwd	CCT GGG ACA TGC AGG AAC AC	RT-qPCR
Umod (THP) rev	GTA GGA GAC CAC TCT GAG CCT	RT-qPCR
VEGF-A fwd	CTT GTT CAG AGC GGA GAA AGC	RT-qPCR
VEGF-A rev	ACA TCT GCA AGT ACG TTC GTT	RT-qPCR
Vhl fwd	CAG CTA CCG AGG TCA TCT TTG	RT-qPCR
Vhl rev	CTG TCC ATC GAC ATT GAG GGA	RT-qPCR
Vim fwd	GCG GCT GCG AGA GAA ATT GCA	RT-qPCR
Vim rev	CCG TTC AAG GTC AAG ACG TGC CA	RT-qPCR
Self-made Adapter rev #1	CAAGCAGAAGACGGCATACGAGATACCTAG GTGACTGGAGTTCAGACGTGTGCTCTTCCGA TCTCTGCCATTTGTCTCGAG	Deep-Sequening
Self-made Adapter rev #2	CAAGCAGAAGACGGCATACGAGATTGGTAC GTGACTGGAGTTCAGACGTGTGCTCTTCCGA TCTCTGCCATTTGTCTCGAG	Deep-Sequening
Self-made Adapter rev #3	CAAGCAGAAGACGGCATACGAGATAACGTG GTGACTGGAGTTCAGACGTGTGCTCTTCCGA TCTCTGCCATTTGTCTCGAG	Deep-Sequening
TruSeq Adapter fwd	AATGATACGGCGACCACCGAGATCTACACTC TTTCCCTACACGACGCTCTTCCGATCTATCTTG TGGAAAGGACGA	Deep-Sequening

TruSeq Adapter rev #1	CAAGCAGAAGACGGCATACGAGATTCAAGT GTGACTGGAGTTCAGACGTGTGCTCTTCCGA TCTCTGCCATTTGTCTCGAG	Deep-Sequening
TruSeq Adapter rev #2	CAAGCAGAAGACGGCATACGAGATCTGATC GTGACTGGAGTTCAGACGTGTGCTCTTCCGA TCT CTGCCATTTGTCTCGAG	Deep-Sequening
TruSeq Adapter rev #3	CAAGCAGAAGACGGCATACGAGATAAGCTA GTGACTGGAGTTCAGACGTGTGCTCTTCCGA TCTCTGCCATTTGTCTCGAG	Deep-Sequening

7.1.6 Plasmids

Vector	Reference	Vendor
Adeno-Cre-GFP	1700	Vector Biolabs
Adeno-GFP	1060	Vector Biolabs
shCdkn1a	TRCN0000042583	Sigma-Aldrich
shCdkn1a	TRCN0000042585	Sigma-Aldrich
shCdkn1a	TRCN0000042586	Sigma-Aldrich
shCdkn1a	TRCN0000042587	Sigma-Aldrich
shCdkn1a	TRCN0000054898	Sigma-Aldrich
shCdkn1a	TRCN0000054901	Sigma-Aldrich
shCdkn1a	TRCN0000054902	Sigma-Aldrich
shCdkn1a	TRCN0000042584	Sigma-Aldrich
shCdkn1a	TRCN0000054899	Sigma-Aldrich
shCdkn1a	TRCN0000054900	Sigma-Aldrich
shCdkn1b	TRCN0000071063	Sigma-Aldrich
shCdkn1b	TRCN0000071064	Sigma-Aldrich
shCdkn1b	TRCN0000071066	Sigma-Aldrich
shCdkn1b	TRCN0000071067	Sigma-Aldrich
shCdkn1b	TRCN0000071065	Sigma-Aldrich
shCdkn1c	TRCN0000042588	Sigma-Aldrich
shCdkn1c	TRCN0000042589	Sigma-Aldrich
shCdkn1c	TRCN0000042590	Sigma-Aldrich
shCdkn1c	TRCN0000042592	Sigma-Aldrich
shCdkn1c	TRCN0000042591	Sigma-Aldrich

shCdkn2a	TRCN0000077815	Sigma-Aldrich
shCdkn2a	TRCN0000077816	Sigma-Aldrich
shCdkn2a	TRCN0000231227	Sigma-Aldrich
shCdkn2a	TRCN0000231228	Sigma-Aldrich
shCdkn2a	TRCN0000231226	Sigma-Aldrich
shCdkn2a	TRCN0000231225	Sigma-Aldrich
shCdkn2a	TRCN0000257162	Sigma-Aldrich
shCdkn2a	TRCN0000222729	Sigma-Aldrich
shCdkn2a	TRCN0000222730	Sigma-Aldrich
shCdkn2a	TRCN0000222731	Sigma-Aldrich
shCdkn2b	TRCN0000042598	Sigma-Aldrich
shCdkn2b	TRCN0000042599	Sigma-Aldrich
shCdkn2b	TRCN0000042600	Sigma-Aldrich
shCdkn2b	TRCN0000042601	Sigma-Aldrich
shCdkn2b	TRCN0000042602	Sigma-Aldrich
shCdkn2b	TRCN0000085033	Sigma-Aldrich
shCdkn2b	TRCN0000085034	Sigma-Aldrich
shCdkn2b	TRCN0000085036	Sigma-Aldrich
shCdkn2b	TRCN0000085037	Sigma-Aldrich
shCdkn2d	TRCN0000085088	Sigma-Aldrich
shCdkn2d	TRCN0000085089	Sigma-Aldrich
shCdkn2d	TRCN0000085090	Sigma-Aldrich
shCdkn2d	TRCN0000085091	Sigma-Aldrich
shCdkn2d	TRCN0000085092	Sigma-Aldrich
Env-IRES-puro	Morita et. al (Morita et al. 2000)	
shHif1a	TRCN0000232222	Sigma-Aldrich
shHif1a	TRCN0000232220	Sigma-Aldrich
shHif1a	TRCN0000232223	Sigma-Aldrich
shLdh-a	TRCN0000308636	Sigma-Aldrich
shLdh-a	TRCN0000308638	Sigma-Aldrich
shLdh-a	TRCN0000041743	Sigma-Aldrich
shLdh-a	TRCN0000041744	Sigma-Aldrich
shLdh-a	TRCN0000308704	Sigma-Aldrich
shPdk1	TRCN0000078810	Sigma-Aldrich

shPdk1	TRCN0000078812	Sigma-Aldrich
pLKO.1 ns	10879	Addgene
pMD2.G	12259	Addgene
psPAX2	12260	Addgene
shRb1	TRCN0000042546	Sigma-Aldrich
shRb1	TRCN0000042547	Sigma-Aldrich
shRb1	TRCN0000055378	Sigma-Aldrich
shRb1	TRCN0000055379	Sigma-Aldrich
shRb1	TRCN0000055380	Sigma-Aldrich
shRb1	TRCN0000055382	Sigma-Aldrich
shRb1	TRCN0000235830	Sigma-Aldrich
shRb1	TRCN0000235829	Sigma-Aldrich
shRb1	TRCN0000235831	Sigma-Aldrich
shRb1	TRCN0000218613	Sigma-Aldrich
shRb1	TRCN0000218099	Sigma-Aldrich
shRb1	TRCN0000042545	Sigma-Aldrich
shRb1	TRCN0000042543	Sigma-Aldrich
shRb1	TRCN0000042544	Sigma-Aldrich
shRb1	TRCN0000055381	Sigma-Aldrich
shRbl1	TRCN0000088103	Sigma-Aldrich
shRbl1	TRCN0000088104	Sigma-Aldrich
shRbl1	TRCN0000088105	Sigma-Aldrich
shRbl1	TRCN0000088106	Sigma-Aldrich
shRbl1	TRCN0000088107	Sigma-Aldrich
shRbl1	TRCN0000234086	Sigma-Aldrich
shRbl1	TRCN0000234087	Sigma-Aldrich
shRbl1	TRCN0000234088	Sigma-Aldrich
shRbl1	TRCN0000218550	Sigma-Aldrich
shRbl2	TRCN0000071273	Sigma-Aldrich
shRbl2	TRCN0000071274	Sigma-Aldrich
shRbl2	TRCN0000071275	Sigma-Aldrich
shRbl2	TRCN0000071276	Sigma-Aldrich
shRbl2	TRCN0000071277	Sigma-Aldrich
SV40 large T-Antigen	pBSSVD2005	Addgene

shTrp53	TRCN0000012358	Sigma-Aldrich
shTrp53	TRCN0000012359	Sigma-Aldrich
shTrp53	TRCN0000012360	Sigma-Aldrich
shTrp53	TRCN0000012361	Sigma-Aldrich
shTrp53	TRCN0000012362	Sigma-Aldrich
shTrp53	TRCN0000054548	Sigma-Aldrich
shTrp53	TRCN0000054550	Sigma-Aldrich
shTrp53	TRCN0000054551	Sigma-Aldrich
shTrp53	TRCN0000054552	Sigma-Aldrich
shTrp53	TRCN0000054549	Sigma-Aldrich
shTrp53	TRCN0000174221	Sigma-Aldrich
shTrp53	TRCN0000204876	Sigma-Aldrich
shTrp63	TRCN0000012749	Sigma-Aldrich
shTrp63	TRCN0000012750	Sigma-Aldrich
shTrp63	TRCN0000012751	Sigma-Aldrich
shTrp63	TRCN0000012752	Sigma-Aldrich
shTrp63	TRCN0000012748	Sigma-Aldrich
shTrp73	TRCN0000012753	Sigma-Aldrich
shTrp73	TRCN0000012754	Sigma-Aldrich
shTrp73	TRCN0000012755	Sigma-Aldrich
shTrp73	TRCN0000012756	Sigma-Aldrich
shTrp73	TRCN0000012757	Sigma-Aldrich

7.2 Virus production

7.2.1 Bacterial strains and media

Plasmid DNA was grown in the bacterial strain Mach1-T1^{R} (Invitrogen). S.O.B. medium (Invitrogen) and Luria Bertani Bouillon medium (Fluka Analytical) was used for growth of bacteria.

7.2.2 Transformation

The plasmid DNA was added to an aliquot of chemically competent bacteria thawed on ice. The DNA/cell mix was incubated on ice for 30 minutes and heat shock was induced for 30 seconds at 42℃ without shaking. Cells were placed on ice for 2 minutes followed by addition of room temperature S.O.C. medium. Cells were incubated at 37℃ for 1 hour at 300 rpm in a shaking incubator (Thermomixer Comfort, Eppendorf). Finally, transformation mix was plated onto pre-

warmed agar plates containing appropriate antibiotic (100 µg/ml ampicillin or 50 µg/ml kanamycin), and incubated at 37°C overnight.

7.2.3 Plasmid isolation

For small-scale preparations, 2 ml of an overnight bacterial culture was centrifuged at 12 000 g for 5 minutes. DNA was isolated using GenElute Plasmid Miniprep Kit (Sigma) according to the manufacturer's instructions. For large-scale preparations, 200 ml of an overnight bacterial culture was centrifuged at 4500 g for 10 minutes. DNA was isolated using Macherey-Nagel NucleoBond Xtra Midi Kit according to manufacturer's instructions. Following resuspension in TE (10 mM Tris, 1 mM EDTA, pH 8), DNA concentration was determined by absorbance at 260 nm.

7.2.4 Production of adenovirus particles

Adenoviruses - Type 5 (dE1/E3) expressing Cre recombinase + GFP (Ad-Cre-GFP) or GFP only (Ad-CMV-GFP) were amplified in HEK-293 cells, cultured in DMEM mix (10 % fetal calf serum (FCS), 2mM glutamine, 10 kU/ml penicillin, 10 mg/ml streptomycin) at atmospheric oxygen levels at 37°C. Cells were infected with adenoviral stocks (7.1.6) at 50 - 80% confluency. Adenovirus-containing cells were harvested 2-3 days after infection when 80-90% of the cells were de-attached and centrifuged at 300 g for 5 minutes. Cell pellets were suspended in PBS, placed for 5 min in liquid nitrogen for thorough freezing, followed by thawing through incubation in a 37℃ water bath. Freezing and thawing cycles were repeated twice. Cell lysate was centrifuged at 2900 g for 15 minutes at room temperature to pellet the cell debris. The supernatant containing viral particles was stored in aliquots at -20℃.

7.2.5 Production of lentivirus particles

Lentiviral vectors (7.1.6) were produced using calcium phosphate-mediated transfection of HEK-293T cells Transfection was performed when the plate was 50-70% confluent. The medium was replaced with fresh DMEM (14 ml / 15 cm dish) two hours before transfection. The following transfection mix for one 15 cm dish was prepared in a 50 ml conical tube: 25 µg transfer vector plasmid, 14.5 µg packaging plasmid (psPAX2), 8 µg amphotropic VSV-G envelope (pMD2.G) or 9 µg ecotropic envelope (Env-IRES-puro^r), 660 µl of 0.1X TE, 180.5 µl of H_2O and 282.5 µl of 1M CaCl2. 1.5 ml of 2xHEBS was added drop wise under constant agitation. The precipitate was left at room temperature for 15 minutes and then added drop wise to the cells, followed by incubation at 37℃ for 16 hours. The medium was aspirated and 14 ml of fresh DMEM was slowly added. The medium containing lentiviral particles was harvested twice every 24 h hours. The

supernatants were cleared by centrifugation at 500 g for 5 minutes, filtered using a 0.45 µm filter unit and stored in aliquots at -80℃.

7.2.6 Determination of viral titer

For titration for lentivirus 5x104 cells were seeded per 6-well plate the day before infection. The next day the virus was diluted in DMEM 1:10^3, 1:10^4 and 1:10^5 and added to the cells together with polybrene (4 µg/ml). 24 hours later the viral supernatant was removed and cells were split 1:4 in triplicates on 6-well plates. Two days after infection, puromycin selection (2 µg/ml) was performed for 7-10 days. To visualize colony growth, the plates were stained with crystal violet (0.3% crystal violet in 70% methanol) at room temperature. After 1 hour, cells were washed in tap water and air dried. The viral titer corresponds to the number of colonies present at the highest dilution containing colonies, multiplied by the dilution factor and by two, to account for the twofold increase of cells during the transduction period and the 1:4 splitting.

7.3 Cell culture assays

7.3.1 Isolation and culturing of mouse embryonic fibroblasts (MEFs)

Mouse embryonic fibroblasts (MEFs) were isolated from embryos of relevant floxed strains at E13.5. After dissecting away the head, internal organs and spinal cord, the remaining tissue was minced with a razorblade, incubated for 15 minutes at 37°C in trypsin EDTA, re-suspended in growth media (DMEM supplemented with 10% fetal calf serum (FCS), 2 mM glutamine, 10 kU/ml penicillin, 10 mg/ml streptomycin and 200 µM β-mercaptoethanol) and plated on a 10 cm dish. Cells were split 2-3 days later into two 15 cm dishes and 2-3 days later frozen at passage two. Cells were cultured in conventional cell culture incubators at 5% oxygen. For low oxygen concentrations (1% oxygen) cells were cultured in an oxygen glove-box incubator (INVIVO$_2$ 400, Ruskinn).

7.3.2 Isolation and culturing of epithelial kidney cells (PKCs)

Kidneys were dissected from 2 month-old floxed mice. After removing the capsule under sterile conditions, kidneys were mashed with a razor blade on ice and digested in collagenase II solution at 37°C and 5% oxygen for 30 min. The cell suspension was filtered through a 70 µm cell strainer and washed in HBSS + 5% FCS. Erythrocytes were lysed for 1 min using standard ACK buffer. Cells were re-suspended in complete K-1 culture medium (Dulbecco's modified Eagle's medium (DMEM) and Hams F12 mixed 1:1, supplemented with 0.5% fetal calf serum, 2 mM glutamine, 10 kU/ml penicillin, 10 mg/ml streptomycin, hormone mix (5 µg/ml insulin, 1.25 ng/ml prostaglandin E_1 (PGE_1), 34 pg/ml triiodothyronine, 5 µg/ml transferrin, 1.73 ng/ml sodium selenite, and 18

ng/ml of hydrocortisone and 25 ng/ml epidermal growth factor (EGF)). Cells were counted and seeded at a density of $1x10^6$ cells on standard 10 cm plastic tissue culture plates. After 5-6 days in culture, cells were infected with adenoviruses expressing GFP or Cre-GFP or lentivirus, respectively (see 7.3.3).

7.3.3 Cell infection

A confluent 10 cm dish of pMEFs was split 1:3, treated with polybrene (4 µg/ml) and infected with an appropriate amount of lentivirus for 24 h. 48 h after infection, cells were selected with puromycin (4 µg/ml) and adenovirus infection was performed identically. PKCs were treated with polybrene at a density of 50% and simultaneously infected with lentivirus and adenovirus. Puromycin selection (2 µg/ml) was performed for three days 24 h after infection.

7.3.4 Cell immortalization

Wild type and *Vhl*$^{fl/fl}$ MEFs were transformed by transfection with a plasmid expressing SV40 large T-Antigen and pools of cells forming colonies after plating at low density were harvested for generation of cell lines. *Vhl*$^{fl/fl}$ *Hif1α*$^{fl/fl}$ cells were immortalized by transfection with the plasmid described above, followed by six passages of serial low density splitting (1:10) (Harding Revised 11/5/2003).

7.4 Cellular and biochemical analysis

7.4.1 Real time PCR-analysis

Total RNA was prepared from cultured cells or from powdered tissue of whole kidneys using NucleoSpin RNA kit and cDNA synthesis was done with random hexadeoxynucleotide primers and Ready-To-Go You-Prime First-Strand Beads. The real-time PCR analysis of cDNA was performed with SYBR Green JumpStart Taq ReadyMix and used primers listed above (7.1.5).

7.4.2 Western blotting

Protein extracts from cultured cells were prepared by washing the cells twice with cold PBS and lysing in RIPA buffer (50 mM Tris–HCl at pH 7.5, 150 mM sodium chloride, 1% NP-40, 1% sodium deoxycholate, 0.1% SDS, 2mM EDTA, 1 mM sodium fluoride, 1 mM Na_3VO_4, 1 mM PMSF, 1 mM dithiothreitol, 1:100 Protease Inhibitor Cocktail).

To assess Hifα protein levels, nuclear extracts were prepared. Cells were washed once in ice cold PBS and subsequently incubated for 20 minutes on ice in lysis buffer (10 mM HEPES, KOH pH 7.9, 10 mM KCl, 0.1 mM EDTA, 0.1 mM EGTA, 1:100 Protease Inhibitor Cocktail, and 1 mM PMSF) followed by adding addition of NP-40 to a final concentration of 0.1%, vortexing and centrifuging

at 5000 rpm. The nuclear pellet was extracted and incubated for 5 min on ice and frozen over night at - 80 °C in protein extraction buffer (400 mM NaCl, 20 mM HEPES, KOH pH 7.9, 1 mM EDTA, 1mM EGTA, 1:100 Protease Inhibitor Cocktail, and 1 mM PMSF). To remove insoluble material the lysates were at 14000 g and 4°C for 10 minutes. Using the Bradford protein assay cleared protein lysates were quantitated using bovine serum albumin as a standard. Prior to use, samples were boiled for 5 minutes at 95°C. Proteins were run on 6–15% acrylamide gels, transferred to nitrocellulose membranes and visualized by semi-dry immunoblotting with antibodies described above (7.1.4). The signal was detected using the Fujifilm Luminescent Image Analyzer LAS4000 mini.

7.4.3 Proliferation assays

For MEF proliferation assays, cells were seeded at densities of either $2x10^5$ or $3x10^5$ cells per 6 cm dish in triplicates and counted after 3 days before reseeding at the same density for the next passage. Proliferation assays shown in all figures are representative of at least 3 independent experiments.

For primary kidney cells, a Sulforhodamine B (SRB) colometric assay was performed (Vichai and Kirtikara 2006). Cells were cultured in K-1 medium containing 10% fetal calf serum for 2 days before seeding for the SRB assay. $2x10^3$ cells per well were seeded and fixed with 5% (wt/vol) trichloroacetic acid at the indicated time points, followed by staining with 0.057% (wt/vol) SRB solution and air drying. SRB was solubilized by incubation in 10 mM Tris base solution (pH 10.5) and OD was measured at 540 nm in a microplate reader (Anthos Lucy 3).

7.4.4 Transformation assays

For low density assays, 5000 cells were seeded per 10 cm plate. After ten days, cells were washed with PBS and stained with crystal violet (0.3% crystal violet in 70% methanol) at room temperature. After 1 h, cells were washed with tap water and air dried.

For soft agar assays, 2% low melting temperature agarose was dissolved in ddH_2O and mixed 1:1 with 2x DMEM mix (20% FCS, 4 mM glutamine, 20 kU/ml penicillin, 20 mg/ml streptomycin, pH 7.4). 1 ml solution was distributed per well of a 12-well plate and allowed to set at room temperature. For the middle layer, 0.8% low melting agarose was dissolved in ddH_2O and mixed 1:1 with 2x DMEM mix containing $1x10^5$ cells per genotype. Subsequently, 1 ml cell suspension was distributed in triplicates (final cell number: $2.5x10^4$ per well), and allowed to set for 30 min at room temperature. Finally, the layers were covered with 0.5 ml normal medium to prevent

dehydration.

For primary kidney cells, 2x K-1 medium (31.2 g/l DMEM/F12, 2.4 g/l sodium bicarbonate, 20% FCS, 20 kU/ml penicillin, 20 mg/ml streptomycin, 5 µg/ml insulin, 1.25 ng/ml prostaglandin E_1 (PGE_1), 34 pg/ml triiodothyronine, 5 µg/ml transferrin, 1.73 ng/ml sodium selenite, and 18 ng/ml of hydrocortisone, pH 7.4) was used instead of 2x DMEM mix.

For anchorage-independent growth assay, $1x10^5$ cells were seeded in untreated polystyrene plates to reduce cell attachment. Medium was changed by filtering the cells in cell strainers (pore size 40 – 100 µm).

7.4.5 ATP measurements

Cells were trypsinized, counted (Beckman counter Vi-Cell XR and Z2) and $1.5x10^5$ cells were re-suspended in 75 µl PBS and 75 µl buffer (CellTiter-Glo Luminescent Cell Viability Assay, Promega). Cells were lysed for 10 min at room temperature and distributed as technical triplicates in an opaque 96-well plate. Luminescence signal was detected with a microplate reader (Anthos Lucy 3). Student's t-test was performed for statistical analysis (P-values: * <0.05, ** <0.01, *** <0.001).

7.4.6 Gain of representation assay

To create a shRNA library for cell cycle regulatory genes, twelve genes of interest were chosen (*Cdkn1a*, *Cdkn1b*, *Cdkn2a*, *Cdkn2b*, *Cdkn2c*, *Cdkn2d*, *Rb1*, *Rbl1*, *Rbl2*, *Trp53*, *Trp63*, *Trp73*) and each gene was represented by 3-14 hairpins (see 7.1.6). Virus was produced in gene batches as described earlier (7.2) and viruses were mixed including a non-silencing (ns) control. $Vhl^{fl/fl}$ and $Vhl^{fl/fl}$ $Hif1a^{fl/fl}$ primary kidney cells were isolated (7.3.2) and cultured in K-1 medium (supplemented with 0.5% FCS). At a confluency of 50%, cells were treated with polybrene (4 µg/ml) and simultaneously infected with adenovirus (Adeno-GFP or Adeno-Cre-GFP) and lentivirus (cell cycle shRNA library, MOI=0.1). Medium was changed to K-1 containing 10% FCS the following day. Two days after infection, puromycin selection (2 µg/ml) was performed for one week. When plates were confluent, 5000 cells per 10 cm plate were seeded for synthetic proliferation screen (6 plates, T1), western blot analysis (1 plate) and crystal violet staining (1 plate). For T0 and Western blot analysis, remaining cells were seeded in two 10 cm plates. Three days later, genomic DNA was isolated using the GenElute Mammalian Genomic DNA Miniprep Kit (Sigma-Aldrich) according to manufacturer's instruction and nuclear extracts were harvested as described earlier (7.4.2).

To visualize colony growth, one plate per genotype was stained with crystal violet 10 days after seeding. For synthetic proliferation screen, colonies were harvested when plates were confluent

and genomic DNA was isolated. shRNA hairpins were amplified and sequencing adapters were added using the primers described in 7.1.5. Primers with different barcode sequences (marked in yellow) were used to distinguish different genotypes. Deep sequencing was performed on an Illumina HiSeq 2000 by the Functional Genomic Centre Zurich (FGCZ).

For the isolation of Hifα protein levels nuclear extracts were prepared. Cells were washed once in ice cold PBS and subsequently incubated for 20 minutes on ice in lysis buffer (10 mM HEPES, KOH pH 7.9, 10 mM KCl, 0.1 mM EDTA, 0.1 mM EGTA, 1:100 Protease Inhibitor Cocktail, and 1 mM PMSF) followed by addition of NP-40 to a final concentration of 0.1%, vortexing and spinning at 5000 g. The nuclear pellet was extracted and incubated for 5 min on ice and frozen over night at - 80 °C in protein extraction buffer (400 mM NaCl, 20 mM HEPES, KOH pH 7.9, 1 mM EDTA, 1mM EGTA, 1:100 Protease Inhibitor Cocktail, and 1 mM PMSF). To remove insoluble material the lysates were centrifuged at 14 000 g at 4°C for 10 minutes. Using the Bradford protein assay cleared protein lysates were quantitated using bovine serum albumin as a standard. Prior to use, samples were boiled for 5 minutes at 95°C. Proteins were run on 6–15% acrylamide gels, transferred to nitrocellulose membranes and visualized by semi-dry immunoblotting with antibodies described above (7.1.4). The signal was detected using the Fujifilm Luminescent Image Analyzer LAS4000 mini.

7.5 Mouse manipulations

7.5.1 Mouse maintenance

Mice were maintained in a specific pathogen-free environment on a 12 hour day/night cycles. Food and water was freely available. Breeding pairs were set up using animals of minimum age 7 weeks and pups were weaned at approximately 3 weeks of age.

7.5.2 Mouse strains

Hif1α$^{fl/fl}$(Ryan et al. 2000), *Vhl*$^{fl/fl}$ (Haase et al. 2001), *Trp53*$^{fl/fl}$ (Jonkers et al. 2001) and *Hif2α*$^{fl/fl}$ (Gruber et al. 2007) mice were crossed with Ksp1.3-Cre/+ (Shao et al. 2002a; Patel et al. 2008)(Patel, Li et al. 2008)(Patel, Li et al. 2008) mice to generate the following mouse lines: Ksp1.3-Cre/+; *Hif1α*$^{fl/f}$, Ksp1.3-Cre/+; *Hif2α*$^{fl/f}$, Ksp1.3-Cre/+; *Vhl*$^{fl/fl}$; *Hif1α*$^{fl/fl}$, Ksp1.3-Cre/+; *Vhl*$^{fl/fl}$; *Hif2α*$^{fl/f}$, *Vhl*$^{fl/fl}$; *Hif1α*$^{fl/fl}$; *Trp53*$^{fl/fl}$ Previously described Ksp1.3-Cre/+; *Vhl*$^{fl/fl}$ (Frew et al. 2008b) and Ksp1.3-Cre/+; *Trp53*$^{fl/fl}$ (Wild et al. 2012) mouse strains were interbred to generate Ksp1.3-Cre/+; *Vhl*$^{fl/fl}$; *Trp53*$^{fl/fl}$ mice. Ksp1.3-Cre/ER^{T2} mice (Patel et al. 2008) was used to generate Ksp1.3-Cre/ER^{T2}; *Vhl*$^{fl/fl}$ mice. Non-Cre transgenic littermate mice served as controls for all cohorts.

SCID/Beige mice (C.B-17/IcrHsd-Prkdc^{scid} Lyst^{bg-J} were obtained from Harlan Laboratories (USA). Wild type cells were isolated from C57BL/6 embryos (Janvier Labs (USA)).

7.5.3 Genotyping

Ear biopsies were digested for 15 min at 95°C in lysis buffer (25 mM NaOH, 0.2 mM EDTA, pH 12) and thereafter neutralised afterwards with the same amount of neutralisation buffer (40 mM Tris-HCl, pH 5). The PCR reaction was carried out according to standard procedures using JumpStart Taq DNA polymerase and the primers shown in 7.1.5. The DNA was analyzed on 1.5% agarose gels in SBE buffer (5 mM NaOH bufferd with boric acid, pH 8.5).

7.5.4 Tamoxifen treatment

Ksp1.3-Cre/ER^{T2} transgenic mice were administered tamoxifen for induction of Cre/loxP recombination. The tamoxifen was dissolved in 100% ethanol and diluted 1:10 in corn oil to a final concentration of 20 mg/ml. Mice were injected intraperitoneal (I.P) with tamoxifen (4 mg/40 g body weight) at the age of 8 weeks. Non-Cre transgenic littermate mice served as controls for all cohorts.

7.5.5 Xenograft assay

3-5x10^6 cells were detached with Trypsin or Accutase and re-suspended in 70 µl DMEM. Cells were placed in a pre-cooled 30 gauge syringe and mixed with 70 µl ice cold matrigel. Syringes were kept on ice to avoid hardening of matrigel. SCID/Beige mice were anaesthetized by inhalation of 2% isofluorane using oxygen as carrier gas, shaved at both flanks and cells were slowly injected subcutaneously. Mice were euthanized the latest when xenograft size reached a size of 1 cm^3. The xenograft was fixed in 10% formalin and processed as described below (7.5.6)

7.5.6 Tissue collection and procedure

Mouse tissues were snap-frozen in liquid nitrogen (protein and mRNA analysis) and stored at -80°C or immersion-fixed in 10% formalin at 4°C overnight and stored in 70% ethanol. After dehydration in serial dilutions (3 h 70% EtOH, 2 h 80% EtOH, 2 h 90% EtOH, 2 h 96% EtOH, 2 h 100% EtOH, 2 h xylene, 3 h paraffin at 65°C), organs were embedded in paraffin and cut into 5 µm sections and fixed on polysine microscope adhesion slides (VWR).

7.5.7 Measurement of feeding parameters in metabolic cages

Single animals were adapted to the metabolic cage (Tecniplast 3600M021) for two days, followed by five measurements every 24 h. Mice were housed on a 12 h day/night cycle and provided with pulverized normal chow and water *ad libitum*. To avoid evaporation, urine collection trays were

covered with mineral oil. Collected urine was centrifuged for 13 000 g at 4°C and the supernatant was frozen at -20°C.

7.5.8 Water restriction test

Single mice were adapted to the metabolic cage and the first measurement was performed for 24 h as described above (see 7.5.7). During water restriction, mice were provided with 50% powder chow in water and the experiment was stopped when a single mouse showed signs of dehydration. Mice were again provided with water and the third measurement was performed for 24 h.

7.5.9 Urine analysis

24 h urine was collected as described above (see 7.5.7). Samples were diluted 1:10 in ddH_2O and osmolality was determined by freezing point osmometry (Osmometer, Roebling). Urine ion levels and urinary creatinine were analyzed with the UniCel® DxC 800 Synchron® Clinical System in cooperation with the ZIRP (University of Zürich). pH was measured with a pH meter from fresh urine (Seven easy, Mettler Toledo).

7.5.10 Blood collection and analysis

Animals were anaesthetized and blood was terminally collected from the vena cava or by puncturing the heart and treated with sodium-heparin. Analysis of hemoglobin and electrolyte levels, blood pH and blood gas values were performed immediately with the ABL825Flex. Hematocrit levels were determined by capillary centrifugation (5 min at 8000 rpm) and the ratio was determined manually. Blood plasma was stored at – 80°C for further analysis. Creatinine, blood urea nitrogen (BUN), albumin and phosphorus were determined using the UniCel® DxC 800 Synchron® Clinical System in cooperation with the ZIRP (University of Zurich).

7.5.11 Micro-computed Tomography (µCT)

Animals were anaesthetized and Visipaque 270 was injected i.v. at 8 µl/g bodyweight (Almajdub et al. 2008) as contrast agent. µCT images were recorded with a Quantum FX microCT (Perkin Elmer) with the following settings: 100 µA, 90 kV, respiratory gating and fine scanning. µCT data were exported as DICOM images to be analyzed in the Quantum FX data format for overview X-ray picture and the CaliperAnalyze 11.0 software was used for for 3D reconstruction.

7.5.12 High-resolution respirometric analysis

Animals were euthanized with CO_2 and dissected immediately. One mm^3 biopsies were taken from cortex and medulla under the microscope and transferred to ice cold PBS. Wet weight was

determined after drying the tissue on a Whatman paper. Biopsies were transferred to modified mitochondrial respiration medium (MiROS, 5 mM $MgCl_2$, 5 mM $KHPO_4^-$, 10 mM HEPES, 70 mM sucrose, 220 M mannitol, 1 mg/ml fatty acid free BSA, pH 7.4) and oxygen consumption was measured using a OROBOROS Oxygraph-2k (ORBOROS INSTRUMENTS Corp, Innsbruck, Austria) according to the following procedure: Leak respiration (LN), representing resting oxygen consumption of an unaltered system, was induced by the addition of malate (2 mM) and octanoyl carnitine (0.2 mM). Adenosine diphosphate (ADP, 5 mM) was added for determination of the maximal electron flow through the electron-transferring flavoprotein (ETF) and fatty acid oxidative capacity (P_{ETF}). P_{CI} (respiratory capacity specific to complex I) was induced by the addition of glutamate (10mM) and pyruvate (5 mM). Maximal state 3 respiration (oxidative phosphorylation capacity P) was measured subsequently to the addition of succinate (10 mM). Finally, complex I was inhibited by rotenone (0.5 µM) to asses maximal state 3 respiration specific to complex II (P_{CII}). Finally, mitochondrial respiration was abrogated by blocking complex III with 2.5 µM antimycin A, allowing the correction of residual O_2. Cytochrome C oxidase activity (complex IV) was assessed by the addition of tetramethylphenylenediamine (TMPD, 0.5 mM) and Ascorbate (2 mM). Values were calculated using the DatLab OROboros 5.1 softare and presented as means ± standard deviation. P-values: * ≤ 0.05. N=6. Experiment was conducted by Michal Rajski, Robert A. Jacobs and Stine Lundby.

7.6 Histological analysis

7.6.1 Haematoxylin and Eosin (H&E) staining

Tissue sections were de-waxed for 3 min in xylene and hydrated for 2 min each in serial dilutions of ethanol washes (100%, 95%, 70%). Nuclei were stained for 4 min in haematoxylin and dipped 3 times in 0.3% acid alcohol (70 % EtOH in ddH_2O acidified with 0.3% HCl 32%) for differentiation. Proteins were stained for 8 min in 1% eosin solution. Finally, specimen were dehydrated for 2 min in serial ethanol dilutions (70%, 95%, 100%) and xylene (3 min) and mounted in entellan.

7.6.2 Immunohistochemistry

Tissue sections were de-waxed in xylene and hydrated in series of ethanol washes (10 min xylene, 10 min 100 % EtOH, 10 min 95% EtOH, 5 min in 70% EtOH) and washed for 5 min in PBS-T (137 mM NaCl, 2.7 mM KCl, 19 mM Na_2HPO_4, 1.7 mM KH_2PO_4, pH 7.4, 0.3% Triton x-100). For antigen retrieval, slides were cooked for 5 min at 110°C in 0.1 M citrate buffer (pH 6) using a standardized pressure cooker (HistosPro, Milestone). Next, specimens were incubated in peroxidase blocking solution (3% H_2O_2 in 10% methanol) for 30 min, circled with a hydrophobic pen and incubated in protein blocking solution (PBS, supplemented with 10% goat serum, 0.3% Triton, 1 drop avadin

per 250 µl solution). Primary antibodies were diluted in PBS, containing 10% goat serum, 0.3% Triton and 1 drop biotin solution per 250 µl blocking buffer) and sections were incubated overnight at 4°C. Biotinylated secondary antibodies were diluted (10% goat serum in PBS) and applied for 1 h at room temperature. Sections were washed and subsequently incubated in TBS for 10 min. For complex formation, 1 drop Avadin DH and and 1 drop biotinylated horseradish peroxidase were mixed in 2.5 ml TBS (50mM Tris, 150 mM NaCl, pH 7.5) 30 min prior to use, and solution was applied for 1 h at room temperature. Next, specimen were washed in TBS and incubated in 50 mM Tris (pH 7.6). 3,3'-diaminobenzidine (DAB) was used as a chromogen according to the manufacturer's instructions. Finally, the specimens were counterstained with hematoxylin solution for 30 s, dehydrated in serial ethanol dilutions (1 min 70% EtOH, 2 min 95% EtOH, 2 min 100% EtOH, 3 min in Xylene) and mounted in entellan. All incubations were performed in a humidified chamber. Between incubations, sections were washed three times for 5 min in PBS, unless otherwise stated.

Immunohistochemistry targeting Hifα proteins was performed using the Dako Catalyzed Signal Amplification (CSA) kit according to the manufacturer's instruction. The following changes were included in the protocol: After peroxidase block, specimen were incubated for 15 min in avadin solution (TBS, supplemented with 1% BSA, 0.1% Tween, 2 drops avadin solution per 250 µl solution), followed by 15 min biotin solution (TBS, containing 1% BSA, 0.1% Tween 20 and 2 drops biotin solution per 250 µl solution). For washing, standard TBS-T (50 mM Tris, 150 mM NaCl, 0.1% Tween 20) was used before primary antibody incubation, whereas high salt TBS-T (0.05 M Tris-HCl pH 7.6 containing 0.3 M NaCl and 0.1 % Tween 20) was used afterwards. Rehydration of sections, antigen retrieval and counterstaining was performed as described above.

7.6.3 Immunofluorescent staining of tissues

For immunofluorescence, specimens were processed as described above (7.6.1) without the avadin/biotin blocking step. After primary antibody incubation, sections were incubated with fluorophor-labelled secondary antibodies for 1 h. Subsequently, slides were washed with PBS and nuclei were stained for 10 min with DAPI (0.5 µg/ml in PBS containing 10% goat serum). After washing in PBS and ddH_2O, sections were mounted in Mowiol.

7.6.4 Immunocytochemistry

Cells were cultured on round glass cover slips placed in a 6-well plate. After washing with PBS the cells were fixed in 4% PFA for 1 h at room temperature. Removal of PFA was followed by a washing step. The cover slips were incubated with blocking solution (10% goat serum/0.3%

Triton/PBS) for 1 h at room temperature. Incubation with antibodies was carried out as described in 7.6.3.

7.6.5 Image acquisition and procession

Brightfield and fluorescence microscopy was performed on either a Zeiss Scope. A1 microscope or an Axiovert 40 CRC microscope. Images were obtained with an Axiocam MRc5 camera using the Axiovision LE64 software and processed with Adobe Photoshop.

8 Results

8.1 Combined mutation of *Vhl* and *Trp53* causes cysts and tumours in mice

During the initial part of my PhD work I participated in a project that investigated the cooperative effects of the deletion of *Vhl* and *Trp53* in the epithelium of mouse kidneys and the genital-urinary tract. This publication presented below forms the first result chapter of this thesis and several conclusions are relevant for the rationale and understanding of the results presented in chapter 8.2, which consists of a manuscript for publication and additional experiments investigating the role of Hifα transcription factors in the early phase of tumour formation.

Briefly, our studies demonstrated that in primary mouse fibroblasts senescence induced by loss of *Vhl* is largely independent of oxygen concentrations and is rescued by the deletion of *Trp53*. However, *Vhl/Trp53* null MEFs still proliferate slower than *Trp53* null cells, indicating that loss of *Vhl* exerts an anti-proliferative barrier even in immortalized cells. Co-deletion of *Vhl* and *Trp53* in the renal epithelium causes the formation of simple cysts, atypical cysts and neoplasms in aged mice. Gene deletions in the genital urinary tract caused dysplasia and tumour formation of the epididymis and uterus and malformation of the vesicular gland (Albers et al. 2013). Furthermore, immunohistochemical analysis of human ccRCC samples demonstrated that *TP53* is mutated in approximately 9% of human ccRCC, supporting the importance of loss of TP53 function in the formation of ccRCC. However, the late onset of the disease in mice indicates that additional oncogenic events have to occur to drive tumourigenesis in Vhl/Trp53 deficient epithelial cells. For this study, I analyzed the effect of loss of *Vhl* on the proliferation of large T antigen transformed MEFs and examined the expression of Hifα in *Vhl/Trp53* deficient kidneys.

Research Article
Kidney cysts and tumours in *Vhl/Trp53* mutant mice

TRANSPARENT PROCESS OPEN ACCESS EMBO Molecular Medicine

Combined mutation of *Vhl* and *Trp53* causes renal cysts and tumours in mice

Joachim Albers[1,2†], *Michal Rajski*[1,3†], *Désirée Schönenberger*[1†], *Sabine Harlander*[1,2,3†], *Peter Schraml*[4], *Adriana von Teichman*[4], *Strahil Georgiev*[5], *Peter J. Wild*[2,4], *Holger Moch*[2,4], *Wilhelm Krek*[2,5], *Ian J. Frew*[1,2,3*]

Keywords: ccRCC; cyst; p53; *VHL*

DOI 10.1002/emmm.201202231

Received November 02, 2012
Revised March 08, 2013
Accepted March 12, 2013

The combinations of genetic alterations that cooperate with von Hippel–Lindau (*VHL*) mutation to cause clear cell renal cell carcinoma (ccRCC) remain poorly understood. We show that the *TP53* tumour suppressor gene is mutated in approximately 9% of human ccRCCs. Combined deletion of *Vhl* and *Trp53* in primary mouse embryo fibroblasts causes proliferative dysregulation and high rates of aneuploidy. Deletion of these genes in the epithelium of the kidney induces the formation of simple cysts, atypical cysts and neoplasms, and deletion in the epithelia of the genital urinary tract leads to dysplasia and tumour formation. Kidney cysts display a reduced frequency of primary cilia and atypical cysts and neoplasms exhibit a pro-proliferative signature including activation of mTORC1 and high expression of Myc, mimicking several cellular and molecular alterations seen in human ccRCC and its precursor lesions. As the majority of ccRCC is associated with functional inactivation of *VHL*, our findings suggest that for a subset of ccRCC, loss of p53 function represents a critical event in tumour development.

INTRODUCTION

Clear cell renal cell carcinoma (ccRCC) accounts for approximately 80% of kidney tumours and thereby approximately 2.5% of all types of human malignancy. The von Hippel–Lindau (*VHL*) tumour suppressor gene is mutated, deleted or epigenetically silenced in up to 85% of all sporadic cases of ccRCC (Maher, 2013). Germline inheritance of a single mutant allele of *VHL* gives rise to the dominantly inherited VHL familial cancer syndrome which predisposes not only to the formation of ccRCC, but also to cystic lesions in the kidney and pancreas as well as to diverse types of tumours in the central nervous system, eye, ear, pancreas, adrenal gland, epididymis and broad ligament (Kaelin, 2002).

The pVHL protein has been ascribed several distinct biochemical activities and implicated in the regulation of diverse cellular processes, dysregulation of any or all of which could be envisaged to play important roles in tumour formation (Frew & Krek, 2007). Two lines of evidence however suggest that loss of pVHL function alone is insufficient for tumour initiation in the kidney. Kidneys of patients with an inherited *VHL* mutation frequently display cystic lesions as well as ccRCC. Since some pVHL-deficient proliferative cysts contain micro-foci of ccRCC, it is believed that, at least in some cases, cysts represent a precursor lesion in the evolution of malignant ccRCC (Lubensky et al, 1996; Walther et al, 1995). Detailed analysis of regions of normal histology in these kidneys revealed that VHL patient kidneys likely contain many thousands of individual isolated cells that are null for pVHL function (Mandriota et al, 2002; Montani et al, 2010). pVHL-deficient cysts and ccRCC apparently arise infrequently in comparison to the total frequency of *VHL* mutation. Secondly, heterozygous deletion of the mouse homologue of the *VHL* gene, *Vhl* (previously referred to as *Vhlh*), in the entire mouse (Haase et al, 2001), or

(1) Institute of Physiology, University of Zurich, Zurich, Switzerland
(2) Competence Center for Systems Physiology and Metabolic Diseases, ETH Zurich and University of Zurich, Zurich, Switzerland
(3) Zurich Center for Integrative Human Physiology, University of Zurich, Zurich, Switzerland
(4) Institute of Surgical Pathology, University Hospital Zurich, Zurich, Switzerland
(5) Institute of Molecular Health Sciences, ETH Zurich, Zurich, Switzerland
***Corresponding author:** Tel: +41 44 635 5004; Fax: +41 44 635 6814; E-mail: ian.frew@access.uzh.ch

†These authors contributed equally to this work.

homozygous deletion under the control of kidney-specific Cre transgenes, does not lead to proliferative dysregulation or tumour formation in the kidney (Frew et al, 2008b; Rankin et al, 2006). Multiple genetic mutations appear to be required to cause proliferation and transformation of pVHL-deficient cells.

Genes that are mutated at high frequency in diverse human epithelial tumours, including *PTEN*, *EGFR*, *ERBB2*, *BRAF*, *RAS* family genes, *RB1* and *APC*, are either not mutated or are mutated at relatively low frequencies (<10%) in ccRCC. Rather, ccRCC frequently (41%) harbour mutations in the chromatin remodelling gene *PBRM1* (Varela et al, 2011) and in several genes involved in histone modification (Dalgliesh et al, 2010) and protein ubiquitination and de-ubiquitination (Guo et al, 2012; Pena-Llopis et al, 2012). Several chromosomal regions are frequently amplified or deleted and numerous genes are frequently hypermethylated in ccRCC (Maher, 2013), implying that there may be many different combinations of genetic alterations that can cooperate with loss of *VHL* function to cause tumour formation. Our previous studies demonstrate that low-frequency mutations could be functionally important in ccRCC formation; co-deletion of *Vhl* and *Pten* in the mouse kidney led to the formation of proliferative cysts, mimicking the precursor lesions of ccRCC that arise in human VHL patients (Frew et al, 2008b). Several studies, including data presented herein, have shown that *TP53* is mutated in a subset of ccRCC (http://cancer.sanger.ac.uk/cosmic). We demonstrate that combined mutation of *Vhl* and *Trp53* causes dysregulation of cellular proliferation in primary mouse embryo fibroblasts (MEFs) and kidney epithelial cells and results in the formation of kidney cysts and neoplastic lesions in kidneys as well as tumours in genital tract organs.

RESULTS

TP53 mutations occur in sporadic ccRCCs

We sequenced the entire *VHL* gene and exons 5–8 of the *TP53* gene in 54 cases of sporadic ccRCC (Table 1). As expected, missense or truncating *VHL* mutations were observed in 73% of the tumours. Immunohistochemistry for the HIF1α-inducible proteins CA9 and Glut1, and for HIF1α itself, revealed moderate or strong expression of at least one of these markers in all but two of the tumours, verifying the well-described hypoxic signature associated with loss of function of pVHL. *TP53* mutations that affected the coding region were detected in 5 (9%) tumours, all of which are either previously described pathogenic mutations or are predicted to be pathogenic. One tumour harboured both *VHL* and *TP53* mutations, while the other four *TP53* mutant tumours were wild-type for *VHL*. While methylation analyses for the *VHL* gene were not possible in these samples, it is likely that pVHL expression may be silenced in these tumours as they showed very high immunohistochemical staining for the HIFα target genes. In agreement with our data, the COSMIC database (http://cancer.sanger.ac.uk/cosmic) lists 30 of 209 (14.4%) tumours that display *TP53* coding region mutations. Unfortunately the *VHL* mutation status of these tumours is in most cases unknown. Thus, *TP53* is mutated in a significant fraction of sporadic ccRCCs.

Trp53 mutation allows immortalisation of *Vhl* mutant primary mouse embryo fibroblasts

We first utilized primary MEFs to investigate potential cooperative interactions of the mouse *Vhl* and *Trp53* genes in proliferative control. Deletion of *Vhl* in primary and transformed MEFs induces proliferation arrest and/or the onset of premature senescence (Mack et al, 2005; Welford et al, 2010; Young et al, 2008). Consistent with these findings, lentiviral-mediated shRNA knockdown of *Vhl* led to rapid loss of proliferative capacity of wild-type MEFs (Fig 1A). In contrast, *Vhl* knockdown had no anti-proliferative effect on $Trp53^{-/-}$ MEFs (Fig 1C). Interestingly, while efficient reduction of pVHL protein was maintained throughout the duration of the experiment in wild-type cells (Fig 1B), the extent of knockdown rapidly diminished with increasing passage in $Trp53^{-/-}$ cells (Fig 1D), suggesting that there is a proliferative selection for those cells in which the knockdown occurs less efficiently. To attempt to overcome this problem of selection, MEFs from wild-type, $Vhl^{fl/fl}$, $Trp53^{fl/fl}$ and $Vhl^{fl/fl}Trp53^{fl/fl}$ mice were infected with adenovirus expressing GFP (Adeno-GFP) as control or with adenovirus expressing a Cre-GFP fusion protein (Adeno-Cre) to delete the floxed genes. *Vhl* knockout MEFs rapidly lost proliferative capacity whereas *Vhl/Trp53* double deletion allowed proliferation, albeit at a slower rate of proliferation than *Trp53* deletion alone (Fig 1E). Consistent with a rescue of senescence, *Vhl/Trp53* double null cells retained the appearance of proliferating cells while *Vhl* deletion caused an enlarged, flattened cell morphology characteristic of senescence (Supporting Information Fig 1). None of the gene deletions allowed the formation of colonies in soft agar, demonstrating that the cells are immortalized but not transformed. Western blotting 4 days after infection confirmed the high efficiency of gene deletion but after approximately 20–30 days of continuous proliferation, a significant restoration of pVHL expression was evident in the $Vhl^{fl/fl}Trp53^{fl/fl}$ Cre-infected cell population (Fig 1F), suggesting a mixed cell population in which *Vhl* null cells have a proliferative disadvantage in comparison to an initially rare population of pVHL-expressing cells (see results below).

In light of recent findings showing that senescence induced by loss of *Vhl* can be rescued by culturing cells at 2 or 5% oxygen (Welford et al, 2010), we conducted a series of experiments in which cells were grown at 5% oxygen. We observed a reproducible but only partial restoration of proliferative capacity following *Vhl* knockout (Fig 1G) when cells were cultured either in a glove box incubator to ensure constant oxygen tension throughout the experiment or in a conventional oxygen incubator where cells were briefly exposed to 21% oxygen every 3 days during passaging. In either incubator, wild-type MEFs did not enter senescence within 50 days of culture at 5% oxygen but typically entered senescence after about 10–12 days at 21% oxygen, verifying our culture system against published data (Parrinello et al, 2003). In light of this partial rescue of proliferation of *Vhl* mutant cells, all subsequent proliferation

Table 1. *VHL* and *TP53* mutations and CA9, GLUT1 and HIF1α immunohistochemistry in sporadic cases of human ccRCC

pT	*VHL* sequencing			Immunohistochemistry			*TP53* sequencing			
	Exon 1	Exon 2	Exon 3	CA9	Glut1	HIF1α	Exon 5	Exon 6	Exon 7	Exon 8
3	–	–	A207CfsX49	2	0	0	–	–	–	–
3b	–	T124RfsX5	–	2	2	1	–	–	–	–
3	–	H115SfsX17	–	2	1	0	–	–	–	–
3b	N78S	–	–	2	2	1	n.a.	–	–	–
3b	–	–	–	1	2	0	K139K	–	–	–
3a	–	V155CfsX4	–	2	0	2	–	–	–	–
3b	–	–	–	1	0	n.a.	Q165X	–	–	–
3	–	–	–	2	1	1	n.a.	–	–	–
3b	–	–	R167_V170del	2	2	2	–	–	–	–
3a	–	–	–	1	1	1	–	–	–	–
3b	P99QfsX60	–	–	2	2	1	–	R213R	–	–
3b	S68T	–	–	2	2	0	–	–	–	–
3a	–	–	–	0	1	0	–	–	–	–
3	S65T	–	–	2	2	0	–	–	–	–
3a	–	–	I180V	2	2	2	–	–	–	–
3	–	V130F	–	2	1	0	–	–	L257L	–
3b	–	L153TfsX21	–	2	1	1	–	R142R	–	–
4	–	–	V170D	2	2	1	–	–	–	–
3a	–	–	L158V	2	n.a.	0	–	–	–	–
3a	–	–	H191H	2	2	0	–	P219L	–	–
3a	–	–	–	2	2	0	H179L	–	–	–
3a	–	W117R	–	2	2	2	–	–	–	–
3b	–	–	R161P	0	0	1	–	–	–	–
4	Y98X	–	–	0	2	1	–	–	–	–
3a	T100SfsX59	–	–	2	2	2	–	–	–	–
4	–	–	–	0	2	n.a.	–	–	–	–
3a	–	–	–	2	2	0	–	–	–	–
3	L101P	–	–	2	2	0	–	–	–	–
3a	–	–	–	2	2	1	–	–	–	–
3a	Y112D	–	–	n.a.	n.a.	0	–	–	–	–
3b	D92AfsX36	–	–	2	2	0	–	–	–	–
3b	V62CfsX5	–	–	1	n.a.	0	–	–	–	–
3	–	–	–	1	2	0	–	–	–	–
3b	c.340 + 1G>T	–	–	2	2	0	–	–	–	–
3	S65L	–	–	2	2	1	–	–	–	–
3	–	c.341-2A>G	–	2	2	0	–	–	–	–
3a	–	–	–	2	2	1	–	–	–	–
4	S68X	–	–	2	2	0	–	–	–	–
3b	Y98N	–	–	2	1	0	–	R213R	–	–
3b	S68X	–	–	2	2	0	–	–	–	–
3b	R107VfsX45	–	–	2	2	1	–	–	–	–
3b	Q73X	–	–	0	2	0	–	–	–	R273C
3a	–	–	R161X	2	n.a.	1	–	–	–	–
3b	–	–	V181KfsX14	n.a.	n.a.	0	–	–	–	–
3	n.d.	n.d.	n.d.	2	2	0	–	–	–	–
3	n.d.	n.d.	n.d.	2	2	0	–	–	–	–
3	n.d.	n.d.	n.d.	2	2	1	–	–	–	–
3	n.d.	n.d.	n.d.	0	1	1	–	–	–	–
3	n.d.	n.d.	n.d.	2	2	2	–	–	–	–
3	n.d.	n.d.	n.d.	0	1	1	–	–	–	–
2	n.d.	n.d.	n.d.	2	1	1	–	–	–	–
4	n.d.	n.d.	n.d.	2	2	0	–	1bp ins*	–	–
3	n.d.	n.d.	n.d.	1	2	1	–	–	–	–
3	n.d.	n.d.	n.d.	2	1	1	–	–	–	–

Grey shading highlights a mutation that causes a coding alteration. Amino acid alterations are shown by single letter code, del = deletion, fs = frame shift, X = new stop codon, n.a. = not analysable, n.d. = not determined, * = bp insertion not identifiable, 0 = no staining, 1 = moderate staining, 2 = strong staining.

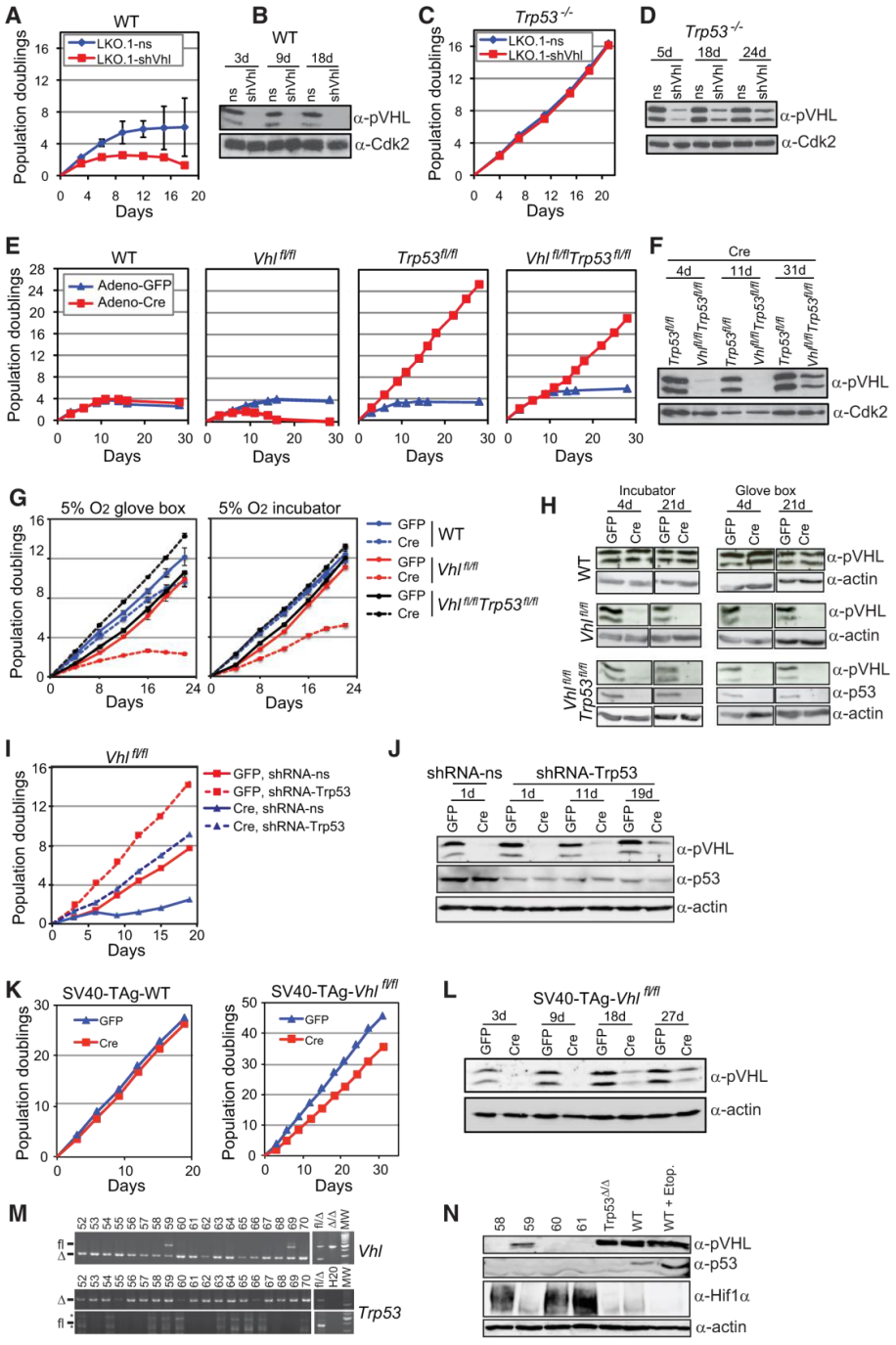

Figure 1.

experiments were conducted at 5% oxygen in a conventional incubator.

To permit comparison of proliferation rates in an isogenic background, we knocked down *Trp53* in $Vhl^{fl/fl}$ MEFs. *Trp53* knockdown rescued the proliferation defect of *Vhl* knockout (Adeno-Cre treated) cells but these cells proliferated more slowly than control (Adeno-GFP treated) cells with *Trp53* knockdown alone (Fig 1I). The *Vhl* knockout/*Trp53* knockdown cultures became enriched with pVHL-expressing cells over time (Fig 1J). A similar reduction in proliferation rate (Fig 1K) and passage-dependent enrichment of pVHL-expressing cells in the cell population (Fig 1L) was also observed in cultures where *Vhl* was deleted from $Vhl^{fl/fl}$ MEFs that had been transformed with SV40 Large T-Antigen to simultaneously inactivate both the p53 and pRB-dependent cell cycle checkpoints. Thus, loss of pVHL compromises cellular proliferation in MEFs in a manner independent of the p53 and pRB cell cycle checkpoints.

Given the strong selection against pVHL-expressing cells in bulk population experiments, we performed experiments using single cells to definitively address the question of whether *Vhl*/*Trp53* double null cells are truly immortalized. While wild-type MEFs undergo cellular senescence when plated as single cells, *Trp53* null cells form colonies allowing the generation of immortalized cell lines founded from single cells. Two days after infection of $Vhl^{fl/fl}Trp53^{fl/fl}$ primary MEFs with Adeno-Cre, cells were plated at a density of 0.5 cells/well in six 96-well plates. Cell lines were generated over a period of 6 weeks and genotyped to detect the floxed or deleted *Vhl* allele, allowing a retrospective assessment of the genotype of the initiating cell of the cell line. From a theoretical maximum of 288 cell lines, 135 cell lines were generated. One hundred and thirty-three of these harboured homozygous deletion of *Vhl*, while two were heterozygous for the floxed and deleted allele (Fig 1M). All cell lines showed homozygous deletion of the floxed *Trp53* gene (Fig 1M). Western blotting of a subset of these cell lines confirmed the PCR genotyping results (Fig 1N). Thus, *Trp53* deletion efficiently allows immortalization of *Vhl* null MEFs. It is likely that the rare cells in which only one floxed *Vhl* allele (but both floxed *Trp53* alleles) has undergone Cre-mediated recombination have a proliferative advantage over the *Vhl*/*Trp53* null cells, allowing them to accumulate over time in bulk populations.

Trp53 mutation rescues proliferation of *Vhl* mutant primary renal epithelial cells

To investigate the cooperative effects of combined *Vhl* and *Trp53* deletion in a disease-relevant cell type we cultured primary mouse renal epithelial cells from the various floxed mouse strains at 5% oxygen and deleted *Vhl* and/or *Trp53* using Adeno-Cre or using Adeno-GFP as control (Fig 2A). While long-term assays of renal epithelial cell behaviour are not possible due to the epithelial to mesenchymal transition that occurs over time, in short term assays we observed that deletion of *Vhl* inhibited the proliferation of renal epithelial cells and co-deletion of *Trp53* rescued this inhibition of proliferation (Fig 2B). Unlike in MEFs, cultures of *Trp53* or *Vhl*/*Trp53* null renal epithelial cells formed colonies when plated at single cell density with very low efficiency (<1%), and did not grow in soft agar, demonstrating that these cells are not immortalized or transformed.

Enhanced rates of aneuploidy in *Trp53* and *Vhl*/*Trp53* mutant MEFs

One driving force in the evolution of tumours is aneuploidy. Loss of pVHL, through an uncharacterized mechanism, results in lower levels of the mitotic checkpoint protein Mad2, which alone causes a moderate elevation of levels of aneuploidy but when combined with reduction in expression of another mitotic spindle checkpoint protein, CENP-E, induces a dramatic increase in aneuploidy (Thoma et al, 2009). Here we confirm that deletion (Fig 3A) or knockdown (Fig 3B) of *Vhl* causes a reduction of Mad2 protein expression. Loss of *Trp53* function in MEFs also causes higher levels of aneuploidy and polyploidy and has been shown to result in aberrantly elevated expression levels of the checkpoint proteins Aurora A (Mao et al, 2007), Mad2 and separase (Pati et al, 2004). Western blotting of

◀ **Figure 1. *Trp53* mutation allows immortalized proliferation of *Vhl* null MEFs.**

A,C. Proliferation assays of wild-type (A) and $Trp53^{-/-}$ (C) MEFs following infection with pLKO.1 lentiviruses expressing a non-silencing sequence (ns) or shRNA directed against *Vhl* (shVhl).

B,D. Western blotting analysis for pVHL in cells from A and C at the time points (number of days after infection) indicated. Immunoblotting using an antibody against Cdk2 served as a loading and transfer control.

E. Proliferation assays of wild-type, $Vhl^{fl/fl}$, $Trp53^{fl/fl}$ or $Vhl^{fl/fl}Trp53^{fl/fl}$ MEFs following infection with adenoviruses expressing GFP (GFP) or Cre-GFP (Cre).

F. Western blotting analysis of $Trp53^{fl/fl}$ and $Vhl^{fl/fl}Trp53^{fl/fl}$ MEFs in E at the indicated time points. Immunoblotting using an antibody against actin served as a loading and transfer control.

G. Proliferation assays of wild-type, $Vhl^{fl/fl}$ and $Vhl^{fl/fl}Trp53^{fl/fl}$ MEFs in 5% oxygen.

H. Western blotting analysis of cells from G at the indicated timepoints.

I. Proliferation assays of $Vhl^{fl/fl}$ MEFs infected with GFP or Cre and lentiviruses expressing an empty miR30 shRNA (shRNA-ns) or miR30-format shRNA directed against *Trp53* (shRNA-Trp53).

J. Western blotting analysis of cells from I at the indicated time points.

K. Proliferation assays of SV40 T-antigen transformed WT and $Vhl^{fl/fl}$ MEFs following GFP or Cre infection.

L. Western blotting analysis of SV40-TAg-$Vhl^{fl/fl}$ from K at the indicated timepoints.

M. Cell lines (52–70) derived from Cre-infected $Vhl^{fl/fl}Trp53^{fl/fl}$ MEFs genotyped for floxed (fl) and deleted (Δ) *Vhl* and *Trp53* alleles. Samples with known *Vhl* and *Trp53* genotypes served as controls, MW: molecular weight markers, * non-specific bands.

N. Western blotting analysis of clones 58–61 for pVHL, p53 and Hif1α, confirming the loss of p53 expression and presence and functionality of pVHL expression in clone 59. Lysates from *Trp53* null MEFs, wild-type MEFs or wild-type MEFs treated with etoposide (10 μM, 6 h) served as controls for the p53 protein.

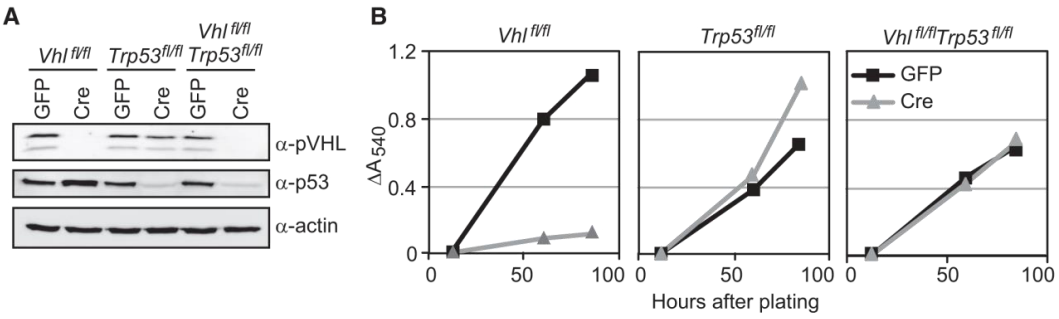

Figure 2. *Trp53* deletion rescues proliferative defects of *Vhl* null primary kidney epithelial cells.

A. Western blotting analysis of primary kidney epithelial cell cultures derived from $Vhl^{fl/fl}$, $Trp53^{fl/fl}$ or $Vhl^{fl/fl}Trp53^{fl/fl}$ mice 3 days after infection with adenoviruses expressing GFP or Cre.

B. Proliferation of cells from A assessed using an SRB assay to detect increase in total protein content of the culture over time.

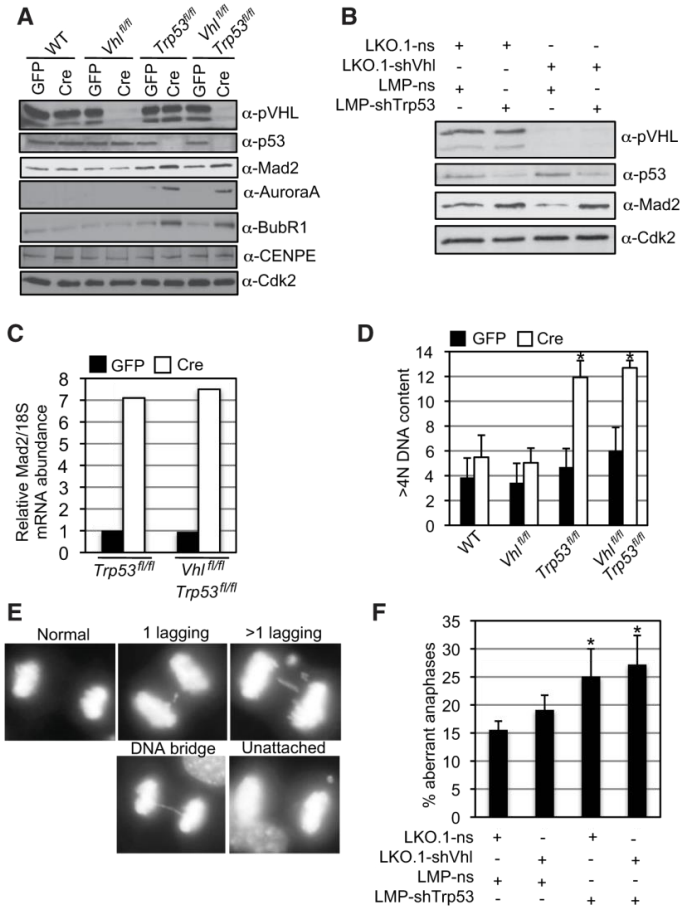

Figure 3. High rates of aneuploidy in *Trp53* and *Vhl*/*Trp53* null MEFs.

A. Western blotting analysis of wild-type, $Vhl^{fl/fl}$, $Trp53^{fl/fl}$ or $Vhl^{fl/fl}Trp53^{fl/fl}$ MEFs infected with adenoviruses expressing GFP (GFP) or Cre-GFP (Cre).

B. Western blotting analysis of wild-type MEFs infected with combinations of pLKO.1 lentiviruses expressing a non-silencing sequence (ns) or shRNA directed against *Vhl* (shVhl) and LMP retroviruses expressing a non-silencing sequence (ns) or shRNA directed against *Trp53* (shTrp53).

C. Real-time quantitative PCR analysis of Mad2 mRNA abundance normalized to 18S mRNA abundance in GFP and Cre infected $Trp53^{fl/fl}$ and $Vhl^{fl/fl}Trp53^{fl/fl}$ MEFs.

D. Frequency of cells with greater than 4N DNA content as assessed by flow cytometric analysis. Results represent mean ± SD of triplicate samples and * represents statistically significant differences between GFP and Cre treated cells of the same genotype (Student's *t*-test, $p < 0.01$).

E. Depiction of a normal anaphase and examples of anaphases showing a range of chromosome segregation defects.

F. Anaphases of cells from B were scored five days after infection according to the scheme shown in E and the percentage of aberrant anaphases calculated. Data represent mean ± SD of triplicate samples (in each $n > 120$ anaphases were counted) and * represents statistically significant differences to cells infected with both ns vectors (Student's *t*-test, $p < 0.01$).

Trp53$^{fl/fl}$ cells infected with Adeno-Cre (Fig 3A) revealed elevated expression levels of Aurora A and Mad2, as well as elevated expression of BubR1, another spindle checkpoint protein, but no change in the expression levels of CENP-E. To our knowledge this is the first report of this effect of p53 on BubR1. Since double mutation of *Mad2* and *Trp53* has been shown to lead to dramatic levels of aneuploidy (Burds et al, 2005), we investigated whether the combined effects of loss of *Vhl* and *Trp53* on the expression of various mitotic spindle checkpoint proteins would have a similar effect. However, *Vhl/Trp53* double knockout (Fig 3A) or double knockdown (Fig 3B) cells displayed higher than normal levels of Mad2. This was presumably due to the elevation in mRNA abundance of *Mad2* in *Trp53* and *Vhl/Trp53* knockout MEFs (Fig 3C), consistent with previous observations that p53 represses *Mad2* mRNA expression (Pati et al, 2004), overriding the effect of loss of *Vhl* in reducing Mad2 expression. Thus, in terms of the expression of several proteins whose levels regulate spindle checkpoint function, *Vhl/Trp53* double null cells are similar to *Trp53* null cells. Functional studies supported this idea. Flow cytometry revealed that cultures of *Trp53* null MEFs accumulated polyploid cells at the same frequency as cultures of *Vhl/Trp53* double null MEFs (Fig 3D). To directly monitor the integrity of the mitotic spindle checkpoint in an isogenic background we performed lentiviral-mediated knockdown of *Vhl* and/or *Trp53* in MEFs and performed fluorescence microscopy to detect aberrant anaphases that are characterized by the presence of lagging or unattached chromosomes or DNA bridges (Fig 3E). Knockdown of *Vhl* led to a slightly increased rate of aberrant anaphases (Fig 3F), *Trp53* knockdown and *Vhl/Trp53* double knockdown both led to a statistically significant increase in the frequency of aberrant anaphases in comparison to control knockdowns, but the two genotypes were not significantly different from one another (Fig 3F).

In summary, while there appear to be no cooperative genetic effects of loss of *Vhl* and *Trp53* function on aneuploidy, *Trp53* mutation in a *Vhl* mutant background may enhance aneuploidy, which may be relevant for tumourigenesis.

Deletion of *Vhl* and *Trp53* in mouse kidney and genital–urinary tract epithelia causes dysplasia and tumour formation

To investigate the consequences of combined deletion of *Vhl* and *Trp53* in epithelial tissues *in vivo*, *Vhl*$^{fl/fl}$ and *Trp53*$^{fl/fl}$ mice were interbred with *Ksp1.3-Cre* transgenic mice to generate *Ksp1.3-Cre*; *Vhl*$^{fl/fl}$ (Frew et al, 2008b), *Ksp1.3-Cre*; *Trp53*$^{fl/fl}$ (Wild et al, 2012) and *Ksp1.3-Cre*; *Vhl*$^{fl/fl}$; *Trp53*$^{fl/fl}$ mice, hereafter referred to as Vhl$^{\Delta/\Delta}$, Trp53$^{\Delta/\Delta}$ and Vhl$^{\Delta/\Delta}$Trp53$^{\Delta/\Delta}$ mice respectively. In the kidney, the *Ksp1.3-Cre* transgene induces gene deletion in the epithelial cells at the urinary pole of the glomerulus, distal tubules, loops of Henle, collecting ducts and also very infrequently in proximal tubular cells. Expression of this transgene in the Wolffian and Müllerian ducts during development also leads to gene deletion in the epithelia of the renal pelvis, ureter, vesicular glands, epididymis, vas deferens and endometrium.

Vhl$^{\Delta/\Delta}$Trp53$^{\Delta/\Delta}$ mice were sub-viable, with approximately 25% of mice dying within the first 3 months of life and with subsequent deaths in an apparently stochastic manner as the mice aged. Autopsy of these mice failed to reveal any obvious cause of death and no tumours were evident in any of the dead mice. This fact complicated the accrual of large cohorts of aged mice. Nonetheless, in combination with previously published analyses (Frew et al, 2008a,b) we analysed cohorts of mice at the following ages: 2–3 months (Vhl$^{\Delta/\Delta}$, $n=8$; Trp53$^{\Delta/\Delta}$, $n=7$; Vhl$^{\Delta/\Delta}$Trp53$^{\Delta/\Delta}$ $n=6$), 4–8 months (Vhl$^{\Delta/\Delta}$, $n=6$; Trp53$^{\Delta/\Delta}$, $n=10$; Vhl$^{\Delta/\Delta}$Trp53$^{\Delta/\Delta}$ $n=10$) and 11–13 months (Vhl$^{\Delta/\Delta}$, $n=9$; Trp53$^{\Delta/\Delta}$, $n=10$; Vhl$^{\Delta/\Delta}$Trp53$^{\Delta/\Delta}$ $n=17$). Littermate mice that were negative for the *Ksp1.3-Cre* transgene served as controls for all of these cohorts.

As previously described, kidneys of Trp53$^{\Delta/\Delta}$ mice developed normally and showed no histological abnormalities within 18 months of age (Wild et al, 2012). Similarly to Vhl$^{\Delta/\Delta}$ mice (Frew et al, 2008b), Vhl$^{\Delta/\Delta}$Trp53$^{\Delta/\Delta}$ mice developed a hydronephrosis phenotype of unknown cause but otherwise showed no defects in the structure of the nephrons at early ages. Mutation of *Trp53* in combination with *Vhl* led to a similar accumulation of nuclear HIF1α and HIF2α in tubular epithelia to that seen in *Vhl* single mutant mice (Supporting Information Fig 2). By 5 months of age small clusters of disorganized cells (Fig 4F) or micro-cysts (not shown) could infrequently be observed in the double knockout mice but not in either of the single mutant mice or control mice, suggestive of a breakdown in normal proliferative control in these cells. In comparison to the normal histological appearance of kidneys from 11- to 13-month-old control and single *Vhl* and *Trp53* mutant mice, kidneys of 13 out of 17 Vhl$^{\Delta/\Delta}$Trp53$^{\Delta/\Delta}$ mice aged 11–13 months mice displayed multiple hyperproliferative lesions (Fig 4G) and mild focal lymphoplasmacellular inflammation. Sections through the midline of 24 kidneys from these mice revealed 399 cysts ranging in diameter from 100 μm to 1 mm. Three hundred and forty-nine of these were lined by a single layered cuboidal epithelium (simple cyst) (Fig 4H) while 50 cysts showed multilayered micro-papillary epithelial growths projecting into the lumen (atypical cyst) (Fig 4I). Some larger cysts showed signs of regression, bleeding, cholesterol accumulation and foam cell macrophage infiltration. An additional 16 neoplastic lesions (diameter 250 μm to 1 mm) were also observed (Fig 4J and K). These lesions were non-invasive, displayed an increased mitotic index, low nuclear grade (Fig 4L) and cells grew either in a micro-papillary (Fig 4J) or solid (Fig 4K and L) growth pattern. Tumour cells typically showed weak cytoplasmic eosin staining (Fig 4L), similar to, but to a lesser extent than, the clear cell morphology seen in human ccRCC. Approximately half of the neoplasms were growing into a cystic space (Fig 4J) whereas the other lesions presented as a solid mass (Fig 4K and L). It was not possible to distinguish whether these latter lesions may represent completely filled cysts or whether they have arisen as a cyst-independent neoplasm. Epithelial cells lining simple and atypical cysts (Fig 4N and O) and neoplastic cells (Fig 4P) displayed frequent labelling for the proliferation marker Ki67. Simple cysts, atypical cysts and neoplasms all displayed high nuclear immunoreactivity for

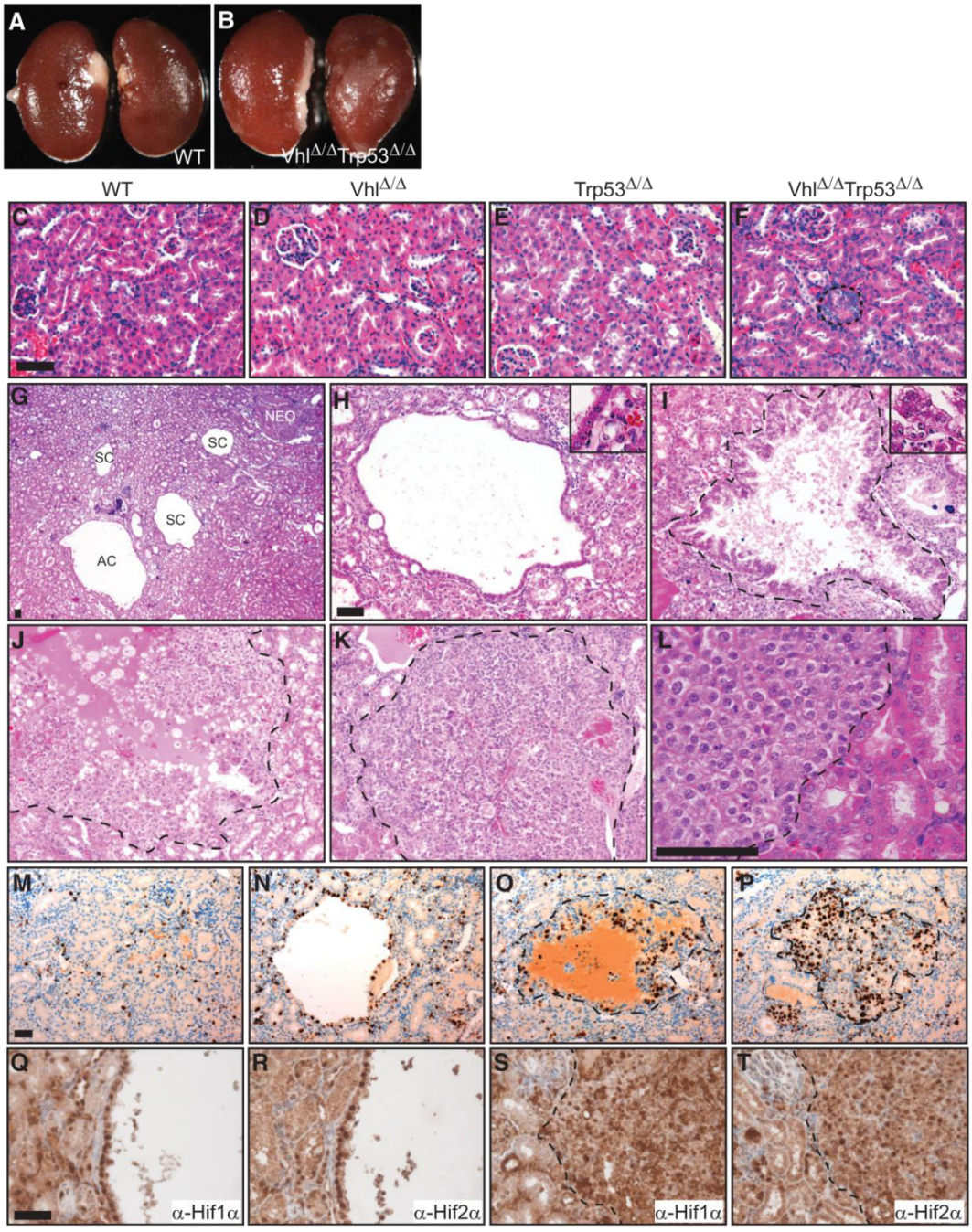

Figure 4.

HIF1α and HIF2α (Fig 4Q–T) verifying that these lesions are derived from *Vhl* null cells. While it is not possible to assay for loss of p53 protein by immunohistochemistry due to the fact that p53 is not detectable in normal kidney cells, PCR genotyping of laser capture micro-dissected simple cysts, atypical cysts and neoplasms demonstrated that the recombined *Trp53* and *Vhl* alleles were present in cells in these lesions (Supporting Information Fig 3). The non-recombined *Trp53* floxed and *Vhl* floxed alleles were also detected, likely due to presence of wild-type ($Vhl^{fl/fl}$;$Trp53^{fl/fl}$) stromal, inflammatory or vascular cells in these lesions.

Immunohistochemical staining using antibodies against NaPi2 (proximal), NCC (distal), THP (thick ascending loop of Henle) and AQP2 (collecting ducts) to mark different tubule segments revealed that most simple cysts express one of these markers (Supporting Information Fig 4), demonstrating that cysts arise from different nephron segments. Very rarely, remnants of the glomerulus could be observed in simple cysts (data not shown), suggesting that these cysts had arisen from the tubular epithelium at the urinary pole of the glomerulus. However, atypical cysts and neoplasms were always negative for all of the tubular markers (Supporting Information Fig 4), preventing assessment of the tubular segment of origin of these lesions and suggesting that the transition to tumour formation involves some degree of de-differentiation. Unlike the findings reported for some precursor lesions in human VHL patient kidneys (Esteban et al, 2006), *Vhl* mutant cystic lesions and neoplasms in the mouse retain expression of the epithelial marker E-cadherin and do not display the mesenchymal marker vimentin (Supporting Information Fig 5).

Thus, *Vhl* and *Trp53* double deletion does not automatically cause proliferative dysregulation of kidney epithelial cells *in vivo* but eventually leads to the evolution of lesions that appear to follow a pathway of simple cyst to atypical cyst to neoplasm that is similar to the proposed disease progression model in kidneys of patients with an inherited *VHL* mutation. Given the apparent morphological similarities and overlapping spectrum of development of atypical cysts and neoplasms, these lesions were grouped together and considered as being distinct from simple cysts in the analyses in the remainder of this study.

$Vhl^{\Delta/\Delta}Trp53^{\Delta/\Delta}$ mice also displayed a variety of dysplasias and tumours in the genital–urinary tract. Deletion of *Trp53* alone caused a moderate disorganisation of the epithelia in epididymal tubules, predominantly in tubules of the corpus and cauda of the epididymis, with an age-dependent accumulation of aberrant nuclei and multi-nucleated cells (Wild et al, 2012, Supporting Information Fig 6E). Epididymides from $Vhl^{\Delta/\Delta}Trp53^{\Delta/\Delta}$ mice appeared externally normal in the first months of life (Supporting Information Fig 6B) but histological analysis of aged cohorts revealed that they displayed a qualitatively more severe phenotype of nuclear abnormalities than the $Trp53^{\Delta/\Delta}$ mice (Supporting Information Fig 6F). At 11–13 months of age, the epididymides of all male $Vhl^{\Delta/\Delta}Trp53^{\Delta/\Delta}$ mice, but not of control or single mutant mice, displayed benign growths (Supporting Information Fig 6H). These growths were predominantly due to squamous metaplasia (Supporting Information Fig 6I) and extensive epithelial dysplasia (Supporting Information Fig 6J). These lesions are histologically identical to those arising in $Vhl^{\Delta/\Delta}Pten^{\Delta/\Delta}$ mice (Frew et al, 2008a). Epididymides also frequently displayed fibrosis, inflammation, foreign body reactions and metaplastic stromal changes, likely as a result of the blockage of tubules by dysplasia and squamous metaplasia. One mouse developed an epididymal clear cell papillary cystadenoma (Supporting Information Fig 7A) that appeared histologically identical to the cystadenomas that arise at high frequency in patients with an inherited *VHL* mutation. Vesicular glands of $Vhl^{\Delta/\Delta}Trp53^{\Delta/\Delta}$ mice (Supporting Information Fig 6L), but not of $Vhl^{\Delta/\Delta}$ or $Trp53^{\Delta/\Delta}$ mice (not shown), were malformed. In contrast to the normal single layered epithelium, vesicular glands of $Vhl^{\Delta/\Delta}Trp53^{\Delta/\Delta}$ mice displayed a disorganized epithelium characterized by multiple convoluted layers of epithelial cells and the formation of gland-like structures (Supporting Information Fig 6P). This phenotype increased in severity with age and two mice exhibited carcinomas in the vesicular gland (Supporting Information Fig 7C). The uterus in all genotypes developed normally (Supporting Information Fig 6R) and displayed a normal organisation of lumenal and glandular endometrial epithelium (Supporting Information Fig 6V). In older $Vhl^{\Delta/\Delta}Trp53^{\Delta/\Delta}$ mice, small foci of disorganized and multilayered epithelial cells could frequently be observed. Consistent with this, one mouse developed a high-grade carcinoma of the endometrium (Supporting Information Fig 7E) and another a high-grade squamous carcinoma of the

◀ **Figure 4. $Vhl^{\Delta/\Delta}Trp53^{\Delta/\Delta}$ mice develop kidney cysts and neoplasms.** C–F and Q–T are all the same magnification, H–K are the same magnification, M–P are the same magnification. Scale bars depict 50 μm. Dotted lines indicate the boundary of normal tissue and atypical cysts or neoplasms.

A,B. Normal external appearance of kidneys from 6 month-old $Vhl^{\Delta/\Delta}Trp53^{\Delta/\Delta}$ mice.

C–F. Histological appearance of cortex of kidneys from 6 month-old wild-type (C), $Vhl^{\Delta/\Delta}$ (D), $Trp53^{\Delta/\Delta}$ (E) and $Vhl^{\Delta/\Delta}Trp53^{\Delta/\Delta}$ (F) mice. The dotted region outlined in F is an example of an abnormal cluster of cells.

G. Example of lesions arising in the cortex of a kidney from a 1-year-old $Vhl^{\Delta/\Delta}Trp53^{\Delta/\Delta}$ mouse. AC: atypical cyst, SC: simple cyst, NEO: neoplasm.

H–K. Examples of lesions found in kidneys of one year-old $Vhl^{\Delta/\Delta}Trp53^{\Delta/\Delta}$ mice; simple tubular cyst (H), atypical cyst (I), neoplasm with cystic precursor (J) and solid neoplasm (K). Insets in H and I show high magnification of the cystic epithelium.

L. High magnification of a solid neoplasm showing clear cell morphology and low nuclear grade.

M–P. Representative Ki67 stainings of histologically normal epithelium (M), a simple cyst (N), an atypical cyst (O) and a neoplasm (P) in $Vhl^{\Delta/\Delta}Trp53^{\Delta/\Delta}$ mouse kidneys.

Q,R. Anti-HIF1α and anti-HIF2α immunohistochemistry of serial sections of a simple cyst.

S,T. Anti-HIF1α and anti-HIF2α immunohistochemistry of serial sections of a neoplastic lesion.

upper cervix (Supporting Information Fig 7G). One mouse displayed a high-grade carcinoma that most likely arose in the urothelium of the renal pelvis and which had also metastasized to the lungs and liver (Supporting Information Fig 7I).

Collectively, these findings demonstrate that mutation of the *Vhl* and *Trp53* tumour suppressor genes ultimately causes dysregulation of epithelial cell proliferation and the evolution of dysplastic and malignant lesions in multiple tissues in mice.

Cooperating pathways in tumour formation in *Vhl/Trp53* double mutant mice

Since we have previously shown a connection between loss of the primary cilium and cyst formation in VHL disease (Frew et al, 2008b; Thoma et al, 2007), we examined whether epithelial cells lining simple cystic lesions that arise in *Vhl/Trp53* double mutant mice displayed a similar loss of primary cilia. Visualising the primary cilium using an antibody against acetylated tubulin revealed that only 40% of cystic epithelial cells but almost 90% of cells in non-cystic tubules displayed a primary cilium (Fig 5A and B). Since only non-proliferating cells exhibit a primary cilium we asked if this reduction in cilia frequency was simply due to the increased proliferation of cystic epithelial cells by staining for Ki67, which labels proliferating cells in all cell cycle stages. On average, 18% of cystic epithelial cells stained positively for Ki67 (Fig 5C), a far lower frequency than the frequency of cells lacking a cilium. Indeed, dual colour immunofluorescence staining experiments revealed that many Ki67 negative cystic cells lacked primary cilia (Fig 5A) demonstrating that the loss of the primary cilium is likely a consequence of loss of pVHL and not an indirect consequence of cellular proliferation and might therefore be causal to cyst formation. Neoplasms displayed a mixed phenotype with respect to cilia, some displayed a very high frequency of ciliated cells (Fig 5D), some displayed an intermediate frequency (Fig 5E) and some were almost completely devoid of cilia (Fig 5F).

We have previously demonstrated that one pathway to cilia loss involves both inactivation of pVHL and inhibition of GSK3β (Frew et al, 2008b; Thoma et al, 2007), which can occur via hyperactivation of the PI3K signalling pathway (Frew et al, 2008b). However, immunohistochemical staining using antibodies against phospho-Thr37/46-4E-BP1 (P-4EBP1) (Fig 6G–I) and phospho-Ser240/244-ribosomal S6 protein (P-S6) (Fig 6J–L), two sensitive and robust downstream markers of activation of the PI3K-mTORC1 signalling pathway, revealed that only about 6–8% of simple cysts displayed mTORC1 pathway

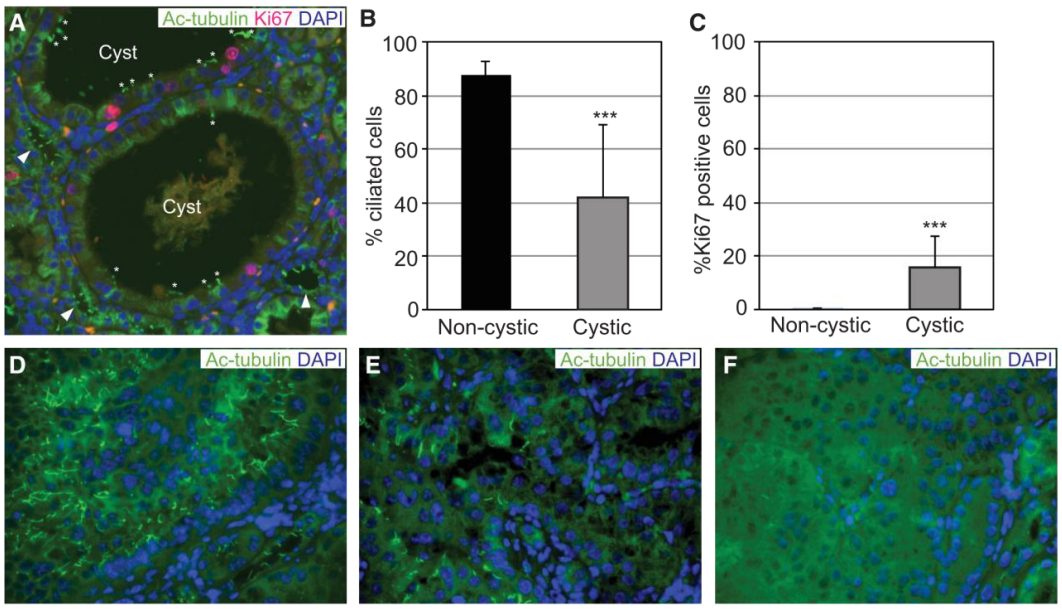

Figure 5. Reduced frequency of primary cilia in cysts.

A. Immunofluorescence staining of formalin-fixed paraffin embedded tissue for acetylated tubulin (green) to mark primary cilia, Ki67 (red) to mark proliferating cells and DAPI (blue) to mark nuclei in a cortical section of kidney from a $Vhl^{\Delta/\Delta}Trp53^{\Delta/\Delta}$ mouse. Arrowheads point to adjacent normal tubules showing a normal frequency of ciliated cells and * highlight primary cilia in cysts. Note the high frequency of Ki67 negative cells that lack a primary cilium.

B,C. Quantification of percentage of epithelial cells displaying a primary cilium (B) or staining for Ki67 (C) in non-cystic tubules ($n = 18$) or simple cysts ($n = 39$) in $Vhl^{\Delta/\Delta}Trp53^{\Delta/\Delta}$ mice. Mean and SD is shown, $^{***}p < 0.001$ Student's *t*-test.

D–F. Examples of neoplasms displaying varying frequencies of primary cilia.

activation above levels seen in histologically normal tubules in the same mice (Fig 6P). Interestingly, atypical cysts and neoplasms were almost always strongly positive for both of these markers (Fig 6P). Approximately half of all simple cystic lesions and almost all atypical cysts or neoplasms displayed elevated levels of the pro-proliferative Myc protein (Fig 6M–P). Thus, multilayered or papillary growth of *Vhl/Trp53* mutant cells into the lumen of cysts or growth as a solid neoplasm correlates with the acquisition of the pro-proliferative signature of mTORC1 activation and Myc expression.

DISCUSSION

We show that *TP53* is mutated in a subset of sporadic human ccRCCs and demonstrate genetically that *Trp53* mutation allows *Vhl* null MEFs to escape senescence and proliferate in an immortalized manner. We also show that combined deletion of *Vhl* and *Trp53* in mice results in the formation of simple and atypical cysts, as well as neoplastic lesions in kidneys and causes tumours to form in other genital tract tissues.

The long latency of tumour formation observed in mice (1 year) is consistent with our primary cell culture data showing that *Vhl/Trp53* mutation causes immortalization but not transformation of MEFs. These findings clarify previous contradictory reports concerning the role of p53 in regulating senescence following loss of *Vhl* in mouse fibroblasts (Welford et al, 2010; Young et al, 2008). *Vhl* null cells nonetheless exhibit a lower proliferation rate than *Vhl* wild-type cells, even in the background of loss of the p53 and pRB cell cycle checkpoints, implying that there may be additional cellular responses that represent barriers that prevent full transformation of *Vhl/Trp53* mutant cells. We suggest that the increase in aneuploidy observed in *Vhl/Trp53* null MEFs might potentially represent a mechanism that could contribute to cellular transformation and tumour evolution *in vivo*.

Our findings strengthen the model derived from studies of human VHL patients that ccRCCs can form via cyst-dependent and cyst-independent pathways (Fig 6Q). *Vhl/Trp53* mutant mice develop an apparent spectrum of cystic lesions beginning with simple cysts lined by a single layer of epithelial cells, followed by atypical cysts that display micro-papillary epithelial growths that project into the lumen of the cyst and finally cysts that are almost entirely filled with neoplastic growth. About half of the neoplasms are a solid mass of cells, preventing assessment of whether they arise via a cystic precursor lesion or not. *Vhl/Trp53* neoplastic lesions display several features of human ccRCC including clear cell-like changes, HIFα stabilisation and high rate of proliferation, but differ in that they exhibit a low nuclear grade and do not invade surrounding tissue. The lack of a capsule surrounding the neoplasms and absence of extra-renal metastases speaks against a malignant ccRCC lesion. *Vhl/Trp53* mutant neoplasms also frequently grow in a micro-papillary pattern, akin to papillary renal cell carcinomas. While the precursor lesions of human renal carcinomas are poorly characterized in general, in papillary type I and type II tumours the size of the lesion is the sole definitive distinguishing criteria. Lesions smaller than 5 mm are classified as adenomas and larger lesions are carcinomas (Eble et al, 2004). Taking the relative sizes of the human and mouse kidney into account, many of the neoplasms in our model would be classified as carcinomas under this definition. Because of the mixed features of the *Vhl/Trp53* null neoplasms we classify these tumours simply as renal neoplasms, rather than as a specific sub-type of renal cell carcinoma.

Epithelial cells lining simple cystic lesions display a reduced frequency of primary cilia, similar to cysts in human VHL patients (Thoma et al, 2007), further supporting the involvement of pVHL in maintenance of primary cilia and suppression of cyst formation. However, in contrast to *Vhl/Pten* mutant mice (Frew et al, 2008b), in *Vhl/Trp53* mutant mice, these simple cysts do not display evidence of over-activation of the PI3K signalling pathway or inactivating phosphorylation of GSK3β (unpublished observations), implying that there may be other unidentified pathways that cooperate with pVHL in maintenance of the primary cilium. In contrast to simple cysts, atypical cysts and neoplasms display hyperactivation of mTORC1 signalling. Since both lesions are characterized by disorganized patterns of cellular growth it is noteworthy that mTORC1 activation has been shown to induce a translational program that promotes cellular invasion (Hsieh et al, 2012). Hyperactivation of mTORC1 predicts poor outcome in ccRCC patients and mTORC1 inhibitors show clinical efficacy against ccRCC (Hudes, 2009). Atypical cysts and neoplasms almost invariably also display high levels of Myc protein. Upregulation of *MYC* expression is common in ccRCC and amplification of *MYC* predicts poor outcome in human ccRCC patients (Monzon et al, 2011; Tang et al, 2009). The combination of *Vhl/Trp53* double mutation with a pro-proliferative signature of mTORC1 activation and high Myc expression therefore correlates with the transition to a neoplastic state.

While approximately 1 in 10 ccRCC tumours harbour *TP53* mutations, in many epithelial malignancies the *TP53* mutation frequency is much higher (50–90%). In ccRCC, several mechanisms have been proposed to act to compromise p53 function, potentially alleviating the selective pressure for *TP53* mutation or deletion during tumour formation. USP10 normally de-ubiquitinates p53 in response to DNA damage, opposing the action of Mdm2 and allowing p53 protein accumulation (Yuan et al, 2010). Interestingly, 90% of ccRCC express lower than normal levels of USP10, possibly leading to reduced p53 activation (Yuan et al, 2010). pVHL itself has been implicated as a factor important for full p53 activation by promoting the recruitment of the p300 acetylase and ATM kinase to p53 (Roe et al, 2006). Knockdown of *VHL* expression reduced p53 activity in response to DNA damage and reintroduction of pVHL expression in *VHL*-deficient RCC cells enhanced damage-induced activation of p53 (Roe et al, 2006). Downstream of loss of pVHL function, activation of HIFα transcription factors may also act to compromise p53 activity. The hypoxia-inducible *PAX2* gene is a transcriptional repressor of *TP53* and is highly upregulated in *VHL* mutant cells and ccRCCs (Luu et al, 2009; Stuart et al, 1995). Elevated HIF2α levels in *VHL*-mutant ccRCC are proposed to induce growth factor expression leading firstly

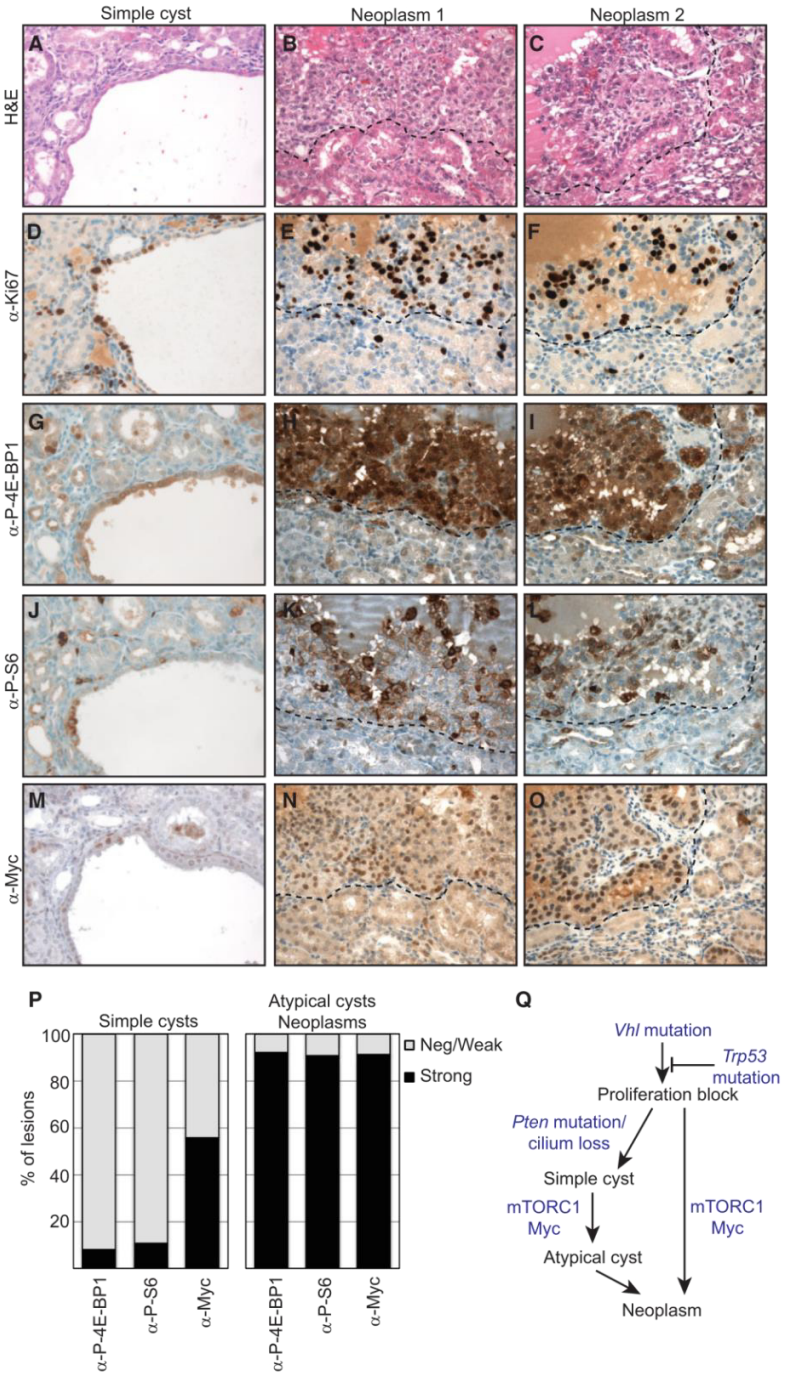

Figure 6.

to the AKT-mediated phosphorylation of HDM2, promoting its ability to degrade p53 (Roberts et al, 2009) or secondly to the suppression of formation of reactive oxygen species which reduce p53 activation (Bertout et al, 2009). *PBRM1* is mutated in 41% of ccRCCs (Varela et al, 2011) and has been shown to be necessary for induction of senescence by p53 (Burrows et al, 2010), thus potentially abrogating part of p53's tumour suppressing activity in the kidney. In our hands however, knockdown of *Pbrm1* failed to alleviate proliferative arrest following *Vhl* knockout in MEFs (unpublished observations). Similarly, *SETD2* is mutated in a small fraction of ccRCCs (Dalgliesh et al, 2010) and has been suggested to regulate a subset of p53 target genes (Xie et al, 2008). Thus, p53 function may either be lost by mutation or compromised by other mechanisms in a large proportion of *VHL*-negative ccRCCs.

It will be important to clarify when *TP53* mutations arise during the process of tumour initiation and progression. In this regard, a study of four ccRCCs utilized deep sequencing of the tumour DNA population to reconstruct the molecular evolutionary history of the tumours (Gerstung et al, 2012). In one of these tumours a single *TP53* truncation mutation was present at about one-fifteenth the frequency of a single *VHL* frameshift mutation, implying that the *TP53* mutation was an event that occurred secondarily to an initiating *VHL* mutation and that it resulted in the formation of a *VHL/TP53* double mutant subclone of the tumour cell population. This finding supports the notion that genetic cooperation between *VHL* and *TP53* mutations promotes tumour progression. Similar analyses of larger numbers of ccRCC samples from different stages of disease progression would test how representative this initial finding is for ccRCCs in general.

In summary, we present strong evidence to support the idea that loss of function of *VHL* and *TP53* is a *bone fide* tumour promoting combination and describe a mouse model that recapitulates many of the steps involved in the formation of *VHL* mutant kidney tumours in humans.

MATERIALS AND METHODS

Mouse genetics

Previously described *Ksp1.3-Cre/+*; $Vhl^{fl/fl}$ (Frew et al, 2008b) and *Ksp1.3-Cre/+*; $Trp53^{fl/fl}$ (Wild et al, 2012) mouse strains were interbred to generate *Ksp1.3-Cre/+*; $Vhl^{fl/fl}$; $Trp53^{fl/fl}$ mice. Non-Cre transgenic littermate mice served as controls for all cohorts. Wild-type cells were isolated from C57BL/6 embryos.

Analyses of human ccRCCs

Tissue samples were from the University Hospital of Zurich (Zurich, Switzerland). The study was approved by the local ethics commission (reference number StV 38-2005). Haematoxylin and eosin stained sections of all paraffin embedded ccRCC specimens were reviewed by H.M. DNA extraction and *VHL* sequencing were performed as previously described (von Teichman et al, 2011). The primers used for PCR and sequencing of *TP53* exons 5–8 are listed in Supporting Information Table S1. PCR was performed with 40 cycles consisting of denaturation at 94°C for 45 s, annealing at 58°C for 45 s and extension at 72°C for 45 s. *VHL* and *TP53* mutations were validated by an independent PCR and sequence analysis. Paraffin sections (2.5 μm) were treated using Ventana Benchmark XT (Tuscon, AZ, USA) or BOND-MAX (Leica Microsystems, Wetzlar, Germany) automated systems. Immunostainings for CAIX, GLUT1 and HIF1α were performed as recently described (Dahinden et al, 2010; Luu et al, 2009). Nuclear HIF1α and membranous CAIX, GLUT1 expression were defined positive if at least 5% of tumour cells showed weak (+1) or strong (+2) staining.

Assays of MEFs

MEFs were isolated from relevant floxed strains and aliquots were frozen at passage 2. $Trp53^{-/-}$ MEFs were a kind gift from Scott Lowe. Cells were cultured either in conventional cell culture incubators at atmospheric oxygen or at 5% oxygen or were cultured in a darkened oxygen glove-box incubator ($INVIVO_2$ 400, Ruskinn) at 5% oxygen in which medium and PBS were equilibrated for 2 h prior to splitting of cells to ensure that cells were exposed to constant oxygen tension throughout the experiment. For proliferation assays, cells were seeded at densities of either 2×10^5 or 3×10^5 cells per 6 cm dish in triplicate dishes and counted after 3 days before reseeding at the same density for the next passage. All proliferation assays shown in the Figures are representative of at least three independent experiments. Wild-type and $Vhl^{fl/fl}$ MEFs were transformed by transfection with a plasmid expressing SV40 large T-Antigen (Addgene, pBSSVD2005) and pools of cells that formed colonies after plating at low density were harvested to generate cell lines. Cells were infected with adenoviruses expressing GFP (Vector Biolabs, 1060) or Cre-GFP (Vector Biolabs, 1700), retroviruses (LMP) expressing non-silencing hairpin or miR30-shRNA against *Trp53* (Dickins et al, 2005), lentiviruses (LKO.1) expressing non-silencing hairpin (Addgene, 10879) or shRNA against *Vhl* (Open Biosystems, TRC0000009735) (Thoma et al, 2007). For lentiviral-mediated knockdown of *Trp53*, we generated a vector (pLenti X1 Puro DEST, Addgene 17297) containing the U6 promoter (derived from pENTR/pSM2 (U6), Addgene 17387) driving expression of a previously described (Dickins et al, 2005) miR30 format shRNA against *Trp53* (1224) or expressing an empty (ns) miR30 backbone. Infections were followed after 48 h by puromycin selection (4 μg/ml) where appro-

Figure 6. mTORC1 activation and Myc expression signature in atypical cysts and neoplasms.

A–O. Serial sections of a simple cyst (A,D,G,J,M) and two neoplasms (B,E,H,K,N and C,F,I,L,O) stained with H&E (A–C) or stained immunohistochemically for Ki67 (D–F), phospho-Thr37/46-4E-BP1 (G–I), phospho-Ser240/244-ribosomal S6 protein (J–L) or Myc (M–O). Dotted lines indicate the boundary of normal tissue and neoplasms.

P. Quantification of the percentage of simple cysts ($n = 68–185$) or atypical cysts and neoplasms ($n = 34–51$) that display higher levels (strong) of staining than adjacent normal tissue in the same section (negative/weak).

Q. Model summarising the proposed sequence of morphological and molecular alterations involved in formation of ccRCC. For details see the Discussion Section.

The paper explained

PROBLEM:

The cooperating genetic events that lead to the formation of clear cell renal cell carcinoma (ccRCC), the most frequent form of kidney cancer in humans, remain unclear. While the vast majority of familial and sporadic forms of ccRCC harbour biallelic inactivation of the von Hippel–Lindau tumour suppressor gene (*VHL*), loss of *VHL* function alone in humans and in mice is insufficient to cause kidney tumour formation. It is presumed that other genetic events must cooperate with loss of *VHL* to cause ccRCC but these cooperating mutations remain poorly understood.

RESULTS:

Here we identify loss of function mutations in *TP53* in a subset of sporadic human ccRCCs and show that kidney-specific combined deletion of *Vhl* and *Trp53* leads to the formation of cysts and tumours in mice, recapitulating the precursor lesions and cellular and molecular alterations that are involved in the formation of *VHL* mutant ccRCC in humans.

IMPACT:

These findings provide the first demonstration that secondary genetic alterations can cooperate with loss of *VHL* to cause kidney tumour formation and implicate *TP53* mutations in the pathogenesis of a subset of human ccRCC.

priate. Genotyping for the floxed or recombined *Vhl* and *Trp53* alleles were performed as described (Biju et al, 2004; Jonkers et al, 2001). Flow cytometry (Frew et al, 2002) and counting of aberrant anaphases (Burds et al, 2005) were performed as described.

Real-time PCR

Real-time PCR was performed as described (Frew et al, 2008b) using the following primer pairs: *18S rRNA* (5′-TGGCCGACCATAAACGATGCC-3′, 5′-TGGTGGTGCCCTTCCGTCAAT-3′), *Mad2* (5′-GTGGCCGAGTTTTTCT-CATTTG-3′, 5′-AGGTGAGTCCATATTTCTGCACT-3′).

Kidney epithelial cell proliferation assays

Kidneys were dissected from 2-month-old floxed mice. After removing the capsule under sterile conditions, kidneys were mashed with a razor blade on ice and digested in collagenase II (Gibco) and soya trypsin inhibitor (Gibco) solution at 37°C for 30 min. The cell suspension was filtered through a 70 μm cell strainer and washed in HBSS + 5% FCS. Erythrocytes were lysed for 1 min using standard ACK buffer. Cells were resuspended in complete K-1 culture medium [Dulbecco's modified Eagle's medium (DMEM):Hams F12] (50:50), supplemented with 0.5% foetal calf serum, hormone mix [5 μg/ml insulin, 1.25 ng/ml prostaglandin E_1 (PGE_1), 34 pg/ml triiodothyronine, 5 μg/ml Apo-transferrin, 1.73 ng/ml sodium selenite and 18 ng/ml of hydrocortisone] and 25 ng/ml epidermal growth factor (EGF). Cells were counted and seeded at a density of 1×10^6 cells on standard 100 mm plastic tissue culture plates. After 5–6 days in culture, cells were infected with adenoviruses expressing GFP (Vector Biolabs, 1060) or Cre-GFP (Vector Biolabs, 1700). Sulforhodamine B (SRB) proliferation assay was performed in 96-well format as described (Vichai & Kirtikara, 2006). Briefly, primary kidney epithelial cells were cultured in K-1 medium containing 10% foetal calf serum for 2 days before seeding for the SRB assay. 2×10^3 cells per well were seeded and fixed in 5% w/v trichloracetic acid at the indicated time points. Cells were stained in 0.057% w/v SRB solution and air dried. SRB was solubilized by incubation in 10 mM Tris base solution (pH 10.5) and OD was measured at 540 nm in a micro-plate reader.

Antibodies, Western blotting, immunofluorescence and immunohistochemistry

Western blotting, immunohistochemistry or immunofluorescence were conducted using previously described methods (Frew et al, 2008b) and the antibodies against the following epitopes: Acetylated tubulin (Sigma, #T6793), Actin (Sigma-Aldrich, A2228), AQP2 (Wagner et al, 2008), Aurora A (Abcam, ab13824), BubR1 (BD Biosciences, 612502), CDK-2 (Santa Cruz, sc-163-g), Cenp-E (Meraldi et al, 2004), E-cadherin (Abcam, ab11512), phospho-Thr37/46-4E-BP1 (Cell Signaling Technology, #2855), HIF1α (Novus Biologicals, NB100-105), HIF2α (Pollard et al, 2007, PM8), Ki67 (DakoCytomation, TEC-3), Mad2 (Bethyl Laboratories, A300301A), Myc (Epitomics, Y69), p53 (Novocastra, NCL-p53-CM5p), NaPi2 (Custer et al, 1994), NCC (Millipore, AB3553), phospho-Ser240/244-ribosomal S6 protein (Cell Signaling Technology, #2215), THP (Santa Cruz Biotechnology, sc-20631), $pVHL(m)_{CT}$ antibody (Hergovich et al, 2003), pVHL (Santa Cruz, sc-5575), Vimentin (Cell Signaling Technology, #5741).

Author contributions

IJF and WK designed the study, IJF, JA, MR, DS, SH, PS, AvT and SG conducted and analysed the experiments, PJW and HM performed histopathological analyses and the manuscript was written by IJF with the assistance of all authors.

Acknowledgements

This work was supported by grants to I.J.F. from SNF Förderungsprofessur (PP00P3_128257) and ERC Starting Grant (260316), to J.A. from the European Community's Seventh Framework Programme (FP7/2007-2013) under grant agreement no. 246539, and to W.K. from the SNF. We are grateful to Johannes Loffing and Jürg Biber for providing antibodies and to the Centre for Microscopy and Imaging Analysis, University of Zurich for assistance with laser capture microdissection.

Supporting Information is available at EMBO Molecular Medicine online.

The authors declare that they have no conflicts of interest.

For more information

For information about the VHL Family Alliance for patients with inherited VHL disease:

http://www.vhl.org

For general information about kidney cancer subtypes and treatments:

http://www.cancer.gov/cancertopics/types/kidney

For information about the genetic mutations that have been found in ccRCC:

http://www.sanger.ac.uk/perl/genetics/CGP/cgp_viewer?action=study;study_id=321

http://www.sanger.ac.uk/genetics/CGP/Studies/Renal/

http://www.sanger.ac.uk/perl/genetics/CGP/cosmic?action=by-hist&s=4&hn=carcinoma&sn=kidney&sh=clear_cell_renal_cell_carcinoma

References

Bertout JA, Majmundar AJ, Gordan JD, Lam JC, Ditsworth D, Keith B, Brown EJ, Nathanson KL, Simon MC (2009) HIF2alpha inhibition promotes p53 pathway activity, tumor cell death, and radiation responses. Proc Natl Acad Sci USA 106: 14391-14396

Biju MP, Neumann AK, Bensinger SJ, Johnson RS, Turka LA, Haase VH (2004) Vhlh gene deletion induces Hif-1-mediated cell death in thymocytes. Mol Cell Biol 24: 9038-9047

Burds AA, Lutum AS, Sorger PK (2005) Generating chromosome instability through the simultaneous deletion of Mad2 and p53. Proc Natl Acad Sci USA 102: 11296-11301

Burrows AE, Smogorzewska A, Elledge SJ (2010) Polybromo-associated BRG1-associated factor components BRD7 and BAF180 are critical regulators of p53 required for induction of replicative senescence. Proc Natl Acad Sci USA 107: 14280-14285

Custer M, Lotscher M, Biber J, Murer H, Kaissling B (1994) Expression of Na-P(i) cotransport in rat kidney: localization by RT-PCR and immunohistochemistry. Am J Physiol 266: F767-F774

Dahinden C, Ingold B, Wild P, Boysen G, Luu VD, Montani M, Kristiansen G, Sulser T, Buhlmann P, Moch H, *et al* (2010) Mining tissue microarray data to uncover combinations of biomarker expression patterns that improve intermediate staging and grading of clear cell renal cell cancer. Clin Cancer Res 16: 88-98

Dalgliesh GL, Furge K, Greenman C, Chen L, Bignell G, Butler A, Davies H, Edkins S, Hardy C, Latimer C, *et al* (2010) Systematic sequencing of renal carcinoma reveals inactivation of histone modifying genes. Nature 463: 360-363

Dickins RA, Hemann MT, Zilfou JT, Simpson DR, Ibarra I, Hannon GJ, Lowe SW (2005) Probing tumor phenotypes using stable and regulated synthetic microRNA precursors. Nat Genet 37: 1289-1295

Eble JN, Sauter G, Epstein JI, Sesterhehn IA (2004) *World Health Organisation Classification of Tumours: Pathology and Genetics of Tumours of the Urinary System and Male Genital Organs.* Lyon: IARC Press

Esteban MA, Tran MG, Harten SK, Hill P, Castellanos MC, Chandra A, Raval R, O'Brien TS, Maxwell PH (2006) Regulation of E-cadherin expression by VHL and hypoxia-inducible factor. Cancer Res 66: 3567-3575

Frew IJ, Dickins RA, Cuddihy AR, Del Rosario M, Reinhard C, O'Connell MJ, Bowtell DD (2002) Normal p53 function in primary cells deficient for Siah genes. Mol Cell Biol 22: 8155-8164

Frew IJ, Krek W (2007) Multitasking by pVHL in tumour suppression. Curr Opin Cell Biol 19: 685-690

Frew IJ, Minola A, Georgiev S, Hitz M, Moch H, Richard S, Vortmeyer AO, Krek W (2008a) Combined VHLH and PTEN mutation causes genital tract cystadenoma and squamous metaplasia. Mol Cell Biol 28: 4536-4548

Frew IJ, Thoma CR, Georgiev S, Minola A, Hitz M, Montani M, Moch H, Krek W (2008b) pVHL and PTEN tumour suppressor proteins cooperatively suppress kidney cyst formation. EMBO J 27: 1747-1757

Gerstung M, Beisel C, Rechsteiner M, Wild P, Schraml P, Moch H, Beerenwinkel N (2012) Reliable detection of subclonal single-nucleotide variants in tumour cell populations. Nat Commun 3: 811

Guo G, Gui Y, Gao S, Tang A, Hu X, Huang Y, Jia W, Li Z, He M, Sun L, *et al* (2012) Frequent mutations of genes encoding ubiquitin-mediated proteolysis pathway components in clear cell renal cell carcinoma. Nat Genet 44: 17-19

Haase VH, Glickman JN, Socolovsky M, Jaenisch R (2001) Vascular tumors in livers with targeted inactivation of the von Hippel-Lindau tumor suppressor. Proc Natl Acad Sci USA 98: 1583-1588

Hergovich A, Lisztwan J, Barry R, Ballschmieter P, Krek W (2003) Regulation of microtubule stability by the von Hippel-Lindau tumour suppressor protein pVHL. Nat Cell Biol 5: 64-70

Hsieh AC, Liu Y, Edlind MP, Ingolia NT, Janes MR, Sher A, Shi EY, Stumpf CR, Christensen C, Bonham MJ, *et al* (2012) The translational landscape of mTOR signalling steers cancer initiation and metastasis. Nature 485: 55-61

Hudes GR (2009) Targeting mTOR in renal cell carcinoma. Cancer 115: 2313-2320

Jonkers J, Meuwissen R, van der Gulden H, Peterse H, van der Valk M, Berns A (2001) Synergistic tumor suppressor activity of BRCA2 and p53 in a conditional mouse model for breast cancer. Nat Genet 29: 418-425

Kaelin WG, Jr (2002) Molecular basis of the VHL hereditary cancer syndrome. Nat Rev Cancer 2: 673-682

Lubensky IA, Gnarra JR, Bertheau P, Walther MM, Linehan WM, Zhuang Z (1996) Allelic deletions of the VHL gene detected in multiple microscopic clear cell renal lesions in von Hippel-Lindau disease patients. Am J Pathol 149: 2089-2094

Luu VD, Boysen G, Struckmann K, Casagrande S, von Teichman A, Wild PJ, Sulser T, Schraml P, Moch H (2009) Loss of VHL and hypoxia provokes PAX2 up-regulation in clear cell renal cell carcinoma. Clin Cancer Res 15: 3297-3304

Mack FA, Patel JH, Biju MP, Haase VH, Simon MC (2005) Decreased growth of Vhl−/− fibrosarcomas is associated with elevated levels of cyclin kinase inhibitors p21 and p27. Mol Cell Biol 25: 4565-4578

Maher ER (2013) Genomics and epigenomics of renal cell carcinoma. Semin Cancer Biol 23: 10-17

Mandriota SJ, Turner KJ, Davies DR, Murray PG, Morgan NV, Sowter HM, Wykoff CC, Maher ER, Harris AL, Ratcliffe PJ, *et al* (2002) HIF activation identifies early lesions in VHL kidneys: evidence for site-specific tumor suppressor function in the nephron. Cancer Cell 1: 459-468

Mao JH, Wu D, Perez-Losada J, Jiang T, Li Q, Neve RM, Gray JW, Cai WW, Balmain A (2007) Crosstalk between Aurora-A and p53: frequent deletion or downregulation of Aurora-A in tumors from p53 null mice. Cancer Cell 11: 161-173

Meraldi P, Draviam VM, Sorger PK (2004) Timing and checkpoints in the regulation of mitotic progression. Dev Cell 7: 45-60

Montani M, Heinimann K, von Teichman A, Rudolph T, Perren A, Moch H (2010) VHL-gene deletion in single renal tubular epithelial cells and renal tubular cysts: further evidence for a cyst-dependent progression pathway of clear cell renal carcinoma in von Hippel-Lindau disease. Am J Surg Pathol 34: 806-815

Monzon FA, Alvarez K, Peterson L, Truong L, Amato RJ, Hernandez-McClain J, Tannir N, Parwani AV, Jonasch E (2011) Chromosome 14q loss defines a molecular subtype of clear-cell renal cell carcinoma associated with poor prognosis. Mod Pathol 24: 1470-1479

Parrinello S, Samper E, Krtolica A, Goldstein J, Melov S, Campisi J (2003) Oxygen sensitivity severely limits the replicative lifespan of murine fibroblasts. Nat Cell Biol 5: 741-747

Pati D, Haddad BR, Haegele A, Thompson H, Kittrell FS, Shepard A, Montagna C, Zhang N, Ge G, Otta SK, *et al* (2004) Hormone-induced chromosomal instability in p53-null mammary epithelium. Cancer Res 64: 5608-5616

Pena-Llopis S, Vega-Rubin-de-Celis S, Liao A, Leng N, Pavia-Jimenez A, Wang S, Yamasaki T, Zhrebker L, Sivanand S, Spence P, *et al* (2012) BAP1 loss defines a new class of renal cell carcinoma. Nat Genet 44: 751-759

Pollard PJ, Spencer-Dene B, Shukla D, Howarth K, Nye E, El-Bahrawy M, Deheragoda M, Joannou M, McDonald S, Martin A, *et al* (2007) Targeted inactivation of fh1 causes proliferative renal cyst development and activation of the hypoxia pathway. Cancer Cell 11: 311-319

Rankin EB, Tomaszewski JE, Haase VH (2006) Renal cyst development in mice with conditional inactivation of the von Hippel-Lindau tumor suppressor. Cancer Res 66: 2576-2583

Roberts AM, Watson IR, Evans AJ, Foster DA, Irwin MS, Ohh M (2009) Suppression of hypoxia-inducible factor 2alpha restores p53 activity via Hdm2 and reverses chemoresistance of renal carcinoma cells. Cancer Res 69: 9056-9064

Roe JS, Kim H, Lee SM, Kim ST, Cho EJ, Youn HD (2006) p53 stabilization and transactivation by a von Hippel-Lindau protein. Mol Cell 22: 395-405

Stuart ET, Haffner R, Oren M, Gruss P (1995) Loss of p53 function through PAX-mediated transcriptional repression. EMBO J 14: 5638-5645

Tang SW, Chang WH, Su YC, Chen YC, Lai YH, Wu PT, Hsu CI, Lin WC, Lai MK, Lin JY (2009) MYC pathway is activated in clear cell renal cell carcinoma and essential for proliferation of clear cell renal cell carcinoma cells. Cancer Lett 273: 35-43

Thoma CR, Frew IJ, Hoerner CR, Montani M, Moch H, Krek W (2007) pVHL and GSK3beta are components of a primary cilium-maintenance signalling network. Nat Cell Biol 9: 588-595

Thoma CR, Toso A, Gutbrodt KL, Reggi SP, Frew IJ, Schraml P, Hergovich A, Moch H, Meraldi P, Krek W (2009) VHL loss causes spindle misorientation and chromosome instability. Nat Cell Biol 11: 994-1001

Varela I, Tarpey P, Raine K, Huang D, Ong CK, Stephens P, Davies H, Jones D, Lin ML, Teague J, *et al* (2011) Exome sequencing identifies frequent mutation of the SWI/SNF complex gene PBRM1 in renal carcinoma. Nature 469: 539-542

Vichai V, Kirtikara K (2006) Sulforhodamine B colorimetric assay for cytotoxicity screening. Nat Protoc 1: 1112-1116

von Teichman A, Comperat E, Behnke S, Storz M, Moch H, Schraml P (2011) VHL mutations and dysregulation of pVHL- and PTEN-controlled pathways in multilocular cystic renal cell carcinoma. Mod Pathol 24: 571-578

Wagner CA, Loffing-Cueni D, Yan Q, Schulz N, Fakitsas P, Carrel M, Wang T, Verrey F, Geibel JP, Giebisch G, *et al* (2008) Mouse model of type II Bartter's syndrome. II. Altered expression of renal sodium- and water-transporting proteins. Am J Physiol Renal Physiol 294: F1373-F1380

Walther MM, Lubensky IA, Venzon D, Zbar B, Linehan WM (1995) Prevalence of microscopic lesions in grossly normal renal parenchyma from patients with von Hippel-Lindau disease, sporadic renal cell carcinoma and no renal disease: clinical implications. J Urol 154: 2010-2014; discussion 2014–2015

Welford SM, Dorie MJ, Li X, Haase VH, Giaccia AJ (2010) Renal oxygenation suppresses VHL loss-induced senescence that is caused by increased sensitivity to oxidative stress. Mol Cell Biol 30: 4595-4603

Wild PJ, Ikenberg K, Fuchs TJ, Rechsteiner M, Georgiev S, Fankhauser N, Noske A, Roessle M, Caduff R, Dellas A, *et al* (2012) p53 suppresses type II endometrial carcinomas in mice and governs endometrial tumour aggressiveness in humans. EMBO Mol Med 4: 808-824

Xie P, Tian C, An L, Nie J, Lu K, Xing G, Zhang L, He F (2008) Histone methyltransferase protein SETD2 interacts with p53 and selectively regulates its downstream genes. Cell Signal 20: 1671-1678

Young AP, Schlisio S, Minamishima YA, Zhang Q, Li L, Grisanzio C, Signoretti S, Kaelin WG, Jr (2008) VHL loss actuates a HIF-independent senescence programme mediated by Rb and p400. Nat Cell Biol 10: 361-369

Yuan J, Luo K, Zhang L, Cheville JC, Lou Z (2010) USP10 regulates p53 localization and stability by deubiquitinating p53. Cell 140: 384-396

8.2 Hif1α stabilization exerts anti-proliferative activities but is necessary for tumour formation

8.2.1 Hif1α reduces oxidative phosphorylation, ATP levels and cellular proliferation but is necessary for initiation of renal cysts and tumours (Manuscript)

Désirée Schönenberger[1], Michal Rajski[1,#], Sabine Harlander[1,2,#], Robert A. Jacobs[1,2], Anne-Kristine Lundby[1,2], Carsten Lundby[1,2] and Ian J. Frew[1,2]

[1] Institute of Physiology, University of Zurich, Zurich, Switzerland

[2] Zurich Center for Integrative Human Physiology, University of Zurich, Zurich, Switzerland

[#] These authors contributed equally

Character count: 53 398

Address for correspondence:

Ian Frew

Institute of Physiology

University of Zurich

Winterthurerstrasse 190

CH-8057 Zurich

Switzerland

Phone: +41 44 635 5004

Fax: +41 44 635 6814

Email: ian.frew@access.uzh.ch

Abstract

The von Hippel-Lindau (*VHL*) gene is biallelically inactivated in most cases of clear cell renal cell carcinoma (ccRCC). The protein product of the *VHL* locus, pVHL, possesses numerous potential tumor suppressor functions, including regulation of the HIF1α and HIF2α transcription factors. However, *Vhl* deletion in mice does not cause renal tumors. Allelic losses of *HIF1A* in *VHL* null ccRCC predict poor patient outcome and HIF1α inhibits, while HIF2α promotes the growth of human ccRCC xenograft tumors, suggesting that HIF1α may function as a tumor suppressor and HIF2α as an oncogene. Consistent with this idea, we show that stabilization of Hif1α, but not Hif2α, alters glucose metabolism resulting in reduced oxygen consumption and ATP levels in *Vhl* mutant primary fibroblasts and in mouse kidneys. Correlating with this energy deficiency, deletion of *Vhl* induces *Hif1a*-dependent, *Hif2a*-independent senescence in primary fibroblasts and inefficient proliferation in immortalized and transformed fibroblasts. However, renal epithelial-specific double deletion of *Vhl*/*Hif1a* or *Vhl*/*Hif2a* does not induce proliferative dysregulation or tumor formation in mouse kidneys. In contrast to its postulated tumor suppressor function, co-deletion of *Hif1a* prevents the formation of cysts and neoplasms in *Vhl/Trp53* double mutant kidneys, showing that *Hif1a* is essential for the first stages of tumor formation. Thus, disruption of the balance of Hif1α and Hif2α signaling together with loss of pVHL's many putative tumor suppressor functions are insufficient to induce ccRCC in mice. Rather, Hif1α stabilization is necessary for the initiation of tumorigenesis.

Introduction

Clear cell renal cell carcinoma (ccRCC) is the most frequent subtype of renal cell carcinoma and up to 92% of ccRCC tumors harbor biallelic inactivation of the von Hippel-Lindau (*VHL*) tumor suppressor gene (Sato et al. 2013). Deep sequencing analyses of intratumoral genetic heterogeneity show that *VHL* mutations represent so-called trunk mutations, indicating that they occur at the earliest stage of tumor formation (Gerlinger et al. 2012; 2014). While studies of ccRCC cell lines grown as xenograft tumors have clearly demonstrated that the absence of pVHL function is necessary for the efficient growth of these fully transformed cell lines in this experimental setting (Iliopoulos et al. 1995; Gnarra et al. 1996), it is also apparent that losing *VHL* function alone is not sufficient to initiate tumor formation from a normal renal epithelial cell in the kidney. This idea is supported by detailed analyses of the relative frequencies of *VHL* mutant single cells in the context of normal kidney tubules compared to the number of ccRCC tumors in kidneys of familial VHL disease patients (Mandriota et al. 2002) and by numerous mouse genetic studies showing that deletion of *Vhl* in renal tubular epithelial cells does not cause tumor formation (Kleymenova 2003; Iguchi et al. 2008; Ma et al. 2003;Rankin et al. 2006;Mathia et al. 2013; Schietke et al. 2012; Frew et al. 2008;Schley et al. 2011; Pritchett et al. 2014). ccRCC tumors frequently harbor mutations in numerous other genes that likely cooperate with loss of *VHL* function to induce tumor initiation and progression (Creighton et al. 2013; Sato et al. 2013). Consistent with this idea, the kidney epithelial cell-specific co-deletion of *Vhl* with *Pten* or *Trp53*, mouse homologs of tumor suppressor genes that are mutated or deleted in human ccRCC, caused the formation of cystic and/or neoplastic lesions that are similar to the lesions that are believed to represent the precursor lesions of ccRCC in human kidneys (Frew et al. 2008; Albers et al. 2013).

The protein encoded by the *VHL* gene, pVHL, controls many biological activities including regulation of the stability of the hypoxia-inducible transcription factors α (HIF1α and HIF2α) (Maxwell et al. 1999), regulation of NFκB activity (Yang et al. 2007), maintenance of the primary cilium (Thoma et al. 2007), activation of p53 (Roe et al. 2006), secretion of extracellular matrix components (Kurban et al. 2008; Ohh et al. 1998), promotion of DNA double strand repair (Metcalf et al. 2013), regulation of the plane of cellular division (Thoma et al. 2009; Hell et al. 2013) and suppression of aneuploidy (Thoma et al. 2009; Hell et al. 2014). It appears likely that the combined loss of all or many of pVHL's functions could contribute to tumor initiation and progression. Of these many potential tumor suppressor activities, the best understood is pVHL's function as the substrate recognition subunit of an E3-ubiquitin ligase complex comprising Elongin B, Elongin C, Rbx1 and Cul2, that targets HIF1α and HIF2α for oxygen-dependent,

ubiquitin-mediated proteolytic degradation (Keith and Simon 2007; Keith et al. 2012; Wenger et al. 2005; Qing and Simon 2009). Loss of function mutations of *VHL* occur in ccRCC mutually exclusively to mutations in *TCEB1*, encoding Elongin C (Sato et al. 2013), and collectively these cause constitutive stabilization of HIF1α and HIF2α in 95% of ccRCC tumors, implying that HIFα activation is a major oncogenic driving force in ccRCC. Indeed, HIF2αis necessary for the growth of *VHL*-deficient ccRCC cell lines as xenografts (Kondo et al. 2003; Raval et al. 2005; Zimmer et al. 2004). Several recent studies have suggested that HIF1α and HIF2α play opposite roles in the context of ccRCC progression. HIF1α inhibits, whereas HIF2α promotes, the proliferation of mouse embryo fibroblasts (Gordan et al. 2007), tumor formation in ccRCC xenografts (Kondo et al. 2003; Raval et al. 2005; Zimmer et al. 2004) and activity of the cell cycle promoting MYC oncoprotein (Gordan et al. 2007). Consistent with the idea that the balance of HIF1α and HIF2α activities might control cellular proliferation of *VHL* null ccRCC tumors, early lesions in VHL patient kidneys predominantly express HIF1α whereas more advanced lesions often express higher levels of HIF2α (Raval et al. 2005). Sporadic ccRCCs expressing HIF1α and HIF2α exhibit reduced MYC activity and lower proliferation rates in comparison to ccRCC cases expressing only HIF2α (Gordan et al. 2008). This apparent shift in the HIF1α/HIF2α balance during ccRCC progression may arise in some cases due to single copy loss of the chromosomal locus harboring the *HIF1A* gene which predicts poor patient outcome (Monzon et al. 2011). ccRCC cell lines frequently express only HIF2α and do not express functional HIF1α due to biallelic alterations of the *HIF1A* locus (Shen et al. 2011). The *VHL* mutant RCC4 cell line is one exception that expresses both wild type HIF1α and HIF2α and knockdown of *HIF1A* in these cells promotes xenograft tumor formation (Shen et al. 2011). Collectively, these studies argue that there is a selection against HIF1α expression or activity during the progression of ccRCC and that HIF1α may act to restrain ccRCC progression whereas HIF2α activity is tumor promoting. These studies however have largely focused on fully transformed, genetically complex ccRCC cell lines derived from advanced tumors. It remains unclear if and how HIF1α and HIF2α contribute to the initiation of ccRCC from cells that initially harbor only mutations in the *VHL* gene.

One of the earliest events following *VHL* mutation is likely to be a profound alteration of cellular metabolic pathways. Numerous HIF1α and/or HIF2α-dependent metabolic changes have recently been reported in ccRCC cell lines, including elevated glucose uptake and conversion to lactate with a concomitant reduction in mitochondrial oxidation of pyruvate, reduced mitochondrial biogenesis, reduced mitochondrial complex I activity, altered cytochrome oxidase activity, increased pentose phosphate pathway flux, decreased oxidative glutaminolysis and increased lipogenesis through reductive glutamine metabolism (Iyer et al. 1998; Papandreou et al. 2006; Kim et al. 2006; Langbein et al. 2008; Luo et al. 2011; Zhang et al. 2007; Metallo et al. 2012; Chan

et al. 2011; Sun and Denko 2014; Tello et al. 2011; Fukuda et al. 2007). A potential confounding factor in the interpretation of these studies is that the ccRCC cell lines that were employed have complex genetic backgrounds that arose during tumor evolution. Some of these mutations potentially represent adaptive mechanisms that were selected because they allow cells to proliferate efficiently in the background of the numerous metabolic pathway constraints that appear to be imposed by constitutive HIFα activity. For example, ccRCCs frequently harbor activating mutations in the PI3K-mTORC1 pathway, inactivating *TP53* mutations or exhibit high levels of MYC expression (Sato et al. 2013; Creighton et al. 2013), all of which are known to influence numerous cellular metabolic pathways (Vander Heiden et al. 2009; Levine and Puzio-Kuter 2010). The contributions of metabolic alterations following *VHL* mutation, in otherwise genetically normal cells, to the earliest stages of tumor formation remain unknown.

Given the apparent importance of correct regulation of HIF1α and HIF2α activities in the kidney epithelium in the context of regulation of metabolism and development of ccRCC tumors, we undertook a systematic approach to genetically delete *Hif1a* or *Hif2a*, alone or together with *Vhl* in renal epithelial cells in mice. We show that while Hif1α activity induces metabolic changes resulting in energy deficiency and inefficient proliferation of cultured primary cells, deletion of *Hif1a* together with *Vhl* is not sufficient to cause kidney tumor formation, arguing that Hif1α activity alone is not a barrier that prevents tumor formation by *Vhl* null kidney cells. In fact, in the tumor-prone *Vhl/Trp53* mutant background, *Hif1a* co-deletion prevented the formation of cysts and neoplasms, arguing that stabilization of Hif1α is essential for the initial stages of tumor formation in the kidney.

Materials and Methods

Mouse strains

Hif1a$^{fl/fl}$ (Ryan et al. 2000) and *Hif2a*$^{fl/fl}$ (Gruber et al. 2007) mice were crossed with *Ksp1.3-Cre;Vhl*$^{fl/fl}$ (Frew et al. 2008), *Ksp1.3-Cre;Vhl*$^{fl/fl}$*;Trp53*$^{fl/fl}$ (Albers et al. 2013) or *Ksp1.3-Cre/+* (Shao et al. 2002a; Patel et al. 2008)(Patel et al. 2008) mice to generate the following mouse lines: *Ksp1.3-Cre/+;Hif1a*$^{fl/fl}$, *Ksp1.3-Cre/+;Hif2a*$^{fl/fl}$, *Ksp1.3-Cre/+;Vhl*$^{fl/fl}$*;Hif1a*$^{fl/fl}$, *Ksp1.3-Cre/+;Vhl*$^{fl/fl}$*;Hif2a*$^{fl/fl}$ and *Ksp1.3-Cre/+;Vhl*$^{fl/fl}$*;Hif1a*$^{fl/fl}$; *Trp53*$^{fl/fl}$. Littermate mice that lacked the Cre transgene served as wild type controls. C57BL/6 mice were obtained from Janvier Labs.

Mouse embryo fibroblasts (MEFs)

MEFs were isolated from E13.5 embryos derived from intercrosses of relevant non-Cre expressing floxed mouse strains or C57BL/6 embryos (for wild type MEFs) and cultured in DMEM supplemented with 10% fetal calf serum (FCS), 2 mM glutamine, 10 kU/ml penicillin, 10 mg/ml

streptomycin and 200 µM β-mercaptoethanol at 5% O_2 and 5% CO_2. WT, *Vhl*$^{fl/fl}$ and *Vhl*$^{fl/fl}$ *Hif1α*$^{fl/fl}$ MEFs were transformed by transfection with a plasmid expressing SV40 large T-Antigen (Addgene, pBSSVD2005), followed by six passages of serial low density splitting (1:10). Cellular proliferation assays were performed according to a 3T3 protocol in which cells were plated at 3 x 10^5 cells per 6 cm dish, counted after 3 days and re-plated at the same starting density. MEFs were infected with adenovirus expressing Cre recombinase and GFP (Ad-Cre-GFP, Vector Biolabs, #1700) or GFP only (Ad-CMV-GFP, Vector Biolabs #1060). Lentiviruses (LKO.1) expressing shRNAs against *Hif1α* (Sigma Mission shRNA, TRCN0000232222, TRCN0000232220) or a non-silencing sequence (Addgene, #10879) were titrated based on puromycin resistance after infection of NIH3T3 cells with serial viral dilutions and MEFs were infected using viruses at MOI of 1-3 in the presence of 4 µg/ml polybrene. 48 hours after infection, cells were selected for 2 days in the presence of 4 µg/mL puromycin.

Metabolic assays of MEFs

For ATP measurements, 1.5 x 10^5 trypsinised cells were resuspended in 75 µl PBS and 75 µl assay buffer (CellTiter-Glo Luminescent Cell Viability Assay, Promega). Cells were lysed for 10 min at room temperature and distributed as technical triplicates in an opaque 96-well plate. Luminescence signal was detected with a microplate reader (Anthos Lucy 3). The Seahorse Bioscience XFe96 Extracellular Flux Analyzer (Seahorse Bioscience, North Billerica, MA, USA) was used for the measurement of mitochondrial oxygen consumption and extracellular acidification rate in MEFs. 5 x 10^4 cells were seeded per well in 12 wells of XFe 96-well cell culture microplates in 200 µl of DMEM and incubated for 16 h at 37°C in 20% O_2. The next day the growth medium was replaced with 175 µl of bicarbonate-free DMEM (25 mM glucose, 110 mg/l sodium pyruvate, 2 mM glutamine, pH 7.4) pre-warmed to 37°C. Before starting the assay procedure cells were preincubated at 37°C for 1 hour. For the measurement of oxygen consumption rate (OCR) and extracellular acidification rate (ECAR) 5 cycles of mix/wait/measure times of 3/3/3 minutes were used. Protein abundance per well was determined via Bradford assay and used to normalize OCR and ECAR values. For measurement of glucose utilization and lactate production, 4 x 10^4 cells were plated per well of a 96 well plate, 8 hours later, medium was removed and replaced with 100 µl DMEM supplemented with 10% FCS, 2 mM glutamine and 2 g/L glucose. Glucose and lactate concentrations in the medium after 50 h of culture were determined using Glucose Assay Kit II (Biovision) and Lactate Assay Kit II (Biovision).

High-resolution respirometric analysis

Animals were euthanized with CO_2 and dissected immediately. 1 mm^3 biopsies were taken from

cortex and medulla under the microscope and transferred to ice cold PBS. Wet weight was determined after drying the tissue on a Whatman paper. Biopsies were transferred to modified mitochondrial respiration medium (5 mM $MgCl_2$, 5 mM $KHPO_4^-$, 10 mM HEPES, 70 mM sucrose, 220 M mannitol, 1 mg/ml fatty acid free BSA, pH 7.4) and oxygen consumption was measured using a OROBOROS Oxygraph-2k (ORBOROS INSTRUMENTS Corp, Innsbruck, Austria) according to the following procedure: Leak respiration (LN), representing resting oxygen consumption of an unaltered system, was induced by the addition of malate (2 mM) and octanoyl carnitine (0.2 mM). ADP (5 mM) was added for determination of the maximal electron flow through the electron-transferring flavoprotein (ETF) and fatty acid oxidative capacity (P_{ETF}). P_{CI} (respiratory capacity specific to complex I) was induced by the addition of glutamate (10mM) and pyruvate (5 mM). Maximal state 3 respiration (oxidative phosphorylation capacity P) was measured subsequently to the addition of succinate (10 mM). Finally, complex I was inhibited by rotenone (0.5 µM) to assess maximal state 3 respiration specific to complex II (P_{CII}). Finally, mitochondrial respiration was abrogated by blocking complex III with 2.5 µM antimycin A, allowing the correction of residual O_2. Cytochrome C oxidase activity (complex IV) was assessed by the addition of TMPD (0.5 mM) and Ascorbate (2 mM). Values were calculated using the DatLab OROboros 5.1 software.

Western blotting

Protein extracts from cultured cells or powdered tissues were prepared using RIPA buffer (50 mM Tris–HCl at pH 7.5, 150 mM sodium chloride, 1% NP-40, 1% sodium deoxycholate, 0.1% SDS, 2mM EDTA, 1 mM sodium fluoride, 1 mM Na_3VO_4, 1 mM PMSF, 1 mM dithiothreitol, 1:100 Protease Inhibitor Cocktail). For detection of Hif1α, nuclear extracts were prepared by washing cells once in ice cold PBS, incubating for 20 minutes on ice in lysis buffer (10 mM HEPES, KOH pH 7.9, 10 mM KCl, 0.1 mM EDTA, 0.1 mM EGTA, 1:100 Protease Inhibitor Cocktail (Sigma-Aldrich), 1 mM PMSF) followed by addition of NP-40 to a final concentration of 0.1%, vortexing and centrifuging at 5000 rpm. The nuclear pellet was extracted and incubated for 5 min on ice in protein extraction buffer (400 mM NaCl, 20 mM HEPES, KOH pH 7.9, 1 mM EDTA, 1mM EGTA, 1:100 Protease Inhibitor Cocktail (Sigma-Aldrich 1 mM PMSF). To remove insoluble material all lysates were centrifuged at 14000 g and 4°C for 10 minutes. Western blotting was performed using the following antibodies: Actin (Sigma-Aldrich, A2228), HIF1α (Novus Biologicals, NB100-479), p53 (Novocastra, NCL-p53-CM5p), pVHL (Santa Cruz, sc-5575), PDK1 (ENZO Life Science, ADI-KAP-PK112-D) LDH-A (Santa Cruz Biotechnology, Sc27230), VDAC1 (Abcam, ab15895), FH (Abcam, ab95947).

Immunohistochemistry

Immunohistochemistry of formalin fixed paraffin embedded tissues was performed as previously described (Albers et al. 2013; Frew et al. 2008) using the following antibodies: HIF1α (Novus Biologicals, NB100-105), HIF2α ((Pollard et al. 2007), PM8) and Glut1 (Abcam, Ab14683).

Mitochondrial mass

After trypsinising, cells were washed twice in pre-warmed PBS and incubated for 30 minutes at 37°C with 100 nM nonyl acridine orange (NAO) in PBS with 10% FCS. Samples were analysed by flow cytometry using a FACScanto II machine.

Real time PCR-analysis

Total RNA was prepared from cultured cells or from powdered tissue of whole kidneys using NucleoSpin RNA kit and cDNA synthesis was done with random hexadeoxynucleotide primers and Ready-To-Go You-Prime First-Strand Beads. The real-time PCR analysis of cDNA was performed with SYBR Green JumpStart Taq ReadyMix using primers listed in Supplementary Table 8.1.

Results

To begin to model the initial genetic events that occur in the progression of ccRCC we utilized primary mouse embryo fibroblasts (MEFs) as a genetically tractable cell culture system and focused on alterations in glucose metabolism. We derived MEFs from *Vhl*$^{fl/fl}$, *Vhl*$^{fl/fl}$*;Hif1α*$^{fl/fl}$, *Vhl*$^{fl/fl}$*;Hif2α*$^{fl/fl}$ and *Vhl*$^{fl/fl}$*;Hif1α*$^{fl/fl}$*;Hif2α*$^{fl/fl}$ embryos, infected them with adenoviruses expressing GFP (Adeno-GFP) or Cre (Adeno-Cre) and investigated the dependence of the expression of key genes that regulate glucose metabolism on *Hif1a* and *Hif2a*. The mRNA levels of *Glut1*, *Pfkfb3*, *Pgk1*, *Ldha* and *Pdk1* were elevated in *Vhl* mutant cells in a *Hif1a*-dependent but *Hif2a*-independent manner (Fig. 8.1A). Deletion of *Vhl* induces premature senescence that can be rescued by co-deletion of *Trp53* (Albers et al. 2013). *Vhl/Trp53* double null MEFs also exhibited higher mRNA abundance of these genes, indicating that the gene expression pattern is not a secondary consequence of senescence. The efficient deletion of all genes in the relevant floxed genotypes was confirmed by real time PCR (Supplementary Fig. 8.6). Since elevated expression of *Ldh-a* and *Pdk1* is expected to promote the conversion of glucose-derived pyruvate into lactate at the expense of entry of pyruvate into the mitochondria for oxidative phosphorylation, we analysed cellular readouts of glycolytic flux. Modest increases in glucose utilization and extracellular acidification rate, as well as increases in the amount of lactate secreted by the cells, were observed in *Vhl* and *Vhl/Trp53* null MEFs (Fig. 8.1B-D). In contrast to these relatively small increases, there was a large decrease in oxygen consumption in *Vhl* and *Vhl/Trp53* null MEFs that was not attributable to reduced mitochondrial abundance, as assessed by NAO staining and protein abundance of the mitochondrial protein VDAC (Fig. 8.1E-G). These results suggest that *Vhl* deletion causes a small increase in glucose uptake and conversion to lactate but a large decrease in the entry of pyruvate into the mitochondrial TCA cycle, reflected by a lowered oxygen consumption rate. The reduced levels of oxidative phosphorylation that are not compensated by a large elevation in glucose flux to lactate suggested that cells may not be able to produce normal levels of ATP. Indeed, *Vhl* and *Vhl/Trp53* deletion caused a decrease in cellular ATP levels that is dependent on *Hif1a* but independent of *Hif2a*, consistent with the transcriptional effects of these gene deletions on glycolytic regulatory genes (Fig. 8.1H-I).

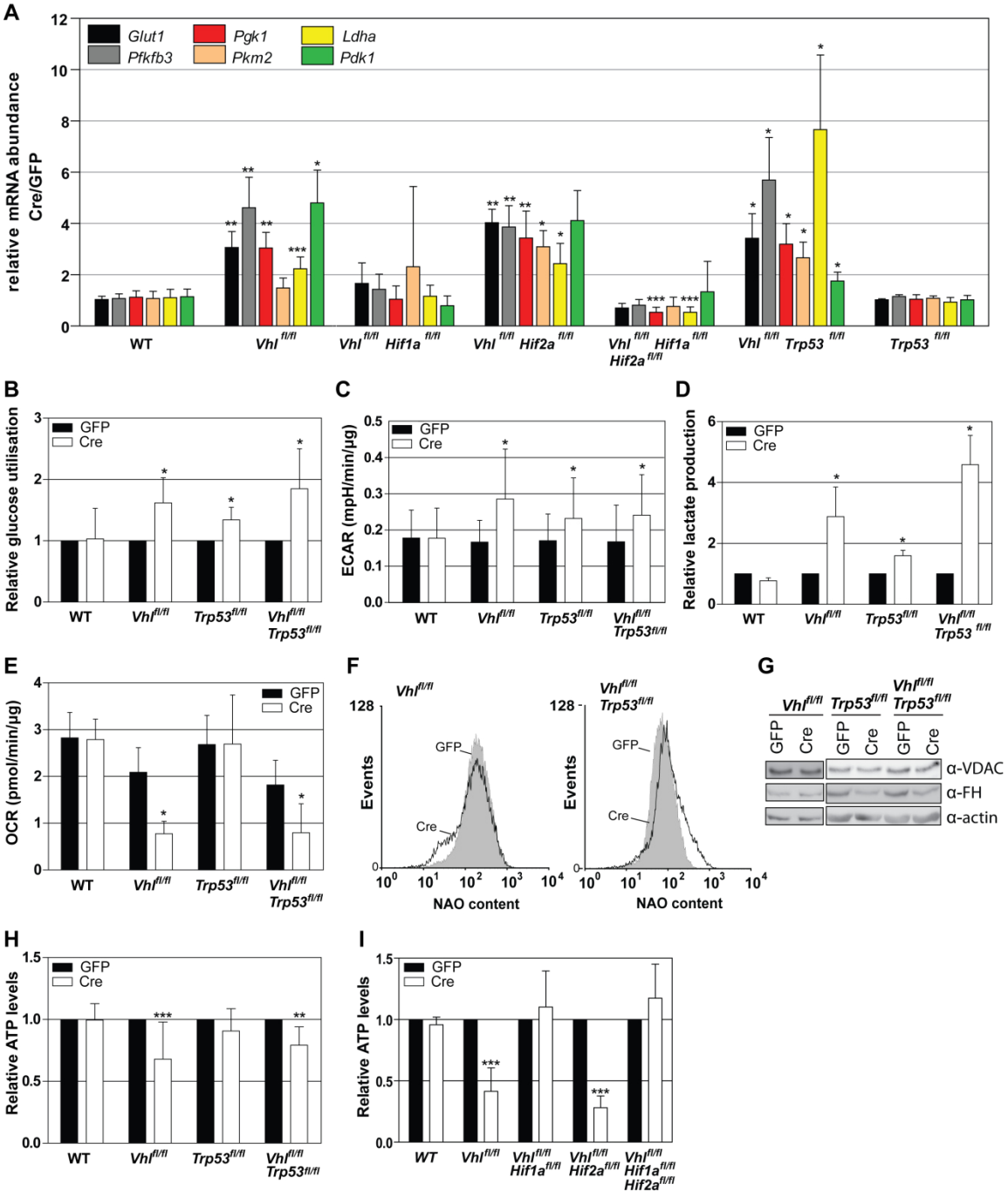

Fig. 8.1 Loss of *Vhl* induces a *Hif1α*-dependent metabolic altereations in pMEFs. (A) Expression analysis of glycolytic genes in pMEFs following infecting with adenoviruses expressing GFP (GFP) or Cre-recombinase (Cre). (B-E) Measurements of glycolytic parameters in wild type, $Vhl^{fl/fl}$, $Trp53^{fl/fl}$ and $Vhl^{fl/fl}$ $Trp53^{fl/fl}$ pMEFs: (B) glucose utilisation (C) extracellular acidification rate (ECAR), (D) relative lactate production, (E) oxygen consumption rate (OCR), (F) FACS analysis of $Vhl^{fl/fl}$, $Trp53^{fl/fl}$ and $Vhl^{fl/fl}$ $Trp53^{fl/fl}$ pMEFs using NAO as a dye for quantification of mitochondria, (G) Western blot analysis for VDAC and FH abundance. Immunoblotting using an antibody against β-actin severed as a loading and transfer control, (H-I) relative intracellular ATP levels for wild type, $Vhl^{fl/fl}$, $Trp53^{fl/fl}$ and $Vhl^{fl/fl}$ $Trp53^{fl/fl}$ pMEFs (H) and $Vhl^{fl/fl}$, $Vhl^{fl/fl}$ $Hif1\alpha^{fl/f}$, $Vhl^{fl/fl}$ $Hif2\alpha^{fl/fl}$ and $Vhl^{fl/fl}$ $Hif1\alpha^{fl/fl}$ $Hif2\alpha^{fl/fl}$ pMEFs.

We reasoned that inefficient ATP production might lead to inefficient cellular proliferation. *Vhl* deletion is known to cause early senescence in MEFs (Welford et al. 2010; Young et al. 2008; Albers et al. 2013). *Hif1a* co-deletion, but not *Hif2a* co-deletion, completely rescued the proliferative defect that followed *Vhl* deletion (Fig. 8.2A). To our knowledge, this is the first form of senescence that has been shown to be genetically dependent on *Hif1a*. To determine whether Hif1α stabilization also impaired proliferation of *Vhl* mutant cells that are unable to enter senescence we infected $Vhl^{fl/fl};Trp53^{fl/fl}$ MEFs with Adeno-GFP or Adeno-Cre as well as with lentiviral vectors expressing shRNA against *Hif1a* and performed proliferation assays. Gene deletion and knockdowns were confirmed by western blotting (Supplementary Fig. 8.7). *Vhl/Trp53* null MEFs are immortalized but proliferate slower than *Trp53* null MEFs (Albers et al. 2013). At least part of this proliferation phenotype is attributable to Hif1α activity since two independent shRNAs directed against *Hif1a* restored ATP levels to levels close to those in wild type cells and enhanced the proliferation rate of *Vhl/Trp53* null MEFs (Fig. 8.2B). Consistently, loss of *Hif1a* in *Vhl/Trp53* deficient pMEFs further increases the size of colonies formed when cells were grown at low density (Fig. 8.2C). Similarly, *Vhl* deletion in SV40 large T-Antigen transformed MEFs caused a reduction in ATP levels and slowed the rate of proliferation of these cells (Fig. 8.2E-F). Both of these effects were abolished when the same experiment was conducted in T-Antigen transformed $Vhl^{fl/fl};Hif1a^{fl/fl}$ MEFs. Thus, Hif1α stabilization following *Vhl* deletion leads to lowered ATP levels and exerts anti-proliferative effects in primary MEFs, immortalized MEFs and transformed MEFs.

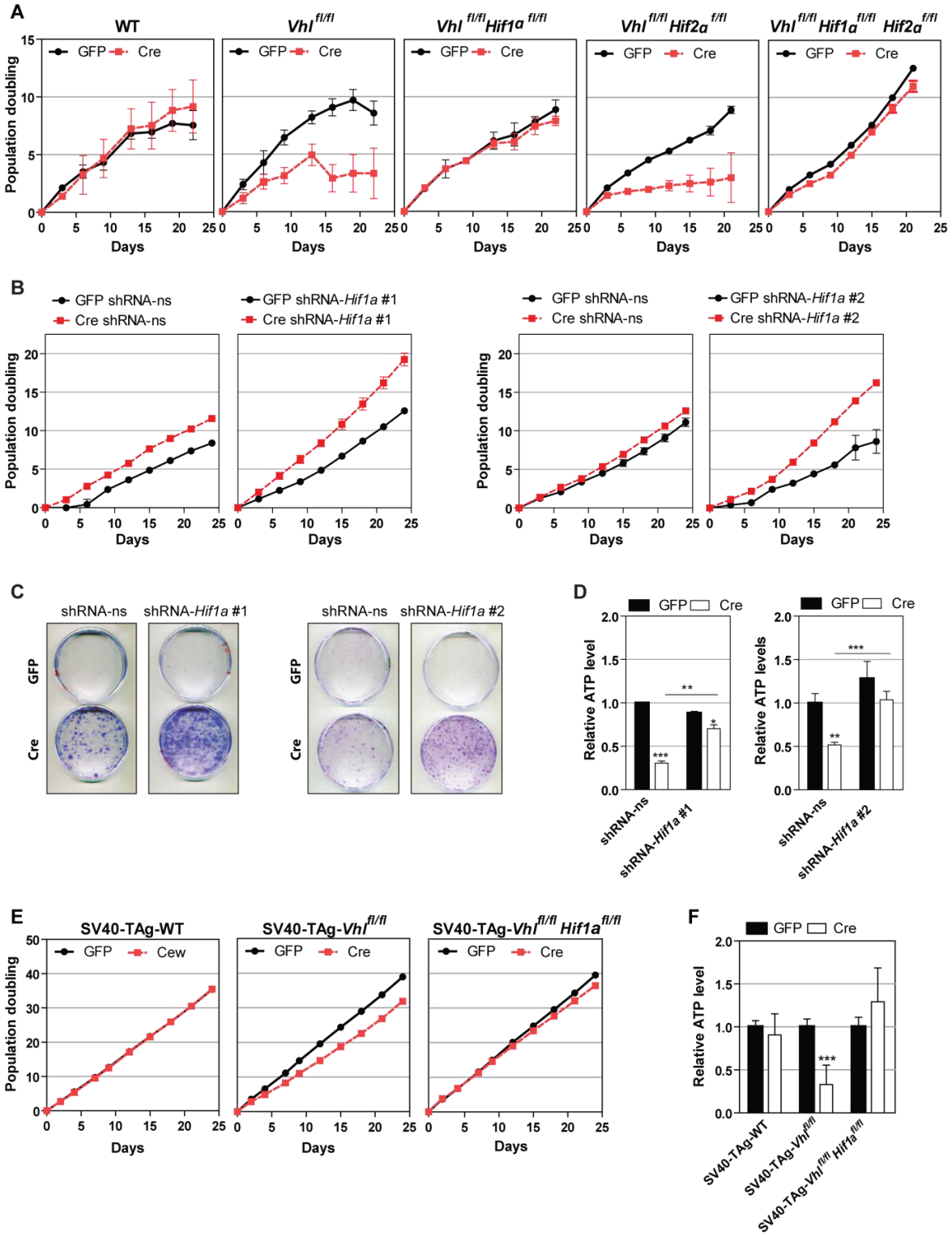

Fig. 8.2 : Hif1α stabilization following *Vhl* deletion exerts anti-proliferative effects in MEFs. (A) Proliferation assay of wild type, $Vhl^{fl/fl}$, $Vhl^{fl/fl}$ $Hif1a^{fl/f}$, $Vhl^{fl/fl}$ $Hif2a^{fl/fl}$ and $Vhl^{fl/fl}$ $Hif1a^{fl/fl}$ $Hif2a^{fl/fl}$ following infection with adenoviruses expression GFP (GFP) or Cre-recombinase (Cre), (B) proliferation assay of $Vhl^{fl/fl}$ $Trp53^{fl/fl}$ pMEFs following co-infection with GFP or Cre and lentiviruses expressing non-silencing sequence (ns) or two different shRNA directed against *Hif1a (*shRNA-*Hif1a* #1 and shRNA-*Hif1a #2)*, (C) cristal violet staining of cells from B after growing for 10 days at low density, (D) relative intracellular ATP levels of cells form B, (E) Proliferation assays of SV40-T-antigen transformed WT, $Vhl^{fl/fl}$ and $Vhl^{fl/fl}$ $Hif1a^{fl/fl}$ following GFP or Cre infection, (F) relative ATP levels from cells in E.

To investigate whether similar metabolic changes also result from *Vhl* deletion and Hif1α or Hif2α dysregulation in renal tubular epithelial cells *in vivo* we generated *Ksp1.3-Cre;Vhl$^{fl/fl}$ (Vhl$^{\Delta/\Delta}$)* (Frew et al. 2008), *Ksp1.3-Cre;Hif1a$^{fl/fl}$* (Hif1a$^{\Delta/\Delta}$), *Ksp1.3-Cre;Hif2a$^{fl/fl}$* (*Hif2a$^{\Delta/\Delta}$*), *Ksp1.3-Cre;Vhl$^{fl/fl}$;Hif1a$^{fl/fl}$* (*Vhl$^{\Delta/\Delta}$Hif1a$^{\Delta/\Delta}$*) and *Ksp1.3-Cre;Vhl$^{fl/fl}$;Hif2a$^{fl/fl}$* (*Vhl$^{\Delta/\Delta}$Hif2a$^{\Delta/\Delta}$*) mice to obtain a panel of mice with different combinations of renal epithelial-specific loss or constitutive stabilization of Hif1α and/or Hif2α. Immunohistochemical staining confirmed the expected stabilization of either or both Hif1α and Hif2α in the relevant *Vhl* mutant genotypes (Fig. 8.3A). Elevated Glut1 protein expression was detected in *Vhl$^{\Delta/\Delta}$* and *Vhl$^{\Delta/\Delta}$Hif2a$^{\Delta/\Delta}$* renal tubules but not in renal tubules in *Vhl$^{\Delta/\Delta}$Hif1a$^{\Delta/\Delta}$* mice (Fig. 8.3B). mRNA abundance of *Pfkfb3*, *Pgk1* and *Ldha* were similarly increased in whole kidney RNA isolations from Vhl$^{\Delta/\Delta}$ and Vhl$^{\Delta/\Delta}$Hif2a$^{\Delta/\Delta}$ mice but not *Vhl$^{\Delta/\Delta}$Hif1a$^{\Delta/\Delta}$* mice (Fig. 8.4A). These results demonstrate that elevated glycolytic gene expression in *Vhl* mutant renal tubular cells is dependent on *Hif1a* but not on *Hif2a*. We next developed a method to analyze mitochondrial oxygen consumption in biopsies of the renal cortex and medulla from mouse kidneys (Fig. 8.4B). *Vhl$^{fl/fl}$* and *Vhl$^{\Delta/\Delta}$* mice were analysed, revealing that *Vhl* deletion in all renal nephron segments except for proximal tubules caused a decrease in total oxygen consumption in the medulla but not cortex of these mice, indicating decreased mitochondrial activity in the renal medulla of *Vhl$^{\Delta/\Delta}$* mice. This is consistent with the fact that the majority of tubules in the medulla are null for *Vhl* and the fact that *Vhl* wild type proximal tubular cells are the most abundant cell type in the cortex. We conclude that Hif1α-dependent metabolic alterations that lead to decreased mitochondrial activity and subsequent ATP deficiency in pMEFS also occur in *Vhl* mutant renal tubular cells *in vivo*. These alterations may therefore be potentially relevant at the earliest stages of tumor formation

.

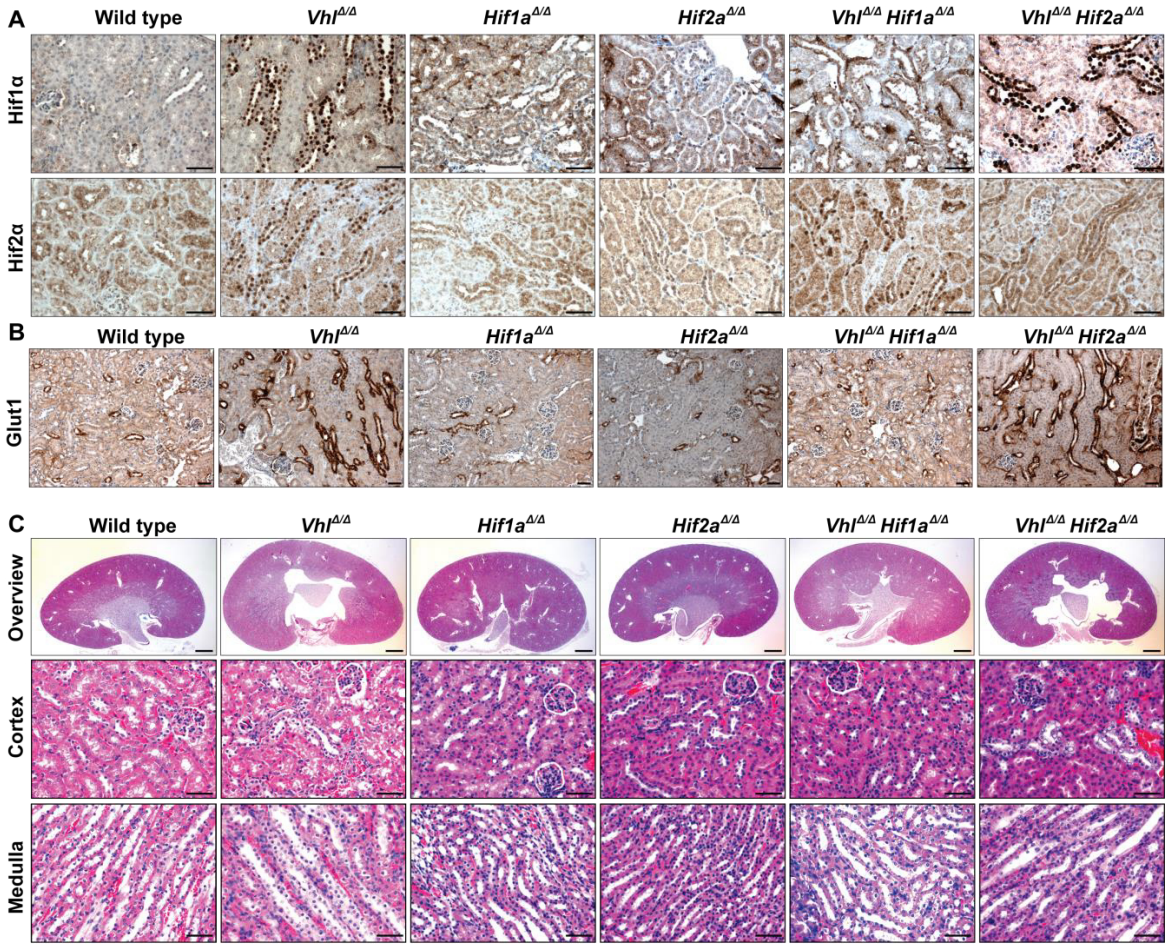

Fig. 8.3: Stabilization of Hif1α, but not Hif2α, elevates Glut1 protein expression in renal tubules. Generation of mice harboring specific deletions of *Vhl, Hif1a* and *Hif2a* in the renal epithelium using the Ksp1.3-Cre transgene. (A) Anti-Glut1 immunohistochemistry of depicted genotypes, (B) Anti-Hif1a and Anti-Hif2a immunohistochemistry, (C) hematoxilin and eosin (H&E) staining of kidneys of 6 month old mice: whole kidney (overview), renal cortex and renal medulla. Non-transgenic littermates were used as controls (WT). Scale bars: 1 mm (overview) and 100 µm (remaining pictures).

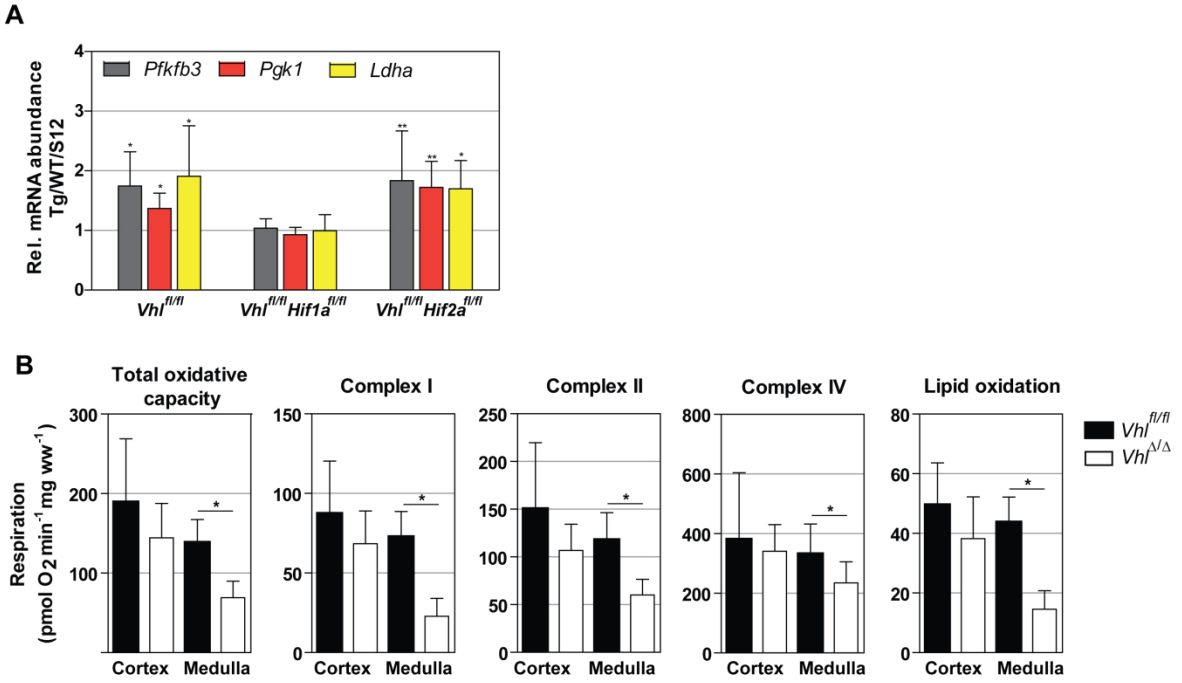

Fig. 8.4: *Vhl* deletion increases expression of glycolytic genes in kidneys and diminishes oxygen consumption rate in renal medulla. mRNA expression levels of glycolytic genes in whole kidney lysates of *Ksp-Cre; Vhl*$^{fl/fl}$ *Ksp-Cre; Vhl*$^{fl/fl}$ *Hif1α*$^{fl/fl}$ and *Ksp-Cre; Vhl*$^{fl/fl}$ *Hif2α*$^{fl/fl}$. Non-transgenic littermates were used as controls (WT). Expression levels of S12 served for internal normalization. (B) High-resolution respirometry for *Vhl*-deficient kidneys (*Vhl*$^{\Delta/\Delta}$) and controls (*Vhl*$^{fl/fl}$). Values are depicted for maximal state 3 respiration (total oxidative phosphorylation capacity, P), capacity for fatty acid oxidation (Lipid oxidation, P_{EFT}), submaximal state 3 respiration through complex I (complex I, PC_I), submaximal state 3 respiration through complex II (Complex II, PC_{II}) and cytochrome C oxidase activity (complex IV, C_{IV}). N=6. Experiment was conducted by Michal Rajski, Robert A. Jacobs and Stine Lundby.

Vhl$^{\Delta/\Delta}$ mice exhibit constitutive stabilization of both Hif1α and Hif2α, but do not display hyperproliferative phenotypes and do not develop ccRCC precursor lesions or tumors (Frew et al. 2008). Since Hif1α-mediated metabolic alterations causing ATP deficiency correlate with reduced proliferation in cell culture, we reasoned that Hif1α might act as an anti-proliferative factor that prevents tumor development following *Vhl* mutation. We therefore analysed cohorts of all of the above-described mutant mice at 6, 12 and 18 months of age. Neither *Hif1α* nor *Hif2α* deletion alone had any effect on the morphology of kidneys (Fig. 8.3C). *Vhl/Hif1α* double deletion, but not *Vhl/Hif2α* double deletion, fully rescued the previously-reported hydronephrosis phenotype caused by *Vhl* deletion (Frew et al. 2008). This phenotypic rescue will be described in detail elsewhere. Importantly, even when aged for up to 18 months, none of the genotypes exhibited cysts, dysplastic lesions or tumors (data not shown). We conclude that the combination of loss of the many putative tumor suppressor functions of pVHL plus constitutive expression of the putative oncoprotein Hif2α plus the absence of the putative tumor suppressor activity of Hif1α, does not affect epithelial homeostasis in the kidney.

While not sufficient to induce tumor formation, we reasoned that loss of *Hif1α* might nonetheless accelerate or enhance renal tumor formation in the *Vhl/Trp53* double mutant tumor-prone genetic background (Albers et al. 2013). We generated *Ksp1.3-Cre;Vhl$^{fl/fl}$;Trp53$^{fl/fl}$;Hif1a$^{fl/fl}$* mice and analyzed cohorts of these mice at 3, 6 and 12 months of age. *Vhl$^{Δ/Δ}$Trp53$^{Δ/Δ}$* mice display hydronephrosis, seminal vesicle developmental abnormalities, sub-fertility and sub-viability and by 12 months of age these mice develop simple and atypical kidney cysts, kidney neoplasms and benign epididymal tumors at high penetrance (Albers et al. 2013). About one third of these mice also develop a variety of genital-urinary tract carcinomas (Albers et al. 2013). All of these phenotypes were completely rescued in the *Vhl$^{Δ/Δ}$Trp53$^{Δ/Δ}$Hif1α$^{Δ/Δ}$* triple mutant background and mice developed no cysts or tumors in any organs (Fig. 8.5A-B). Thus, in contrast to our initial hypothesis, Hif1α activity is indispensable for the initiation of kidney cyst and tumor formation.

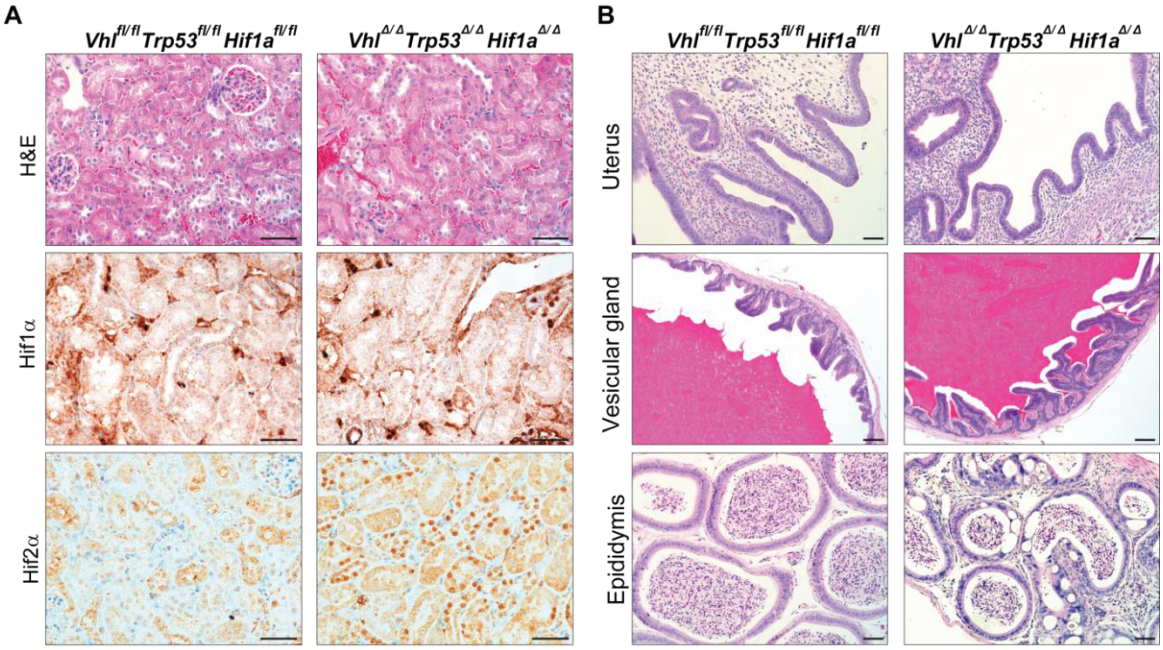

Fig. 8.5: Deletion of *Hif1α* prevents tumor formation in *Vhl$^{fl/fl}$ Trp53$^{fl/fl}$* deficient mice. Generation of mice harboring specific deletions of *Vhl, Trp53* and *Hif1α* in the renal epithelium using the Ksp1.3-Cre transgene ((*Vhl$^{Δ/Δ}$ Trp53$^{Δ/Δ}$ Hif1α$^{Δ/Δ}$*) mice. (A) H&E staining and (B) anti-Hif1α and anti-Hif2α immunochemistry of kidneys, (B) H&E staining of uterus, vesicular gland and epididymis. Non-transgenic littermates were used as controls *Vhl$^{fl/fl}$ Trp53$^{fl/fl}$ Hif1α$^{fl/fl}$*) . Scale bar: 50 µm.

Discussion

ccRCC is one of the few remaining major human cancer types for which there is no autochthonous mouse model, demonstrating that there are large gaps in our understanding of the molecular and cellular causes of this disease. A large body of correlative evidence in human ccRCC and functional genetic evidence in ccRCC cell lines has demonstrated that HIF1α stabilization exerts a tumor suppressor-like activity while HIF2α behaves oncogenically in the context of proliferation of tumor cells.

In keeping with this idea, our studies of the metabolism of primary MEFs in cell culture revealed that *Vhl* deletion causes Hif1α-dependent and Hif2α-independent induction of glycolytic genes, including *Pdk1*, that induce large decreases in mitochondrial oxygen consumption accompanied by relatively smaller increases in glucose uptake and metabolism to lactate, resulting in a deficiency of ATP production. Similar *Hif1α*-dependent and *Hif2α*-independent induction of glycolytic target genes and decreased mitochondrial oxygen consumption were observed following deletion of *Vhl* in renal epithelial cells in mouse kidneys. Many genes encoding glycolytic enzymes, including *HK1*, *HK2*, *PGK1*, *PFKFB4*, *ALDOC*, *TPI1, ENO2*, *PDK1*, and *PDK3* have been demonstrated to be specific targets of *HIF1A* in ccRCC cell lines (Shen et al. 2011) and quantitatively similar *VHL*-dependent phenotypes in terms of glucose uptake, lactate secretion, oxygen consumption and ATP deficiencies have been observed in RCC4 cells which express functional HIF1α and HIF2α (Zhang et al. 2007; Chan et al. 2011). Thus, *Vhl* or *VHL* loss in mouse and human cells, respectively, causes a Warburg-like shift in glucose metabolism from oxidative phosphorylation to anaerobic glycolysis that results in a state of cellular energy deficiency. In primary *Vhl* mutant MEFs, this ATP deficiency correlates with the induction of cellular senescence. Both phenotypes are completely rescued by co-deletion of *Hif1α* but not of *Hif2α*. This result contradicts a previous account that senescence induced by loss of *Vhl* is independent of Hifα activity (Young et al. 2008). One experimental difference that may account for these opposite conclusions is that our experiments were conducted at 5% O_2 while the previous publication used 20% O_2. It has been argued that culturing *Vhl* deficient MEFs under more physiologically relevant O_2 concentrations (2-5%) is sufficient to rescue cellular senescence (Welford et al. 2010), however, in our hands, we observe only a partial rescue of proliferation under these conditions (Albers et al. 2013) and a full rescue of proliferative capacity is achieved only with the combination of 5% O_2 and co-deletion of *Hif1α*. To the best of our knowledge this is the first demonstration of a form of senescence that is dependent on Hif1α.

The inhibitory effects of Hif1α stabilization on cellular proliferation are partially, but not fully, rescued by co-deletion of *Trp53* or transformation with SV40 large T-Antigen, since *Vhl* null cells in these genetic backgrounds were able to escape cellular senescence and proliferate in an immortalized manner (Albers et al. 2013), yet the proliferation rate of these cells was further enhanced by knockdown or knockout of *Hif1a*, which also rescued ATP levels. These results obtained in defined genetic backgrounds parallel previous results obtained using several *VHL*-deficient ccRCC cell lines where knockdown of *HIF1A* enhanced the proliferation of cells that express functional HIF1α and HIF2α, whereas *HIF1A* overexpression decreased the proliferation of *HIF1A*-mutant cells that express only functional HIF2α but did not decrease the proliferation of cells expressing functional HIF1α and HIF2α. Collectively, these results suggest that the MEF *Vhl* deletion model recapitulates many of the metabolic and proliferative features of ccRCC cell lines.

Since these findings added further evidence to the idea that Hif1α stabilization acts to impair proliferation of *Vhl* mutant cells, we asked whether removing this putative barrier may allow hyperproliferation of *Vhl* mutant kidney epithelial cells *in vivo*, potentially allowing cysts or ccRCC tumors to form. However, even when aged for 1.5 years, $Vhl^{\Delta/\Delta}Hif1a^{\Delta/\Delta}$ mice exhibited no renal proliferative abnormalities. Similar mouse models in which *Vhl* and *Hif1a* were deleted in renal epithelial cells under the control of different nephron segment-specific Cre transgenes also did not lead to tumor formation (Rankin et al. 2006; Pritchett et al. 2014). In the reverse experiment, $Vhl^{\Delta/\Delta}Hif2a^{\Delta/\Delta}$ mice similarly did not develop renal proliferative phenotypes. Thus, despite the numerous putative tumor suppressor functions of *Vhl*, its deletion together with constitutive stabilization of HIF1α and HIF2α alone or together are insufficient for renal tumor formation. Previous studies also support the idea that activation of the Hifα transcription factors alone is not oncogenic. Combinatorial deletion of *PHD1*, *PHD2* and *PHD3* in mouse kidney epithelial cells results in constitutive HIF1α and HIF2α stabilization and activation of HIFα target genes but does not cause tumor formation (Adam et al. 2011) and transgenic expression of constitutively active, non-degradable mutants of HIF1α or HIF2α alone, or in combination, in kidney epithelial cells also failed to induce tumor formation beyond the stage of simple cysts or small dysplastic lesions that could be envisaged as ccRCC precursor lesions (Schietke et al. 2012; Fu et al. 2011; 2013). While insufficient for tumor formation, Hif1α and Hif2α activities may modify the phenotype of tumors that arise in other genetic backgrounds. *Vhl/Trp53* deletion leads to the formation of *Vhl* mutant simple and atypical renal cysts, renal neoplasms as well as carcinomas in other organs of the genital tract (Albers et al. 2013). Based on the evidence that Hif1α suppresses cellular proliferation, we anticipated that the tumor phenotype in these mice might be enhanced by *Hif1a* co-deletion. In fact, the opposite result was obtained and all phenotypes in these mice were

completely rescued. Insofar as the *Vhl/Trp53* deletion model mimics the initial stages of evolution of ccRCCs, these findings demonstrate that Hif1α stabilization plays an essential oncogenic role in tumor formation.

Based on these findings we propose a new working model to explain ccRCC initiation and progression. Following biallelic inactivation of *VHL*, activation of HIF1α or HIF2α alone or together are insufficient for tumor formation, but likely provide an initial permissive environment that facilitates tumor formation once other cooperating genetic alterations arise, for example by inducing angiogenesis, promoting growth factor production and evading apoptotic responses. Additional HIFα-independent consequences of loss of pVHL function such as loss of planar cell division (Thoma et al. 2009; Hell et al. 2013) and sensitization to lose the primary cilium in response to extracellular signals (Thoma et al. 2007; Frew et al. 2008) may contribute to initial cellular dysplasia and cyst formation, while elevated levels of aneuploidy (Thoma et al. 2009; Hell et al. 2013) and inefficient repair of DNA damage (Metcalf et al. 2013) could lead to increased rates of generation of cooperating secondary mutations. In this context, it is likely that genetic alterations commonly found in ccRCCs that affect the PI3K-mTORC1 and p53 pathways, or the *PBRM1*, *SETD2* or *BAP1* tumor suppressors might act as cooperating mutations that initiate tumor formation (Creighton et al. 2013; Sato et al. 2013). HIF1α activity appears to be essential for the emergence of ccRCC precursor lesions, at least in the background of cooperating *TP53* mutations. However, since HIF1α stabilization also induces metabolic alterations that result in lowered oxygen consumption and ATP levels and impaired cellular proliferation, it is likely there is a selection for tumor cells that can proliferate most efficiently in this genetic and metabolic background. One mechanism of evading these potential metabolic and proliferative constraints may be to select for functional losses of the *HIF1A* gene (Shen et al. 2011) or for other post-transcriptional alterations that impair HIF1α stability or activity. Alternatively or additionally, mutations in other metabolism-regulating genes may act to further alter cellular metabolic pathways to achieve a balance of high rates of glycolytic flux and sufficient oxidative phosphorylation to provide the glycolytic and TCA cycle metabolic intermediates, as well as sufficient amounts of ATP, that are necessary to fuel efficient biosynthesis, cellular proliferation and tumor growth.

Acknowledgements

We are grateful to Strahil Georgiev and Wilhelm Krek for providing *Vhl*$^{fl/fl}$ *Hif1α*$^{fl/fl}$ and *Vhl*$^{fl/fl}$ *Hif2α*$^{fl/fl}$ mice and to Tatiana Simka for assistance with SeaHorse assays. This work was supported by grants to I.J.F. from SNF Förderungsprofessur (PP00P3_128257), SNF NCCR Kidney.CH and ERC Starting Grant (260316).

Supplement

Gene (primer)	**Oligonucleotide sequence (5´-3´)**
Hif1a (fwd)	TGC TCAT CAG TTG CCA CTT C
Hif1a (rev)	CCT CAT GGT CAC ATG GAT GA
Hif2a (fwd)	CTG ATG GCC AGG CGC ATG ATG
Hif2a (rev)	CTG ATG GCC AGG CGC ATG ATG
Ldha (fwd)	TGG CTT TCC CAA AAA CCG AGT
Ldha (rev)	CCA TCA GGT AAC GGA ACC GC
Trp53 (fwd)	GCG TAA ACG CTT CGA GAT GTT
Trp53 (rev)	TTT TTA TGG CGG GAA GTA GAC TG
Pdk1 (fwd)	AGG ATC AGA AAC CGG CAC AAT
Pdk1 (rev)	GTG CTG GTT GAG TAG CAT TCT A
Pfkfb3 (fwd)	CAA CTC CCC AAC CGT GAT TGT
Pfkfb3 (rev)	TGA GGT AGC GAG TCA GCT TCT
Pgk1 (fwd)	TGG AGC CAA CTC CGT TGT C
Pgk1 (rev)	CAG GCA TTC TCG ACT TCT GGG
Pkm2 (fwd)	TCG AGG AAC TCC GCC GCC TG
Pkm2 (rev)	CCA CGG CAC CCA CGG CGG CA
S12 (fwd)	GAA GCT GCC AAA GCC TTA GA
S12 (rev)	AAC TGC AAC CAA CCA CCT TC
Vhl (fwd)	CAG CTA CCG AGG TCA TCT TTG
Vhl rev	CTG TCC ATC GAC ATT GAG GGA

Supplementary Table 8.1: 5`-3` sequences of primers used for real time PCR analyses

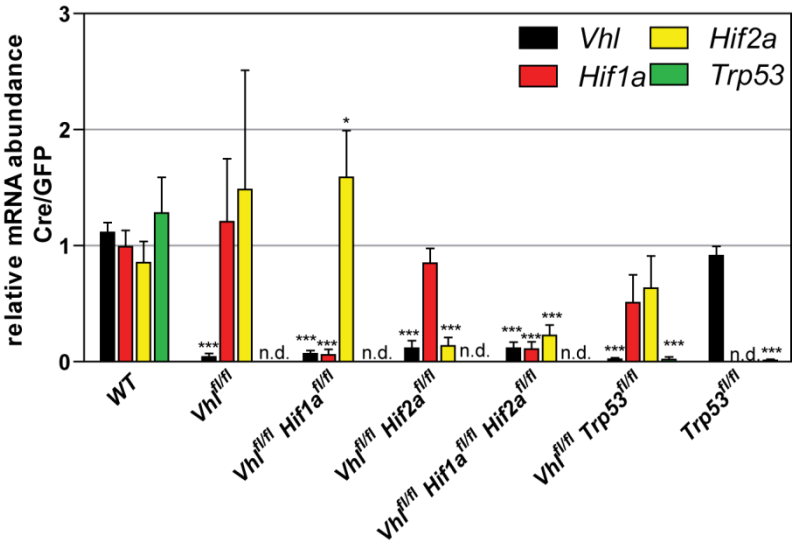

Supplementary Fig. 8.6: Efficient gene deletion in pMEFs from Fig. 8.1. RT-qPCR analysis of mRNA expression for *Vhl*, *Hif1a*, *Hif2a* and *Trp53*. S12 mRNA abundance was used for internal normalization.

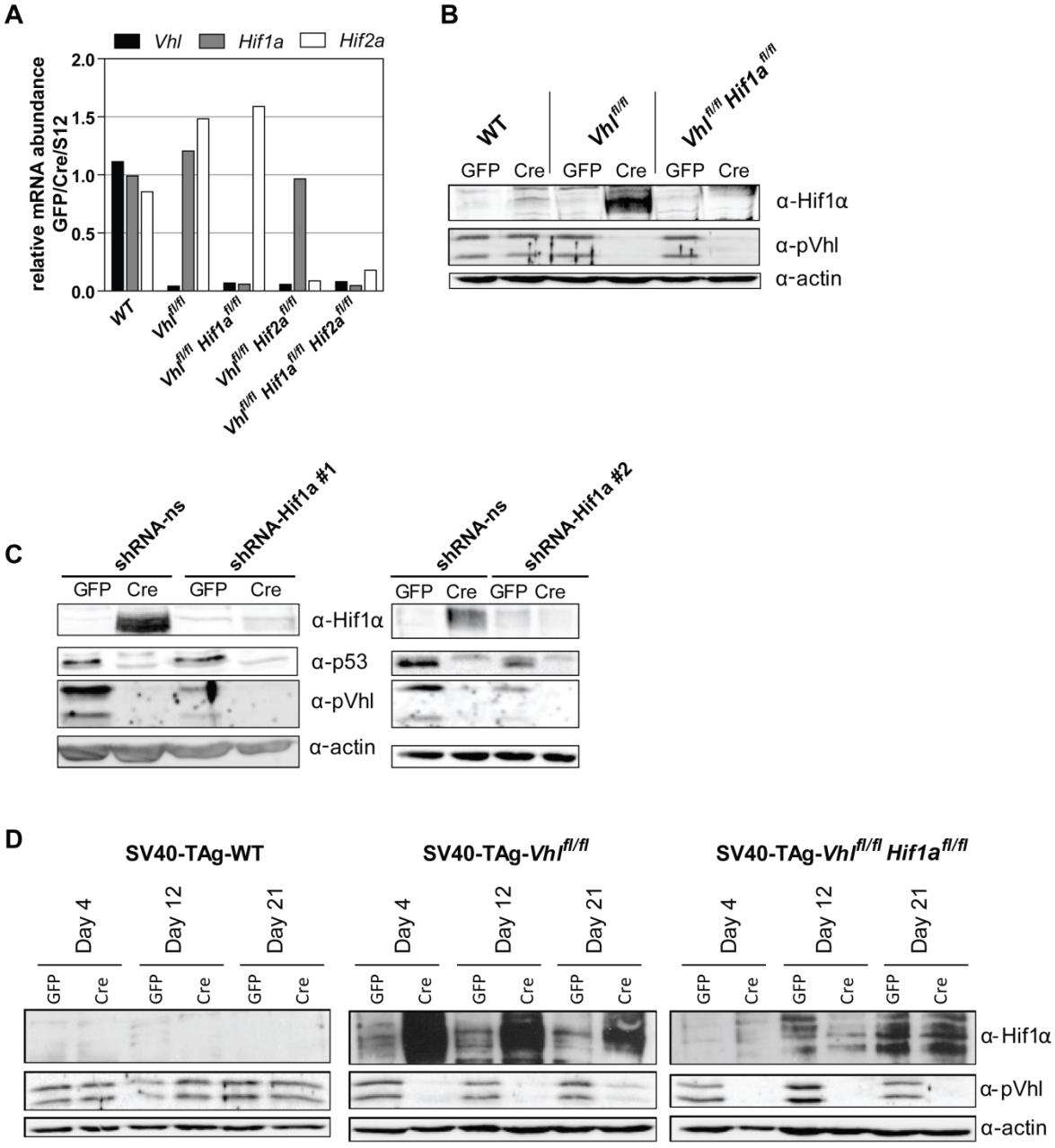

Supplementary Fig. 8.7 Confirmation of efficient gene knockdowns and gene deletions from cells used in Fig. 8.2. (A) mRNA abundance of *Vhl, Hif1a* and *Hif2a* of depicted genotypes. Expression levels of S12 were used as for internal normalization (B-C) Western blot analysis using antibodies against Hif1α, p53 and pVhl. (D) Western blot analysis using antibodies against Hif1α and pVhl. Cell lysate was harvested at depicted time points. Immunoblotting using an antibody against β-actin severed as a loading and transfer control

References

Adam J, Hatipoglu E, O'Flaherty L, Ternette N, Sahgal N, Lockstone H, Baban D, Nye E, Stamp GW, Wolhuter K, et al. 2011. Renal cyst formation in Fh1-deficient mice is independent of the Hif/Phd pathway: roles for fumarate in KEAP1 succination and Nrf2 signaling. *Cancer cell* **20**: 524–537.

Albers J, Rajski M, Schönenberger D, Harlander S, Schraml P, Teichman von A, Georgiev S, Wild PJ, Moch H, Krek W, et al. 2013. Combined mutation of Vhl and Trp53 causes renal cysts and tumours in mice. *EMBO Mol Med* **5**: 949–964.

Chan DA, Sutphin PD, Nguyen P, Turcotte S, Lai EW, Banh A, Reynolds GE, Chi J-T, Wu J, Solow-Cordero DE, et al. 2011. Targeting GLUT1 and the Warburg effect in renal cell carcinoma by chemical synthetic lethality. *Science translational medicine* **3**: 94ra70.

Creighton CJ, Morgan M, Gunaratne PH, Wheeler DA, Gibbs RA, Gordon Robertson A, Chu A, Beroukhim R, Cibulskis K, Signoretti S, et al. 2013. Comprehensive molecular characterization of clear cell renal cell carcinoma. *Nature*.

Frew IJ, Thoma CR, Georgiev S, Minola A, Hitz M, Montani M, Moch H, Krek W. 2008. pVHL and PTEN tumour suppressor proteins cooperatively suppress kidney cyst formation. *EMBO J* **27**: 1747–1757.

Fu L, Wang G, Shevchuk MM, Nanus DM, Gudas LJ. 2013. Activation of HIF2 in Kidney Proximal Tubule Cells Causes Abnormal Glycogen Deposition but not Tumorigenesis. *Cancer Research* **73**: 2916–2925.

Fu L, Wang G, Shevchuk MM, Nanus DM, Gudas LJ. 2011. Generation of a Mouse Model of Von Hippel-Lindau Kidney Disease Leading to Renal Cancers by Expression of a Constitutively Active Mutant of HIF1. *Cancer Research* **71**: 6848–6856.

Fukuda R, Zhang H, Kim J-W, Shimoda L, Dang CV, Semenza GL. 2007. HIF-1 regulates cytochrome oxidase subunits to optimize efficiency of respiration in hypoxic cells. *Cell* **129**: 111–122.

Gerlinger M, Horswell S, Larkin J, Rowan AJ, Salm MP, Varela I, Fisher R, McGranahan N, Matthews N, Santos CR, et al. 2014. Genomic architecture and evolution of clear cell renal cell carcinomas defined by multiregion sequencing. *Nature genetics* 1–12.

Gerlinger M, Rowan AJ, Horswell S, Larkin J, Endesfelder D, Gronroos E, Martinez P, Matthews N, Stewart A, Tarpey P, et al. 2012. Intratumor heterogeneity and branched evolution revealed by multiregion sequencing. *The New England journal of medicine* **366**: 883–892.

Gnarra JR, Zhou S, Merrill MJ, Wagner JR, Krumm A, Papavassiliou E, Oldfield EH, Klausner RD, Linehan WM. 1996. Post-transcriptional regulation of vascular endothelial growth factor mRNA by the product of the VHL tumor suppressor gene. *Proc Natl Acad Sci USA* **93**: 10589–10594.

Gordan JD, Bertout JA, Hu CJ, Diehl JA, Simon MC. 2007. HIF-2alpha promotes hypoxic cell proliferation by enhancing c-myc transcriptional activity. *Cancer cell* **11**: 335–347.

Gordan JD, Lal P, Dondeti VR, Letrero R, Parekh KN, Oquendo CE, Greenberg RA, Flaherty KT, Rathmell WK, Keith B, et al. 2008. HIF-alpha effects on c-Myc distinguish two subtypes of sporadic VHL-deficient clear cell renal carcinoma. *Cancer cell* **14**: 435–446.

Gruber M, Hu C-J, Johnson RS, Brown EJ, Keith B, Simon MC. 2007. Acute postnatal ablation of Hif-2alpha results in anemia. *Proc Natl Acad Sci USA* **104**: 2301–2306.

Hell MP, Duda M, Weber TC, Moch H, Krek W. 2013. Tumor Suppressor VHL Functions in the Control of Mitotic Fidelity. *Cancer Research* **74**: 2422–2431.

Hell MP, Thoma CR, Fankhauser N, Christinat Y, Weber TC, Krek W. 2014. miR-28-5p promotes chromosomal instability in VHL-associated cancers by inhibiting Mad2 translation. *Cancer Research*.

Iguchi M, Kakinuma Y, Kurabayashi A, Sato T, Shuin T, Hong S-B, Schmidt LS, Furihata M. 2008. Acute Inactivation of the *VHL* Gene Contributes to Protective Effects of Ischemic Preconditioning in the Mouse Kidney. *Nephron Exp Nephrol* **110**: e82–e90.

Iliopoulos O, Kibel A, Gray S, Kaelin WG. 1995. Tumour suppression by the human von Hippel-Lindau gene product. *Nat Med* **1**: 822–826.

Iyer NV, Kotch LE, Agani F, Leung SW, Laughner E, Wenger RH, Gassmann M, Gearhart JD, Lawler AM, Yu AY, et al. 1998. Cellular and developmental control of O2 homeostasis by hypoxia-inducible factor 1 alpha. *Genes & development* **12**: 149–162.

Keith B, Johnson RS, Simon MC. 2012. HIF1α and HIF2α: sibling rivalry in hypoxic tumour growth and progression. *Nature reviews Cancer* **12**: 9–22.

Keith B, Simon MC. 2007. Hypoxia-inducible factors, stem cells, and cancer. *Cell* **129**: 465–472.

Kim J-W, Tchernyshyov I, Semenza GL, Dang CV. 2006. HIF-1-mediated expression of pyruvate dehydrogenase kinase: A metabolic switch required for cellular adaptation to hypoxia. *Cell metabolism* **3**: 177–185.

Kleymenova E. 2003. Susceptibility to vascular neoplasms but no increased susceptibility to renal carcinogenesis in Vhl knockout mice. *Carcinogenesis* **25**: 309–315.

Kondo K, Kim WY, Lechpammer M, Kaelin WGJ. 2003. Inhibition of HIF2alpha is sufficient to suppress pVHL-defective tumor growth. *PLoS biology* **1**: E83.

Kurban G, Duplan E, Ramlal N, Hudon V, Sado Y, Ninomiya Y, Pause A. 2008. Collagen matrix assembly is driven by the interaction of von Hippel-Lindau tumor suppressor protein with hydroxylated collagen IV alpha 2. *Oncogene* **27**: 1004–1012.

Langbein S, Frederiks WM, Hausen zur A, Popa J, Lehmann J, Weiss C, Alken P, Coy JF. 2008. Metastasis is promoted by a bioenergetic switch: new targets for progressive renal cell

cancer. *International journal of cancer* **122**: 2422–2428.

Levine AJ, Puzio-Kuter AM. 2010. The control of the metabolic switch in cancers by oncogenes and tumor suppressor genes. *Science (New York, NY* **330**: 1340–1344.

Luo W, Hu H, Chang R, Zhong J, Knabel M, O'Meally R, Cole RN, Pandey A, Semenza GL. 2011. Pyruvate kinase M2 is a PHD3-stimulated coactivator for hypoxia-inducible factor 1. *Cell* **145**: 732–744.

Ma W, Tessarollo L, Hong SB, Baba M, Southon E, Back TC, Spence S, Lobe CG, Sharma N, Maher GW, et al. 2003. Hepatic vascular tumors, angiectasis in multiple organs, and impaired spermatogenesis in mice with conditional inactivation of the VHL gene. *Cancer research* **63**: 5320–5328.

Mandriota SJ, Turner KJ, Davies DR, Murray PG, Morgan NV, Sowter HM, Wykoff CC, Maher ER, Harris AL, Ratcliffe PJ, et al. 2002. HIF activation identifies early lesions in VHL kidneys: evidence for site-specific tumor suppressor function in the nephron. *Cancer cell* **1**: 459–468.

Mathia S, Paliege A, Koesters R, Peters H, Neumayer HH, Bachmann S, Rosenberger C. 2013. Action of hypoxia-inducible factor in liver and kidney from mice with Pax8-rtTA-based deletion of von Hippel-Lindau protein. *Acta Physiol* **207**: 565–576.

Maxwell PH, Wiesener MS, Chang GW, Clifford SC, Vaux EC, Cockman ME, Wykoff CC, Pugh CW, Maher ER, Ratcliffe PJ. 1999. The tumour suppressor protein VHL targets hypoxia-inducible factors for oxygen-dependent proteolysis. *Nature* **399**: 271–275.

Metallo CM, Gameiro PA, Bell EL, Mattaini KR, Yang J, Hiller K, Jewell CM, Johnson ZR, Irvine DJ, Guarente L, et al. 2012. Reductive glutamine metabolism by IDH1 mediates lipogenesis under hypoxia. *Nature* **481**: 380–384.

Metcalf JL, Bradshaw PS, Komosa M, Greer SN, Meyn MS, Ohh M. 2013. K63-Ubiquitylation of VHL by SOCS1 mediates DNA double-strand break repair. *Oncogene* **33**: 1055–1065.

Monzon FA, Alvarez K, Peterson L, Truong L, Amato RJ, Hernandez-McClain J, Tannir N, Parwani AV, Jonasch E. 2011. Chromosome 14q loss defines a molecular subtype of clear-cell renal cell carcinoma associated with poor prognosis. *Mod Pathol* **24**: 1470–1479.

Ohh M, Yauch RL, Lonergan KM, Whaley JM, Stemmer-Rachamimov AO, Louis DN, Gavin BJ, Kley N, Kaelin WGJ, Iliopoulos O. 1998. The von Hippel-Lindau tumor suppressor protein is required for proper assembly of an extracellular fibronectin matrix. *Molecular cell* **1**: 959–968.

Papandreou I, Cairns RA, Fontana L, Lim AL, Denko NC. 2006. HIF-1 mediates adaptation to hypoxia by actively downregulating mitochondrial oxygen consumption. *Cell metabolism* **3**: 187–197.

Pollard PJ, Spencer-Dene B, Shukla D, Howarth K, Nye E, El-Bahrawy M, Deheragoda M, Joannou

M, McDonald S, Martin A, et al. 2007. Targeted inactivation of fh1 causes proliferative renal cyst development and activation of the hypoxia pathway. *Cancer cell* **11**: 311–319.

Pritchett TL, Bader HL, Henderson J, Hsu T. 2014. Conditional inactivation of the mouse von Hippel. **0**: 1–9.

Qing G, Simon MC. 2009. Hypoxia inducible factor-2alpha: a critical mediator of aggressive tumor phenotypes. *Current opinion in genetics & development* **19**: 60–66.

Rankin EB, Tomaszewski JE, Haase VH. 2006. Renal cyst development in mice with conditional inactivation of the von Hippel-Lindau tumor suppressor. *Cancer research* **66**: 2576–2583.

Raval RR, Lau KW, Tran MG, Sowter HM, Mandriota SJ, Li JL, Pugh CW, Maxwell PH, Harris AL, Ratcliffe PJ. 2005. Contrasting properties of hypoxia-inducible factor 1 (HIF-1) and HIF-2 in von Hippel-Lindau-associated renal cell carcinoma. *Mol Cell Biol* **25**: 5675–5686.

Roe JS, Kim H, Lee SM, Kim ST, Cho EJ, Youn HD. 2006. p53 stabilization and transactivation by a von Hippel-Lindau protein. *Molecular cell* **22**: 395–405.

Ryan HE, Poloni M, McNulty W, Elson D, Gassmann M, Arbeit JM, Johnson RS. 2000. Hypoxia-inducible factor-1alpha is a positive factor in solid tumor growth. *Cancer research* **60**: 4010–4015.

Sato Y, Yoshizato T, Shiraishi Y, Maekawa S, Okuno Y, Kamura T, Shimamura T, Sato-Otsubo A, Nagae G, Suzuki H, et al. 2013. Integrated molecular analysis of clear-cell renal cell carcinoma. *Nature genetics*.

Schietke RE, Hackenbeck T, Tran M, Günther R, Klanke B, Warnecke CL, Knaup KX, Shukla D, Rosenberger C, Koesters R, et al. 2012. Renal tubular HIF-2α expression requires VHL inactivation and causes fibrosis and cysts. *PloS one* **7**: e31034.

Schley G, Klanke B, Schodel J, Forstreuter F, Shukla D, Kurtz A, Amann K, Wiesener MS, Rosen S, Eckardt KU, et al. 2011. Hypoxia-Inducible Transcription Factors Stabilization in the Thick Ascending Limb Protects against Ischemic Acute Kidney Injury. *Journal of the American Society of Nephrology* **22**: 2004–2015.

Shen C, Beroukhim R, Schumacher SE, Zhou J, Chang M, Signoretti S, Kaelin WG. 2011. Genetic and functional studies implicate HIF1α as a 14q kidney cancer suppressor gene. *Cancer Discov* **1**: 222–235.

Sun RC, Denko NC. 2014. Short Article. *Cell metabolism* **19**: 285–292.

Tello D, Balsa E, Acosta-Iborra B, Fuertes-Yebra E, Elorza A, Ordóñez A, Corral-Escariz M, Soro I, López-Bernardo E, Perales-Clemente E, et al. 2011. Induction of the Mitochondrial NDUFA4L2 Protein by HIF-1a Decreases Oxygen Consumptionby Inhibiting Complex I Activity. *Cell metabolism* **14**: 768–779.

Thoma CR, Frew IJ, Hoerner CR, Montani M, Moch H, Krek W. 2007. pVHL and GSK3beta are

components of a primary cilium-maintenance signalling network. *Nat Cell Biol* **9**: 588–595.

Thoma CR, Toso A, Gutbrodt KL, Reggi SP, Frew IJ, Schraml P, Hergovich A, Moch H, Meraldi P, Krek W. 2009. VHL loss causes spindle misorientation and chromosome instability. *Nat Cell Biol* **11**: 994–1001.

Vander Heiden MG, Cantley LC, Thompson CB. 2009. Understanding the Warburg effect: the metabolic requirements of cell proliferation. *Science (New York, NY* **324**: 1029–1033.

Welford SM, Dorie MJ, Li X, Haase VH, Giaccia AJ. 2010. Renal oxygenation suppresses VHL loss-induced senescence that is caused by increased sensitivity to oxidative stress. *Mol Cell Biol* **30**: 4595–4603.

Wenger RH, Stiehl DP, Camenisch G. 2005. Integration of oxygen signaling at the consensus HRE. *Sci STKE* **2005**: re12.

Yang H, Minamishima YA, Yan Q, Schlisio S, Ebert BL, Zhang X, Zhang L, Kim WY, Olumi AF, Kaelin WGJ. 2007. pVHL Acts as an adaptor to promote the inhibitory phosphorylation of the NF-kappaB agonist Card9 by CK2. *Molecular cell* **28**: 15–27.

Young AP, Schlisio S, Minamishima YA, Zhang Q, Li L, Grisanzio C, Signoretti S, Kaelin WGJ. 2008. VHL loss actuates a HIF-independent senescence programme mediated by Rb and p400. *Nat Cell Biol* **10**: 361–369.

Zhang H, Gao P, Fukuda R, Kumar G, Krishnamachary B, Zeller KI, Dang CV, Semenza GL. 2007. HIF-1 inhibits mitochondrial biogenesis and cellular respiration in VHL-deficient renal cell carcinoma by repression of C-MYC activity. *Cancer cell* **11**: 407–420.

Zimmer M, Doucette D, Siddiqui N, Iliopoulos O. 2004. Inhibition of hypoxia-inducible factor is sufficient for growth suppression of VHL-/- tumors. *Molecular cancer research : MCR* **2**: 89–95.

8.2.2 Cooperative effects of loss of *Vhl* and *Hif1α* in primary kidney cells

The work described in the manuscript above showed that the deletion of *Hif1α* in pMEFs rescues *Vhl*-dependent senescence and accelerates growth of *Vhl/Trp53*-deficient pMEFs. Next, we aimed to confirm these findings in a more disease-relevant cell type. We isolated primary epithelial kidney cells (PKCs) from mice harbouring floxed alleles of our genes of interest and induced gene deletion by the infection of cells with adenovirus expressing Cre recombinase or GFP as control. First, we measured the short term proliferation capacity by a sulforhodamine B colorimetric assay. Whereas loss of *Vhl* impairs growth as expected, this growth defect was not rescued by co-deletion of *Hif1α*, contradicting our observations in pMEFs (Fig. 8.8A-C). Furthermore, gene deletions did not cause immortalization of PKCs, as demonstrated by low density seeding of cells (Fig. 8.8B). Simultaneous deletion of *Vhl* and *Trp53* in PKCs induces enhanced cell proliferation, which is not affected by silencing of *Hif1α* (Fig. 8.8D), in contrast to our findings with MEFs. These results indicate that HIF1α has no observable effect on the proliferation of primary kidney cells in these short term assays. In longer term low density colony forming and proliferation assays however, silencing of *Hif1α* in *Vhl/Trp53* null PKCs apparently increases the rate of proliferation of immortalized cells as it resulted in the formation of more and bigger colonies (Fig. 8.8E). In contrast, loss of *Hif1α* does not induce immortalization in cells expressing wild type *Trp53* (Fig. 8.8B). Another feature of cell transformation is the ability to proliferate in an anchorage-independent manner. We therefore seeded cells in unmodified polystyrene dishes, where cell attachment of wild type cells is prevented due to the hydrophobic nature of the plate. Interestingly, *Vhl/Trp53* null PKCs frequently as floating spheres and are also able to attach to the bottom of the plate forming an epithelial monolayer. This phenotype was not altered by silencing of *Hif1α* (Fig. 8.8F). These results indicate that *Vhl/Trp53* null transformed PKCs are capable to grow with no or only very little integrin interaction. To exclude any off-target effects, we validated these results using *Vhl/p53/Hif1α* triple floxed PKCs. Consistently, Cre but not GFP expressing cells are immortalized, proliferate faster and frequently form spheres in low-attachment plates (Fig. 8.8H-J). Finally, we tested the tumour-forming capacity of *Vhl/Trp53* negative cells *in vivo* by the subcutaneous injection of cells into the flank of SCID mice. While *Vhl/Trp53* null cells were not able to establish any tumours, one out of two *Vhl/Trp53/Hif1α* null xenografts formed a tumour after 6 months, indicating that loss of Hif1α might favour tumour growth in xenografts (Fig. 8.8K-L), however the fact that only one of two clones allowed a tumour to form and that this occurred at a very late timepoint, indicates that other modifying genetic events have presumably occurred in this tumourigenic clone. In contrast, *Vhl/p53*-deficient as well as *Vhl/p53/ Hif1α*-deficient pMEFs did not growth as xenografts (data not shown).

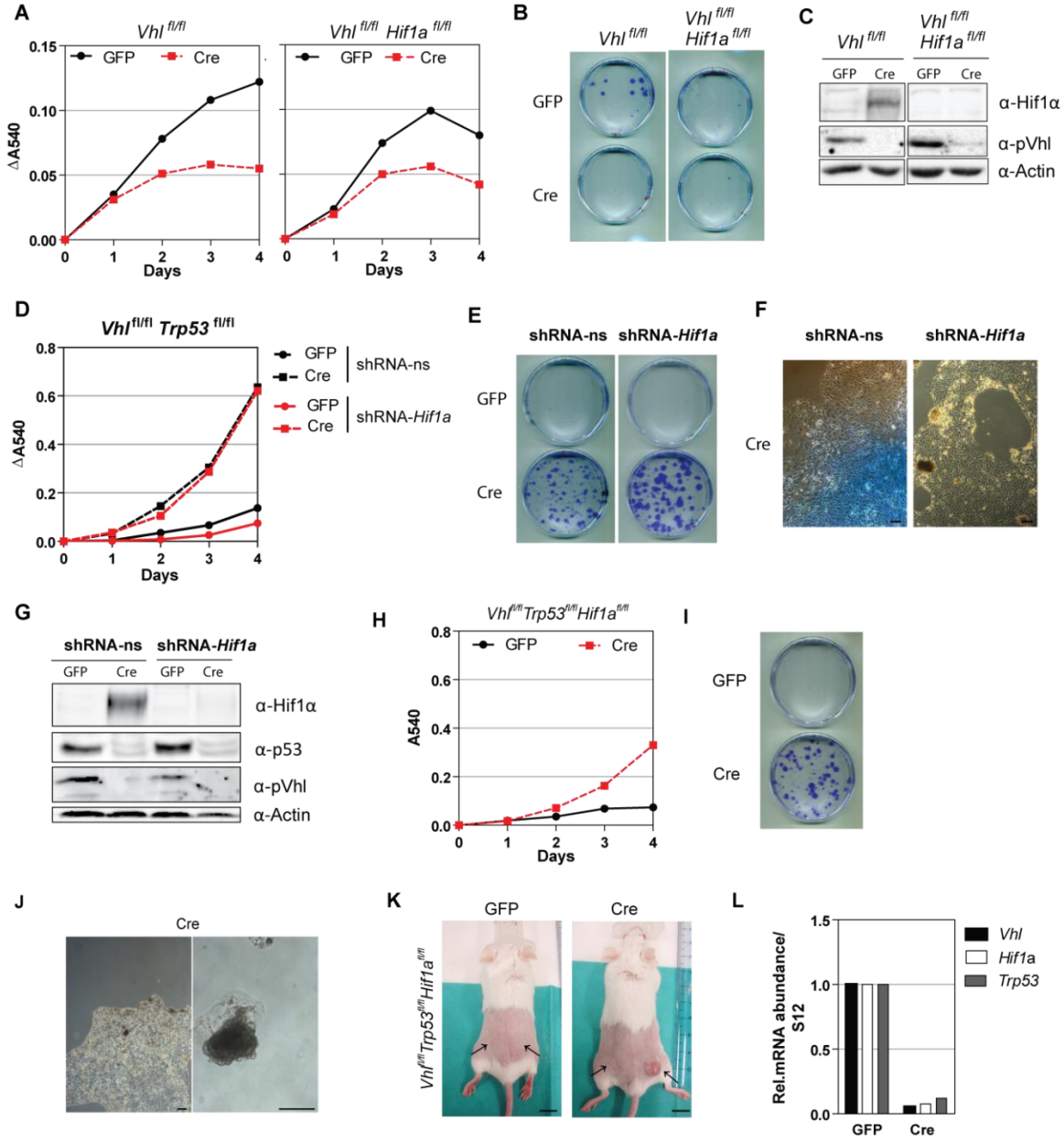

Fig. 8.8: Loss of *Hif1a* transforms *Vhl/Trp53* deficient primary kidney cells. (A) Sulforhodamine B colorimetric proliferation assay (SRB) for $Vhl^{fl/f}$ and $Vhl^{fl/f}$ $Hif1a^{fl/fl}$ primary kidney cells (PKCs) infected with adenoviruses expressing GFP or Cre recombinase, (B) low density assay for cells from A, (C) Western blot analysis for gene deletions from cells from A, (D) SRB assays for $Vhl^{fl/fl}Trp53^{fl/fl}$ PKCs infected with GFP or Cre and lentiviruses expressing a non-silencing sequence (shRNA-ns) or shRNA against *Hif1a,*(E) low density assay, (F) anchorage-independent growth assay and (G) western blot analysis for cells from D, (H) SRB assay for $Vhl^{fl/fl}$ $Trp53^{fl/fl}$ $Hif1a^{fl/fl}$ PKCs expressing GFP or Cre. (I) Low density assay, (J) anchorage-independent growth, and (K) subcutaneous injection of xenografts with cells from H. (L) Confirmation of gene deletion for cells from H by RT-qPCR. Scale bars: 50 µm (F and J) and 1 cm (K).

Despite extensive research, the origin of ccRCC is still under debate. Given that our primary cell culture system consists of a mix of renal epithelial cells, we speculated that a specific cell type might be more susceptible to oncogenic mutations than others. To address this question, we induced gene deletions in *Vhl/Trp53/Hif1a* floxed PKCs, isolated mRNA 3 days (T0) and 14 days (T1) after infection and quantified mRNA levels of markers for different tubular segments. mRNA

for NaPi-IIa (proximal tubules), Tamm-Horsfall protein (Thp, TAL) and Aqp2 (collecting ducts) were detectable at both time points, demonstrating that cells arising from different tubular segments are able to proliferate in culture (Fig. 8.9A-C). However, the relative population of *Thp* and *Aqp2* expressing *Vhl/Trp53/Hif1α* negative cells doubled over time, whereas NaPi-IIa mRNA abundance slightly decreased. These results indicate that cells deriving from TAL and collecting ducts harbour a mild growth advantage over cells deriving from proximal tubules. As Hif1α activity promotes epithelial to mesenchymal transition (EMT) (Luo et al. 2006; Higgins et al. 2007), we also measured the expression levels of E-cadherin (marker for epithelial cells) and vimentin (mesenchymal cells) (Fig. 8.9D-E). *E-cadherin* mRNA levels decreased in GFP as well as Cre expressing cells whereas *Vimentin* abundance increased over time, either suggesting that epithelial cells undergo EMT or that mesenchymal cells proliferate faster than epithelial cells and therefore are enriched in the population. Gene deletions were confirmed by RT-qPCR (Fig. 8.9F-H). To validate the knock out results, we repeated the experiment by silencing *Hif1α* in *Vhl/Trp53* null PKCs. Although we could confirm that all cells are able to growth in culture, the expression pattern of tubular and EMT markers were not reproducible (Fig. 8.9I-P). This difference might be due to residual Hif1α levels or intracellular changes caused by lentiviral introduction of shRNA.

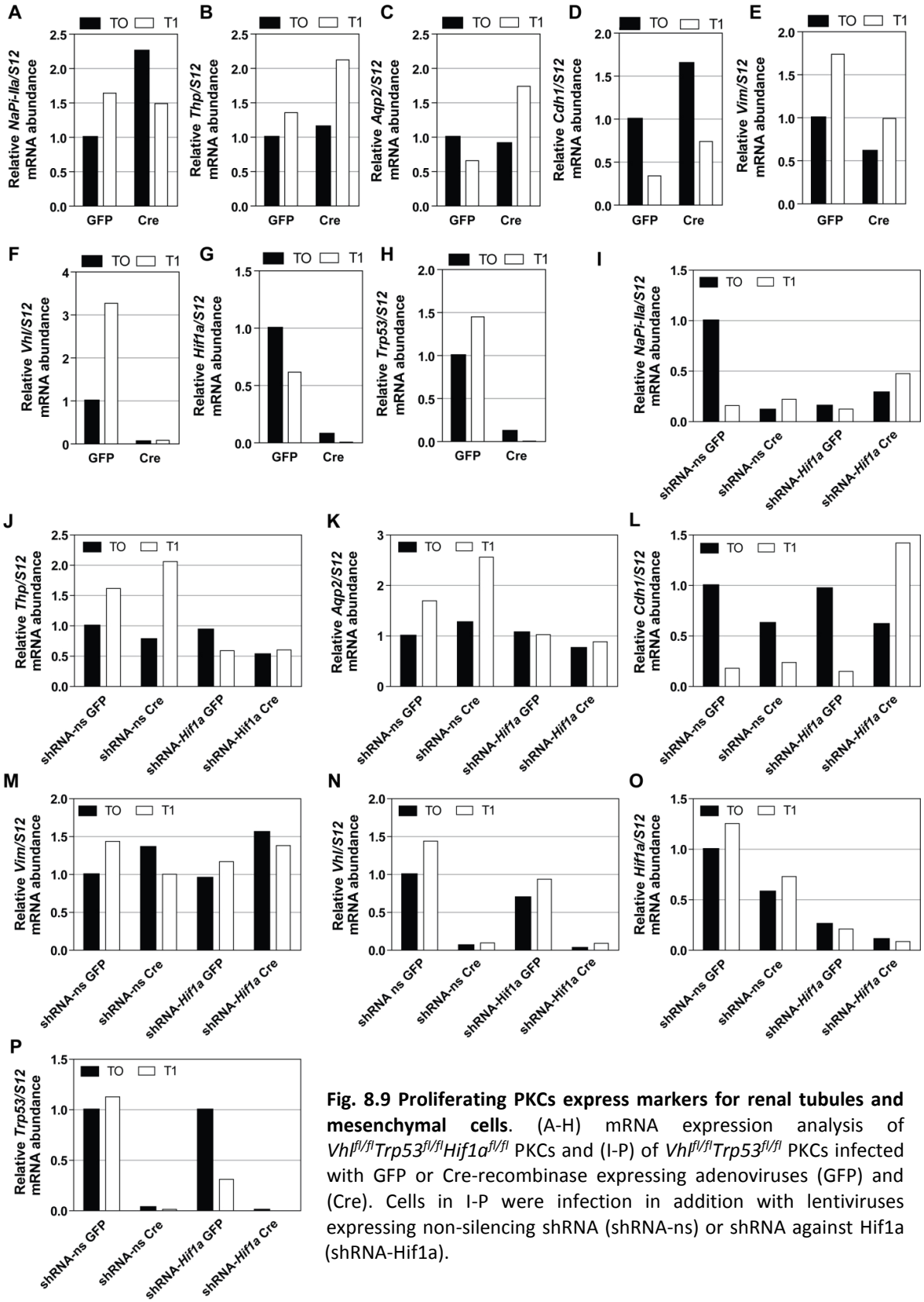

Fig. 8.9 Proliferating PKCs express markers for renal tubules and mesenchymal cells. (A-H) mRNA expression analysis of $Vhl^{fl/fl}Trp53^{fl/fl}Hif1a^{fl/fl}$ PKCs and (I-P) of $Vhl^{fl/fl}Trp53^{fl/fl}$ PKCs infected with GFP or Cre-recombinase expressing adenoviruses (GFP) and (Cre). Cells in I-P were infection in addition with lentiviruses expressing non-silencing shRNA (shRNA-ns) or shRNA against Hif1a (shRNA-Hif1a).

The analysis of *Vhl/Hif1a* deficient mice demonstrated that deletion of *Hif1a* in *Hif2a*-expressing renal epithelial cells is not sufficient to induce tumourigenesis. To identify cooperative mutations that further increase the tumourigenic capacity of kidney epithelial cells, we performed a synthetic transformation genetic screen by silencing different cell cycle inhibitors in PKCs. We

simultaneously infected freshly isolated *Vhl* and *Vhl/Hif1a* floxed PKCs with adenovirus expressing GFP or Cre and a lentiviral based shRNA library harbouring 4-5 hairpins against each of 12 cell cycle regulatory genes (*Cdkn1a, Cdkn1b, Cdkn1c, Cdkn2a, Cdkn2b, Cdkn2c, Cdkn2d, Rb1, Rbl1, Rbl2, Trp53, Trp63 and Trp73*). Low density assays revealed that loss of function of cell cycle inhibitors can cause the immortalization of PKCs, which is fully abrogated by the loss of *Vhl* but restored by co-deletion of *Vhl* and *Hif1a* (Fig. 8.10A-B), consistent with the idea that *Hif1a* suppresses cellular transformation. To further investigate the transformation capacity of the cells, we tested the colony formation capacity in soft agar as well as the ability for anchorage-independent growth. However, no colonies or spheres formation were observed in either *Vhl* or *Vhl/Hif1a* null populations infected with the shRNA library indicating that these genetic alterations are not sufficient to cause cellular transformation (Fig. 8.10C-D). To identify hairpins responsible for the immortalization of PKCs or those that provide a proliferative advantage to *Vhl/Hif1a* deficient PKC, we performed a population based gain-of-representation screen: genomic DNA of PKCs was harvested 3 days after infection with the lentiviral shRNA library (T0) and from colonies that formed when plated at low density for a further 10 days (T1) and the relative abundance of each of the integrated hairpins in the total population was assessed by deep sequencing. As at least one hairpin per target gene was present at T0 as well as at T1, indicating that inactivation of all cell cycle inhibitors represented in the library causes cell immortalization in wild type as well as in *Vhl/Hif1a* deficient PKC (Fig. 8.10E). Furthermore, we found that 10 hairpins targeting 5 different genes are enriched at T1 compared to T0 in Cre expressing but not in GFP expressing cells (5 hairpins targeting *Cdkn1a*, 2 targeting *Trp53* and one each against *Rb1*, *Rbl1* and *Trp63),* suggesting that the inactivation of these genes causes a proliferation advantage in a *Vhl/Hif1a* deficient context. These results demonstrate that loss of *Vhl* in renal epithelial cells causes a *Hif1a*-dependent proliferation barrier, which cannot be overcome by mutations of the cell cycle inhibitors chosen for the screen. Furthermore, loss of *Cdkn1a*, *Trp53*, *Trp63*, *Rb1* and *Rbl1* enhance the proliferation of *Vhl/Hif1a* null kidney cells and might represent other oncogenic hits during tumour evolution.

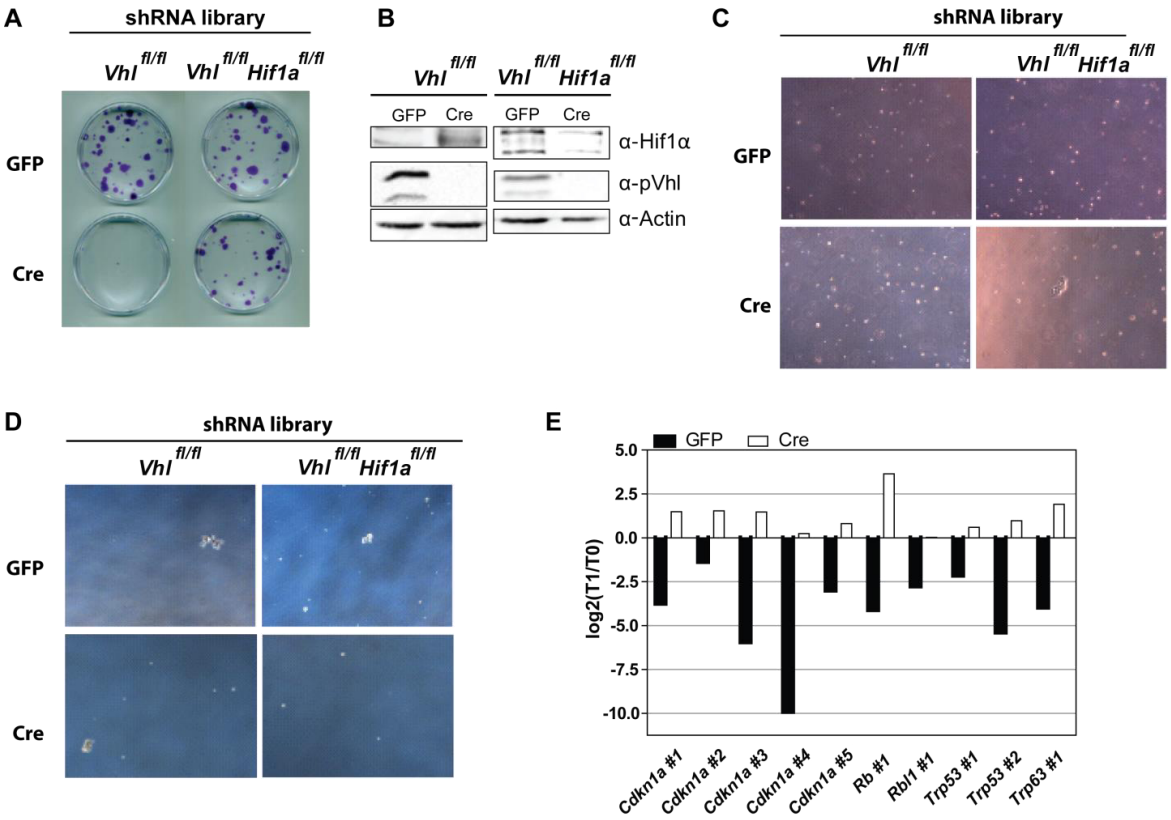

Fig. 8.10 Loss of *Vhl* causes a *Hif1α*-dependent proliferation barrier. *Vhl*$^{fl/fl}$ and *Vhl*$^{fl/fl}$*Hif1α*$^{fl/fl}$ PKCs were co-infected with adenovirus expressing Cre-recombinase (Cre) or GFP (GFP) and a lentivirus-based library containing shRNA hairpins targeting different cell cycle inhibitors (*Cdkn1a, Cdkn1b, Cdkn1c, Cdkn2a, Cdkn2b, Cdkn2c, Cdkn2d, Rb1, Rbl1, Rbl2, Trp53, Trp63).* (A) Crystal violet staining of cells growing 14 days at low density seeding, (B) Confirmation of gene deletions, (C) soft agar assay, (D) anchorage-independent growth assay, (E) gain of representation screen with cells from A-D: Deep-sequencing of starting population 3 days after infection (T0) and of colonies growing at low density (T1).

8.2.3 Discussion

To confirm the findings from our studies performed in pMEFS in a more disease-relevant cell type, we established a new culturing system for primary epithelial kidney cells (PKCs) that were freshly isolated from different transgenic mice. Gene expression analyses and antibody stainings for nephron markers revealed a mixed population of cells arising from different nephron segments, which express E-cadherin for several days of culturing and confirm the epithelial nature of PKCs (results from Holger Lehmann and Michal Rajski). Therefore, our culturing system enables us to target cells from all nephron segments that have been shown give rise to ccRCC (Droz et al. 1990; Motzer et al. 1996; Paraf et al. 2000; Mandriota et al. 2002; Straube et al. 2011).

Our studies show that loss of *Vhl* impairs growth of PKCs, which is not rescued by the deletion of *Hif1α,* contrasting our previous findings in pMEFS (Fig. 8.8A and Fig. 8.2A). The observed difference between these 2 cell types might be due to the very low proliferation rate of PKCs

which is barely above background levels obscuring the detection of significant differences in growth. Loss of *Trp53 in Vhl*-deficient PKCs, however, accelerates proliferation and enables cell growth at low density, a feature of immortalized cells. Interestingly, although there is no effect on the measurable short term proliferation rate of PKCs, loss of *Hif1α* in *Vhl/Trp53* deficient PKCs further increased the size of colonies formed when cells were grown at low density (Fig. 8.1D-F). Moreover, we found that loss of *Vhl* prevents the immortalization of PKCs caused by the inactivation of cell cycle inhibitors. Loss of *Hif1α* enables the overcoming of this barrier and enables the formation of colonies in low density assays (Fig. 8.10A). In line with our observations in pMEFs, these observations suggest that loss of *Hif1α* promotes the aggressiveness of cancer cells, presumably contributing to the bad prognosis of patients with loss of chromosome 14q (Monzon et al. 2011).

Gene expression profiling of PKCs performed by Michal Rajski demonstrated an increased expression of glycolytic genes in *Vhl*-deficient PKCs, which is abrogated by the deletion of *Hif1α* as well as of *Hif2α*. It remains to be investigated whether these changes also result in restricted availability of ATP, as observed in pMEFS. To finally prove our hypothesis that the reprogramming of the cellular metabolism is responsible for the impaired proliferation of PKCs and pMEFS, we aim to mimic the effects of loss of *Hif1α* by the downregulation of *Pdk1* in *Vhl* and *Vhl/Trp53* cells, again enabling the entry of pyruvate into the TCA cycle (Fig. 6.5). We expect that loss of Pdk1 activity enables again the re-entry of pyruvate into the TCA cycle, increasing the production of ATP and subsequently facilitates cell proliferation. However, given that other Hif1α targets are also likely to contribute to the reduced ATP levels upon loss of *Vhl,* loss of *Pdk1* might only cause a partial rescue of the phenotype. For instance, expression of LON and NDUFA4L2 have been shown to attenuate mitochondrial activity, probably further diminishing ATP production (Fukuda et al. 2007; Tello et al. 2011).

Contradictory to our finding in mouse kidneys, where *Hif1α* is necessary for the initiation of *Vhl/Trp53* negative tumours, one out of two subcutaneous injections of *Vhl/Trp53/Hif1α*-deficient PKCs lead to the formation of a tumour (Fig. 8.8K). We hypothesized earlier that Hif1α activity is needed to establish a pro-tumorigenic environment in the kidney. Given that xenograft assays in immunosuppressed mice represent a rather artificial system with very distinct environmental conditions compared to the mouse kidney, it is plausible that *Hif1α* is not necessary to establish a niche for xenograft growth. Furthermore, additional mutations might have occurred in these lines of *Vhl/Trp53/Hif1*-deficient cells, since the deletion of *Vhl* and *Trp53* are not sufficient to drive xenograft growth (data not shown). A plausible oncogenic event might be the activation of c-myc, concordantly with other studies performed in our lab where

overexpression of c-myc in *Trp53* negative PKCs enables xenograft growth, irrespectively of *Vhl* activity (Tomas Hejhal, oral communication).

To find potential driver mutations in *Vhl/Hif1a* negative cells, we performed a gain of representation screen in PKCs. We found that deletion of *Cdkn1a*, *Trp53*, *Trp63*, *Rb1* and *Rbl1* enhances the proliferation of *Vhl/Hif1a* deficient cells, potentially representing other oncogenic hits during tumour evolution (Fig. 8.10E). Mutations in cell cycle regulatory genes frequently occur in human cancers and several mouse tumour models have been generated by the inactivation of cell cycle kinases (Sotillo et al. 2001; Ko et al. 2005; Sotillo et al. 2005; Malumbres and Barbacid 2009). In ccRCC, the TCGA study identified mutations in cell cycle control genes in 18% of the cases. The genes showing up in our screen were only mutated in 4% (Cerami et al. 2012; Gao et al. 2013). Although the percentage is rather low, it is likely that mutations in these genes or in upstream or downstream targets can exert important driver functions in a subset of ccRCC. The significance of Rb mutations is supported by work from our lab performed by Sabine Harlander, which demonstrates that deletion of *Rb1* rescues the loss of *Vhl*-dependent senescence phenotype in pMEFs. Furthermore, $Vhl^{\Delta/\Delta}$ $Trp53^{\Delta/\Delta}$ $Rb1^{\Delta/\Delta}$ mice develop renal lesions already after 3 months. Given that other studies report higher frequencies of mutations in *RB1* and also in *TP53* in ccRCC biopsies, it is possible that the number of mutations in *Rb*, *Trp53* and potentially also in other cell cycle regulators is underestimated in the study mentioned above (Shuin et al. 1995; Albers et al. 2013). Therefore, it would be valuable to further validate these genes in different cell culture systems, for instance in a colony-forming assay. Finally, it would be interesting to induce the inactivation of these genes in the kidney of *Vhl/Hif1a* deficient mice, for instance by a lentiviral-based approach and monitor the formation of potential tumours *in vivo*. Based on our finding that *Hif1a* is crucial for tumour initiation in the mouse kidney it might be necessary to develop a model that allows the time-delayed inactivation of genes to identify additional driver mutations in ccRCC.

8.3 Renal Hif1α stabilization impairs renal water reabsorption and causes hydronephrosis

8.3.1 Introduction

Hydronephrosis is characterized by the expansion of the renal pelvis and the collecting system and is the most frequently diagnosed prenatal abnormality, occurring in approximately 1% of all pregnancies (Dudley et al. 1997; Thom and Rosenblum 2013). Most cases show stabilization or even a normalization of kidney morphology within the first two years after birth; however 10 – 25% of the young patients show persistent severe dilatation and require medical or surgical intervention to prevent kidney insufficiency (Woodward and Frank 2002). The underlying mechanism often remains unclear, however possible causes are obstructions of the urogenital tract or excess urine production. Conversely, hydronephrosis is also a common symptom in renal disorders that are caused by reduced renal ion transport or aquaporin expression therefore impairing renal urine reabsorption (Gargollo and Diamond 2007; Moon et al. 2009). Furthermore, kidney stones, pelvic neuroblastoma, pregnancy or impaired ureteral peristaltic activity can cause hydronephrosis in adults and therefore is a common complication in a broad range of human diseases (Au et al. 1985; Woo et al. 2013). Untreated hydronephrosis causes chronic kidney insufficiency and end stage renal disease, however, the precise mechanism is not yet fully understood (Rasouly and Lu 2013).

We previously published that epithelial deletion of *Vhl* causes hydronephrosis in mice, however the underlying mechanism remained unclear (Frew et al., 2008). Importantly, in contrast to other published mouse models for hydronephrosis, *Vhl*-deficient mice display a normal life span and also kidneys from older mice are largely morphologically intact – except for the expanded renal pelvis, which leads to a partial thinning of the renal cortex. These observations indicate a new potential mechanism for the formation of hydronephrosis at least in mice. Therefore, in the second part of the thesis, we investigated the effect of loss of *Vhl* on kidney function more closely, aiming to understand the underlying etiologies of the hydronephrosis phenotype.

8.3.2 Results

As shown in the first part of this thesis, *Vhl*-deficient kidneys display a bilateral hydronephrosis that is rescued in *Vhl/Hif1a*-deficient, but not in *Vhl/Hif2a*-deficient mice (Fig. 8.3C). Hydronephrosis is defined by the increased diameter of one or more components of the renal collecting system (Thom and Rosenblum 2013). Sectioning of *Vhl*-deficient kidneys in different planes confirmed the expansion of the renal pelvis and a thinning of the renal medulla when compared to $Vhl^{fl/fl}$ control kidneys (Fig. 8.11).

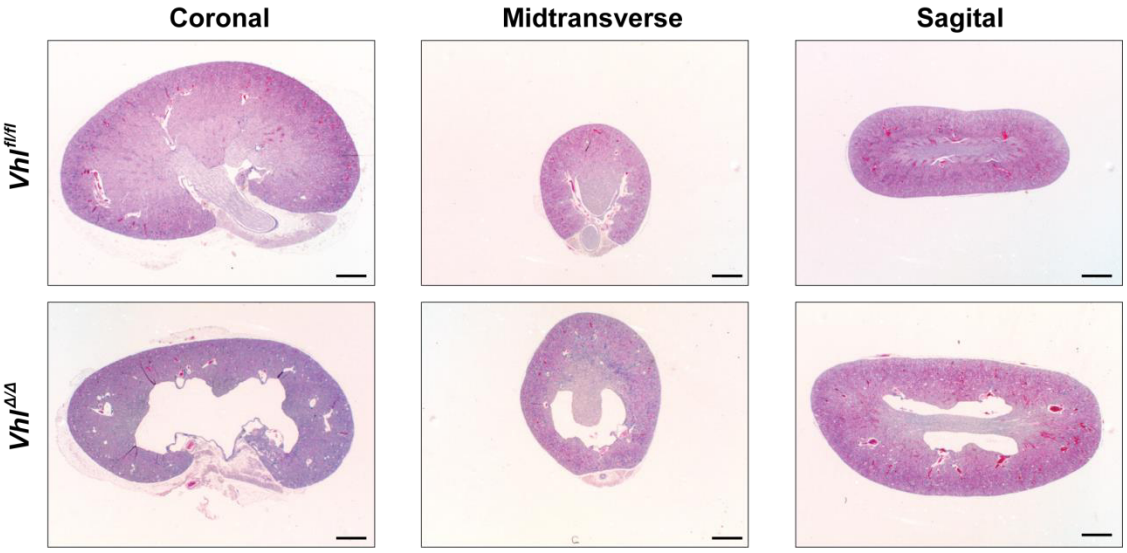

Fig. 8.11: Loss of *Vhl* causes hydronephrosis. H&E staining of different section planes of adult Ksp-Cre; $Vhl^{fl/fl}$ kidneys ($Vhl^{\Delta/\Delta}$) and controls (+/+, $Vhl^{fl/fl}$). N=2, Scalebar = 1 mm.

Given that hydronephrosis is often caused by an obstruction or dysplasia of the ureter (Peters 1995; Thom and Rosenblum 2013), we visualized the morphology of the urinary system by micro-computed tomography (µCT) (Fig. 8.12A). $Vhl^{\Delta/\Delta}$ kidneys display a clearly changed morphology with an expanded renal pelvis and almost no medullary structures. Furthermore, the cortical structures displayed a much weaker signal from the contrast agent when compared to the cortex of wild type kidneys, suggesting changes in urine flow or renal filtration. However, we did not notice any obvious delay in renal clearance of the contrast agent and 3-D rendering of the kidney volume, ureter and bladder did not show any urinary obstruction or development of hydroureter, a dilation of the ureter (Shopfner 1966). Interestingly, measurement of kidney size *in vivo* demonstrated an increase in renal diameter by approximately 20%, possibly compensating for space lost by the expansion of the pelvis (Fig. 8.12B and C).

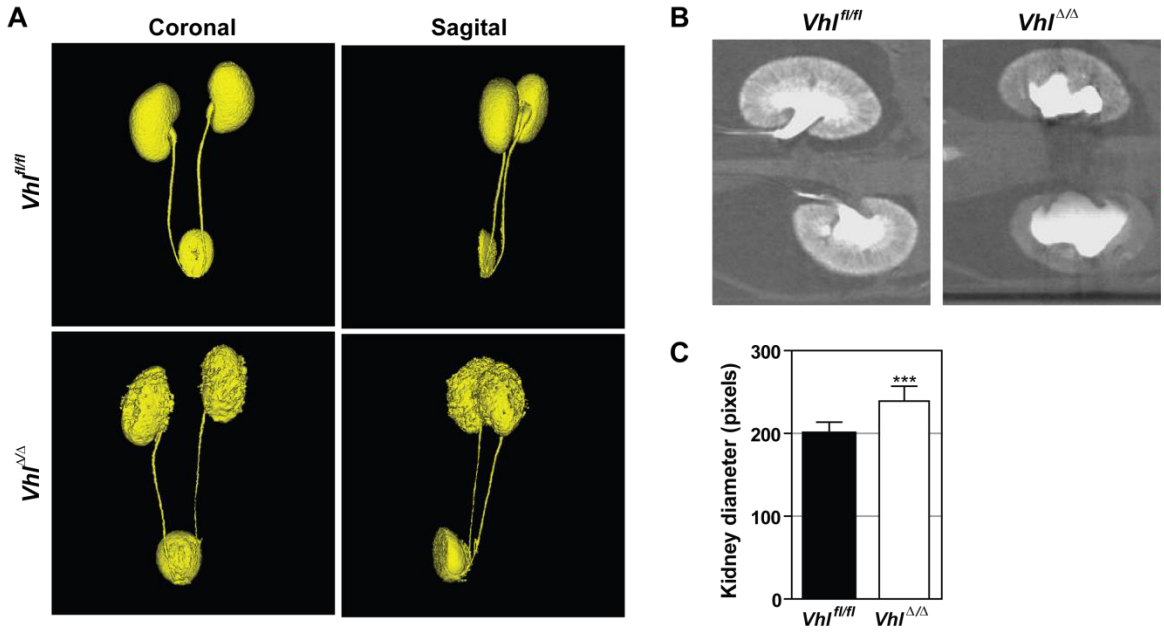

Fig. 8.12: Hydronephrosis is not caused by kidney obstruction. (A) Three-dimensional reconstruction of kidney, ureter and bladder. (B) Coronal view of a two-dimensional image of control (*Vhl*$^{fl/fl}$) and *Vhl*-deficient kidneys (*Vhl*$^{\Delta/\Delta}$), (C) Measurement of kidney diameter *in vivo.* Caliper µCT analysis. Contrast agent: Visipaque.

Fetal kidneys produce four to six times more urine before than after birth (Walsh PC 2002). A common hypothesis for the development of congenital non-obstructive hydronephrosis is a dilation of the renal pelvis caused by increased urine volume (Thom and Rosenblum 2013). To investigate whether an overproduction of urine might cause hydronephrosis, we subjected single *Vhl*$^{\Delta/\Delta}$ mice to 24h urine collection for several consecutive days. Indeed, measurement of water consumption and urine output revealed severe polyuria and polydipsia, with 24h urine production being increased by a factor of 10 in *Vhl*$^{\Delta/\Delta}$ mice (Fig. 8.13A-B). Furthermore, urine osmolality was decreased by almost 90% (Fig. 8.13G), whereas food consumption and feces production remain unchanged (Fig. 8.13C-D). No difference in mouse bodyweight was observed in either genotype (Fig. 8.13E). Whilst *Vhl/Hif2a*-deficient mice display a similar phenotype, co-deletion of *Vhl* and *Hif1a* does not disturb water homeostasis in mice, again indicating a *Hif1a*-dependent phenotype. Loss of both *Hifa* isoforms alone had no impact on kidney function. Further urine analysis demonstrated that stabilization of Hif1α but not of Hif2α increases urine pH, presumably either due to impaired renal pH regulation or the dilution of protons due to polyuria (Fig. 8.13F). Since blood pH is normal (see below), the second reason appears to be the most likely explanation. Taken together, we hypothesize that the excess of urine production in *Vhl*-deficient mice exceeds the ability of the ureter to remove the urine, subsequently building up a back pressure on the kidney, causing a slow expansion of the renal pelvis and collecting system and finally leading to the development of hydronephrosis.

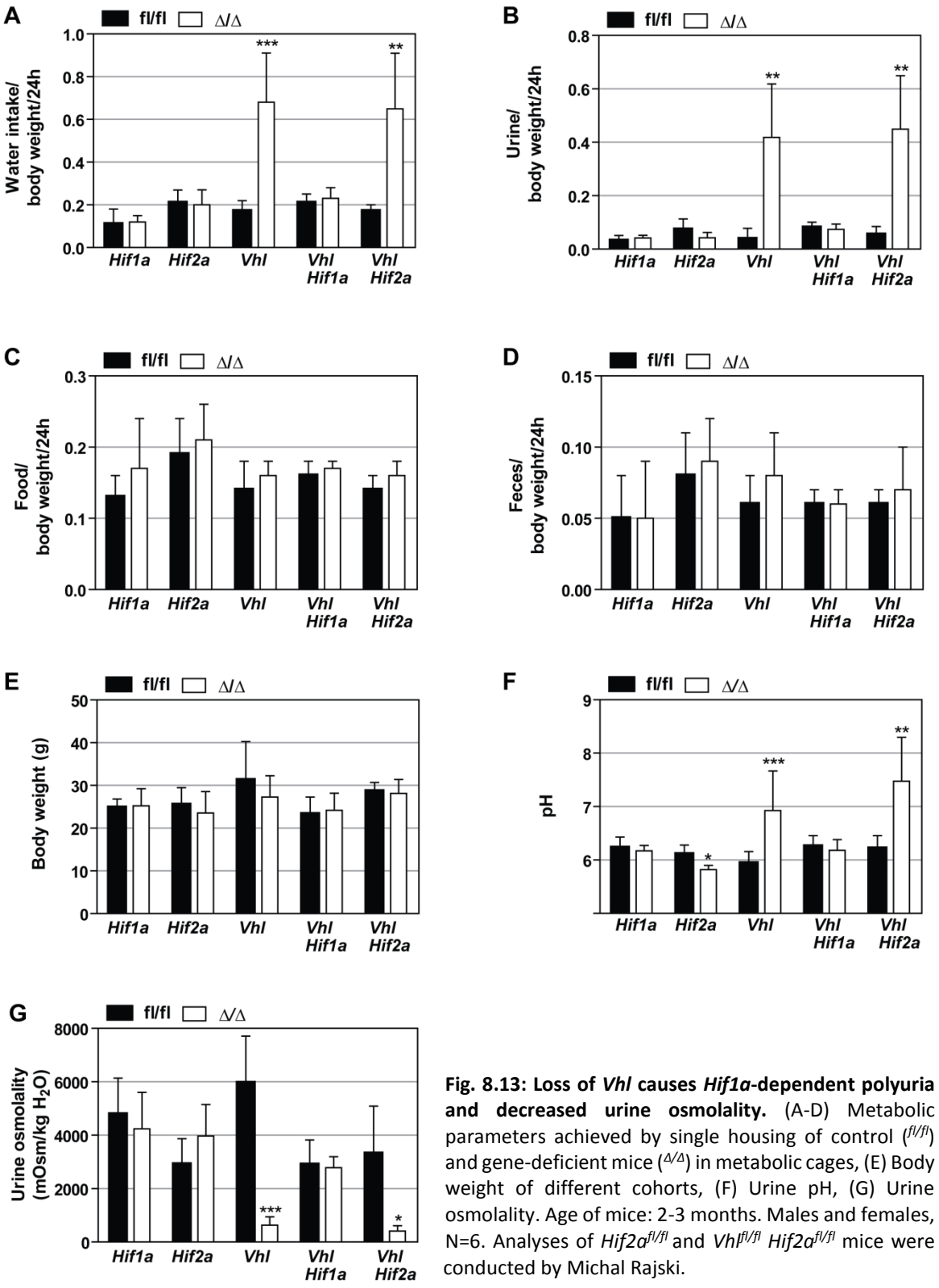

Fig. 8.13: Loss of *Vhl* causes *Hif1α*-dependent polyuria and decreased urine osmolality. (A-D) Metabolic parameters achieved by single housing of control ($^{fl/fl}$) and gene-deficient mice ($^{\Delta/\Delta}$) in metabolic cages, (E) Body weight of different cohorts, (F) Urine pH, (G) Urine osmolality. Age of mice: 2-3 months. Males and females, N=6. Analyses of *Hif2α*$^{fl/fl}$ and *Vhl*$^{fl/fl}$ *Hif2α*$^{fl/fl}$ mice were conducted by Michal Rajski.

Since progressive hydronephrosis and polyuria can lead to glomerular sclerosis, interstitial inflammation and tubular atrophy (Takahashi, Chernavvsky et al. 2000, Ampawong, Klincomhum et al. 2012, Mesrobian and Mirza 2012), we next investigated the effect of Hif1α dysregulation and subsequent occurrence of hydronephrosis and polyuria on kidney function. Analysis of blood

samples showed that loss of *Vhl* alone or together with a deletion of *Hif1a* or *Hif2a* does not alter kidney parameters such as blood creatinine, blood urea nitrogen (BUN) and electrolytes levels, indicating fully functional kidneys (Fig. 8.14A and B). Nevertheless, loss of *Hif1a* decreases blood phosphate concentration, whereas $Hif2a^{\Delta/\Delta}$ mice display elevated potassium levels. Importantly, despite observed *Hif1a*-dependent increase in urine pH (Fig. 8.13F), blood pH levels remain unchanged, indicating intact renal pH regulation.

A

	Na^+ (mmol/l)	Ca^{2+} (mmol/l)	Cl^- (mmol/l)	K^+ (mmol/l)	Alb (mg/dl)	Phos (mg/dl)	Blood pH
$Hif1a^{fl/fl}$	143.00 ± 1.67	1.24 ± 0.04	115.83 ± 0.98	4.17 ± 0.4	1.32 ± 0.14	6.97 ± 0.48	7.29 ± 0.05
$Hif1a^{\Delta/\Delta}$	142.00 ± 1.41	1.22 ± 0.018	116.17 ± 1.47	4.58 ± 0.58	1.42 ± 0.13	**5.78 ± 0.29*** **	7.35 ± 0.04
$Hif2a^{fl/fl}$	144.00 ± 1.58	1.26 ± 0.03	116.20 ± 0.84	3.78 ± 0.15	1.42 ± 0.04	6.54 ± 0.65	7.26 ± 0.08
$Hif2a^{\Delta/\Delta}$	142.57 ± 1.40	1.25 ± 0.04	116.00 ± 2.16	**4.40 ± 0.51***	1.50 ± 0.07	6.91 ± 0.85	7.26 ± 0.06
$Vhl^{fl/fl}$	146.40 ± 2.70	1.35 ± 0.07	115.60 ± 2.30	3.52 ± 0.29	1.25 ± 0.06	5.85 ± 0.59	7.32 ± 0.08
$Vhl^{\Delta/\Delta}$	148.83 ± 1.82	1.33 ± 0.05	117.17 ± 3.35	3.60 ± 0.39	1.30 ± 0.16	7.20 ± 0.86	7.37 ± 0.09
$Vhl^{fl/fl}$ $Hif1a^{fl/fl}$	144.00 ± 1.90	1.32 ± 0.03	110.83 ± 1.47	4.60 ± 0.40	1.40 ± 0.11	8.05 ± 1.04	7.25 ± 0.08
$Vhl^{\Delta/\Delta}$ $Hif1a^{\Delta/\Delta}$	144.33 ± 2.58	1.29 ± 0.04	111.00 ± 1.67	4.48 ± 0.67	1.35 ± 0.10	7.82 ± 0.95	7.29 ± 0.08
$Vhl^{fl/fl}$ $Hif2a^{fl/fl}$	138.50 ± 3.94	1.21 ± 0.06	121.17 ± 5.98	4.93 ± 0.52	1.20 ± 0.08	7.05 ± 1.22	7.04 ± 0.20
$Vhl^{\Delta/\Delta}$ $Hif2a^{\Delta/\Delta}$	**142.33 ± 2.94***	1.21 ± 0.04	120.33 ± 1.37	5.03 ± 0.69	1.16 ± 0.12	7.30 ± 0.87	7.12 ± 0.26

B

	BUN (g/dl)	Crea (mg/dl)
$Hif1a^{fl/fl}$	21.33 ± 3.83	0.09 ± 0.03
$Hif1a^{\Delta/\Delta}$	19.67 ± 2.16	0.10 ± 0.04
$Hif2a^{fl/fl}$	25.00 ± 4.58	0.09 ± 0.02
$Hif2a^{\Delta/\Delta}$	23.86 ± 4.06	0.07 ± 0.03
$Vhl^{fl/fl}$	16.25 ± 3.30	0.12 ± 0.05
$Vhl^{\Delta/\Delta}$	23.67 ± 6.71	0.14 ± 0.04
$Vhl^{fl/fl}$ $Hif1a^{fl/fl}$	27.00 ± 6.84	0.13 ± 0.04
$Vhl^{\Delta/\Delta}$ $Hif1a^{\Delta/\Delta}$	25.83 ± 3.54	0.10 ± 0.03
$Vhl^{fl/fl}$ $Hif2a^{fl/fl}$	18.09 ± 3.86	0.08 ± 0.05
$Vhl^{\Delta/\Delta}$ $Hif2a^{\Delta/\Delta}$	18.42 ± 3.34	0.12 ± 0.03

Fig. 8.14: $Vhl^{\Delta/\Delta}$ mice display intact kidney function. (A) Blood parameters of transgenic control mice ($^{fl/fl}$) and gene-deficient mice ($^{\Delta/\Delta}$), (B) Kidney function parameters. Age of mice: 2-3 months. Males and females, N=6. Analyses of $Hif2a^{fl/fl}$ and $Vhl^{fl/fl}$ $Hif2a^{fl/fl}$ mice were conducted by Michal Rajski.

Although $Vhl^{\Delta/\Delta}$ mice display a normal life span, we speculated that excessive urine production could harm the kidney over time, leading to kidney insufficiency in aged mice. We therefore repeated all metabolic experiments with ten to twelve month old mice. Surprisingly, we could not detect any significant changes in urine output or water consumption upon loss of *Vhl* (Fig. 8.15A). Closer examination of *Vhl*-deficient animals revealed that only two out of four mice displayed hydronephrosis, although all kidneys stained positively for Hif1α and Hif2α. Taking only hydronephrotic animals in consideration, we could confirm the occurrence of polyuria and decreased osmolality in these mice. Blood analysis demonstrated a slight increase in blood urea nitrogen, but no change in creatinine or electrolyte levels was detected, indicating intact kidney function (Fig. 8.15B-C).

A

	$Vhl^{fl/fl}$	$Vhl^{\Delta/\Delta}$	Hydronephrosis
Water intake/bodyweight/24h	0.11 ± 0.03	0.24 ± 0.11	0.30 ± 0.07
Urine output/bodyweight/24h	0.03 ± 0.02	0.09 ± 0.05	**0.12 ± 0.01*****
Food intake/bodyweight/24h	0.07 ± 0.03	0.09 ± 0.12	0.09 ± 0.02
Feces/bodyweight/24h	0.03 ± 0.02	0.02 ± 0.02	0.02 ± 0.02
Bodyweight (g)	39.99 ± 4.08	40.96 ± 2.76	40.28 ± 2.91
Urine osmolality (mOsm/kg H_2O)	2828 ± 1160	1214.00 ± 1031	**624.00 ± 18.95****
Urine pH	6.08 ± 0.25	6.85 ± 0.95	7.12 ± 0.43

B

	BUN (g/dl)	Crea (mg/dl)
$Vhl^{fl/fl}$	19.50 ± 4.04	0.20 ± 0
$Vhl^{\Delta/\Delta}$	**28.00 ± 4.24***	0.20 ± 0

C

	Na^+ (mmol/l)	Ca^{2+} (mmol/l)	Cl^- (mmol/l)	K^+ (mmol/l)	Alb (mg/dl)	Phos (mg/dl)	Blood pH
$Vhl^{fl/fl}$	150.17 ± 4.02	1.36 ± 0.02	119.50 ± 2.51	4.53 ± 0.58	1.87 ± 0.05	8.22 ± 1.26	7.23 ± 0.05
$Vhl^{\Delta/\Delta}$	152.50 ± 0.71	1.34 ± 0.03	118.00 ± 0	4.00 ± 0.42	1.90 ± 0.14	7.35 ± 0.07	7.28 ± 0.01

Fig. 8.15: Aged *Vhl*-deficient mice exhibit slight kidney insufficiency. (A) Metabolic parameters and urine analysis from control ($Vhl^{fl/fl}$) and *Vhl*-deficient mice ($Vhl^{\Delta/\Delta}$) and mice with hydronephrosis, (B) Blood kidney function parameters: creatinine (Crea) and blood urea nitrogen (BUN), (C) Blood electrolyte levels. Mixed gender, N=4, Significant values are highlighted in red.

Polyuria has been described as a symptom of several genetic disorders in humans. In the following sections we investigate whether similar mechanisms may contribute to the polyuria phenotype observed in *Vhl*-deficient mice. For instance, excess urine production is a common feature of nephrogenic diabetes insipidus (NDI) (Robertson 1988). NDI is characterized by an impaired renal response to arginine vasopressin (AVP) stimulation, consequently causing a failure in renal water reabsorption (Fujiwara et al. 1995). To investigate the urine concentration capacity of *Vhl*-deficient kidneys, we performed a water restriction test. After two days adaptation in the metabolic cage, we provided mice with food and water for 24 hours *ad libitum* (Fig. 8.16A). Next, we restricted the mice from drinking water, however providing them with an equal mix of water and food to attenuate the effect of dehydration. After 5.5 h of water restriction *Vhl*-deficient mice showed signs of dehydration and the experiment was aborted. Analysis of the urine demonstrated that $Vhl^{\Delta/\Delta}$ mice produced 5 times more urine than control mice, whereas the urine concentration was 4x lower (Fig. 8.16B). During water restriction, urine of control mice was more diluted when compared to the 24 h measurement at day 1, probably due to lack of sleep during the measurement period. Interestingly, absence of drinking water was not compensated by increased wet food consumption in dehydrated mice (Fig. 8.16B). Kidney values returned to normal again when mice were provided with sufficient water (Fig. 8.16C). These results demonstrate that *Vhl*-deficient mice are not able to concentrate urine, even when challenged by water restriction. Immunofluorescent detection of renal AQP2 expression showed increased apical staining of the vasopressin-sensitive water channel AQP2 even in unchallenged mice,

suggesting functional vesicle trafficking and vasopressin stimulation (Fig 8.17). Taken together, these results indicate that loss of *Vhl* causes polyuria, which cannot be overcome by the activation of the AVP system.

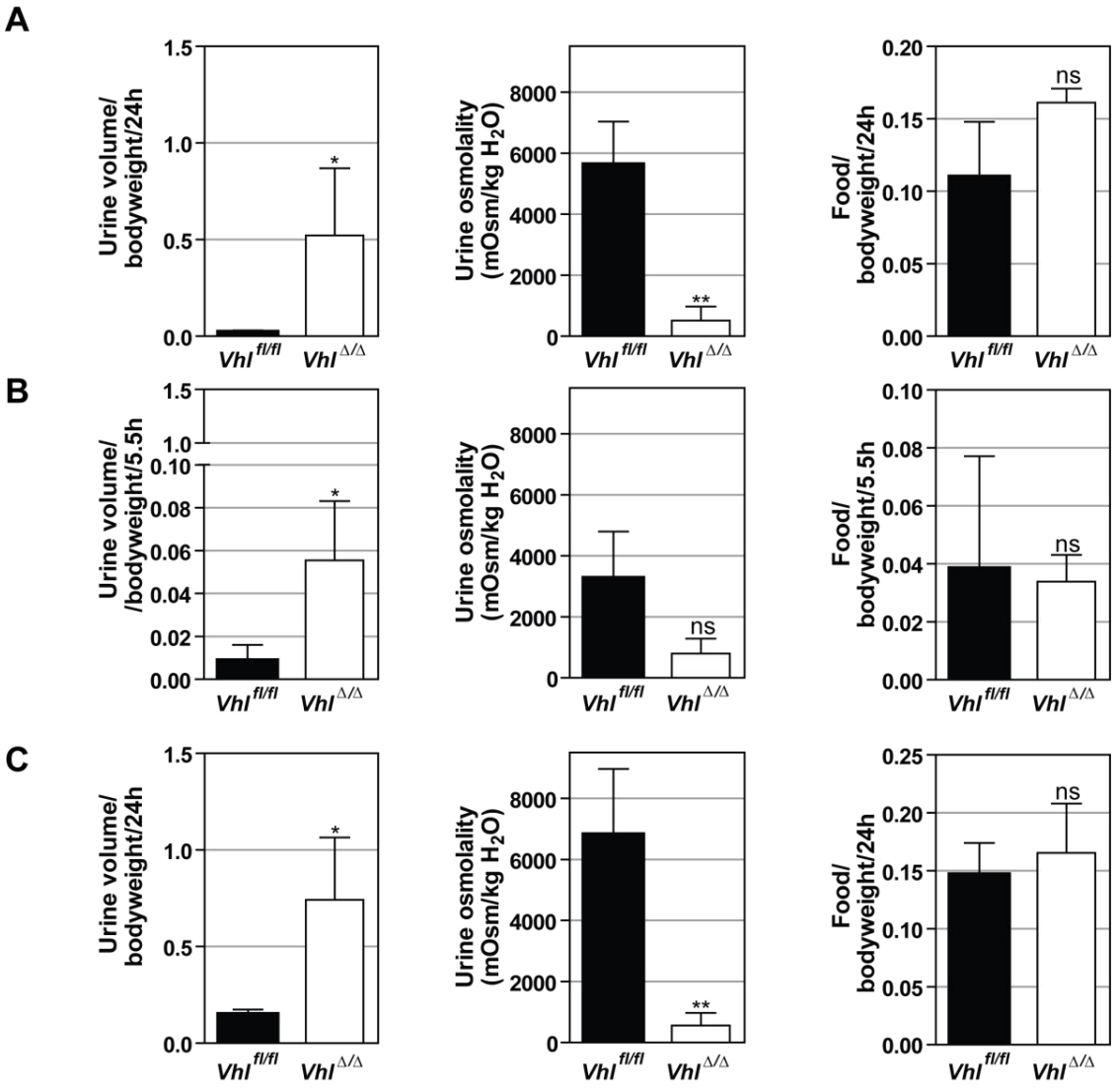

Fig. 8.16: *Vhl*-deficient mice fail to concentrate urine under water deprivation. Mice were housed in metabolic cages for three consecutive measurements. (A) Water ad libitum for 24 h (day 1), (B) Water restriction (day 2, mice provided with wet food for 5.5 h), (C) Water ad libitum for 24 h (day 3). Values are depicted for urine volume, urine osmolality and food intake. Age of mice: 2-3 months. Males and females, N=4.

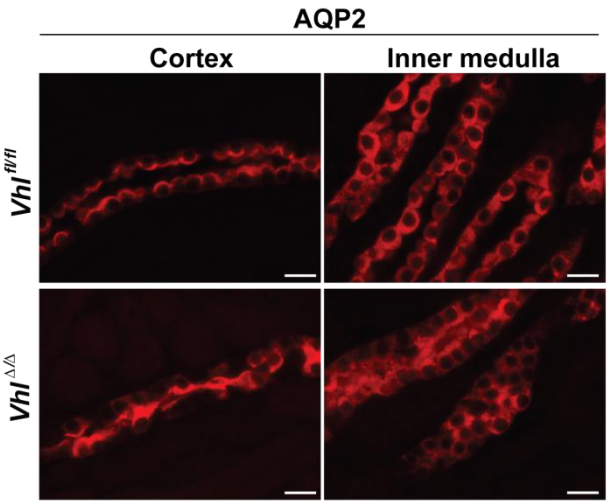

Fig 8.17: Increased apical localization of Aqp2 in collecting ducts of *Vhl*-deficient in unchallenged *Vhl*-deficient mice. Immunofluorescence staining of Aqp2 expression in 14 day old kidneys. N=10. Scale bar = 25 µm.

Examination of polyuric patients and the generation of several mouse models uncovered that mutations in renal aquaporins (Aqp) can cause polyuria and hydronephrosis (Ampawong et al. 2012; Li et al. 2012), hence we analyzed the expression of aquaporins in the kidney. Gene expression analysis of kidneys of adult mice revealed decreased abundance of *Aqp1*, *Aqp2*, *Aqp3* and *Aqp7* mRNA (Fig. 8.18A). Decreased renal protein levels of Aqp2 could be confirmed by Western blot analysis (Fig. 8.18C). Consistently, immunofluorescent staining exhibits less Aqp1 and Aqp2 staining in the renal medulla of young $Vhl^{\Delta/\Delta}$ kidneys when compared to controls (Fig. 8.18B). Taken together, these results indicate that epithelial loss of *Vhl* reduces renal abundance of Aqp, potentially decreasing the rate of renal urine reabsorption and finally causing polyuria. However, studies show that *Aqp* expression in mice can also decrease in response to ureter obstruction induced by the mechanical clamping, mimicking the situation in obstructive hydronephrosis. Therefore, we cannot rule out the possibility that decreased *Aqp* expression in *Vhl*-deficient kidneys is rather a secondary effect than a cause (Li et al. 2012).

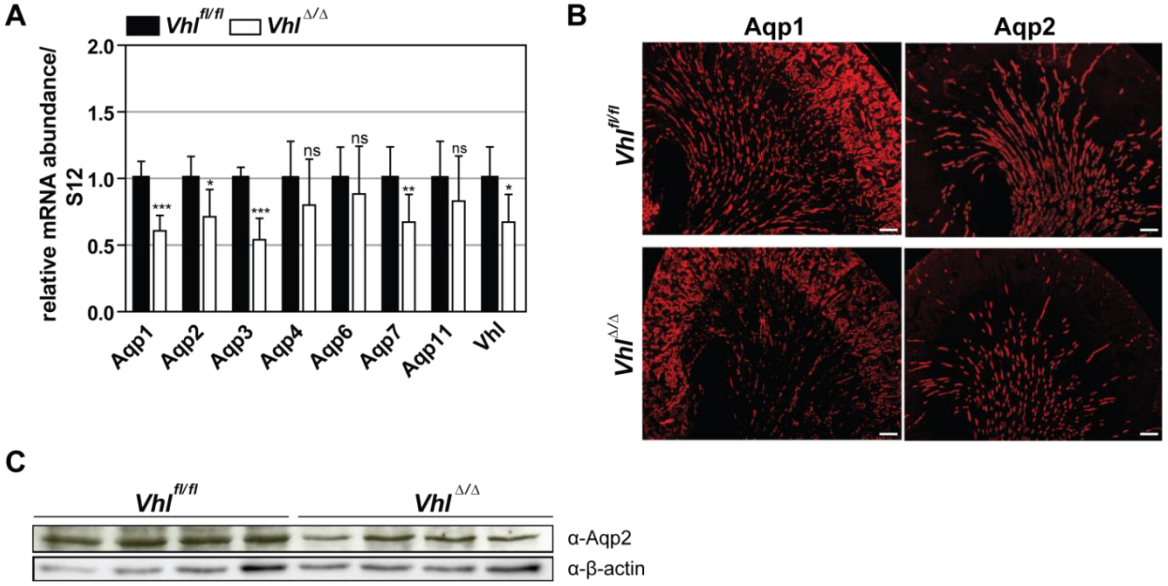

Fig. 8.18: Deletion of *Vhl* causes decreased expression of several aquaporins in the adult kidney. (A) Gene expression analysis, S12 was used as internal standard, N=6, (B) Immunofluorescence staining of Aqp1 and Aqp2 levels in 14 day old kidneys, N=10, Scale bar = 200 µm. (C) Protein expression level for Aqp2 in adult kidneys.

Another possible cause of polyuria is an impaired function or expression of renal ion transporters (Takahashi et al. 2000). We therefore performed immunofluorescence staining on kidneys of young *Vhl*-deficient mice for specific renal ion transporters along the nephron, confirming the expression of transporters in the proximal tubules (NaPi-IIa, ATPV1B1), thick ascending limb of Henle (THP, NKCC2) and distal tubules (NCC). However, it remained unclear whether expression levels were changed upon loss of *Vhl (*Fig. 8.19A). Gene expression analysis in adult mice revealed decreased mRNA abundance of *Slc34a1* (NaPi-II), *Atp6v1b1* (ATPV1B1) and *Slc26a4* (Pendrin, proximal tubules and cortical collecting ducts), but not of *Umod* (THP) and *Slc12a1* (NKCC2) (Fig. 8.19B). Consistently, Western blot analysis showed similar protein levels for NCC and NKCC2 in $Vhl^{\Delta/\Delta}$ and control animals. However, decreased *Slc34a1* transcript levels did not translate into decreased protein abundance for NaPi-IIa (Fig. 8.19 C).

We did not expect any changes in proximal tubule gene expression since the Ksp.1.3 promoter is only very weakly expressed in the proximal tubules, causing Hifα stabilization only in rare cells in this nephron segment. To further investigate the down regulation of *Slc34a1* expression, we examined renal mRNA levels of two additional markers for proximal tubules, *Slc5a1* (Sglt1) and *Cubn* (Cublin). Abundance of both markers was reduced. Given that the apparent reductions in markers of different tubule segments occur in both *Vhl* wild type and *Vhl* null nephron segments,

the most likely explanation is that there is progressive damage of the kidney caused by permanent hydronephrosis, leading to a moderate loss of nephrons in adult mice (Fig. 8.19A).

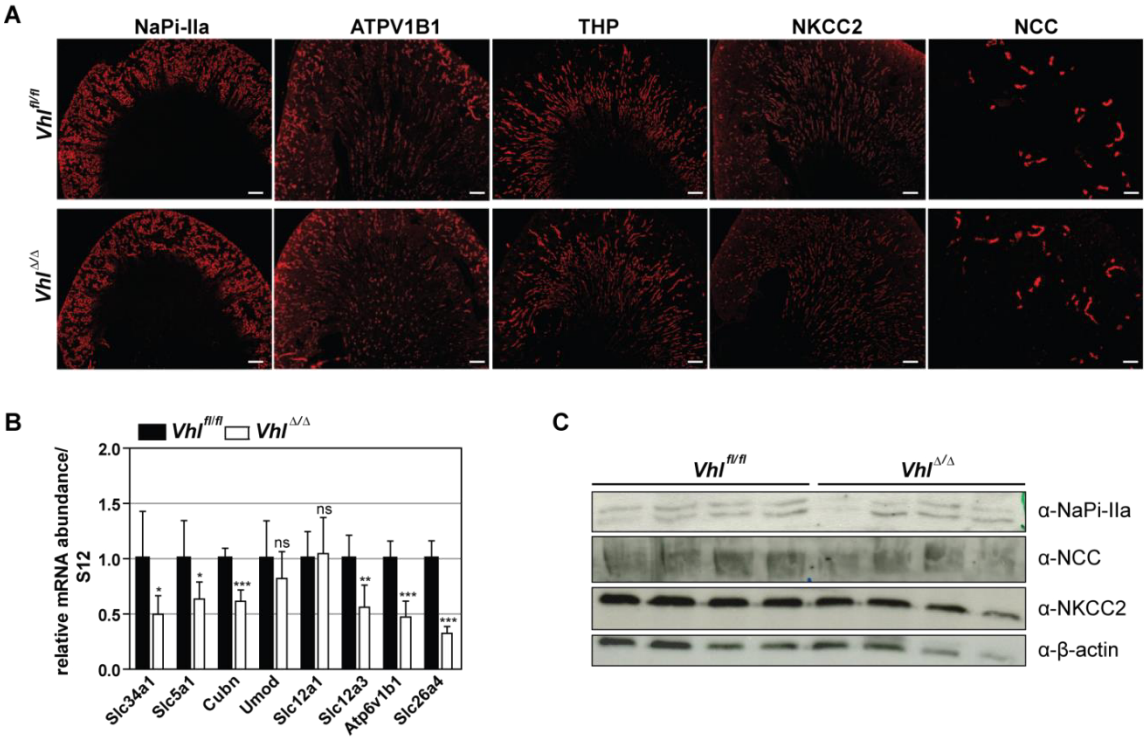

Fig. 8.19: Decreased expression of renal ion transporters in upon loss of *Vhl.* (A) Immunofluorescence staining of depicted renal ion transporter abundance in kidneys of 14 days old mice, N=10, Scale bar = 200 µm. (A) Gene expression analysis of transporter expression in adult kidneys: *Slc34a1* (NaPi-II), *Slc5a1* (SGLT1), *Cubn* (Cublin), *Umod* (THP), *Slc12a1* (NKCC2), *Slc12a3* (NCC), *Atp6v1b1* (ATPV1B1) and *Slc26a4* (Pendrin), S12 was used as internal standard, N=6, (C) Protein expression level in kidneys of adult mice.

Next, we investigated whether changes in transporter expression impairs renal ion reabsorption. Urine analysis revealed that $Vhl^{\Delta/\Delta}$ mice excrete 1.5- to 2-fold more salt within 24 h than control mice (Fig. 8.20A). However, it is likely that the total amount of salt excretion in $Vhl^{\Delta/\Delta}$ mice is overestimated compared to wild type animals, as urine recovery from the metabolic cages is more efficient in mice with polyuria, since a smaller fraction of urine is lost on the wires and tubes. A more precise method to assess deregulated renal reabsorption is the calculation of the fractional excretion rate (FE), which expresses the amount of salt excreted in the urine compared to the amount filtered by the glomeruli (Espinel 1976). We could not detect any difference in FE for sodium, potassium or calcium, indicating intact renal ion reabsorption (Fig. 8.20B). Considering the normal electrolytes levels in the blood of *Vhl*-deficient mice, these results argue against a failure of ion transporter expression or activity as a cause of polyuria. Nevertheless, we could only calculate the fractional excretion rate for 2 out of 6 animals since urine creatinine level was below detection range. Therefore, we cannot rule out the possibility that FE is changed in these mice.

A

	Vhl$^{fl/fl}$	*Vhl*$^{\Delta/\Delta}$
Na^+ (µmol/24h)	112.900 ± 27.31	206.1 ± 52.31**
K^+ (µmol/24h)	481.85 ± 107.05	713.3 ± 149.12*
Mg^+ (mg/24h)	0.570 ± 0.46	1.120 ± 0.73
Ca^{2+} (mg/24h)	0.098 ± 0.09	0.36 ± 0.06**
Creatinine (mg/24h)	0.43 ± 0.11	0.65 ± 0.01

B

	Vhl$^{fl/fl}$	*Vhl*$^{\Delta/\Delta}$
FE_{Na} (%)	0.180 ± 0.03	0.197 ± 0.07
FE_K (%)	33.68 ± 13.50	29.48 ± 6.03
FE_{Ca} (%)	0.540 ± 0.54	1.117 ± 0.12

Fig. 8.20: Loss of *Vhl* does not disturb renal ion reabsorption in mice. Urine was collected from mice housed in metabolic cages. (A) Urine ion excretion within 24h, N=6 (B) Fractional excretion rate (FE) = ($[Na]_{urine}/[Na]_{plasma}$) ($[Cre]_{urine}/[Cre]_{plasma}$) of depicted electrolytes, Creatinine levels were determined in Fig. 8.14B, N=2. Significant values are highlighted in red.

Another possible mechanism for the development of hydronephrosis is a defect in kidney development. To investigate in which age the phenotype first occurs we analyzed the morphology of kidneys at different time points. Fetal kidneys dissected at day E18.5 as well as from newborns (day 1-7) display normal morphology. However, kidneys from mice aged 14 days display an expanded renal pelvis, indicating the development of hydronephrosis between day 7 and 14 after birth (Fig. 8.21). In rodents, nephrogenesis continues after birth for another 10 to 14 days, until nephron maturation and vascularization are completed (Song and Yosypiv 2012). Our results suggest that a defect in late renal development or the increase in renal work load cause polyuria and hydronephrosis in *Vhl*-deficient mice.

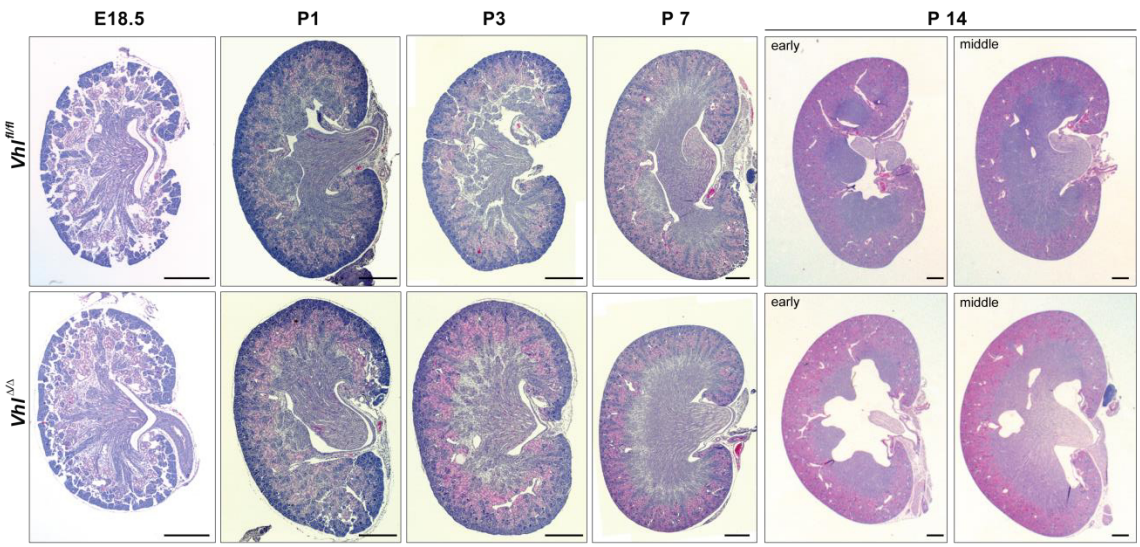

Fig. 8.21: Hydronephrosis in *Vhl*-deficient mice develops between postnatal day 7 and 14. Hematoxilin and Eosin (H&E) staining of cytoplasma (pink) and nuclei (blue) of kidney sections at depicted timepoints (Embryonal day 18.5, postnatal day P1-P14), N=2-10). Scale bar = 500 µm.

Given that loss of *Vhl* causes impaired growth in pMEFs we hypothesized that deletion of *Vhl* in renal tubules might cause the cells to proliferate more slowly during development, presumably causing shorter renal nephrons, which might reduce the concentrating power of the kidney, leading to diluted urine. An established assay to address tissue proliferation is the immunohistochemical staining for Ki67, a protein that is expressed in all non-quiescent cells (Gerdes et al. 1984). Although *Vhl*-deficient kidneys exhibit more cells that are positive for Ki67 staining, particularly in the inner medulla, closer examination indicated that many positive cells were peritubular cells and therefore not part of the renal nephron (Fig. 8.22). We therefore conducted further experiments to directly determine whether loss of *Vhl* alters tubular cell proliferation capacity.

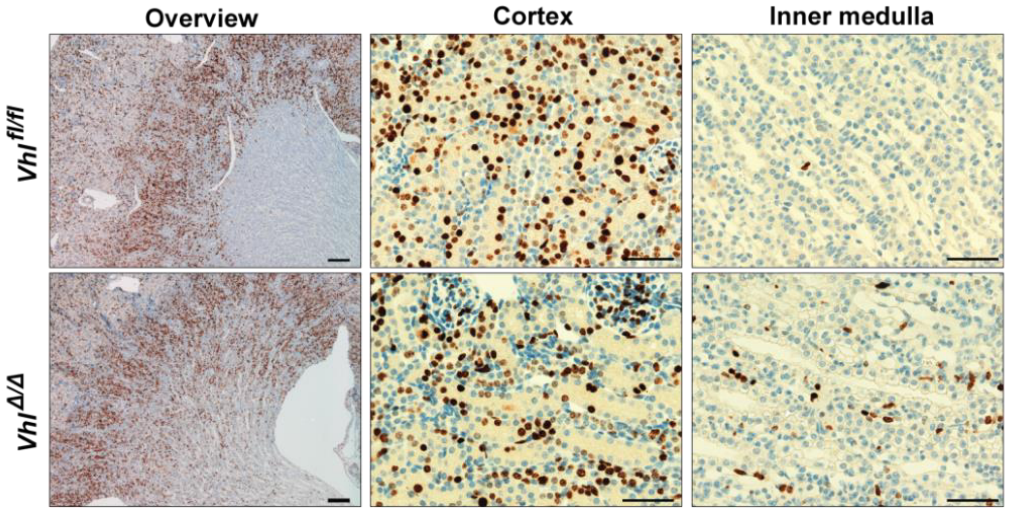

Fig. 8.22: *Vhl*-deficient kidneys display increased staining for non-quiescent cells. Ki67 immunohistochemical staining of kidney sections of 14 days old *Vhl*-deficient or corresponding control mice. Scale bars: overview 200 µm, cortical and medullar sections: 50 µm. N=10.

A more direct method to assay for cell proliferation is the Bromodeoxyuridine (BrdU) incorporation assay. The nucleotide analog is injected into mice and incorporated in the DNA of proliferating cells during S-Phase, where it can be later visualized by antibody staining. We injected BrdU in 7 and 14 day old mice two hours prior to dissection. Co-staining of BrdU and specific markers of different nephron segments revealed that there were no differences between wild type and *Vhl* mutant kidneys in the percentage of proliferating cells in proximal tubules, in the thick ascending loops of Henle (TAL) and the collecting ducts (Fig. 8.23A-D).

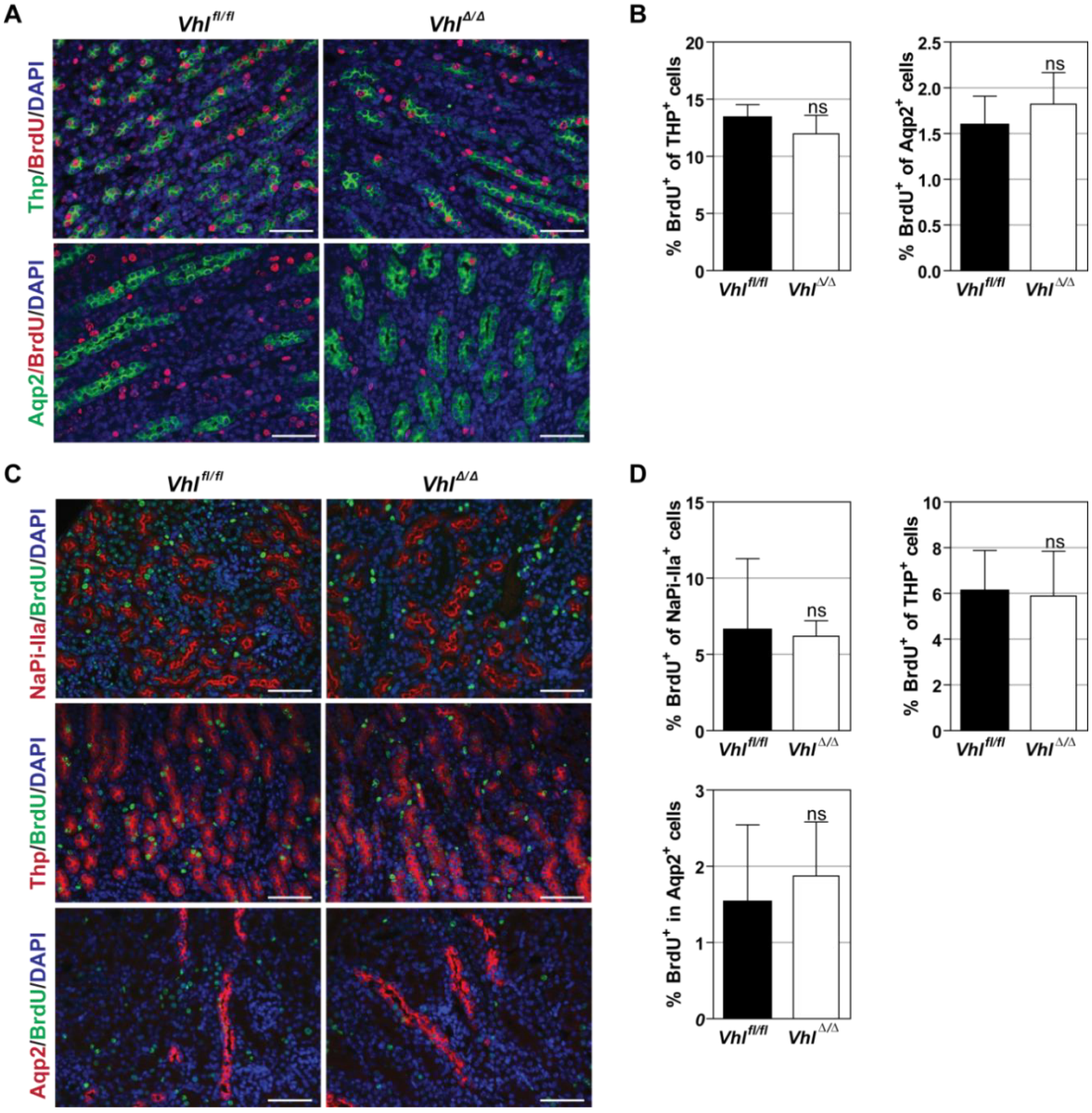

Fig. 8.23: Loss of *Vhl* does not alter proliferation capacity of renal tubular cells at day 7 and 14. (A) BrdU was injected in neonatal mice 2 h prior to dissection at postnatal day 7 (B) Quantification from A. Data was collected from 500-1000 positive cells per tubular marker. N=3. (C) BrdU injection 48 h before dissection at day 12, (D) Quantification from 1500 – 2500 positive cells per marker from D. N=4. Co-staining of DAPI, BrdU, and NaPi-IIa (proximal tubules), THP (thick ascending limb of Henle) or AQP2 (collecting ducts). Respective colors are depicted in the figure. Scale bar = 50 µm.

Next, we hypothesized that increased peritubular Ki67 staining in *Vhl*-deficient kidneys might be due to increased tissue vascularization, since Hif1α regulates the expression of vascular epithelial growth factor (VEGF), a major molecular mediator of angiogenesis (Connolly et al. 1989). Therefore, we measured *Vegf-a* transcript levels in kidneys of transgenic mice, demonstrating that adult *Vhl*-deficient mice exhibit elevated renal *Vegf-a* expression (Fig. 8.24D). Whereas loss *Hif1α* clearly abrogates the *Vhl*-dependent increase in *Vegf-a* expression, *Vhl/Hif2α*-deficient mice display a clear but not significant increase of transcripts, possibly because of tissue loss due

to more severe hydronephrosis in these mice. Visualization of renal blood vessels by immunohistochemial staining for von Willebrand factor (vWF) and CD31, two established markers of endothelial cells, confirmed a *Hif1*a-dependent regulation of kidney vascularization (Fig. 8.24A-C). Whereas we could not detect any difference in vWF expression in the renal cortex, stabilization of Hif1α, but not of Hif2α massively increases the density of endothelial vessels in the renal medulla (Fig. 8.24A, compare upper row for cortex and lower row for medulla). This observation could be confirmed by vWF and CD31 staining in young *Vhl*-deficient mice (Fig. 8.24B-C).

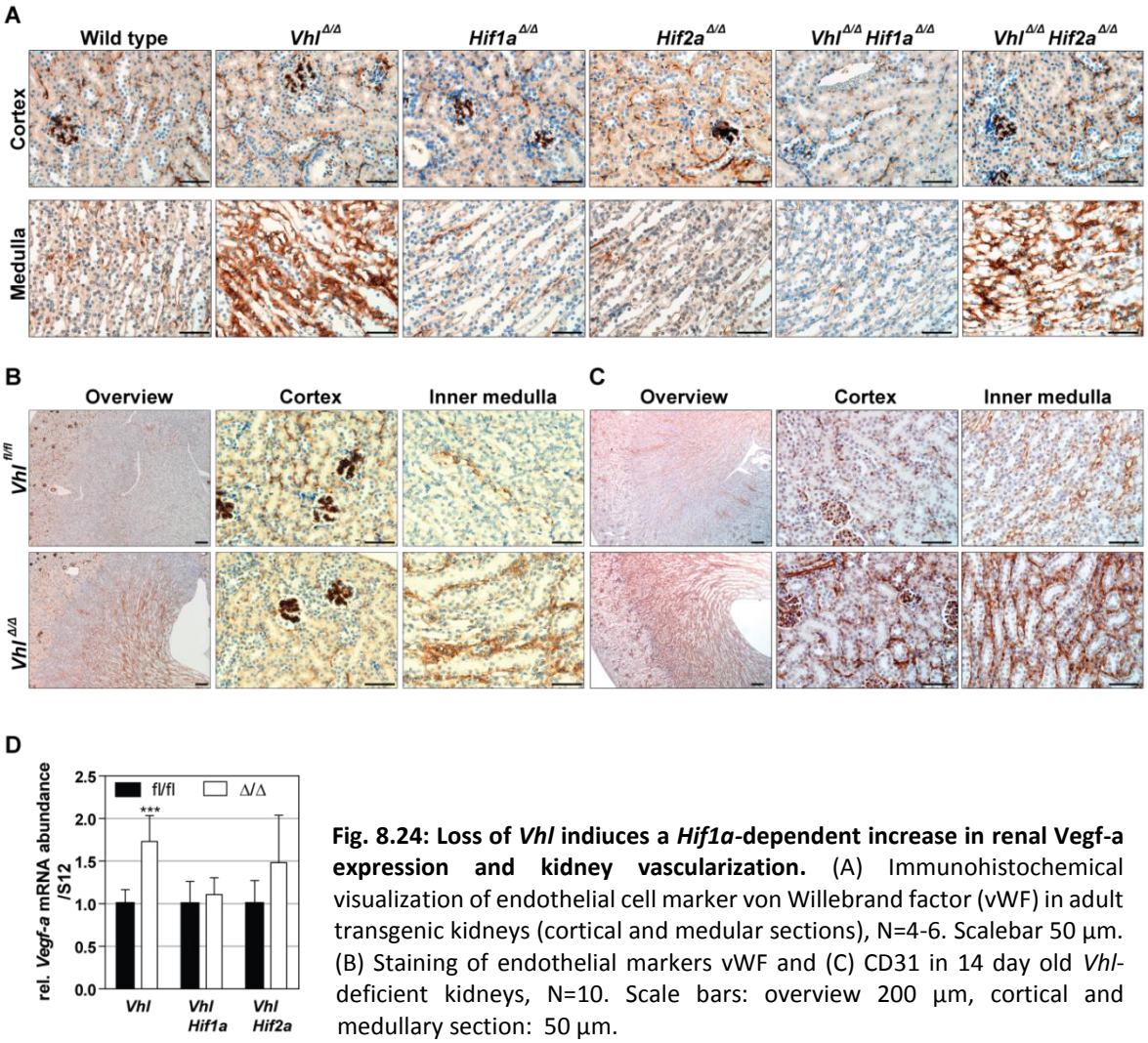

Fig. 8.24: Loss of *Vhl* indiuces a *Hif1α*-dependent increase in renal Vegf-a expression and kidney vascularization. (A) Immunohistochemical visualization of endothelial cell marker von Willebrand factor (vWF) in adult transgenic kidneys (cortical and medular sections), N=4-6. Scalebar 50 µm. (B) Staining of endothelial markers vWF and (C) CD31 in 14 day old *Vhl*-deficient kidneys, N=10. Scale bars: overview 200 µm, cortical and medullary section: 50 µm.

As the kidney is important for the regulation of the hematopoietic system in adults, we next tested whether changes in renal vascularization have an impact on blood homeostasis. Under low oxygen levels renal interstitial fibroblasts secrete erythropoietin (EPO), thereby promoting the production of red blood cells (Wenger and Hoogewijs 2010). Although the precise mechanism of oxygen-sensing in the kidney is still controversial, it is known that EPO expression is controlled

by Hif2α. As shown in Fig. 8.25A, loss of *Vhl* causes a *Hif1α*-dependent decrease in hemoglobin concentration in adult mice. Diminished hematocrit levels could be confirmed by an independent method in $Vhl^{\Delta/\Delta}$ and $Vhl^{\Delta/\Delta}Hif2a^{\Delta/\Delta}$ animals (data not shown). Interestingly, the difference is more pronounced in males than in females (Fig. 8.25B). Reduced hemoglobin levels were also shown in aged $Vhl^{\Delta/\Delta}$ mice (Fig. 8.25C). Given that the Ksp.1.3 promoter drives Cre expression only in epithelial but not in interstitial cells, decreased hemoglobin and hematocrit levels probably reflect a secondary adaption to *Vhl* deletion in the nephron due to increases in renal vascularization. However, changes in *Epo* gene expression could not be detected by RT-qPCR (Fig. 8.25D)

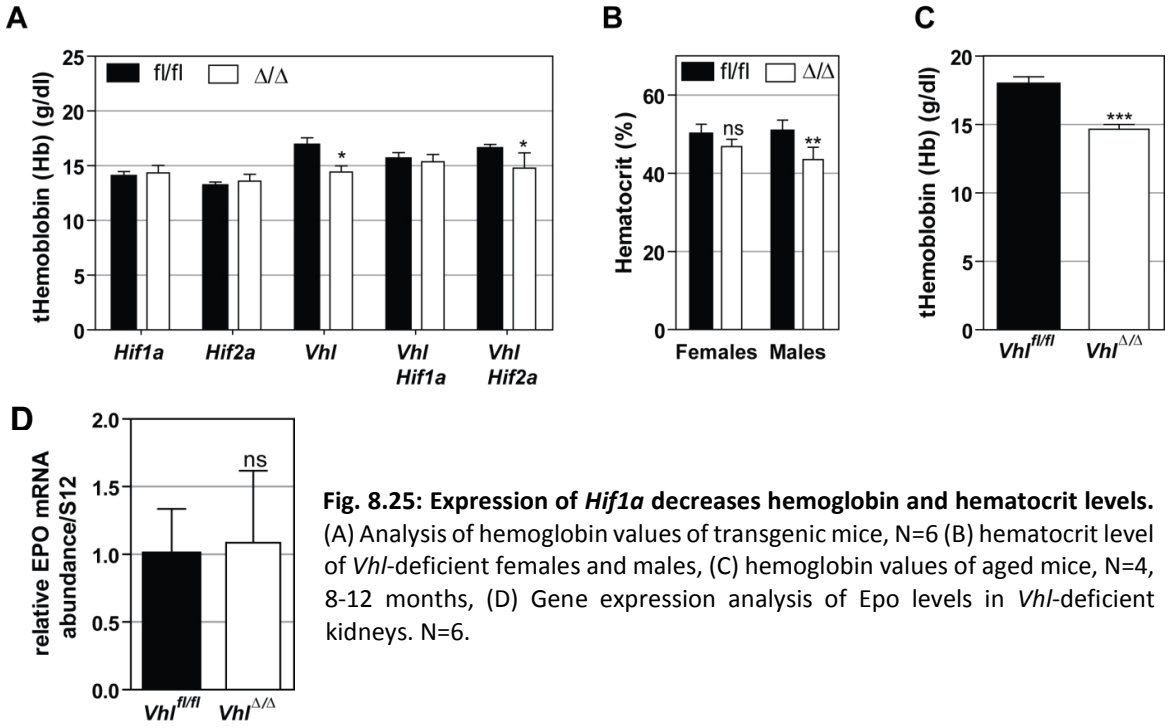

Fig. 8.25: Expression of *Hif1α* decreases hemoglobin and hematocrit levels. (A) Analysis of hemoglobin values of transgenic mice, N=6 (B) hematocrit level of *Vhl*-deficient females and males, (C) hemoglobin values of aged mice, N=4, 8-12 months, (D) Gene expression analysis of Epo levels in *Vhl*-deficient kidneys. N=6.

Taken together, we showed that stabilization of Hif1α increases renal vascularization in *Vhl*-deficient kidneys. We hypothesize that changes in medullary blood flow disrupts the osmotic gradient, essentially washing out salt from the renal interstitium and thereby preventing urinary concentration and urine reabsorption. The excess production of urine causes a back pressure on the kidney, leading to the expansion of the renal pelvis. To test this idea, we generated *Vhl* floxed mice harboring a tamoxifen-inducible Cre-recombinase (Ksp1.3-CreER^{T2}; $Vhl^{fl/fl}$) allowing the specific activation of Hifα in the adult kidney and thereby circumventing potential effects of *Vhl* deletion during renal development. µCT analysis and urine analysis did not show any significant changes in urine production or kidney morphology *in vivo* more than six months after tamoxifen induction, contradicting to our hypothesis (Fig. 8.26A-D). However, immunohistochemical analysis of Hifα protein expression revealed very few Hifα positive nuclei, indicating low

recombination efficiency (Fig. 8.26E). It is therefore very likely that renal expression of Hif1α was not sufficient to induce vascularization of the renal medulla and impair renal urine absorption.

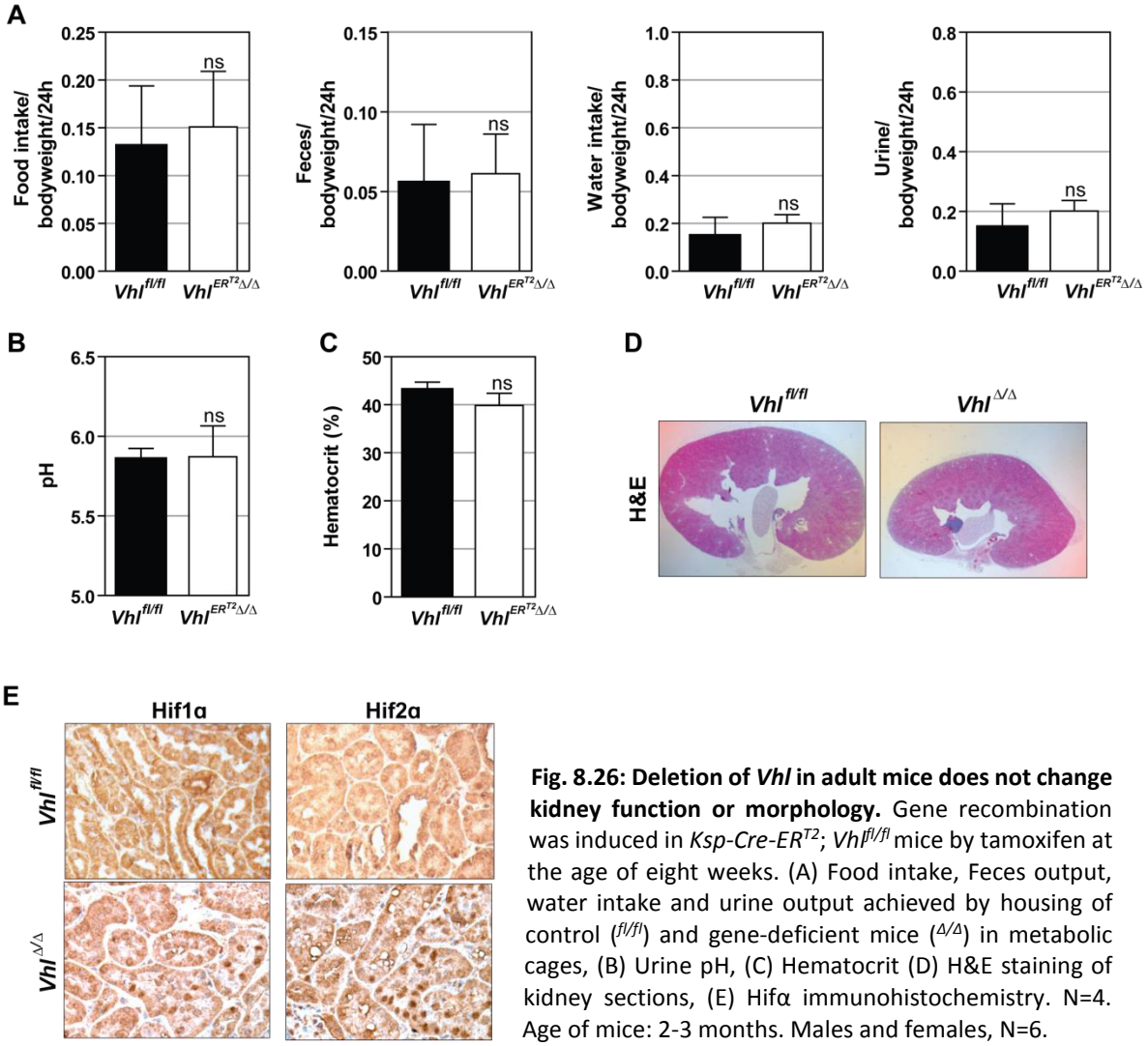

Fig. 8.26: Deletion of *Vhl* in adult mice does not change kidney function or morphology. Gene recombination was induced in *Ksp-Cre-ER^{T2}*; *Vhl$^{fl/fl}$* mice by tamoxifen at the age of eight weeks. (A) Food intake, Feces output, water intake and urine output achieved by housing of control (*$^{fl/fl}$*) and gene-deficient mice (*$^{Δ/Δ}$*) in metabolic cages, (B) Urine pH, (C) Hematocrit (D) H&E staining of kidney sections, (E) Hifα immunohistochemistry. N=4. Age of mice: 2-3 months. Males and females, N=6.

8.3.3 Discussion

We previously published that epithelial deletion of *Vhl* causes bilateral hydronephrosis in mice, however the underlying mechanism remains unclear (Frew et al. 2008a). In this study, we aimed to identify the ethology of hydronephrosis in *Vhl$^{Δ/Δ}$* mice and its consequence on kidney function. We could show that 24h urine production of *Vhl$^{Δ/Δ}$* mice is increased by a factor of 10 when compared to non-transgenic litter mates, accompanied by a massively reduced urine osmolality **(**Fig. 8.13A-B, G), pointing towards a non-obstructive cause for the formation of hydronephrosis. This notion is further supported by µCT-based visualization of the urogenital tract, which revealed no obvious delay in renal clearance of the contrast agent and an intact morphology of the ureter and the bladder in *Vhl$^{Δ/Δ}$* mice (Fig. 8.12A-B). These data demonstrate that *Vhl* deficient mice do

not suffer from any malformation or obstructions of the urogenital tract in contrast to several mouse models for hydronephrosis (Cain et al. 2011; Ekman et al. 2014). Consistently, hydronephrosis appears between postnatal day 10 and 14, further excluding an impairment of early renal development. Instead, excess urine production in *Vhl*-deficient mice most likely exceeds the ability of the ureter to remove the urine, subsequently building up pressure on the kidney and slowly expanding the renal pelvis and the collecting system. Consistently, µCT imaging revealed a weaker signal of the contrast agent from the cortex of $Vhl^{\Delta/\Delta}$ mice compared to $Vhl^{fl/fl}$ mice, presumably due to changes in urine flow or renal filtration rate.

Non-obstructive hydronephrosis represents the majority of cases diagnosed in humans and several human disorders are associated with polyuria and subsequent formation of non-obstructive hydronephrosis (Woodward and Frank 2002; Hebert 2003; Jin et al. 2009; Moon et al. 2009). To find the underlying cause of polyuria in *Vhl*-deficient mice we investigated several potential mechanisms that are known to impair renal water absorption in human disorders or corresponding mouse models. For instance, nephrogenic diabetes insipidus (NDI) is caused by a failure of the recruitment of the arginine vasopressin (AVP)-sensitive water transporters AQP2 to the apical membrane of collecting ducts, thereby impairing concentration of urine (Fujiwara et al. 1995). In $Vhl^{\Delta/\Delta}$ mice, AQP2 staining is predominantly localized to the apical membrane of collecting ducts, indicating that these cells are sensitive to AVP stimulation (Fig 8.17). In clinics, NDI is commonly diagnosed by the lack of response to desmopressin injections, an AVP analogue (Fenske and Allolio 2012). Therefore, AVP-sensitivity in *Vhl*-deficient mice could be further confirmed by desmopressin injections. However, given that the recruitment of AQP2 to the cell membrane was already observed under unchallenged conditions, we speculate that $Vhl^{\Delta/\Delta}$ mice already exhibit a maximal activation of the AVP system to prevent dehydration and thereby would not respond to an additional stimulation with desmopressin. This hypothesis also provides an explanation for the inability of *Vhl*-deficient mice to respond to water restriction despite functional AQP2 recruitment (Fig. 8.16B). Consequently, we would expect an even more pronounced polyuria when mice were treated with an AVP V2-receptor antagonist such as tolvapan (Yamamura et al. 1998).

Not only the loss of function of AQP2 but also deletions of AQP1, 3 and 4 are associated with polyuria in mice (Yang et al. 2001; McDill et al. 2006; Ampawong et al. 2012). Examination of AQP gene expression in $Vhl^{\Delta/\Delta}$ kidneys revealed a decreased abundance of AQP1, 2, 3 and 7, proposing that lower levels of water channels in $Vhl^{\Delta/\Delta}$ mice might at least partially contribute to the phenotype (Fig. 8.18A,C). Together with the concomitant decrease in gene expression of different segment markers such as NaPi-IIa (proximal tubules), NCC (distal tubules) and Pendrin (proximal

tubules and cortical collecting ducts), these data indicate a general shortening of the renal nephron, presumably as a consequence of the expansion of the renal pelvis (Fig. 8.19B). This notion is supported by the antibody staining to label specific renal segments which are particularly reduced in the renal medulla (Fig. 8.18B and Fig. 8.19A). To circumvent any secondary effects of changes in renal morphology, we aim to further investigate the expression of renal transporters in neonatal mice.

In the kidney the Na-K-ATPase consumes the majority of ATP produced in the cell to transport solutes though the membrane (Soltoff 1986). Given that loss of *Vhl* recues cellular ATP production in MEFs, it is appealing to speculate that low ATP levels in the renal epithelium might impair the maintenance of renal ion gradients, which are necessary for the efficient reabsorption of water. However, we found normal plasma levels for various electrolytes and similar renal reabsorption rates for sodium, potassium and calcium in *Vhl*-deficient mice compared to wild type mice, arguing against a problem with renal ion transport (Fig. 8.20B and Fig. 8.14A). Furthermore, $Vhl^{\Delta/\Delta}$ mice exhibit normal blood levels of creatinine and blood urea nitrogen (BUN), further indicating unaffected kidney function. Consistently, aged mice exhibit a largely preserved renal function and histology (Fig. 8.15A-C). This is in strong contrast to most other published mouse models with polyuria, which suffer from kidney insufficiency and severe renal damage. For instance, mice suffering from NDI show progressive hydronephrosis, kidney insufficiency, growth retardation and reduced survival (Yang et al. 2001; McDill et al. 2006). Mouse models for Bartter syndrome, a group of genetic disorders caused by mutations in renal ion transporters, display an even more severe phenotype as they exhibit an imbalance in electrolytes in addition to the other symptoms (Takahashi et al. 2000; Yan et al. 2008). We therefore speculate that loss of pVhl in the renal epithelium provides a new model for non-obstructive hydronephrosis in mice.

The investigation of *Vhl/Hif1a* and *Vhl/Hif2a*-deficient mice revealed that the deletion of *Hif1a*, but not H*if2a*, fully restores renal morphology and function, demonstrating a Hif1α dependent mechanism. Although the stabilization of Hif1α impairs cell proliferation *in vitro* (Fig. 8.2A) nwe did not detect any difference in the proliferation of tubular cells of $Vhl^{\Delta/\Delta}$ mice compared to controls at day 7 and 14 (Fig. 8.23A-D). Similarly, initial experiments at day 14 also did not show any difference in apoptosis of tubular cells (data not shown). It remains to be tested whether increased apoptosis at an earlier time point might contribute to the formation of hydronephrosis.

Loss of *Vhl* causes an elevated expression of *Vegf-a* in the kidney, which is abrogated by co-deletion of *Hif1a* but not *Hif2a* (Fig. 8.24D). *Vegf-a* is a known *Hif1a* target gene and serves as major mediator of angiogenesis (Connolly et al. 1989). Staining for two independent endothelial cell markers confirmed that the increased renal abundance of *Vegf-a* mRNA is translated into an

increased vascularization of renal medulla of *Vhl*$^{\Delta/\Delta}$ and *Vhl*$^{\Delta/}$*Hif2α*$^{\Delta/\Delta}$ mice (Fig. 8.24A-C). Although it has earlier been shown that co-expression of Vegf and Hif1a induces the formation of mature vessels in the skin, we aim to confirm the functionality of the vasculature by the generation of vascular erosion casts of *Vhl*$^{\Delta/\Delta}$ kidneys and investigate the architecture of the medullary capillaries by electron microscopy (Elson et al. 2001). In mice, the maturation of the renal vasculature continues until approximately 10 days after birth (Machura 2007). Therefore, we hypothesize that an increased medullary blood flow (MBF) in *Vhl*-deficient kidneys during this time period allows a more efficient absorption of salts from the renal interstitium, thereby disrupting the osmotic gradient which is the driving force for urine concentration. Therefore, the lower osmolality of the interstitium prevents efficient uptake of water in the renal tubules, resulting in an excess production of urine. This urine subsequently induces a back pressure on the kidney, causing an expansion of the renal pelvis. Several other studies confirm that renal blood flow is a central mediator of ion and water absorption in the kidney (Lu et al. 1992; Zou et al. 2001). For instance, selective infusion of vasodilators in the renal medulla of rats increases MBF, accompanied by diuresis and natriuresis (Mattson and Cowley 1993). In contrast, vasoconstrictors decreased MBF and lowered the excretion of water and sodium (Rajapakse and Mattson 2011). Therefore, it would be interesting to test whether local inhibition of Vegf-a and subsequent reduction of medullary capillary abundance restores normal urine output in *Vhl*$^{\Delta/\Delta}$ mice. Intriguingly, hydronephrosis has not been reported in any other model of *Vhl*-deletion in the renal epithelium, although an increase in renal vasculature and Vegf production has also been observed in some cases (Ma et al. 2003; Rankin et al. 2006; Schley et al. 2011; Mathia et al. 2013; Pritchett et al. 2014). Given that these mice seem to exhibit a milder increase in renal vascularization compared to our mouse model it is feasible that a moderate increase in renal blood flow is not sufficient to disturb the renal osmotic gradient.

Polyuria appears to have opposing effects on haematocrit levels in mice, probably depending on the underlying cause and the severity of the phenotype. Loss of *Vhl* lowers haemoglobin and haematocrit levels in mice, similar to mice suffering from prenatal hydronephrosis (Fig. 8.25A-C) (Wu et al. 2009). In contrast, polyuria in other mouse models has either no effect or even increases Hct levels, presumably due to dehydration (Takahashi et al. 2000; Schley et al. 2011). We speculate that in *Vhl*$^{\Delta/\Delta}$ mice increased renal vascularization improves the oxygenation of the tissue, which in turn lowers renal Epo production and subsequently diminishes erythropoiesis. An alternative – or additional – explanation for reduced erythropoiesis could be a change in renal oxygen consumption. As shown in figure 8.4B, loss of *Vhl* in the nephron decreases mitochondrial respiration in the tissue due to *Hif1a*-dependent changes in cellular energy metabolism and mitochondrial activity. These changes possibly lead to a higher oxygen concentration in the tissue

leading to decreased renal Epo production. Although, Epo mRNA abundance did not change in the kidney, serum Epo levels remain to be tested (Fig. 8.25D).

Increased renal vascularization might also provide an explanation for the milder effect of polyuria on kidney function compared to other mouse models with polyuria. Administration of VEGF has been shown to enhance capillary repair and improve renal function in renal disorders or after injury (Kim et al. 2000; Kang et al. 2001). Furthermore, diminished *Vegf-a* expression and capillary density in patients with diabetic nephropathy is associated with disease progression (Lindenmeyer et al. 2007). Therefore, we speculate that the pressure-induced expansion of the renal pelvis might damage the renal capillaries, promoting renal destruction. In contrast, increased VEGF expression in *Vhl*-deficient mice improves renal blood flow and thereby prevents kidney damage. Conversely, however, other studies report a deleterious role of VEGF overproduction in several renal pathologies or mouse models (Kang and Johnson 2003). It is likely that the expression of other Hifα target genes also exert renoprotective effects, for instance by the decreased production of reactive oxygen species (ROS) or promoting cell survival (Haase 2013). Consistently, genetic activation of Hifα has been shown to protect the kidney during acute ischemic injuries (Manotham et al. 2005; Schley et al. 2011).

9 General Discussion and Outlook

Tumours evolve through the accumulation of driver mutations and other genetic alterations that provide a proliferation and survival advantage to the cell. Epidemiologic studies suggest that solid tumours require five to eight of these "hits" for their development (Armitage and Doll 1954). However, cells also gather a large number of passenger mutations over time that have no impact on tumour growth. During recent years, large whole genome profiling studies revealed a broad range of genetic alterations in established tumours such as ccRCC. However, it remains unclear which mutations or combinations of mutations are driving tumourigenesis, as well as in which order they have to occur. One aim of this thesis was to investigate the cooperative effects of four commonly mutated genes in ccRCC (*Vhl*, *Hif1α, Hif2α* and *Trp53*) and their relevance in tumour initiation. We found that loss of *Hif1α* in a *Vhl/Trp53* negative background provides a proliferation advantage to cells in culture, however *Hif1α* is crucial for tumour initiation *in vivo*. To test whether loss of *Hif1α* is beneficial for tumour growth in already established lesions, it would be necessary to develop animal models that allow staggered inactivation of genes to model the physiological process of tumour evolution. One possibility would be to combine different inducible systems to mediate gene deletions *in vivo*, such as the Cre/LoxP and the Flp/FRT systems (Sauer and Henderson 1989; O'Gorman et al. 1991). However, since the generation of classical conditional mouse models is a time-consuming process that requires a lot of personnel and financial resources, new approaches are desirable. Our lab recently developed a promising lentiviral-based vector system called MuLE (Multiple Lentiviral expression), which allows the simultaneous introduction of multiple genetic alterations into mammalian cells *in vivo* and *in vitro (Albers et al. 2014, unpublished data).* This system enables the generation of polycistronic lentiviruses which can be directly injected in the kidney or other organs of interest to induce gene overexpressions or deletions. At the same time, fluorescent (e.g. iRFP, tdTomato, mCherry) or enzymatic reporters (luciferase, lacZ) can be expressed to monitor tumour growth *in vivo*. For instance, it would be interesting to produce lentivirus particles expressing Cre recombinase, luciferase and an inducible shRNA targeting *Hif1α* (e.g. isopropyl-b-D-thio-galactoside (IPTG)-inducible shRNA, Sigma-Aldrich), inject them into the kidney of $Vhl^{fl/fl}Trp53^{fl/fl}$ mice and monitor the formation of renal lesions by *in vivo* imaging. Subsequently, the effect of loss of *Hif1α* on these lesions can be examined by the induction of the shRNA hairpin expression. Similarly, it would be possible to screen for other driver mutations or oncogenic gene combinations *in vivo*. Promising candidate genes would be the genes found in our gain of representation screen (*Cdkn1a*, *Trp53*, *Trp63*, *Rb1* and *Rbl1*) or *PBRM1*, *BAP1*, *SETD2* and members of the TOR pathway as they have recently been shown to be commonly mutated in ccRCC (Sato et al. 2013). Importantly, due to the broad range

of cells that can be infected by lentiviruses the MuLE system allows targeting of not only epithelial cells but also other cell types that might contribute to tumour formations, such as renal stem cells (Funke et al. 2008; Axelson and Johansson 2013).

To identify additional candidates, it would be interesting to repeat our gain of representation screen with an shRNA library targeting a larger number of commonly mutated genes or even the whole kinome or genome and additionally test cooperative effects in different backgrounds such as in *Vhl/Trp53* or *Vhl/Cdkn2a* null PKCs. Additionally, it would be possible to use other gene libraries based on the RNA-guided CRISPR-Cas9 nuclease system that allows the generation of gene knockouts in mammalian cells (Ran et al. 2013). Another approach to identify potential driver mutations in ccRCC is the whole genome sequencing of micro-dissected lesions that arise in *Vhl/Trp53* mice. Given that tumour growth is initiated almost a year after the deletion of *Vhl* and *Trp53,* we speculate that additional oncogenic alterations occur in the already tumour prone *Vhl/Trp53* null epithelial cells to drive proliferation. Therefore, these mutations represent a key step in tumour evolution and might provide promising targets for future treatment approaches.

The mouse models generated by the approaches discussed above would provide new insights into the molecular mechanisms underlying the formation of ccRCC that are necessary for the development of efficient treatments for advanced ccRCC. For instance, cell lines generated from lesions at different stages could be used to screen different chemical libraries for potential new drug targets. Eventually, new drugs could be validated in these mouse models by assessing tumour response over time by *in vivo* imaging.

In the second part of this thesis we identified a new mechanism that leads to the formation of hydronephrosis in mice, which might help to understand so far unexplainable cases of hydronephrosis in humans and especially in children. The most intriguing finding was that in contrast to other polyuric mouse models, the kidneys of *Vhl*-deficient mice do not suffer from renal insufficiency or renal damage. The finding that stabilization of Hif1α exhibits renoprotective functions provides new perspectives for the treatment of patients suffering from hydronephrosis or chronic kidneys diseases. Therefore, it would be interesting to test whether the stabilization of Hif1α could prevent or attenuate renal damage also in other mouse models with polyuria, for instance by the pharmacological activation of specific Hif1α targets in the kidney, such as the stimulation of renal angiogenesis or by reducing ROS production. Of special interest could be the treatment of mice with a mutation in AQP2, a model for NDI (McDill et al. 2006). Although primary NDI is a rather rare syndrome, secondary NDI is a common complication of other genetic disorders (e.g. Bartter's syndrome) or as side effect of pharmacological interventions (e.g. lithium

treatment), thereby affecting a large number of patients worldwide (Bockenhauer and Bichet 2013).

11 References

Abreu-Rodriguez I, Sanchez Silva R, Martins AP, Soveral G, Toledo-Aral JJ, Lopez-Barneo J, Echevarria M. 2011. Functional and transcriptional induction of aquaporin-1 gene by hypoxia; analysis of promoter and role of Hif-1alpha. *PLoS One* **6**(12): e28385.

Albers J, Brandt S, Bode P, Bode-Lesniewska B, Wild P, Frew IJ. 2014. The MuLE lentiviral vector system facilitates combinatorial genetics and reveals genetic cooperation between H-RAS and CDK2a in rhabdomyosarcomas.

Albers J, Rajski M, Schönenberger D, Harlander S, Schraml P, von Teichman A, Georgiev S, Wild PJ, Moch H, Krek W et al. 2013. Combined mutation of Vhl and Trp53 causes renal cysts and tumours in mice. *EMBO Molecular Medicine* **5**(6): 949-964.

Almajdub M, Magnier L, Juillard L, Janier M. 2008. Kidney volume quantification using contrast-enhanced in vivo X-ray micro-CT in mice. *Contrast Media Mol Imaging* **3**(3): 120-126.

Ampawong S, Klincomhum A, Likitsuntonwong W, Singha O, Ketjareon T, Panavechkijkul Y, Zaw KM, Kengkoom K. 2012. Expression of aquaporin-1, -2 and -4 in mice with a spontaneous mutation leading to hydronephrosis. *J Comp Pathol* **146**(4): 332-337.

Ang SO, Chen H, Hirota K, Gordeuk VR, Jelinek J, Guan Y, Liu E, Sergueeva AI, Miasnikova GY, Mole D et al. 2002. Disruption of oxygen homeostasis underlies congenital Chuvash polycythemia. *Nat Genet* **32**(4): 614-621.

Armitage P, Doll R. 1954. The age distribution of cancer and a multi-stage theory of carcinogenesis. *British journal of cancer* **8**(1): 1-12.

Asim Amin ERP, Jeffrey R. Infante, Marc S. Ernstoff, Brian I. Rini, David F. McDermott, Jennifer J. Knox, Sumanta Kumar Pal, Martin Henner Voss, Padmanee Sharma, Christian K. Kollmannsberger, Daniel Yick Chin Heng, Jennifer L. Spratlin, Yun Shen, John F. Kurland, Paul Gagnier, Hans J. Hammers;

Atkins M, Ravaud, A., Gravis, G, et. al. 2012. Safety and efficacy of AMG 386 in combination with sunitinib in patients with metastatic renal cell carcinoma (mRCC) in an open-label multicenter phase II study. *Journal of clinical oncology : official journal of the American Society of Clinical Oncology*.

Au KK, Woo JS, Tang LC, Liang ST. 1985. Aetiological factors in the genesis of pregnancy hydronephrosis. *The Australian & New Zealand journal of obstetrics & gynaecology* **25**(4): 248-251.

Axelson H, Johansson ME. 2013. Renal stem cells and their implications for kidney cancer. *Seminars in cancer biology* **23**(1): 56-61.

Bailey RR, Lynn KL, Robson RA. 1994. End-stage reflux nephropathy. *Renal failure* **16**(1): 27-35.

Banumathy G, Cairns P. 2010. Signaling pathways in renal cell carcinoma. *Cancer Biol Ther* **10**(7): 658-664.

Bardos JI, Ashcroft M. 2004. Hypoxia-inducible factor-1 and oncogenic signalling. *Bioessays* **26**(3): 262-269.

Barontini M, Dahia PL. 2010. VHL disease. *Best practice & research Clinical endocrinology & metabolism* **24**(3): 401-413.

Berndt JD, Moon RT, Major MB. 2009. Beta-catenin gets jaded and von Hippel-Lindau is to blame. *Trends in biochemical sciences* **34**(3): 101-104.

Berndt TJ, Knox FG. 1992. *The Kidney, Physiology and Pathophysiology.* Raven Press, New York.

Bertout JA, Majmundar AJ, Gordan JD, Lam JC, Ditsworth D, Keith B, Brown EJ, Nathanson KL, Simon MC. 2009. HIF2alpha inhibition promotes p53 pathway activity, tumor cell death, and radiation responses. *Proc Natl Acad Sci U S A* **106**(34): 14391-14396.

Birn H, Fyfe JC, Jacobsen C, Mounier F, Verroust PJ, Orskov H, Willnow TE, Moestrup SK, Christensen EI. 2000. Cubilin is an albumin binding protein important for renal tubular albumin reabsorption. *The Journal of clinical investigation* **105**(10): 1353-1361.

Biswas S, Troy H, Leek R, Chung YL, Li JL, Raval RR, Turley H, Gatter K, Pezzella F, Griffiths JR et al. 2010. Effects of HIF-1alpha and HIF2alpha on Growth and Metabolism of Clear-Cell Renal Cell Carcinoma 786-0 Xenografts. *J Oncol* **2010**: 757908.

Blankenship C, Naglich JG, Whaley JM, Seizinger B, Kley N. 1999. Alternate choice of initiation codon produces a biologically active product of the von Hippel Lindau gene with tumor suppressor activity. *Oncogene* **18**(8): 1529-1535.

Bockenhauer D, Bichet DG. 2013. Inherited secondary nephrogenic diabetes insipidus: concentrating on humans. *American journal of physiology Renal physiology* **304**(8): F1037-1042.

Braga LH, Ruzhynsky V, Pemberton J, Farrokhyar F, Demaria J, Lorenzo AJ. 2014. Evaluating practice patterns in postnatal management of antenatal hydronephrosis: a national survey of Canadian pediatric urologists and nephrologists. *Urology* **83**(4): 909-914.

Bukowski RM, Kabbinavar FF, Figlin RA, Flaherty K, Srinivas S, Vaishampayan U, Drabkin HA, Dutcher J, Ryba S, Xia Q et al. 2007. Randomized phase II study of erlotinib combined with bevacizumab compared with bevacizumab alone in metastatic renal cell cancer. *Journal of clinical oncology : official journal of the American Society of Clinical Oncology* **25**(29): 4536-4541.

Cain JE, Islam E, Haxho F, Blake J, Rosenblum ND. 2011. GLI3 repressor controls functional development of the mouse ureter. *The Journal of clinical investigation* **121**(3): 1199-1206.

Caubit X, Lye CM, Martin E, Core N, Long DA, Vola C, Jenkins D, Garratt AN, Skaer H, Woolf AS et al. 2008. Teashirt 3 is necessary for ureteral smooth muscle differentiation downstream of SHH and BMP4. *Development* **135**(19): 3301-3310.

Cerami E, Gao J, Dogrusoz U, Gross BE, Sumer SO, Aksoy BA, Jacobsen A, Byrne CJ, Heuer ML, Larsson E et al. 2012. The cBio cancer genomics portal: an open platform for exploring multidimensional cancer genomics data. *Cancer discovery* **2**(5): 401-404.

Chen L, Cai A, Wang X, Wang B, Li J. 2010. Two- and three-dimensional prenatal sonographic diagnosis of prune-belly syndrome. *Journal of clinical ultrasound : JCU* **38**(5): 279-282.

Cheung KL, Lafayette RA. 2013. Renal physiology of pregnancy. *Advances in chronic kidney disease* **20**(3): 209-214.

Chevalier RL, Kaiser DL. 1984. Chronic partial ureteral obstruction in the neonatal guinea pig. I. Influence of uninephrectomy on growth and hemodynamics. *Pediatric research* **18**(12): 1266-1271.

Chitalia VC, Foy RL, Bachschmid MM, Zeng L, Panchenko MV, Zhou MI, Bharti A, Seldin DC, Lecker SH, Dominguez I et al. 2008. Jade-1 inhibits Wnt signalling by ubiquitylating beta-catenin and mediates Wnt pathway inhibition by pVHL. *Nat Cell Biol* **10**(10): 1208-1216.

Cho HK, Kim SY, Kim KH, Kim HH, Cheong J. 2013. Tumor suppressor protein VHL inhibits Hedgehog-Gli activation through suppression of Gli1 nuclear localization. *FEBS letters* **587**(7): 826-832.

Choi H, Chun YS, Kim TY, Park JW. 2010. HIF-2alpha enhances beta-catenin/TCF-driven transcription by interacting with beta-catenin. *Cancer Res* **70**(24): 10101-10111.

Choyke PL, Glenn GM, Wagner JP, Lubensky IA, Thakore K, Zbar B, Linehan WM, Walther MM. 1997. Epididymal cystadenomas in von Hippel-Lindau disease. *Urology* **49**(6): 926-931.

Connolly DT, Heuvelman DM, Nelson R, Olander JV, Eppley BL, Delfino JJ, Siegel NR, Leimgruber RM, Feder J. 1989. Tumor vascular permeability factor stimulates endothelial cell growth and angiogenesis. *The Journal of clinical investigation* **84**(5): 1470-1478.

Costantini F, Kopan R. 2010. Patterning a complex organ: branching morphogenesis and nephron segmentation in kidney development. *Developmental cell* **18**(5): 698-712.

Di Iorgi N, Napoli F, Allegri AE, Olivieri I, Bertelli E, Gallizia A, Rossi A, Maghnie M. 2012. Diabetes insipidus--diagnosis and management. *Hormone research in paediatrics* **77**(2): 69-84.

Dressler GR. 2009. Advances in early kidney specification, development and patterning. *Development* **136**(23): 3863-3874.

Droz D, Zachar D, Charbit L, Gogusev J, Chretein Y, Iris L. 1990. Expression of the human nephron differentiation molecules in renal cell carcinomas. *The American journal of pathology* **137**(4): 895-905.

Dudley JA, Haworth JM, McGraw ME, Frank JD, Tizard EJ. 1997. Clinical relevance and implications of antenatal hydronephrosis. *Archives of disease in childhood Fetal and neonatal edition* **76**(1): F31-34.

Eckardt KU, Koury ST, Tan CC, Schuster SJ, Kaissling B, Ratcliffe PJ, Kurtz A. 1993. Distribution of erythropoietin producing cells in rat kidneys during hypoxic hypoxia. *Kidney Int* **43**(4): 815-823.

Ekman M, Uvelius B, Albinsson S, Sward K. 2014. HIF-mediated metabolic switching in bladder outlet obstruction mitigates the relaxing effect of mitochondrial inhibition. *Lab Invest* **94**(5): 557-568.

Elson DA, Thurston G, Huang LE, Ginzinger DG, McDonald DM, Johnson RS, Arbeit JM. 2001. Induction of hypervascularity without leakage or inflammation in transgenic mice overexpressing hypoxia-inducible factor-1alpha. *Genes Dev* **15**(19): 2520-2532.

Espinel CH. 1976. The FENa test. Use in the differential diagnosis of acute renal failure. *JAMA : the journal of the American Medical Association* **236**(6): 579-581.

Esteban MA, Tran MG, Harten SK, Hill P, Castellanos MC, Chandra A, Raval R, O'Brien T S, Maxwell PH. 2006. Regulation of E-cadherin expression by VHL and hypoxia-inducible factor. *Cancer Res* **66**(7): 3567-3575.

Everett LA, Glaser B, Beck JC, Idol JR, Buchs A, Heyman M, Adawi F, Hazani E, Nassir E, Baxevanis AD et al. 1997. Pendred syndrome is caused by mutations in a putative sulphate transporter gene (PDS). *Nat Genet* **17**(4): 411-422.

Fang JS, Gillies RD, Gatenby RA. 2008. Adaptation to hypoxia and acidosis in carcinogenesis and tumor progression. *Seminars in cancer biology* **18**(5): 330-337.

Fenske W, Allolio B. 2012. Clinical review: Current state and future perspectives in the diagnosis of diabetes insipidus: a clinical review. *The Journal of clinical endocrinology and metabolism* **97**(10): 3426-3437.

Freeburg PB, Abrahamson DR. 2003. Hypoxia-inducible factors and kidney vascular development. *J Am Soc Nephrol* **14**(11): 2723-2730.

Freedman DA, Levine AJ. 1999. Regulation of the p53 protein by the MDM2 oncoprotein--thirty-eighth G.H.A. Clowes Memorial Award Lecture. *Cancer Res* **59**(1): 1-7.

Frew IJ, Minola A, Georgiev S, Hitz M, Moch H, Richard S, Vortmeyer AO, Krek W. 2008a. Combined VHLH and PTEN mutation causes genital tract cystadenoma and squamous metaplasia. *Mol Cell Biol* **28**(14): 4536-4548.

Frew IJ, Thoma CR, Georgiev S, Minola A, Hitz M, Montani M, Moch H, Krek W. 2008b. pVHL and PTEN tumour suppressor proteins cooperatively suppress kidney cyst formation. *EMBO J* **27**(12): 1747-1757.

Fujiwara TM, Morgan K, Bichet DG. 1995. Molecular biology of diabetes insipidus. *Annual review of medicine* **46**: 331-343.

Fukuda R, Zhang H, Kim JW, Shimoda L, Dang CV, Semenza GL. 2007. HIF-1 regulates cytochrome oxidase subunits to optimize efficiency of respiration in hypoxic cells. *Cell* **129**(1): 111-122.

Funke S, Maisner A, Muhlebach MD, Koehl U, Grez M, Cattaneo R, Cichutek K, Buchholz CJ. 2008. Targeted cell entry of lentiviral vectors. *Molecular therapy : the journal of the American Society of Gene Therapy* **16**(8): 1427-1436.

Gao J, Aksoy BA, Dogrusoz U, Dresdner G, Gross B, Sumer SO, Sun Y, Jacobsen A, Sinha R, Larsson E et al. 2013. Integrative analysis of complex cancer genomics and clinical profiles using the cBioPortal. *Science signaling* **6**(269): pl1.

Gargollo PC, Diamond DA. 2007. Therapy insight: What nephrologists need to know about primary vesicoureteral reflux. *Nature clinical practice Nephrology* **3**(10): 551-563.

Georgas K, Rumballe B, Valerius MT, Chiu HS, Thiagarajan RD, Lesieur E, Aronow BJ, Brunskill EW, Combes AN, Tang D et al. 2009. Analysis of early nephron patterning reveals a role for distal RV proliferation in fusion to the ureteric tip via a cap mesenchyme-derived connecting segment. *Developmental biology* **332**(2): 273-286.

Gerdes J, Lemke H, Baisch H, Wacker HH, Schwab U, Stein H. 1984. Cell cycle analysis of a cell proliferation-associated human nuclear antigen defined by the monoclonal antibody Ki-67. *Journal of immunology* **133**(4): 1710-1715.

Gilbert SF. 2003. Developmental Biology. (Seventh Edition).

Glick PL, Harrison MR, Noall RA, Villa RL. 1983. Correction of congenital hydronephrosis in utero III. Early mid-trimester ureteral obstruction produces renal dysplasia. *Journal of pediatric surgery* **18**(6): 681-687.

Gnarra JR, Ward JM, Porter FD, Wagner JR, Devor DE, Grinberg A, Emmert-Buck MR, Westphal H, Klausner RD, Linehan WM. 1997. Defective placental vasculogenesis causes embryonic lethality in VHL-deficient mice. *Proc Natl Acad Sci U S A* **94**(17): 9102-9107.

Gomez RA, Norwood VF, Tufro-McReddie A. 1997. Development of the kidney vasculature. *Microscopy research and technique* **39**(3): 254-260.

Gordan JD, Bertout JA, Hu CJ, Diehl JA, Simon MC. 2007. HIF-2alpha promotes hypoxic cell proliferation by enhancing c-myc transcriptional activity. *Cancer Cell* **11**(4): 335-347.

Gordan JD, Lal P, Dondeti VR, Letrero R, Parekh KN, Oquendo CE, Greenberg RA, Flaherty KT, Rathmell WK, Keith B et al. 2008. HIF-alpha effects on c-Myc distinguish two subtypes of sporadic VHL-deficient clear cell renal carcinoma. *Cancer Cell* **14**(6): 435-446.

Greene F. 2002. *AJCC Cancer Staging Manual*. Springer.

Grignon A, Filion R, Filiatrault D, Robitaille P, Homsy Y, Boutin H, Leblond R. 1986. Urinary-Tract Dilatation Inutero - Classification and Clinical-Applications. *Radiology* **160**(3): 645-647.

Grosfeld A, Stolze IP, Cockman ME, Pugh CW, Edelmann M, Kessler B, Bullock AN, Ratcliffe PJ, Masson N. 2007. Interaction of hydroxylated collagen IV with the von hippel-lindau tumor suppressor. *J Biol Chem* **282**(18): 13264-13269.

Gruber M, Hu CJ, Johnson RS, Brown EJ, Keith B, Simon MC. 2007. Acute postnatal ablation of Hif-2alpha results in anemia. *Proc Natl Acad Sci U S A* **104**(7): 2301-2306.

Gu YZ, Moran SM, Hogenesch JB, Wartman L, Bradfield CA. 1998. Molecular characterization and chromosomal localization of a third alpha-class hypoxia inducible factor subunit, HIF3alpha. *Gene Expr* **7**(3): 205-213.

Gunaratnam L, Morley M, Franovic A, de Paulsen N, Mekhail K, Parolin DA, Nakamura E, Lorimer IA, Lee S. 2003. Hypoxia inducible factor activates the transforming growth factor-alpha/epidermal growth factor receptor growth stimulatory pathway in VHL(-/-) renal cell carcinoma cells. *J Biol Chem* **278**(45): 44966-44974.

Haase VH. 2013. Mechanisms of hypoxia responses in renal tissue. *J Am Soc Nephrol* **24**(4): 537-541.

Haase VH, Glickman JN, Socolovsky M, Jaenisch R. 2001. Vascular tumors in livers with targeted inactivation of the von Hippel-Lindau tumor suppressor. *Proc Natl Acad Sci U S A* **98**(4): 1583-1588.

Haeri S, Devers PL, Kaiser-Rogers KA, Moylan VJ, Jr., Torchia BS, Horton AL, Wolfe HM, Aylsworth AS. 2010. Deletion of hepatocyte nuclear factor-1-beta in an infant with prune belly syndrome. *American journal of perinatology* **27**(7): 559-563.

Hakimi AA, Pham CG, Hsieh JJ. 2013. A clear picture of renal cell carcinoma. *Nat Genet* **45**(8): 849-850.

Hamanaka RB, Chandel NS. 2009. Mitochondrial reactive oxygen species regulate hypoxic signaling. *Current opinion in cell biology* **21**(6): 894-899.

Hanahan D, Weinberg RA. 2000. The hallmarks of cancer. *Cell* **100**(1): 57-70.

Hara S, Hamada J, Kobayashi C, Kondo Y, Imura N. 2001. Expression and characterization of hypoxia-inducible factor (HIF)-3alpha in human kidney: suppression of HIF-mediated

gene expression by HIF-3alpha. *Biochemical and biophysical research communications* **287**(4): 808-813.

Harding HP. Revised 11/5/2003. Immortalization of MEF with SV40 T antigen.

Harrison RB, Ramchandani P, Allen JT. 1979. Psychogenic polydipsia: unusual cause for hydronephrosis. *AJR American journal of roentgenology* **133**(2): 327-328.

Hashim H, Woodhouse CRJ. 2012. Ureteropelvic Junction Obstruction. *Eur Urol Suppl* **11**(2): 25-32.

Hassett S, Smith GH, Holland AJ. 2012. Prune belly syndrome. *Pediatric surgery international* **28**(3): 219-228.

Hayden MS, Ghosh S. 2008. Shared principles in NF-kappaB signaling. *Cell* **132**(3): 344-362.

Hebert SC. 2003. Bartter syndrome. *Current opinion in nephrology and hypertension* **12**(5): 527-532.

Hell MP, Duda M, Weber TC, Moch H, Krek W. 2014. Tumor suppressor VHL functions in the control of mitotic fidelity. *Cancer Res* **74**(9): 2422-2431.

Hergovich A, Lisztwan J, Barry R, Ballschmieter P, Krek W. 2003. Regulation of microtubule stability by the von Hippel-Lindau tumour suppressor protein pVHL. *Nat Cell Biol* **5**(1): 64-70.

Herrmann E, Marschner N, Grimm MO, Ohlmann CH, Hutzschenreuter U, Overkamp F, Groschek M, Blumenstengel K, Puhse G, Steiner T. 2011. Sequential therapies with sorafenib and sunitinib in advanced or metastatic renal cell carcinoma. *World journal of urology* **29**(3): 361-366.

Higgins DF, Kimura K, Bernhardt WM, Shrimanker N, Akai Y, Hohenstein B, Saito Y, Johnson RS, Kretzler M, Cohen CD et al. 2007. Hypoxia promotes fibrogenesis in vivo via HIF-1 stimulation of epithelial-to-mesenchymal transition. *The Journal of clinical investigation* **117**(12): 3810-3820.

Hollstein M, Rice K, Greenblatt MS, Soussi T, Fuchs R, Sorlie T, Hovig E, Smith-Sorensen B, Montesano R, Harris CC. 1994. Database of p53 gene somatic mutations in human tumors and cell lines. *Nucleic acids research* **22**(17): 3551-3555.

Holmquist-Mengelbier L, Fredlund E, Lofstedt T, Noguera R, Navarro S, Nilsson H, Pietras A, Vallon-Christersson J, Borg A, Gradin K et al. 2006. Recruitment of HIF-1alpha and HIF-2alpha to common target genes is differentially regulated in neuroblastoma: HIF-2alpha promotes an aggressive phenotype. *Cancer Cell* **10**(5): 413-423.

Hoyer JR, Sisson SP, Vernier RL. 1979. Tamm-Horsfall glycoprotein: ultrastructural immunoperoxidase localization in rat kidney. *Lab Invest* **41**(2): 168-173.

Huang Y, Murakami T, Sano F, Kondo K, Nakaigawa N, Kishida T, Kubota Y, Nagashima Y, Yao M. 2009. Expression of aquaporin 1 in primary renal tumors: a prognostic indicator for clear-cell renal cell carcinoma. *European urology* **56**(4): 690-698.

Hutson TE, Davis ID, Machiels JP, De Souza PL, Rottey S, Hong BF, Epstein RJ, Baker KL, McCann L, Crofts T et al. 2010. Efficacy and safety of pazopanib in patients with metastatic renal cell carcinoma. *Journal of clinical oncology : official journal of the American Society of Clinical Oncology* **28**(3): 475-480.

Iliopoulos O, Ohh M, Kaelin WG, Jr. 1998. pVHL19 is a biologically active product of the von Hippel-Lindau gene arising from internal translation initiation. *Proc Natl Acad Sci U S A* **95**(20): 11661-11666.

Jeck N, Reinalter SC, Henne T, Marg W, Mallmann R, Pasel K, Vollmer M, Klaus G, Leonhardt A, Seyberth HW et al. 2001. Hypokalemic salt-losing tubulopathy with chronic renal failure and sensorineural deafness. *Pediatrics* **108**(1): E5.

Jiang P, Du W, Wang X, Mancuso A, Gao X, Wu M, Yang X. 2011. p53 regulates biosynthesis through direct inactivation of glucose-6-phosphate dehydrogenase. *Nat Cell Biol* **13**(3): 310-316.

Jin XD, Chen ZD, Cai SL, Chen SW. 2009. Nephrogenic diabetes insipidus with dilatation of bilateral renal pelvis, ureter and bladder. *Scandinavian journal of urology and nephrology* **43**(1): 73-75.

Johnston LB, Chew SL, Lowe D, Reznek R, Monson JP, Savage MO. 2001. Investigating familial endocrine neoplasia syndromes in children. *Hormone research* **55 Suppl 1**: 31-35.

Jonasch E, Futreal PA, Davis IJ, Bailey ST, Kim WY, Brugarolas J, Giaccia AJ, Kurban G, Pause A, Frydman J et al. 2012. State of the science: an update on renal cell carcinoma. *Molecular cancer research : MCR* **10**(7): 859-880.

Jonkers J, Meuwissen R, van der Gulden H, Peterse H, van der Valk M, Berns A. 2001. Synergistic tumor suppressor activity of BRCA2 and p53 in a conditional mouse model for breast cancer. *Nat Genet* **29**(4): 418-425.

Joseph A, Yao H, Hinton BT. 2009. Development and morphogenesis of the Wolffian/epididymal duct, more twists and turns. *Developmental biology* **325**(1): 6-14.

Kamura T, Sato S, Iwai K, Czyzyk-Krzeska M, Conaway RC, Conaway JW. 2000. Activation of HIF1α ubiquitination by a reconstituted von Hippel-Lindau (VHL) tumor suppressor complex. *Proceedings of the National Academy of Sciences* **97**(19): 10430-10435.

Kang DH, Hughes J, Mazzali M, Schreiner GF, Johnson RJ. 2001. Impaired angiogenesis in the remnant kidney model: II. Vascular endothelial growth factor administration reduces renal fibrosis and stabilizes renal function. *J Am Soc Nephrol* **12**(7): 1448-1457.

Kang DH, Johnson RJ. 2003. Vascular endothelial growth factor: a new player in the pathogenesis of renal fibrosis. *Current opinion in nephrology and hypertension* **12**(1): 43-49.

Kaplan MR, Plotkin MD, Lee WS, Xu ZC, Lytton J, Hebert SC. 1996. Apical localization of the Na-K-Cl cotransporter, rBSC1, on rat thick ascending limbs. *Kidney Int* **49**(1): 40-47.

Kathel BL. 1971. Radioisotope renography as a renal function test in the newborn. *Archives of disease in childhood* **46**(247): 314-320.

Keith B, Johnson RS, Simon MC. 2012. HIF1alpha and HIF2alpha: sibling rivalry in hypoxic tumour growth and progression. *Nature reviews Cancer* **12**(1): 9-22.

Kim JW, Tchernyshyov I, Semenza GL, Dang CV. 2006. HIF-1-mediated expression of pyruvate dehydrogenase kinase: a metabolic switch required for cellular adaptation to hypoxia. *Cell metabolism* **3**(3): 177-185.

Kim YG, Suga SI, Kang DH, Jefferson JA, Mazzali M, Gordon KL, Matsui K, Breiteneder-Geleff S, Shankland SJ, Hughes J et al. 2000. Vascular endothelial growth factor accelerates renal recovery in experimental thrombotic microangiopathy. *Kidney Int* **58**(6): 2390-2399.

Kitamoto Y, Tokunaga H, Tomita K. 1997. Vascular endothelial growth factor is an essential molecule for mouse kidney development: glomerulogenesis and nephrogenesis. *The Journal of clinical investigation* **99**(10): 2351-2357.

Kiuru M, Lehtonen R, Arola J, Salovaara R, Jarvinen H, Aittomaki K, Sjoberg J, Visakorpi T, Knuutila S, Isola J et al. 2002. Few FH mutations in sporadic counterparts of tumor types observed in hereditary leiomyomatosis and renal cell cancer families. *Cancer Res* **62**(16): 4554-4557.

Ko MA, Rosario CO, Hudson JW, Kulkarni S, Pollett A, Dennis JW, Swallow CJ. 2005. Plk4 haploinsufficiency causes mitotic infidelity and carcinogenesis. *Nat Genet* **37**(8): 883-888.

Koh MY, Darnay BG, Powis G. 2008. Hypoxia-associated factor, a novel E3-ubiquitin ligase, binds and ubiquitinates hypoxia-inducible factor 1alpha, leading to its oxygen-independent degradation. *Mol Cell Biol* **28**(23): 7081-7095.

Koh MY, Lemos R, Jr., Liu X, Powis G. 2011. The hypoxia-associated factor switches cells from HIF-1alpha- to HIF-2alpha-dependent signaling promoting stem cell characteristics, aggressive tumor growth and invasion. *Cancer Res* **71**(11): 4015-4027.

Kondo K, Kim WY, Lechpammer M, Kaelin WG, Jr. 2003. Inhibition of HIF2alpha is sufficient to suppress pVHL-defective tumor growth. *PLoS Biol* **1**(3): E83.

Kondo K, Klco J, Nakamura E, Lechpammer M, Kaelin WG, Jr. 2002. Inhibition of HIF is necessary for tumor suppression by the von Hippel-Lindau protein. *Cancer Cell* **1**(3): 237-246.

Koshiji M, Huang LE. 2004. Dynamic balancing of the dual nature of HIF-1alpha for cell survival. *Cell cycle* **3**(7): 853-854.

Koshiji M, Kageyama Y, Pete EA, Horikawa I, Barrett JC, Huang LE. 2004. HIF-1alpha induces cell cycle arrest by functionally counteracting Myc. *EMBO J* **23**(9): 1949-1956.

Koury ST, Koury MJ, Bondurant MC, Caro J, Graber SE. 1989. Quantitation of erythropoietin-producing cells in kidneys of mice by in situ hybridization: correlation with hematocrit, renal erythropoietin mRNA, and serum erythropoietin concentration. *Blood* **74**(2): 645-651.

Kroemer G, Pouyssegur J. 2008. Tumor cell metabolism: cancer's Achilles' heel. *Cancer Cell* **13**(6): 472-482.

Kubbutat MH, Jones SN, Vousden KH. 1997. Regulation of p53 stability by Mdm2. *Nature* **387**(6630): 299-303.

Kuznetsova AV, Meller J, Schnell PO, Nash JA, Ignacak ML, Sanchez Y, Conaway JW, Conaway RC, Czyzyk-Krzeska MF. 2003. von Hippel-Lindau protein binds hyperphosphorylated large subunit of RNA polymerase II through a proline hydroxylation motif and targets it for ubiquitination. *Proc Natl Acad Sci U S A* **100**(5): 2706-2711.

Lai LP, Gibson-Gill CM, Gombas G, Claffey K, Tanks S, Garstang S. 2014. Hydronephrosis: an unusual complication of neurogenic bowel in a patient with spinal cord injury: a case report. *Spinal cord* **52 Suppl 1**: S9-s10.

Langbein S, Frederiks WM, zur Hausen A, Popa J, Lehmann J, Weiss C, Alken P, Coy JF. 2008. Metastasis is promoted by a bioenergetic switch: new targets for progressive renal cell cancer. *International journal of cancer Journal international du cancer* **122**(11): 2422-2428.

Latif F, Tory K, Gnarra J, Yao M, Duh FM, Orcutt ML, Stackhouse T, Kuzmin I, Modi W, Geil L et al. 1993. Identification of the von Hippel-Lindau disease tumor suppressor gene. *Science* **260**(5112): 1317-1320.

Lehninger AL, Nelson DL, Cox MM. 1993. *Principles of Biochemistry*. Worth, New York.

Li B, Qiu B, Lee DSM, Walton ZE, Ochocki JD, Mathew LK, Mancuso A, Gade TPF, Keith B, Nissim I et al. 2014. Fructose-1,6-bisphosphatase opposes renal carcinoma progression. *Nature* **advance online publication**.

Li C, Wang W, Kwon TH, Isikay L, Wen JG, Marples D, Djurhuus JC, Stockwell A, Knepper MA, Nielsen S et al. 2001. Downregulation of AQP1, -2, and -3 after ureteral obstruction is associated with a long-term urine-concentrating defect. *American journal of physiology Renal physiology* **281**(1): F163-171.

Li ZZ, Xing L, Zhao ZZ, Li JS, Xue R, Chandra A, Norregaard R, Wen JG. 2012. Decrease of renal aquaporins 1-4 is associated with renal function impairment in pediatric congenital hydronephrosis. *World J Pediatr* **8**(4): 335-341.

Liang H, Ward WF. 2006. PGC-1alpha: a key regulator of energy metabolism. *Advances in physiology education* **30**(4): 145-151.

Lim JH, Chun YS, Park JW. 2008. Hypoxia-inducible factor-1alpha obstructs a Wnt signaling pathway by inhibiting the hARD1-mediated activation of beta-catenin. *Cancer Res* **68**(13): 5177-5184.

Lindenmeyer MT, Kretzler M, Boucherot A, Berra S, Yasuda Y, Henger A, Eichinger F, Gaiser S, Schmid H, Rastaldi MP et al. 2007. Interstitial vascular rarefaction and reduced VEGF-A expression in human diabetic nephropathy. *J Am Soc Nephrol* **18**(6): 1765-1776.

Linehan WM, Pinto PA, Bratslavsky G, Pfaffenroth E, Merino M, Vocke CD, Toro JR, Bottaro D, Neckers L, Schmidt LS et al. 2009. Hereditary kidney cancer: unique opportunity for disease-based therapy. *Cancer* **115**(10 Suppl): 2252-2261.

Linehan WM, Srinivasan R, Schmidt LS. 2010. The genetic basis of kidney cancer: a metabolic disease. *Nature reviews Urology* **7**(5): 277-285.

Lisy K, Peet DJ. 2008. Turn me on: regulating HIF transcriptional activity. *Cell Death Differ* **15**(4): 642-649.

Lisztwan J, Imbert G, Wirbelauer C, Gstaiger M, Krek W. 1999. The von Hippel-Lindau tumor suppressor protein is a component of an E3 ubiquitin-protein ligase activity. *Genes Dev* **13**(14): 1822-1833.

Livera LN, Brookfield DS, Egginton JA, Hawnaur JM. 1989. Antenatal ultrasonography to detect fetal renal abnormalities: a prospective screening programme. *BMJ* **298**(6685): 1421-1423.

Lofstedt T, Fredlund E, Holmquist-Mengelbier L, Pietras A, Ovenberger M, Poellinger L, Pahlman S. 2007. Hypoxia inducible factor-2alpha in cancer. *Cell cycle* **6**(8): 919-926.

Lonergan KM, Iliopoulos O, Ohh M, Kamura T, Conaway RC, Conaway JW, Kaelin WG, Jr. 1998. Regulation of hypoxia-inducible mRNAs by the von Hippel-Lindau tumor suppressor protein requires binding to complexes containing elongins B/C and Cul2. *Mol Cell Biol* **18**(2): 732-741.

Lu S, Roman RJ, Mattson DL, Cowley AW, Jr. 1992. Renal medullary interstitial infusion of diltiazem alters sodium and water excretion in rats. *The American journal of physiology* **263**(5 Pt 2): R1064-1070.

Luo W, Hu H, Chang R, Zhong J, Knabel M, O'Meally R, Cole Robert N, Pandey A, Semenza Gregg L. 2011. Pyruvate Kinase M2 Is a PHD3-Stimulated Coactivator for Hypoxia-Inducible Factor 1. *Cell* **145**(5): 732-744.

Luo Y, He DL, Ning L, Shen SL, Li L, Li X. 2006. Hypoxia-inducible factor-1alpha induces the epithelial-mesenchymal transition of human prostatecancer cells. *Chinese medical journal* **119**(9): 713-718.

Ma W, Tessarollo L, Hong SB, Baba M, Southon E, Back TC, Spence S, Lobe CG, Sharma N, Maher GW et al. 2003. Hepatic vascular tumors, angiectasis in multiple organs, and impaired spermatogenesis in mice with conditional inactivation of the VHL gene. *Cancer Res* **63**(17): 5320-5328.

Machura K. 2007. Zeitlich-räumlche Entwicklung der Reninexpression in der Mausniere. Universität Regensburg.

Mack FA, Patel JH, Biju MP, Haase VH, Simon MC. 2005. Decreased growth of Vhl-/- fibrosarcomas is associated with elevated levels of cyclin kinase inhibitors p21 and p27. *Mol Cell Biol* **25**(11): 4565-4578.

Maddocks OD, Vousden KH. 2011. Metabolic regulation by p53. *Journal of molecular medicine* **89**(3): 237-245.

Madsen K, Marcussen N, Pedersen M, Kjaersgaard G, Facemire C, Coffman TM, Jensen BL. 2010. Angiotensin II promotes development of the renal microcirculation through AT1 receptors. *J Am Soc Nephrol* **21**(3): 448-459.

Maher ER, Iselius L, Yates JR, Littler M, Benjamin C, Harris R, Sampson J, Williams A, Ferguson-Smith MA, Morton N. 1991. Von Hippel-Lindau disease: a genetic study. *Journal of medical genetics* **28**(7): 443-447.

Maher ER, Neumann HP, Richard S. 2011. von Hippel-Lindau disease: a clinical and scientific review. *European journal of human genetics : EJHG* **19**(6): 617-623.

Mahon PC, Hirota K, Semenza GL. 2001. FIH-1: a novel protein that interacts with HIF-1alpha and VHL to mediate repression of HIF-1 transcriptional activity. *Genes Dev* **15**(20): 2675-2686.

Malumbres M, Barbacid M. 2009. Cell cycle, CDKs and cancer: a changing paradigm. *Nature reviews Cancer* **9**(3): 153-166.

Mandriota SJ, Turner KJ, Davies DR, Murray PG, Morgan NV, Sowter HM, Wykoff CC, Maher ER, Harris AL, Ratcliffe PJ et al. 2002. HIF activation identifies early lesions in VHL kidneys: evidence for site-specific tumor suppressor function in the nephron. *Cancer Cell* **1**(5): 459-468.

Manivel JC, Pettinato G, Reinberg Y, Gonzalez R, Burke B, Dehner LP. 1989. Prune belly syndrome: clinicopathologic study of 29 cases. *Pediatric pathology / affiliated with the International Paediatric Pathology Association* **9**(6): 691-711.

Manotham K, Tanaka T, Ohse T, Kojima I, Miyata T, Inagi R, Tanaka H, Sassa R, Fujita T, Nangaku M. 2005. A biologic role of HIF-1 in the renal medulla. *Kidney Int* **67**(4): 1428-1439.

Mao S, Zhang A, Huang S. 2014. The signaling pathway of uromodulin and its role in kidney diseases. *Journal of receptor and signal transduction research*: 1-5.

Mathia S, Paliege A, Koesters R, Peters H, Neumayer HH, Bachmann S, Rosenberger C. 2013. Action of hypoxia-inducible factor in liver and kidney from mice with Pax8-rtTA-based deletion of von Hippel-Lindau protein. *Acta physiologica* **207**(3): 565-576.

Mattson DL, Cowley AW, Jr. 1993. Kinin actions on renal papillary blood flow and sodium excretion. *Hypertension* **21**(6 Pt 2): 961-965.

Maxwell PH, Wiesener MS, Chang GW, Clifford SC, Vaux EC, Cockman ME, Wykoff CC, Pugh CW, Maher ER, Ratcliffe PJ. 1999. The tumour suppressor protein VHL targets hypoxia-inducible factors for oxygen-dependent proteolysis. *Nature* **399**(6733): 271-275.

McDill BW, Li SZ, Kovach PA, Ding L, Chen F. 2006. Congenital progressive hydronephrosis (cph) is caused by an S256L mutation in aquaporin-2 that affects its phosphorylation and apical membrane accumulation. *Proc Natl Acad Sci U S A* **103**(18): 6952-6957.

Mekhail TM, Abou-Jawde RM, Boumerhi G, Malhi S, Wood L, Elson P, Bukowski R. 2005. Validation and extension of the Memorial Sloan-Kettering prognostic factors model for survival in patients with previously untreated metastatic renal cell carcinoma. *Journal of clinical oncology : official journal of the American Society of Clinical Oncology* **23**(4): 832-841.

Miyazaki Y, Oshima K, Fogo A, Hogan BLM, Ichikawa I. 2000. Bone morphogenetic protein 4 regulates the budding site and elongation of the mouse ureter. *Journal of Clinical Investigation* **105**(7): 863-873.

Montani M, Heinimann K, von Teichman A, Rudolph T, Perren A, Moch H. 2010. VHL-gene deletion in single renal tubular epithelial cells and renal tubular cysts: further evidence for a cyst-dependent progression pathway of clear cell renal carcinoma in von Hippel-Lindau disease. *Am J Surg Pathol* **34**(6): 806-815.

Monzon FA, Alvarez K, Peterson L, Truong L, Amato RJ, Hernandez-McClain J, Tannir N, Parwani AV, Jonasch E. 2011. Chromosome 14q loss defines a molecular subtype of clear-cell renal cell carcinoma associated with poor prognosis. *Modern pathology : an official journal of the United States and Canadian Academy of Pathology, Inc* **24**(11): 1470-1479.

Moon SS, Kim HJ, Choi YK, Seo HA, Jeon JH, Lee JE, Lee JY, Kwon TH, Kim JG, Kim BW et al. 2009. Novel mutation of aquaporin-2 gene in a patient with congenital nephrogenic diabetes insipidus. *Endocr J* **56**(7): 905-910.

Morita S, Kojima T, Kitamura T. 2000. Plat-E: an efficient and stable system for transient packaging of retroviruses. *Gene therapy* **7**(12): 1063-1066.

Motzer RJ, Bander NH, Nanus DM. 1996. Renal-cell carcinoma. *The New England journal of medicine* **335**(12): 865-875.

Motzer RJ, Mazumdar M, Bacik J, Berg W, Amsterdam A, Ferrara J. 1999. Survival and prognostic stratification of 670 patients with advanced renal cell carcinoma. *Journal of clinical oncology : official journal of the American Society of Clinical Oncology* **17**(8): 2530-2540.

Narumi Y, Kosho T, Tsuruta G, Shiohara M, Shimazaki E, Mori T, Shimizu A, Igawa Y, Nishizawa S, Takagi K et al. 2010. Genital abnormalities in Pallister-Hall syndrome: Report of two patients and review of the literature. *American journal of medical genetics Part A* **152A**(12): 3143-3147.

Neumann HP, Bender BU, Berger DP, Laubenberger J, Schultze-Seemann W, Wetterauer U, Ferstl FJ, Herbst EW, Schwarzkopf G, Hes FJ et al. 1998. Prevalence, morphology and biology of renal cell carcinoma in von Hippel-Lindau disease compared to sporadic renal cell carcinoma. *The Journal of urology* **160**(4): 1248-1254.

Nickerson ML, Warren MB, Toro JR, Matrosova V, Glenn G, Turner ML, Duray P, Merino M, Choyke P, Pavlovich CP et al. 2002. Mutations in a novel gene lead to kidney tumors, lung wall

defects, and benign tumors of the hair follicle in patients with the Birt-Hogg-Dube syndrome. *Cancer Cell* **2**(2): 157-164.

O'Gorman S, Fox DT, Wahl GM. 1991. Recombinase-mediated gene activation and site-specific integration in mammalian cells. *Science* **251**(4999): 1351-1355.

Ohh M, Park CW, Ivan M, Hoffman MA, Kim TY, Huang LE, Pavletich N, Chau V, Kaelin WG. 2000. Ubiquitination of hypoxia-inducible factor requires direct binding to the beta-domain of the von Hippel-Lindau protein. *Nat Cell Biol* **2**(7): 423-427.

Ohh M, Yauch RL, Lonergan KM, Whaley JM, Stemmer-Rachamimov AO, Louis DN, Gavin BJ, Kley N, Kaelin WG, Jr., Iliopoulos O. 1998. The von Hippel-Lindau tumor suppressor protein is required for proper assembly of an extracellular fibronectin matrix. *Mol Cell* **1**(7): 959-968.

Okuda H, Saitoh K, Hirai S, Iwai K, Takaki Y, Baba M, Minato N, Ohno S, Shuin T. 2001. The von Hippel-Lindau tumor suppressor protein mediates ubiquitination of activated atypical protein kinase C. *J Biol Chem* **276**(47): 43611-43617.

Pan Y, Metzenberg A, Das S, Jing B, Gitschier J. 1992. Mutations in the V2 vasopressin receptor gene are associated with X-linked nephrogenic diabetes insipidus. *Nat Genet* **2**(2): 103-106.

Papandreou I, Cairns RA, Fontana L, Lim AL, Denko NC. 2006. HIF-1 mediates adaptation to hypoxia by actively downregulating mitochondrial oxygen consumption. *Cell metabolism* **3**(3): 187-197.

Paraf F, Chauveau D, Chretien Y, Richard S, Grunfeld JP, Droz D. 2000. Renal lesions in von Hippel-Lindau disease: immunohistochemical expression of nephron differentiation molecules, adhesion molecules and apoptosis proteins. *Histopathology* **36**(5): 457-465.

Parry L, Maynard JH, Patel A, Clifford SC, Morrissey C, Maher ER, Cheadle JP, Sampson JR. 2001. Analysis of the TSC1 and TSC2 genes in sporadic renal cell carcinomas. *British journal of cancer* **85**(8): 1226-1230.

Patel V, Li L, Cobo-Stark P, Shao X, Somlo S, Lin F, Igarashi P. 2008. Acute kidney injury and aberrant planar cell polarity induce cyst formation in mice lacking renal cilia. *Human molecular genetics* **17**(11): 1578-1590.

Paunescu TG, Russo LM, Da Silva N, Kovacikova J, Mohebbi N, Van Hoek AN, McKee M, Wagner CA, Breton S, Brown D. 2007. Compensatory membrane expression of the V-ATPase B2 subunit isoform in renal medullary intercalated cells of B1-deficient mice. *American journal of physiology Renal physiology* **293**(6): F1915-1926.

Pause A, Lee S, Worrell RA, Chen DY, Burgess WH, Linehan WM, Klausner RD. 1997. The von Hippel-Lindau tumor-suppressor gene product forms a stable complex with human CUL-2, a member of the Cdc53 family of proteins. *Proc Natl Acad Sci U S A* **94**(6): 2156-2161.

Peters CA. 1995. Urinary tract obstruction in children. *The Journal of urology* **154**(5): 1874-1883; discussion 1883-1874.

Peters CA, Mandell J, Lebowitz RL, Colodny AH, Bauer SB, Hendren WH, Retik AB. 1989. Congenital obstructed megaureters in early infancy: diagnosis and treatment. *The Journal of urology* **142**(2 Pt 2): 641-645; discussion 667-648.

Philips GK, Atkins MB. 2014. New agents and new targets for renal cell carcinoma. *American Society of Clinical Oncology educational book / ASCO American Society of Clinical Oncology Meeting*: e222-227.

Podevin G, Mandelbrot L, Vuillard E, Oury JF, Aigrain Y. 1996. Outcome of urological abnormalities prenatally diagnosed by ultrasound. *Fetal diagnosis and therapy* **11**(3): 181-190.

Presta LG, Chen H, O'Connor SJ, Chisholm V, Meng YG, Krummen L, Winkler M, Ferrara N. 1997. Humanization of an anti-vascular endothelial growth factor monoclonal antibody for the therapy of solid tumors and other disorders. *Cancer Res* **57**(20): 4593-4599.

Pritchett TL, Bader HL, Henderson J, Hsu T. 2014. Conditional inactivation of the mouse von Hippel-Lindau tumor suppressor gene results in wide-spread hyperplastic, inflammatory and fibrotic lesions in the kidney. *Oncogene* **0**.

Qian CN. 2013. Hijacking the vasculature in ccRCC--co-option, remodelling and angiogenesis. *Nature reviews Urology* **10**(5): 300-304.

Rajapakse NW, Mattson DL. 2011. Role of L-arginine uptake mechanisms in renal blood flow responses to angiotensin II in rats. *Acta physiologica* **203**(3): 391-400.

Ran FA, Hsu PD, Wright J, Agarwala V, Scott DA, Zhang F. 2013. Genome engineering using the CRISPR-Cas9 system. *Nat Protoc* **8**(11): 2281-2308.

Rankin EB, Tomaszewski JE, Haase VH. 2006. Renal cyst development in mice with conditional inactivation of the von Hippel-Lindau tumor suppressor. *Cancer Res* **66**(5): 2576-2583.

Rasouly HM, Lu W. 2013. Lower urinary tract development and disease. *Wiley interdisciplinary reviews Systems biology and medicine* **5**(3): 307-342.

Raval RR, Lau KW, Tran MG, Sowter HM, Mandriota SJ, Li JL, Pugh CW, Maxwell PH, Harris AL, Ratcliffe PJ. 2005. Contrasting properties of hypoxia-inducible factor 1 (HIF-1) and HIF-2 in von Hippel-Lindau-associated renal cell carcinoma. *Mol Cell Biol* **25**(13): 5675-5686.

Richards FM, Payne SJ, Zbar B, Affara NA, Ferguson-Smith MA, Maher ER. 1995. Molecular analysis of de novo germline mutations in the von Hippel-Lindau disease gene. *Human molecular genetics* **4**(11): 2139-2143.

Rinkevich Y, Montoro DT, Contreras-Trujillo H, Harari-Steinberg O, Newman AM, Tsai JM, Lim X, Van-Amerongen R, Bowman A, Januszyk M et al. 2014. In vivo clonal analysis reveals lineage-restricted progenitor characteristics in mammalian kidney development, maintenance, and regeneration. *Cell reports* **7**(4): 1270-1283.

Roberts AM, Watson IR, Evans AJ, Foster DA, Irwin MS, Ohh M. 2009. Suppression of hypoxia-inducible factor 2alpha restores p53 activity via Hdm2 and reverses chemoresistance of renal carcinoma cells. *Cancer Res* **69**(23): 9056-9064.

Robertson GL. 1988. Differential diagnosis of polyuria. *Annual review of medicine* **39**: 425-442.

Rodier F, Campisi J. 2011. Four faces of cellular senescence. *J Cell Biol* **192**(4): 547-556.

Roe JS, Kim H, Lee SM, Kim ST, Cho EJ, Youn HD. 2006. p53 stabilization and transactivation by a von Hippel-Lindau protein. *Mol Cell* **22**(3): 395-405.

Ryan HE, Poloni M, McNulty W, Elson D, Gassmann M, Arbeit JM, Johnson RS. 2000. Hypoxia-inducible factor-1alpha is a positive factor in solid tumor growth. *Cancer Res* **60**(15): 4010-4015.

S Silbernagl AD. 2003. *Taschenatlas der Physiologie* Thieme.

Sahali D, Mulliez N, Chatelet F, Dupuis R, Ronco P, Verroust P. 1988. Characterization of a 280-kD protein restricted to the coated pits of the renal brush border and the epithelial cells of the yolk sac. Teratogenic effect of the specific monoclonal antibodies. *The Journal of Experimental Medicine* **167**(1): 213-218.

Samnakay N, Orford J, Barker A, Charles A, Terry P, Newnham J, Moss T. 2006. Timing of morphologic and apoptotic changes in the sheep fetal kidney in response to bladder outflow obstruction. *Journal of pediatric urology* **2**(4): 216-224.

Sandock DS, Seftel AD, Resnick MI. 1995. A new protocol for the followup of renal cell carcinoma based on pathological stage. *The Journal of urology* **154**(1): 28-31.

Santos P, Pimenta T, Taveira-Gomes A. 2014. Hereditary Pheochromocytoma. *International journal of surgical pathology*.

Sato Y, Yoshizato T, Shiraishi Y, Maekawa S, Okuno Y, Kamura T, Shimamura T, Sato-Otsubo A, Nagae G, Suzuki H et al. 2013. Integrated molecular analysis of clear-cell renal cell carcinoma. *Nat Genet* **45**(8): 860-867.

Sauer B, Henderson N. 1989. Cre-stimulated recombination at loxP-containing DNA sequences placed into the mammalian genome. *Nucleic acids research* **17**(1): 147-161.

Saxén L LE. 1987. Embryonic kidney in organ culture. *Differentiation,* **36:2-11**.

Schedl A. 2007. Renal abnormalities and their developmental origin. *Nature reviews Genetics* **8**(10): 791-802.

Schley G, Klanke B, Schodel J, Forstreuter F, Shukla D, Kurtz A, Amann K, Wiesener MS, Rosen S, Eckardt KU et al. 2011. Hypoxia-inducible transcription factors stabilization in the thick

ascending limb protects against ischemic acute kidney injury. *J Am Soc Nephrol* **22**(11): 2004-2015.

Schmidt L, Duh FM, Chen F, Kishida T, Glenn G, Choyke P, Scherer SW, Zhuang Z, Lubensky I, Dean M et al. 1997. Germline and somatic mutations in the tyrosine kinase domain of the MET proto-oncogene in papillary renal carcinomas. *Nat Genet* **16**(1): 68-73.

Schofield CJ, Ratcliffe PJ. 2004. Oxygen sensing by HIF hydroxylases. *Nat Rev Mol Cell Biol* **5**(5): 343-354.

Scott DA, Wang R, Kreman TM, Sheffield VC, Karniski LP. 1999. The Pendred syndrome gene encodes a chloride-iodide transport protein. *Nat Genet* **21**(4): 440-443.

Sebastian S, Azzariti A, Silvestris N, Porcelli L, Russo A, Paradiso A. 2010. p53 as the main traffic controller of the cell signaling network. *Frontiers in bioscience (Landmark edition)* **15**: 1172-1190.

Semenza GL. 2003. Targeting HIF-1 for cancer therapy. *Nature reviews Cancer* **3**(10): 721-732.

Semenza GL, Roth PH, Fang HM, Wang GL. 1994. Transcriptional regulation of genes encoding glycolytic enzymes by hypoxia-inducible factor 1. *J Biol Chem* **269**(38): 23757-23763.

Shao X, Johnson JE, Richardson JA, Hiesberger T, Igarashi P. 2002a. A minimal Ksp-cadherin promoter linked to a green fluorescent protein reporter gene exhibits tissue-specific expression in the developing kidney and genitourinary tract. *J Am Soc Nephrol* **13**(7): 1824-1836.

Shao X, Somlo S, Igarashi P. 2002b. Epithelial-specific Cre/lox recombination in the developing kidney and genitourinary tract. *J Am Soc Nephrol* **13**(7): 1837-1846.

Shen C, Beroukhim R, Schumacher SE, Zhou J, Chang M, Signoretti S, Kaelin WG, Jr. 2011. Genetic and functional studies implicate HIF1alpha as a 14q kidney cancer suppressor gene. *Cancer discovery* **1**(3): 222-235.

Shopfner CE. 1966. Nonobstructive hydronephrosis and hydroureter. *The American journal of roentgenology, radium therapy, and nuclear medicine* **98**(1): 172-180.

Shuin T, Torigoe S, Kubota Y, Kishida T, Hosaka M, Horikoshi T, Yao M, Kondo K, Sakai N, Danenberg K et al. 1995. Retinoblastoma gene mutation in primary human renal cell carcinoma. *Oncology research* **7**(2): 63-66.

Sikri KL, Foster CL, MacHugh N, Marshall RD. 1981. Localization of Tamm-Horsfall glycoprotein in the human kidney using immuno-fluorescence and immuno-electron microscopical techniques. *Journal of anatomy* **132**(Pt 4): 597-605.

Soleimani M, Greeley T, Petrovic S, Wang Z, Amlal H, Kopp P, Burnham CE. 2001. Pendrin: an apical Cl-/OH-/HCO3- exchanger in the kidney cortex. *American journal of physiology Renal physiology* **280**(2): F356-364.

Soltoff SP. 1986. ATP and the regulation of renal cell function. *Annual review of physiology* **48**: 9-31.

Song R, Yosypiv IV. 2012. Development of the kidney medulla. *Organogenesis* **8**(1): 10-17.

Sotillo R, Dubus P, Martin J, de la Cueva E, Ortega S, Malumbres M, Barbacid M. 2001. Wide spectrum of tumors in knock-in mice carrying a Cdk4 protein insensitive to INK4 inhibitors. *EMBO J* **20**(23): 6637-6647.

Sotillo R, Renner O, Dubus P, Ruiz-Cabello J, Martin-Caballero J, Barbacid M, Carnero A, Malumbres M. 2005. Cooperation between Cdk4 and p27kip1 in tumor development: a preclinical model to evaluate cell cycle inhibitors with therapeutic activity. *Cancer Res* **65**(9): 3846-3852.

Srinivas S, Goldberg MR, Watanabe T, D'Agati V, al-Awqati Q, Costantini F. 1999. Expression of green fluorescent protein in the ureteric bud of transgenic mice: a new tool for the analysis of ureteric bud morphogenesis. *Developmental genetics* **24**(3-4): 241-251.

Stebbins CE, Kaelin WG, Jr., Pavletich NP. 1999. Structure of the VHL-ElonginC-ElonginB complex: implications for VHL tumor suppressor function. *Science* **284**(5413): 455-461.

Straube T, Elli AF, Greb C, Hegele A, Elsasser HP, Delacour D, Jacob R. 2011. Changes in the expression and subcellular distribution of galectin-3 in clear cell renal cell carcinoma. *Journal of experimental & clinical cancer research : CR* **30**: 89.

Sudarshan S, Linehan WM, Neckers L. 2007. HIF and fumarate hydratase in renal cancer. *British journal of cancer* **96**(3): 403-407.

Sunela KL, Kataja MJ, Lehtinen ET, Salminen TK, Kujala PM, Virman JP, Kellokumpu-Lehtinen PL. 2009. Prognostic factors and long-term survival in renal cell cancer patients. *Scandinavian journal of urology and nephrology* **43**(6): 454-460.

Takahashi N, Chernavvsky DR, Gomez RA, Igarashi P, Gitelman HJ, Smithies O. 2000. Uncompensated polyuria in a mouse model of Bartter's syndrome. *Proc Natl Acad Sci U S A* **97**(10): 5434-5439.

Tello D, Balsa E, Acosta-Iborra B, Fuertes-Yebra E, Elorza A, Ordonez A, Corral-Escariz M, Soro I, Lopez-Bernardo E, Perales-Clemente E et al. 2011. Induction of the mitochondrial NDUFA4L2 protein by HIF-1alpha decreases oxygen consumption by inhibiting Complex I activity. *Cell metabolism* **14**(6): 768-779.

The Cancer Genome Atlas Research N. 2013. Comprehensive molecular characterization of clear cell renal cell carcinoma. *Nature* **499**(7456): 43-49.

Thom RP, Rosenblum ND. 2013. A translational approach to congenital non-obstructive hydronephrosis. *Pediatric nephrology* **28**(9): 1757-1761.

Thoma CR, Frew IJ, Hoerner CR, Montani M, Moch H, Krek W. 2007. pVHL and GSK3beta are components of a primary cilium-maintenance signalling network. *Nat Cell Biol* **9**(5): 588-595.

Thoma CR, Toso A, Gutbrodt KL, Reggi SP, Frew IJ, Schraml P, Hergovich A, Moch H, Meraldi P, Krek W. 2009. VHL loss causes spindle misorientation and chromosome instability. *Nat Cell Biol* **11**(8): 994-1001.

Thut CJ, Goodrich JA, Tjian R. 1997. Repression of p53-mediated transcription by MDM2: a dual mechanism. *Genes Dev* **11**(15): 1974-1986.

Tomlinson IP, Alam NA, Rowan AJ, Barclay E, Jaeger EE, Kelsell D, Leigh I, Gorman P, Lamlum H, Rahman S et al. 2002. Germline mutations in FH predispose to dominantly inherited uterine fibroids, skin leiomyomata and papillary renal cell cancer. *Nat Genet* **30**(4): 406-410.

Toschi A, Lee E, Gadir N, Ohh M, Foster DA. 2008. Differential dependence of hypoxia-inducible factors 1 alpha and 2 alpha on mTORC1 and mTORC2. *J Biol Chem* **283**(50): 34495-34499.

Treuting PM, Kowalewska J. 2012. 16 - Urinary System. In *Comparative Anatomy and Histology*, (ed. PM Treuting, SM Dintzis), pp. 229-251. Academic Press, San Diego.

Tripathi P, Wang Y, Casey AM, Chen F. 2012. Absence of canonical Smad signaling in ureteral and bladder mesenchyme causes ureteropelvic junction obstruction. *J Am Soc Nephrol* **23**(4): 618-628.

Trowe MO, Airik R, Weiss AC, Farin HF, Foik AB, Bettenhausen E, Schuster-Gossler K, Taketo MM, Kispert A. 2012. Canonical Wnt signaling regulates smooth muscle precursor development in the mouse ureter. *Development* **139**(17): 3099-3108.

Tsai SJ, Ting H, Ho CC, Bih LI. 2001. Use of sonography and radioisotope renography to diagnose hydronephrosis in patients with spinal cord injury. *Archives of physical medicine and rehabilitation* **82**(1): 103-106.

Uchida T, Rossignol F, Matthay MA, Mounier R, Couette S, Clottes E, Clerici C. 2004. Prolonged hypoxia differentially regulates hypoxia-inducible factor (HIF)-1alpha and HIF-2alpha expression in lung epithelial cells: implication of natural antisense HIF-1alpha. *J Biol Chem* **279**(15): 14871-14878.

Uribarri J, Kaskas M. 1993. Hereditary nephrogenic diabetes insipidus and bilateral nonobstructive hydronephrosis. *Nephron* **65**(3): 346-349.

Vaidyanathan S, Soni BM, Hughes PL, Singh G, Mansour P, Oo T. 2009. Long-term nephrostomy in an adult male spinal cord injury patient who had normal upper urinary tracts but

developed bilateral hydronephrosis following penile sheath drainage: pyeloplasty and balloon dilatation of ureteropelvic junction proved futile: a case report. *Cases journal* **2**: 9335.

van Lieburg AF, Knoers NV, Monnens LA. 1999. Clinical presentation and follow-up of 30 patients with congenital nephrogenic diabetes insipidus. *J Am Soc Nephrol* **10**(9): 1958-1964.

Vander Heiden MG, Cantley LC, Thompson CB. 2009. Understanding the Warburg effect: the metabolic requirements of cell proliferation. *Science* **324**(5930): 1029-1033.

Verkman AS. 2008. Dissecting the roles of aquaporins in renal pathophysiology using transgenic mice. *Seminars in nephrology* **28**(3): 217-226.

Vichai V, Kirtikara K. 2006. Sulforhodamine B colorimetric assay for cytotoxicity screening. *Nat Protoc* **1**(3): 1112-1116.

W F Boron ELB. 2009. *Medical Physiology*. Elsevier Saunders.

Wagner CA, Loffing-Cueni D, Yan Q, Schulz N, Fakitsas P, Carrel M, Wang T, Verrey F, Geibel JP, Giebisch G et al. 2008. Mouse model of type II Bartter's syndrome. II. Altered expression of renal sodium- and water-transporting proteins. *American journal of physiology Renal physiology* **294**(6): F1373-1380.

Walsh PC RA, Vaughan ED, Wein AJ, Kavoussi LR, Novick AC, Partin AWm Peters CA. 2002. Campbell's Urology. (8th edition).

Weber S, Thiele H, Mir S, Toliat MR, Sozeri B, Reutter H, Draaken M, Ludwig M, Altmuller J, Frommolt P et al. 2011. Muscarinic Acetylcholine Receptor M3 Mutation Causes Urinary Bladder Disease and a Prune-Belly-like Syndrome. *American journal of human genetics* **89**(5): 668-674.

Welford SM, Dorie MJ, Li X, Haase VH, Giaccia AJ. 2010. Renal oxygenation suppresses VHL loss-induced senescence that is caused by increased sensitivity to oxidative stress. *Mol Cell Biol* **30**(19): 4595-4603.

Wenger RH, Hoogewijs D. 2010. Regulated oxygen sensing by protein hydroxylation in renal erythropoietin-producing cells. *American journal of physiology Renal physiology* **298**(6): F1287-1296.

Wenger RH, Stiehl DP, Camenisch G. 2005. Integration of oxygen signaling at the consensus HRE. *Science's STKE : signal transduction knowledge environment* **2005**(306): re12.

Wheeler H, Hanchey P. 1971. Pinocytosis and membrane dilation in uranyl-treated plant roots. *Science* **171**(3966): 68-71.

Wiesener MS, Jurgensen JS, Rosenberger C, Scholze CK, Horstrup JH, Warnecke C, Mandriota S, Bechmann I, Frei UA, Pugh CW et al. 2003. Widespread hypoxia-inducible expression of HIF-2alpha in distinct cell populations of different organs. *FASEB J* **17**(2): 271-273.

Wild PJ, Ikenberg K, Fuchs TJ, Rechsteiner M, Georgiev S, Fankhauser N, Noske A, Roessle M, Caduff R, Dellas A et al. 2012. p53 suppresses type II endometrial carcinomas in mice and governs endometrial tumour aggressiveness in humans. *EMBO Mol Med* **4**(8): 808-824.

Wilting RH, Dannenberg JH. 2012. Epigenetic mechanisms in tumorigenesis, tumor cell heterogeneity and drug resistance. *Drug resistance updates : reviews and commentaries in antimicrobial and anticancer chemotherapy* **15**(1-2): 21-38.

Woo JR, Sisul D, Kaplan G, Chiang G. 2013. Urologic outcomes of pediatric pelvic neuroblastoma presenting in acute urinary retention. *Pediatric hematology and oncology* **30**(7): 662-667.

Woods AG, Brandon DH. 2007. Prune belly syndrome. A focused physical assessment. *Advances in neonatal care : official journal of the National Association of Neonatal Nurses* **7**(3): 132-143; quiz 144-135.

Woodward M, Frank D. 2002. Postnatal management of antenatal hydronephrosis. *BJU international* **89**(2): 149-156.

Wright EM, Hirayama BA, Loo DF. 2007. Active sugar transport in health and disease. *Journal of internal medicine* **261**(1): 32-43.

Wu W, Kitamura S, Truong DM, Rieg T, Vallon V, Sakurai H, Bush KT, Vera DR, Ross RS, Nigam SK. 2009. Beta1-integrin is required for kidney collecting duct morphogenesis and

maintenance of renal function. *American journal of physiology Renal physiology* **297**(1): F210-217.

Wu X, Bayle JH, Olson D, Levine AJ. 1993. The p53-mdm-2 autoregulatory feedback loop. *Genes Dev* **7**(7A): 1126-1132.

Wullschleger S, Loewith R, Hall MN. 2006. TOR signaling in growth and metabolism. *Cell* **124**(3): 471-484.

Yamacake KG, Nguyen HT. 2013. Current management of antenatal hydronephrosis. *Pediatric nephrology* **28**(2): 237-243.

Yamamura Y, Nakamura S, Itoh S, Hirano T, Onogawa T, Yamashita T, Yamada Y, Tsujimae K, Aoyama M, Kotosai K et al. 1998. OPC-41061, a highly potent human vasopressin V2-receptor antagonist: pharmacological profile and aquaretic effect by single and multiple oral dosing in rats. *The Journal of pharmacology and experimental therapeutics* **287**(3): 860-867.

Yan Q, Yang X, Cantone A, Giebisch G, Hebert S, Wang T. 2008. Female ROMK null mice manifest more severe Bartter II phenotype on renal function and higher PGE2 production. *American journal of physiology Regulatory, integrative and comparative physiology* **295**(3): R997-r1004.

Yang B, Ma T, Verkman AS. 2001. Erythrocyte water permeability and renal function in double knockout mice lacking aquaporin-1 and aquaporin-3. *J Biol Chem* **276**(1): 624-628.

Yang H, Minamishima YA, Yan Q, Schlisio S, Ebert BL, Zhang X, Zhang L, Kim WY, Olumi AF, Kaelin WG, Jr. 2007. pVHL acts as an adaptor to promote the inhibitory phosphorylation of the NF-kappaB agonist Card9 by CK2. *Mol Cell* **28**(1): 15-27.

Yashima T, Noguchi Y, Kawashima Y, Rai T, Ito T, Kitamura K. 2010. Novel ATP6V1B1 mutations in distal renal tubular acidosis and hearing loss. *Acta oto-laryngologica* **130**(9): 1002-1008.

Young AP, Schlisio S, Minamishima YA, Zhang Q, Li L, Grisanzio C, Signoretti S, Kaelin WG, Jr. 2008. VHL loss actuates a HIF-independent senescence programme mediated by Rb and p400. *Nat Cell Biol* **10**(3): 361-369.

Yu J, Carroll TJ, McMahon AP. 2002. Sonic hedgehog regulates proliferation and differentiation of mesenchymal cells in the mouse metanephric kidney. *Development* **129**(22): 5301-5312.

Yun J, Schoneberg T, Liu J, Schulz A, Ecelbarger CA, Promeneur D, Nielsen S, Sheng H, Grinberg A, Deng C et al. 2000. Generation and phenotype of mice harboring a nonsense mutation in the V2 vasopressin receptor gene. *The Journal of clinical investigation* **106**(11): 1361-1371.

Zbar B, Tory K, Merino M, Schmidt L, Glenn G, Choyke P, Walther MM, Lerman M, Linehan WM. 1994. Hereditary papillary renal cell carcinoma. *The Journal of urology* **151**(3): 561-566.

Zhang H, Bosch-Marce M, Shimoda LA, Tan YS, Baek JH, Wesley JB, Gonzalez FJ, Semenza GL. 2008. Mitochondrial autophagy is an HIF-1-dependent adaptive metabolic response to hypoxia. *J Biol Chem* **283**(16): 10892-10903.

Zhang H, Gao P, Fukuda R, Kumar G, Krishnamachary B, Zeller KI, Dang Chi V, Semenza GL. 2007a. HIF-1 Inhibits Mitochondrial Biogenesis and Cellular Respiration in VHL-Deficient Renal Cell Carcinoma by Repression of C-MYC Activity. *Cancer Cell* **11**(5): 407-420.

Zhang H, Gao P, Fukuda R, Kumar G, Krishnamachary B, Zeller KI, Dang CV, Semenza GL. 2007b. HIF-1 inhibits mitochondrial biogenesis and cellular respiration in VHL-deficient renal cell carcinoma by repression of C-MYC activity. *Cancer Cell* **11**(5): 407-420.

Zhou MI, Wang H, Foy RL, Ross JJ, Cohen HT. 2004. Tumor suppressor von Hippel-Lindau (VHL) stabilization of Jade-1 protein occurs through plant homeodomains and is VHL mutation dependent. *Cancer Res* **64**(4): 1278-1286.

Zou AP, Li N, Cowley AW, Jr. 2001. Production and actions of superoxide in the renal medulla. *Hypertension* **37**(2 Pt 2): 547-553.

Zundel W, Schindler C, Haas-Kogan D, Koong A, Kaper F, Chen E, Gottschalk AR, Ryan HE, Johnson RS, Jefferson AB et al. 2000. Loss of PTEN facilitates HIF-1-mediated gene expression. *Genes Dev* **14**(4): 391-396.